Cooling Fractures in Lavas: Mechanisms and Environments of Formation

Thesis

UNRESTRICTED

Cooling fractures in lavas: mechanisms and environments of formation

A thesis submitted for the degree of Doctor of Philosophy in the Earth Sciences

By
Anne Forbes BA, MSci (Cantab)

Department of Environment, Earth and Ecosystems, The Open University
December 2012

Date of Submission: 21 December 20
Date of Award: 31 July 2013 12
Date of Award: 31 July 2013

Abstract

The focus of this study is cooling fractures in lavas that are associated with environments containing ice, snow or liquid water. Two main fracture types feature in this study: columnar jointing and pseudopillow fractures. This thesis addresses how and why these fractures form in particular environments.

Columnar jointing in rhyolite lava is particularly common in subglacial environments and rare in subaerial or purely subaqueous environments. Five subglacial rhyolites are studied with the presentation of the first set of measurements from subglaical rhyolite columns, showing considerably smaller column sizes and striae widths than in basalts. Some simple modelling was undertaken in order to explain these differences.

Pseudopillow fractures consist of a large, metre-scale, master fracture with many smaller, centimetre-scale, subsidiary fractures perpendicular to the master fracture. They are found in lava compositions from basalt to rhyolite. All documented occurrences are in lavas that have been inferred to have interacted with liquid water, ice or snow. The term *pseudopillow fracture system* is proposed to describe the consistent package of two different fracture types occurring together. Pseudopillow fracture systems were studied in two different trachyandesite lava flows. Three different master fracture types were identified on the basis of fracture surface textures displaying either chisel marks, cavitation dimples, or river lines and rough/smooth textures. Two types of subsidiary fractures were identified on the basis of their morphology: polygonal and planar subparallel.

The fractures in entablature, a formation common in basalt lava flows that have been inundated with water, were studied. Entablature was found to contain pseudopillow fracture systems and columnar jointing, which interact to form chevron fracture patterns. Master fractures form by ductile fracture of evolved residual melt, and show evidence of rapid cooling, related to coolant ingress. Two end members were identified: cube-jointing and column-bearing entablature, resulting from faster cooling in cube-jointed entablature.

Acknowledgements

First and foremost thanks to my supervisors Steve Blake, Dave McGarvie and Hugh Tuffen, for introducing me to the exhilarating world of fractures in lavas, taking me exciting places on fieldwork and for always being so encouraging.

Special thanks go, in particular, to Steve, my supervisor based here in Milton Keynes. Without his tireless reading and correcting of my work, amazing attention to detail, help with modelling, answering all my daft questions and kindness through the last 3 years this thesis would never have got finished.

Thank you to Iceland and the people there, in particular Ditta, Helga and the Landmannalaugar crew for looking after me and taking us in during a storm and feeding us cake. Thanks also to the wardens of Snæfellsnes national park for taking us through the lava tunnels and for also sheltering us from a storm.

To Ashea, the 'mum' of VDG, special thanks for looking after us so well.

Huge thanks are due to so many people who helped me collect data. Thanks to John Watson for help with XRF, Michelle Higgins and Kay Green for fun times in the thin section lab and all their help with endless polishing, Andy Tindle for very kindly letting me use his snazzy photomicroscopes, Clare Warren for the use of her photomicroscope and Chris MacDonnald for helping me use it. To Wesley Fraser for helping me fix the FTIR over the phone from Edinburgh, and to Susanne Schwenzer for going well above and beyond the call of duty helping me with the EPMA, at one point until 8pm on a bank holiday Saturday.

Many thanks to Tom Shaw, who field assisted the first time I was in Iceland. Sorry about the weather! Thank for being so cheery, even when we were hitch hiking in the rain, and being so much fun to have along.

Thanks also to Jacqui, for the fun time we spent in the field together, the fun times we've had in MK with the FTIR, baking, at conferences and generally over email. It was so nice to know you were just an email away.

My office mates deserve enormous thanks. They have put up with my jokes, songs, ballistic objects and occasional dancing with good humour and a great sense of fun. They are: Guillermo, Saskia, Susan, Mel, Bea, Marc, Sam, Leanne, Sion, Peter F, Alex, Natalie, Lucy, Liz and Lottie. They all have the patience of saints.

The community in the EEE department has made the time I have spent at the OU so much fun. Thanks to all the makers, doers, organisers, bakers, knitters, coffee drinkers, beer drinkers, crisp eaters, funsters, punsters and Santas, secret or otherwise.

To my housemates over the years, thank you Millie, Lucy, Jinni, Catherine, Liz, Guillermo and Peter M, for removing spiders, cooking me dinner, knitting, watching films, playing with glitter and generally keeping me entertained.

Thank you to Sam and Wes, for letting me play in your allotment, even if I dig up the wrong things!

To my family, for being so supportive and even listening to me witter on about rocks, thank you!

Thanks to Sion Hughes and Hazel Rymer for taking me off to north Iceland for two weeks. So much more fun than writing up!

John Murray for the institution that is VDG tea and a trip to (and particularly from) Mt. Etna that I will never forget, thank you!

Ane finally, thanks to Andy Wilson, field assistant, excellent lava scale, tent warmer, field-coffee maker, rock carrier, weather protector, general gadget man, scientific advisor and husband extraordinaire – I couldn't have done it without you. Thank you.

List of Figures

Chapter 1

Chapter 2

Chapter 3

Chapter 4

Chapter 5

Chapter 6

Appendix 7

List of tables

Chapter 2

Chapter 3

Chapter 4

Chapter 5

Appendix 1

Appendix 2

Appendix 3

Appendix 4

Appendix 5

Appendix 6

Appendix 7

Chapter 1: Introduction

1.1 Introduction

This thesis is concerned with the study of cooling fractures in lavas that have interacted in some way with ice, snow or water. As fractures in lavas are generally formed by contraction in response to cooling, fractures may therefore reflect the cooling environment in which they formed. They can be especially useful when studying lava from unusual cooling environments, such as those containing additional coolant in the form of ice, snow or water. Cooling fractures can lead to an interpretation of the lava flow environment (e.g. Lescinsky and Sisson, 1998; Lescinsky and Fink, 2000; Tuffen et al., 2001; Tuffen et al., 2002; Mee et al., 2006; Stevenson et al., 2006; Mee et al., 2009) and so an idea of the palaeoenvironmental setting. Given accurate dating of lava flows this can be used as an alternative proxy for the past environment. Previously, subglacial volcanic deposits have been used to great effect in inferring otherwise unobtainable details about the past environment, such as ice thickness (e.g. Tuffen et al., 2001; Tuffen et al., 2010; Owen et al., 2012), and they have the potential for recognising wet environments on other planets (e.g. Milazzo et al., 2009).

There are a number of hazards associated with lavas in environments containing ice, snow and/or water, such as jokulhlaups (glacial outburst floods) from subglacial eruptions (e.g. Guðmundsson et al., 1997; Snorrason et al., 2009) which are particularly problematic in Iceland, and lahars from lava-snow and lava-ice interaction (e.g. Waitt Jr et al., 1983; Lube et al., 2009; Waythomas, 2010). These hazards may be influenced by the rate of ice or snow melting, which is strongly influenced by the surface area of lava available to transfer heat (e.g. Höskuldsson and Sparks, 1997), and so by the amount and types of fractures present. Subglacial lava in lava-ice interaction ice-melting models is generally treated as

either fragmental particles or as pillow lavas (e.g. Höskuldsson and Sparks, 1997; Guðmundsson, 2003; Tuffen, 2007; Woodcock et al., 2012) but not as fractured coherent lava. Explosive lava-water/ice/snow interactions are a type of interaction phenomenon beyond the scope of this project. Pillow lava is rare in felsic lavas, and columnar jointing may instead be the dominant lava facies (e.g. Lescinsky and Fink, 2000; Tuffen et al., 2001; Stevenson et al., 2006). It is not possible to incorporate this into a model without knowing the amount of hot lava surface area that might be created by this fracturing. It is therefore important to understand the types of fractures that may occur in these settings to better inform us of the hazards they might influence. By studying lavas from environments dominated by different forms of coolant enables the broadest possible approach to understanding links between cooling fractures and cooling environments.

1.2 Fracture types

A number of cooling fracture types are commonly found associated with environments containing ice, snow or water, namely columnar jointing, pseudopillow fractures, 'sheet-like' fractures and hackly fractures, as outlined below. There are a number of gaps in our understanding of these cooling fractures. This study mainly focuses on pseudopillow fractures (Chapters 2, 4 and 5) and columnar jointing (Chapters 3 and 4) and touches briefly on sheet-like fractures, as they appear with columnar jointing (Chapter 3). Of primary importance is to increase our understanding of how these fractures form and why they form in these wet environments. In addition, this study also aims to enable environmental information to be extracted not just from the presence of particular fracture types but from the fractures themselves.

1.2.1 Pseudopillow fractures

A pseudopillow fracture (Fig. 1.1) consists of two fracture types, a single primary or master fracture which may be planar or curvi-planar and many secondary fractures that form perpendicular to this. Pseudopillow fractures may show a preferred orientation of formation (Lodge and Lescinsky, 2009) or can be more randomly oriented (Watanabe and Katsui, 1976; Mee et al., 2006). They occur in lavas which range in composition from rhyolite to basalt, but only form in lavas that have interacted with either ice, snow or liquid water (Watanabe and Katsui, 1976; Yamagishi et al., 1989; Yamagishi, 1991; Lescinsky and Fink, 2000; Mee et al., 2006; McGarvie et al., 2007; Lodge and Lescinsky, 2009; Tucker and Scott, 2009; Forbes et al., 2012). Thus they are intimately linked to the environment of lava emplacement.

Primary fractures are thought to form as a result of stresses caused by melting of underlying snow combined with rapid cooling (Mee et al., 2006), or due to the release of stresses caused by the flow movement and cooling contraction (Watanabe and Katsui, 1976) or by quench contraction of the solid lava (Yamagishi, 1991). Secondary fractures are polygonal, appearing as small versions of columnar jointing, and so are thought to form when water or steam infiltrates into the primary fracture causing cooling and contraction of the lava (Watanabe and Katsui, 1976; Yamagishi, 1991; Lescinsky and Fink, 2000; Mee et al., 2006). They propagate away from the primary fracture as demonstrated by striae propagation directions (e.g. DeGraff and Aydin, 1987) observed on the secondary fractures (Lescinsky and Fink, 2000; Lodge and Lescinsky, 2009).

Mud, palagonite and coarse grained glassy ash have been observed in primary fractures (Lescinsky and Fink, 2000; Mee et al., 2006), which is taken as evidence of particle bearing coolant fluxing through the lava. This is particularly relevant in the study of the

Santa Gertrudis lava at Nevados de Chillán volcano, Chile, by Mee et al. (2006) because the height of pseudopillow fractures in the lava is a few meters above the coolant source, in this case snow. Therefore the coolant is most likely to be steam rather than water, which will of course be present in abundance in any environment where hot lava interacts with a water-based coolant in any form.

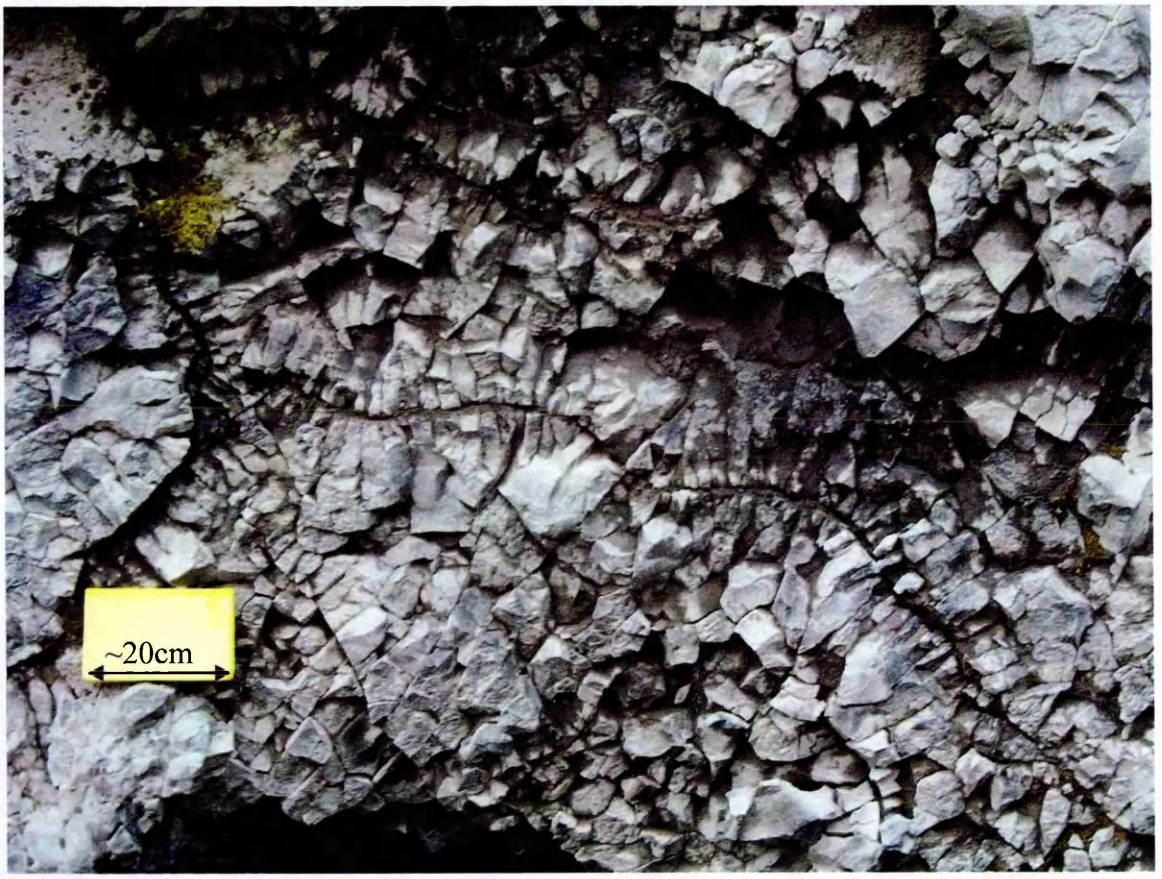

Fig. 1.1 Pseudopillow fractures, showing curvi-planar primary fracture and many small secondary fractures. This exposure is from the trachyandesite Slaga lava flow, Iceland, investigated in Chapter 5. Note book is 20 cm long.

Pseudopillow fractures have only been documented in a handful of studies, a common feature of all documented occurrences is the influence of additional coolant as either water, snow or ice. A key question of pseudopillow fractures must be directed to why they only form in environments that contain a coolant source. What about this combination of two fracture types (primary and secondary) means that they only form in 'wet' places?

Secondary fractures are relatively well understood: they are polygonal cooling contraction fractures (Watanabe and Katsui, 1976; Yamagishi, 1991; Lescinsky and Fink, 2000; Mee et al., 2006), similar to columnar jointing. This type of fracture therefore, like columnar jointing, can occur in any environment, with or without a coolant source. So instead the primary fracture may contain some critical information relating to the environment of formation. No detailed descriptions of primary fractures exist and this is clearly an important objective in understanding pseudopillow fractures better. To do this it is necessary to know how primary fractures form and what type of fracture they are.

1.2.2 Columnar jointing

Columnar jointing (Figs. 1.2 and 1.3) is characterised by a tessellated array of polygonal fracture patterns that extend into a lava flow normal to the cooling surfaces, and are typified by formations such as the Giant's Causeway in Northern Ireland. Much is known about how columns form and they have been an irresistible enigma for some time (e.g. Bulkeley, 1693; O'Reilly, 1879; Iddings, 1886; Tomkeieff, 1940; Beard, 1959; Spry, 1962). They form incrementally due to cooling contraction in a uniform stress environment (Spry, 1962; Lodge and Lescinsky, 2009) with each increment of fracture leaving behind a band on the column bounding fracture, known as a stria or a chisel mark (Ryan and Sammis, 1978). Columnar jointing can be found in lavas ranging in composition from rhyolite to basalt, in both intrusive and extrusive igneous rocks, and in environments from arid to subglacial (DeGraff and Aydin, 1993; Budkewitsch and Robin, 1994; Grossenbacher and McDuffie, 1995; Allen and McPhie, 2002; Tuffen et al., 2002; Stevenson et al., 2006; Goehring and Morris, 2008). They produce a large surface area within a lava flow, and so can increase the rate of heat loss from the lava to the surroundings.

Fig. 1.2 Columnar jointing in basalt, from Kirkugólf, near Kirkjubæjarklaustur, south Iceland. Pink pencil in centre is approx 15 cm, scale bar at bottom left is 30 cm.

Columnar jointing appears to be rare in rhyolite lavas, however it is prevalent in subglacial rhyolites, to the point that the presence of columnar jointing in rhyolite (and other felsic lavas) has be used as an indicator of subglacial emplacement (Lescinsky and Sisson, 1998; Lescinsky and Fink, 2000; Tuffen et al., 2001; Tuffen et al., 2002; Stevenson et al., 2006). Columns are, however, uncommon in both subaerial and subaqueous rhyolite. There are no detailed studies of columns in rhyolite lavas equivalent to those in basalts, although there is a wealth of studies of basaltic lava flows detailing measurements of column size, measured as column side width, striae widths and numbers of sides of columns (Beard, 1959; Ryan and Sammis, 1978; DeGraff and Aydin, 1993; Grossenbacher and McDuffie, 1995; Goehring and Morris, 2008; Hetényi et al., 2012). The ratio of striae widths to column side width has been found from field studies to be approximately 1:7 (Ryan and Sammis, 1978; DeGraff and Aydin, 1993; Grossenbacher and McDuffie, 1995; Goehring and Morris, 2008). It is unknown if this relationship or anything similar occurs in rhyolitic columns.

Likewise, it is unknown if columns in rhyolite show a dominance of column shapes other than hexagons as in some basalts (e.g. Beard, 1959). In fact we know almost nothing about columnar jointing in rhyolite, not even why it appears to form in subglacial environments and yet is so rare in subaerial rhyolite lava flows.

The presence of a coolant source cannot be the cause of the subglacial columnar jointing as columns are not common in purely subaqueous settings either (e.g. Scutter et al., 1998; DeRita et al., 2001). The only references to columnar jointing in subaerial rhyolite appears to be from very thick lava flows (e.g. Bonnichsen and Kauffman, 1987; Henry et al., 1990; Allen and McPhie, 2002; Allen et al., 2008; McPhie et al., 2008). If we can understand why columnar jointing occurs in subglacial rhyolite perhaps we can use this to gain a better understanding of the environment.

So much is unknown about columnar jointing in rhyolite. Do they behave like columns in basalt? Are they governed by the same scaling relationships? Do they appear the same statistically? In basalt both column size and striae width are controlled by cooling rate, with faster cooling rates leading to smaller columns and smaller striae widths (Spry, 1962; Ryan and Sammis, 1978; Goehring and Morris, 2008; Hetényi et al., 2012). Gathering this type of data for rhyolite columns in subglacial environments may enable a better understanding of cooling rates and so a better determination of the exact environment of subglacial lavas.

Fig. 1.3 Colonnade and entablature from Staffa, Scotland, showing the famous Fingle's cave exposure. The entablature is the irregular upper tier and the colonnade is the lower tier of large, vertical, regular columns. The entablature forms from the top downwards and the colonnade forms from the base upwards, they meet in the middle at a distinct contact. The lava is resting on a layer of tephra visible in the left hand side of the image. The height of this section is approximately 20 m. Photo courtesy of Peter Sheldon.

1.2.3 Entablature

A particular type of irregular columnar jointing, called entablature (Fig. 1.3), forms predominantly in the upper parts of basalt lava flows that have interacted with water from lava dammed rivers (Swanson, 1967; Sæmundsson, 1970; Long and Wood, 1986; DeGraff et al., 1989; Walker, 1993; Lyle, 2000) or subglacial melt water (e.g. Smellie, 2008). This is an interesting formation, and allows an interpretation of the emplacement environment of an entablature bearing lava flow from its broad scale appearance. However, entablature alone does not tell us of the source of this water, for example subglacially produced water on melting of overlying ice or subaerial invasion of water from a river. The fracturing in entablature has been studied by Spry (1962), who draws attention to a range of interesting shapes that are formed from a combination of columns and 'master' fractures, and DeGraff

and Aydin (1987) demonstrated that entablature forms from the top downwards by studying striae propagation directions in entablature.

The environments of entablature formation have been extensively studied (Spry, 1962; Swanson, 1967; Sæmundsson, 1970; Long and Wood, 1986; DeGraff et al., 1989; Lyle, 2000) and are fairly well understood. However the fractures and fracture types occurring in entablature have not been investigated previously. 'Master' fractures which appear to form early in the fracture history have been described but the type and formation mechanisms of these master fractures are not known (Spry, 1962; DeGraff and Aydin, 1987; Lyle, 2000). These may influence some of the fracture morphologies that appear in entablature tiers, such as chevrons and fans (Spry, 1962; DeGraff and Aydin, 1987).

1.2.4 Sheet-like fractures

Sheet-like fractures (Lescinsky and Fink, 2000; Lodge and Lescinsky, 2009) are described from ice-contact lavas of andesite to dacite composition in the Cascades, USA. They are long planar fractures, generally up to 5 m long, occurring in parallel sets. Smaller cross-cutting fractures can occur roughly perpendicularly between pairs of sheet-like fractures, creating crude four-sided columns. They have striae on their fracture surfaces which are continuous across the entire fracture, across the adjacent crude columns.

A fracture type termed 'intermediate' fractures are very similar to sheet-like fractures, being intermediate in morphology between sheet-like and polygonal (columnar) fractures (Lodge and Lescinsky, 2009). They have a jagged, saw-tooth appearance rather than the straighter shape of sheet-like fractures. Cross cutting fractures form polygonal shapes between the intermediate fractures. They have only been described by Lodge and Lescinsky (2009), occurring in andesite and dacite lava flows in ice-contact settings.

Sheet-like and intermediate fractures have only been described from lava-ice interaction sites from the Cascades. These fractures are interpreted to be the result of marginal bulging and gravitational settling of a flow occurring when supporting ice melts away from the lava allowing bulging of the flow (Lodge and Lescinsky, 2009). These fracture types could therefore be a good indication of lava-ice interaction as ice appears to be integral to their formation; they have not been observed in lavas in non-glacial environments (although they are only mentioned in two studies).

1.2.5 Hackly fractures

Hackly fractures are common in all places where there is a source of coolant in the form of either water, snow or ice (Lescinsky and Fink, 2000; Mee et al., 2006; Tucker and Scott, 2009; Stevenson et al., 2012). They are chaotic closely spaced fractures with a range of orientations that intersect to form irregularly shaped angular blocks. They are thought to form under conditions of rapid cooling, possibly enhanced by steam explosions (Lescinsky and Fink, 2000), leaving no time for the formation of ordered fracture patterns to establish themselves. They are a product of random brittle fracturing due to fast cooling.

1.3 Key research questions

Six key research questions are apparent from this introduction to cooling fractures, these are: 1) how do pseudopillow fracture systems form and 2) why do they only form in 'wet' environments? 3) Why is columnar jointing so common in subglacial rhyolite and 4) what information can these columns give us about the cooling environment? 5) What fracture types occur in entablature in basalt and 6) how do they form? This thesis sets out to answer these questions through studies of lava flows containing these fracture types.

1.4 Research techniques

In addition to conventional geological techniques such as field measurement, petrography and physical modelling, this study utilises an area of material science known as fractography, which is the study of fractures through the topography of fracture surface textures. The topography of a surface created while a crack is growing is characteristic of the microstructure of the material and of the conditions under which the material fractured (Hull, 1999). This is of primary industrial importance in materials such as metals, soda lime glass and ceramics and so most fractography studies are of industrially important materials, rather than rocks or lavas. However many fracture features that occur in these materials also occur in lava, which although at a different scale, can still be interpreted in the same way. This study uses evidence from fracture surface textures to understand and reconstruct fracture nucleation and propagation directions. Various fracture surface textures are seen in lavas from this study such as river lines, also known as twist-hackle (e.g. Kulander and Dean, 1995; Roberts, 1995; Weinberger, 2001) resulting from mixed mode I/III brittle fracturing, hackle, also known as plumose structures, resulting from accelerating brittle fracture propagation, and cavitation, a ductile fracture texture more commonly found in ductile materials such as metals (fracture textures outlined in Fig. 1.4).

In general the formation of columnar jointing and the fractography of column bounding fractures is well understood (Ryan and Sammis, 1978; DeGraff and Aydin, 1987), whereas those in pseudopillow fractures have so far remained totally enigmatic. So while this study makes use of advances in the understanding of fracture formation and fractography in columnar jointing, to enhance the study of columns in subglacial and water inundation environments, it must 'start from scratch' in the study of pseudopillow fractures, particularly their primary fractures.

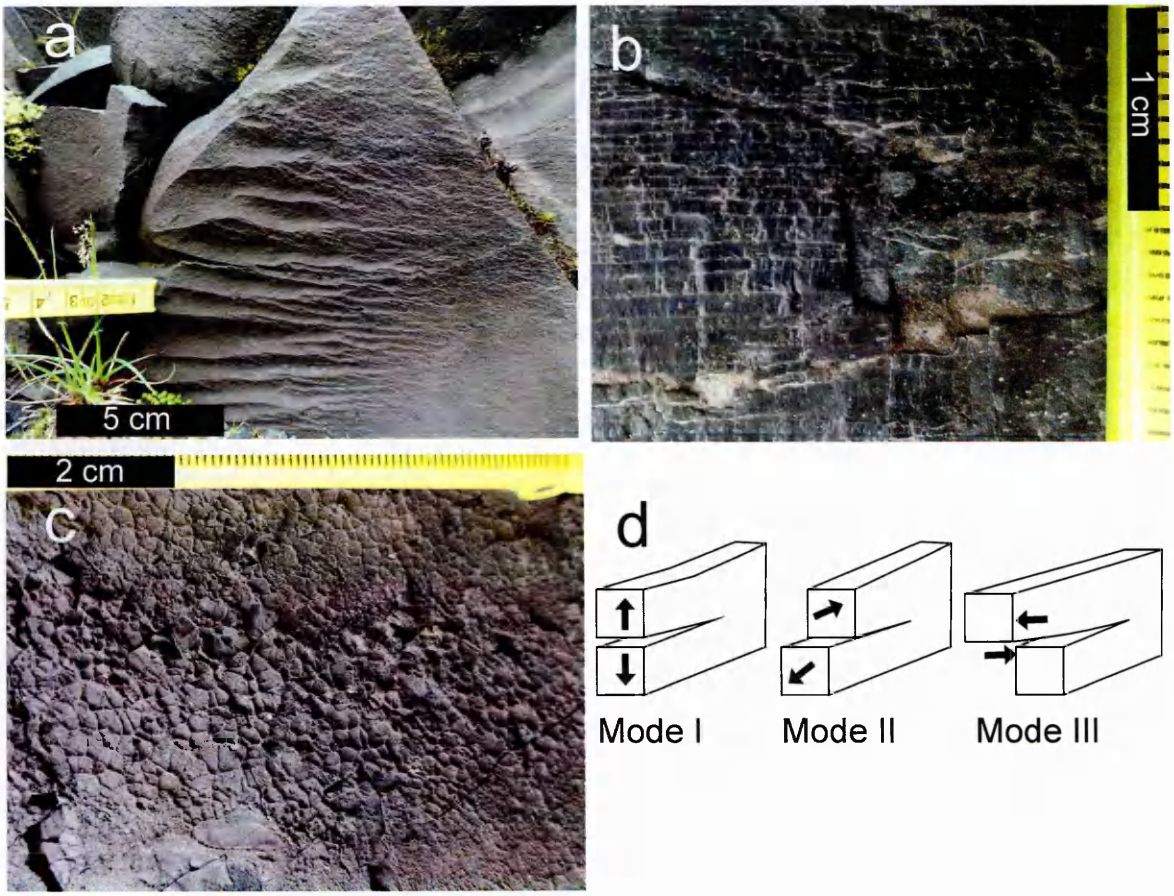

Fig. 1.4 a) River lines (also known as twist-hackles) propagating from right to left from the Slaga lava flow, Iceland, investigated in Chapter 5. They are a series of steps that amalgamate into fewer, larger steps as they propagate forward. They result from mixed mode I/III fracture. b) Hackle on closely spaced striae (horizontal) propagating upwards, from the Slaga lava flow. c) Dimpled cavitation fracture surface texture, resulting from ductile fracture, from the Tangahraun lava flow of Chapter 2, and d) the modes of fracture showing pure tension (I), shear parallel to the direction of fracture propagation (II) and shear normal to the direction of fracture propagation (III).

1.5 Aims and structure of the thesis

Chapter 2 deals with understanding the formation of pseudopillow fractures, providing detailed descriptions of the two fractures that form pseudopillow fractures, from the Tangahraun lava flow, Snæfellsnes, west Iceland. A new non-genetic nomenclature system for pseudopillow fractures is provided. This study focuses on a trachyandesite lava flow that has probably interacted with liquid water, flowing into the sea. This chapter aims to link this fracture type to the emplacement environment of the lava flow.

Chapter 3 focuses on columnar jointing in subglacial rhyolites from a number of localities from Torfajökull and Öræfajökull volcanoes, Iceland. A data set of column measurements (column side width, striae widths and number of column sides) from rhyolite columns is presented and these are compared to their subaerial basalt equivalents. Physical properties of basalt and rhyolite lavas are analysed to understand whether differences in columnar jointing in these two lava compositions are due to environmental or compositional differences.

Chapter 4 looks at the fracture types in entablature in the Þjorsádalur valley, southwest Iceland, and attempts to relate these, and their formation, to their environments. Two end member types of entablature are studied, cube-jointing and column bearing entablature. Both contain pseudopillow fractures, and these show evidence of evolved melt migration as part of their formation mechanism.

Chapter 5 uses the understanding gained from the study of cooling fractures in lava, particularly pseudopillow fractures, to understand a lava flow from an unknown cooling environment from the southwest flanks of Öræfajökull volcano. Fractures and other features in the lava are described in detail and used to interpret the emplacement environment of this lava flow. This chapter demonstrates the usefulness of cooling fractures in helping to provide a detailed understanding of the emplacement environment of lava flows.

Chapter 6 summarises and synthesises chapters 1-5, bringing together observations and new findings, to look at how these have changed the way we understand cooling fractures in lavas and how they can be used to gain a better understanding of a lava flow.

Chapter 2: Pseudopillow fracture systems in lavas: Insights into cooling mechanisms and environments from lava flow fractures

This chapter is published as:

Forbes, A.E.S., Blake, S., McGarvie, D.W. and Tuffen, H., (2012). Pseudopillow fracture systems in lavas: Insights into cooling mechanisms and environments from lava flow fractures. Journal of Volcanology and Geothermal Research, 245-246: 68-80.

Abstract

Detailed field observations of structures within the flow front of a Holocene trachyandesite lava from Snæfellsnes, Iceland, are presented. The lava provides exceptional three-dimensional exposure of complex brittle and ductile deformation textures that record processes of lava fracture and quenching driven by external water.

The flow front interior is characterised by structures consisting of a large (metre-scale) curviplanar master fracture with many smaller (centimetre-scale) subsidiary fractures perpendicular to the master fracture. Such structures have previously been recognised in a range of lava compositions from basalt to dacite and called pseudopillows or pseudopillow fractures. We propose the term *pseudopillow fracture systems* to emphasise the consistent package of different fracture types occurring together. All documented occurrences of pseudopillow fracture systems are in lavas that have been inferred to interact with an aqueous coolant (i.e. liquid water, ice or snow).

We use fracture surface textures and their orientation in relation to flow banding to identify three distinct types of master fracture and two types of subsidiary fractures. Master fracture

surface textures used to identify fracture mechanisms include striae (chisel marks), cavitation dimples, river lines and rough/smooth fracture surface textures. These indicate both brittle and ductile fracture happening on different types of master fracture. Striae on subsidiary fractures indicate comparative cooling rates, cooling directions and isotherm orientations at the time of fracture. We propose a model for pseudopillow fracture system formation taking into account all the various fracture types, textures and fracture propagation mechanisms and discuss their implications for interaction mechanisms between lava flows and external coolants.

2.1 Introduction

Cooling related fractures in lavas have long been used to give information on how lava cools, deforms and fractures during emplacement in various environments. One type of fracture that has been extensively studied in this respect is columnar jointing. Column size has been linked to the cooling rate of the lava (e.g. Grossenbacher and McDuffie, 1995; Goehring and Morris, 2008), columns in rhyolite and dacite lavas have been used to infer the presence of ice (Lescinsky and Sisson, 1998; Tuffen et al., 2001; Tuffen et al., 2002; Stevenson et al., 2006) and entablature-type columnar jointing has been argued to occur when water floods the upper surface of a cooling lava flow (Saemundsson, 1970; Long and Wood, 1986; Lyle, 2000). Pseudopillow fractures, so called because they split the lava into shapes with a rudimentary similarity to those of subaqueous lava pillows when first observed (Watanabe and Katsui, 1976), fall into this category of fracture types that may contain environmental information.

Pseudopillow fractures (also called *pseudopillows*) are complex fracture systems that comprise two distinct types of fractures (see Fig. 2.1). The most prominent is a large curviplanar fracture, commonly called the *primary* fracture (e.g. Lescinsky and Fink, 2000)

but also the *master* fracture (Tucker and Scott, 2009). Each side of the master fracture is then cut by many small *secondary* fractures. The secondary fractures extend perpendicularly from the master fracture into the surrounding lava for up to 30 cm and are spaced a few mm to a few cm apart. We propose to call pseudopillow 'fractures' *pseudopillow fracture systems* in recognition of the intricate interaction of the two fracture types that form these distinctive fracture systems. We propose to retain the term *master* fracture but change the previously termed secondary fractures to *subsidiary* fractures. This change in nomenclature enables a more generic terminology that avoids assumptions about the order of events, and allows improved description of the complex fracture systems we have observed in this study.

The term 'pseudopillow' originated from the fact that this fracture system has a basic similarity to the outer edge of contraction-fractured pillow lavas. They were also first observed in a subaqueous lava, where one might expect to find pillow lavas (Watanabe and Katsui, 1976). *Pseudopillow fracture* or *pseudopillow fracture system* may not be the best name for these fracture systems as they have no genetic similarity to pillow lavas and little similarity to the appearance of pillow lavas. However, as this term has been in use for more than 30 years and is subsequently ingrained in studies of lava-coolant interaction I continue with the use of the term *pseudopillow*. Pillow lavas are entirely unlike pseudopillow fracture systems and will not be discussed further in this thesis.

Fig. 2.1 A pseudopillow fracture system: the master fracture is parallel to the flow banding horizontally across the centre of the image and the subsidiary fractures extend vertically away from either side of the master fracture. Paler alteration of some flow bands occurs either side of the master fracture. The ruler is 25 cm long.

It has been inferred that subsidiary fractures are formed when water or steam infiltrates the master fracture causing cooling and contraction of the surrounding lava (Watanabe and Katsui, 1976; Yamagishi, 1991; Lescinsky and Fink, 2000; Mee et al., 2006). Mud, palagonite (altered glass) and coarse-grained glassy ash have been observed in master fractures (Lescinsky and Fink, 2000; Mee et al., 2006), and interpreted as evidence for movement of particle-laden steam or water coolant through the fractures. There is no consensus on the mode or cause of formation of master fractures. Existing models include: lava deformation due to melting and withdrawal of underlying snow (Mee et al., 2006), release of stresses caused by the flow movement and cooling contraction (Watanabe and Katsui, 1976) and quench contraction of the solid lava (Yamagishi, 1991). In contrast, Lodge and Lescinsky (2009) and Walker (1992, 1993) suggest that master fractures are expansion fractures because of the wide gap sometimes observed on the master fracture.

Pseudopillow fracture systems have only been documented in a handful of studies, however they have been observed in a broad range of lava compositions and environments, as summarised in Table 2.1. A common feature of all documented occurrences of pseudopillow fracture systems in lavas is the influence of additional coolant, such as water, snow or ice.

Table 2.1 Previously published literature concerning pseudopillow fracture systems, their form and environment.

Literature source	Lava composition	Environment	Form	Subsidiary jointing
Watanabe & Katsui (1976)	Dacite	Water, caldera lake	Arcuate, can form lenticular bodies	Polygonal
Yamagishi et al. (1989)	Basalt	Submarine		
Yamagishi (1991)	Andesite	Submarine	Forms isolated bodies 'pseudopillows'	Polygonal
Walker (1992)	Andesite			Polygonal
Lescinsky & Fink (2000)	Andesite/ basaltic-and.	Ice on stratovolcano	Arcuate	Polygonal
Mee et al. (2006)	Dacite	Snow	Arcuate, can form pillow-like bodies	Polygonal
Tucker & Scott (2009)	Basalt/ basaltic-and.	Water >100m deep	Arcuate, also in subparallel sets	
Lodge & Lescinsky (2009)	Andesite-dacite	Ice on stratovolcano	Semi-parallel, some arcuate	Polygonal

The objectives of this study are to more fully describe and understand pseudopillow fracture systems. We provide field descriptions of an exceptionally well-exposed lava flow from Snæfellsnes, west Iceland, that contains pseudopillow fracture systems. We use evidence from the fracture surface morphologies, textures and inter-relationships to reconstruct the nucleation and advance of fractures and propose new models of pseudopillow fracture system growth and their environmental significance.

2.2 Geological setting and nature of the Tangahraun lava

The lava flow in this study is located on the southwest coast of the Snæfellsnes peninsula, Iceland, informally named Tangahraun. Major element data from XRF analysis (Table 2.2) show that this flow-banded lava is of trachyandesite composition. It is post-glacial in age, showing sparse plagioclase and clinopyroxene phenocrysts < 5 mm and prominent flow ridges (ogives; Fig. 2.2).

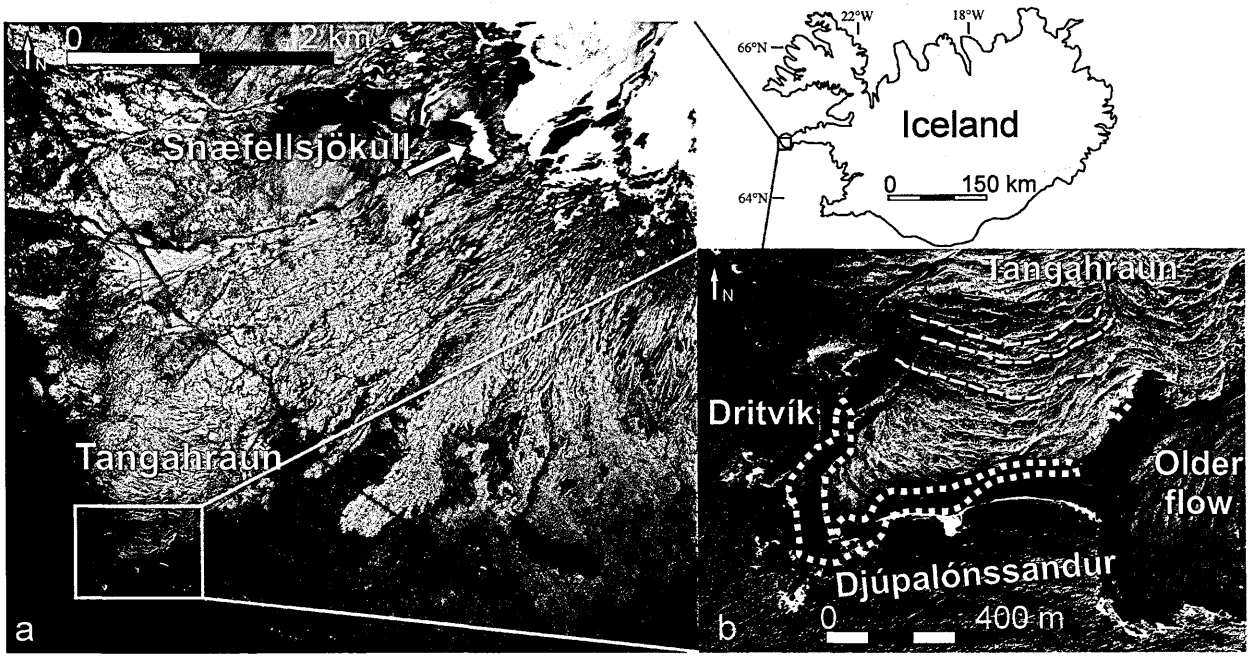

Fig. 2.2 Outline map of Iceland and aerial photographs showing (a) the southwest part of the Snæfellsnes peninsula and (b) a magnification of the boxed area in (a) which is the area of study. The extent of pseudopillow fracture systems is marked in dotted lines, and the traces of some ogives, or flow ridges, are marked on in dashed lines. The names of the two bays referred to in the text (Djúpalónssandur and Dritvík) are indicated in (b).

Table 2.2 XRF data of a single representative sample from the Tangahraun lava flow.

wt. %	Tangahraun
SiO_2	57.62
TiO_2	1.507
Al_2O_3	16.08
Fe_2O_3	9.25
MnO	0.243
MgO	2.10
CaO	5.01
Na_2O	5.03
K_2O	2.63
P_2O_5	0.606
LOI	-0.11
Total	99.95

The inland part of the flow is largely covered in grassy vegetation and is poorly exposed showing some flow top breccia and bodies of crudely polygonal jointed lava. It is substantially different in appearance to the shore front exposures. No pseudopillow fracture systems have been observed in the inland part of the lava (see Fig. 2.2).

Exposure at the eroded flow front interior is excellent between the bays of Djúpalónssandur and Dritvík (see Figs. 2.2 and 2.3), although the base of the flow is not visible. The total flow front exposure showing pseudopillow fracture systems is approximately 1 km long (Fig. 2.2). The exposed flow thickness is approximately 10-15 m and can be seen in the cliff along the north side of the beach at Djúpalónssandur (Fig. 2.3). The top few metres typically consist of vesicular flow top breccia containing ribbons/intrusions of solid lava up to 1 m wide, similar to the lava intrusions that occur in rubbly topped basaltic a'a lava flows (e.g. Guilbaud, 2006). Below this the lava forms increasingly coherent lobes, amalgamating into substantial lava bodies at lower elevations. Further south across the beach isolated stacks of coherent lava are present. These are commonly thicker than the solid lava that forms the lobes in the cliff and often have some residual flow top breccia preserved on top. Strongly coloured alteration (white, red and yellow) can be seen in some highly fractured areas of the lava, which appears as a thin coating on these fractured rocks.

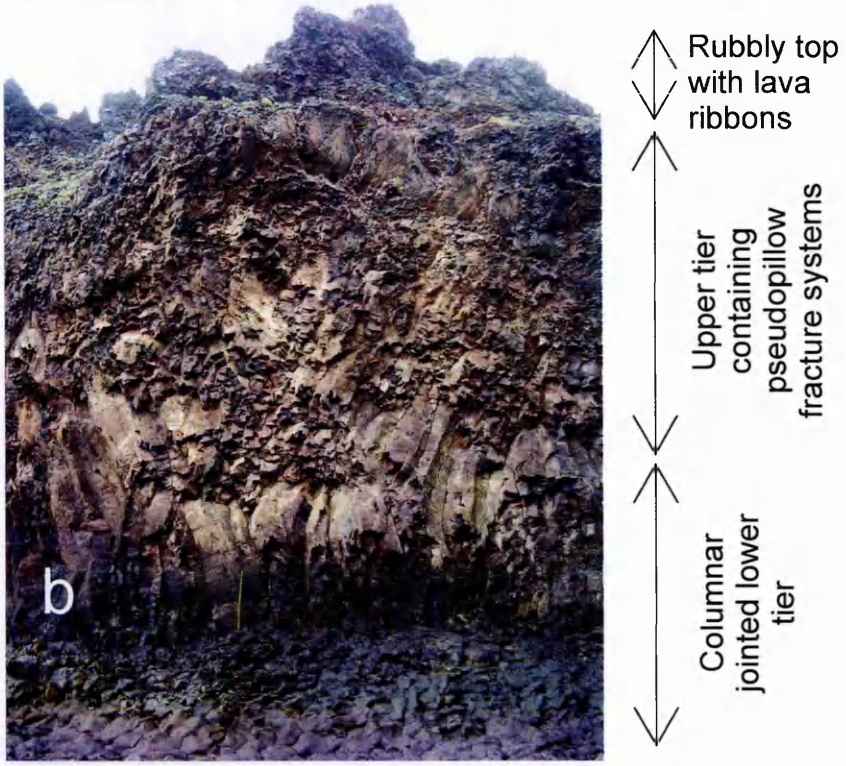

Fig. 2.3 (a) Overview of the western end of Djúpalónssandur looking west. Note colonnade-type columnar jointing on the left in the cliff face and flow top breccia on the right containing small solid ribbons of lava within. Isolated stacks of lava on the beach give excellent exposure of the lava and its fractures. Cliff on right hand side is about 15 m high. (b) Close up of cliff section showing cross-section through lava. The lower tier contains irregular columnar jointing and the upper tier is dominated by pseudopillow fracture systems. This is capped by a rubbly flow top with ribbons of coherent material within the flow top breccia. Cliff section here is about 10 m high, yellow metre rule for scale.

As the Tangahraun lava flowed towards the sea it appears to have increased in thickness and shows fewer individual lobes. The lobes on the present-day shore front seem to have

coalesced to create a large thick solid body of lava, perhaps as a result of the lava entering the sea or coming into contact with sea water, slowing down and backing up, while the flow was inflating.

There are two tiers of fractures in the Tangahraun lava flow. In the upper tier pseudopillow fracture systems can be found in all of the coherent lava at the beach front, from the ribbons of lava surrounded by flow top breccia downwards. They particularly dominate the fractures in the thicker lava seen along the beach between western Dritvík and eastern Djúpalónssandur (Fig. 2.2). The southernmost part of the lava, visible only at low tide, has an erosional surface dipping gently towards the south. The lower tier of fractures, visible at the shore front and on the south side of some stacks of lava, contains subvertical columnar jointing, and subvertical pseudopillow fracture systems that can form one or more of the column-bounding fractures.

2.3 Description of pseudopillow fracture systems at Tangahraun

2.3.1 Master fractures

We have found three distinct types of master fracture that we term F-type, X-type and G-type. They can be distinguished on the basis of their fractography (i.e. the topography of a fracture surface; e.g. Hull, 1999) and their orientation with respect to flow bands in the lava. F-type are parallel to the flow banding (F for flow banding), X-type cross cut the flowbanding (X for cross- or X-cutting) and G-type occur in glassier lava (G for Glassy). The master fracture name also provides the name to the pseudopillow fracture system type as a whole.

2.3.1.1 F-type master fractures

F-type master fractures (Fig. 2.4) form parallel with flow banding in the lava, commonly occurring in parallel sets (Fig. 2.4a). Flow bands are generally planar but occasionally contorted or folded. They are laterally extensive and generally subhorizontal at the shore front steepening up to become steeply dipping (dip direction is south, towards the sea) at the cliff face on the flow front exposure at Djúpalónssandur. They also occur as bulbous 'onion skin' type shapes in the centres of some flow lobes.

F-type are the dominant master fracture type at Tangahraun and may be several metres across. There is frequently a yellow alteration of some flow bands up to approximately 10 cm either side of an F-type master fracture (Fig. 2.1), other flow bands appear not to be affected by this alteration and retain their dark grey colour. Alternating dark grey and yellow stripes up to approximately 1 cm wide commonly appear across the surface of some F-type master fractures.

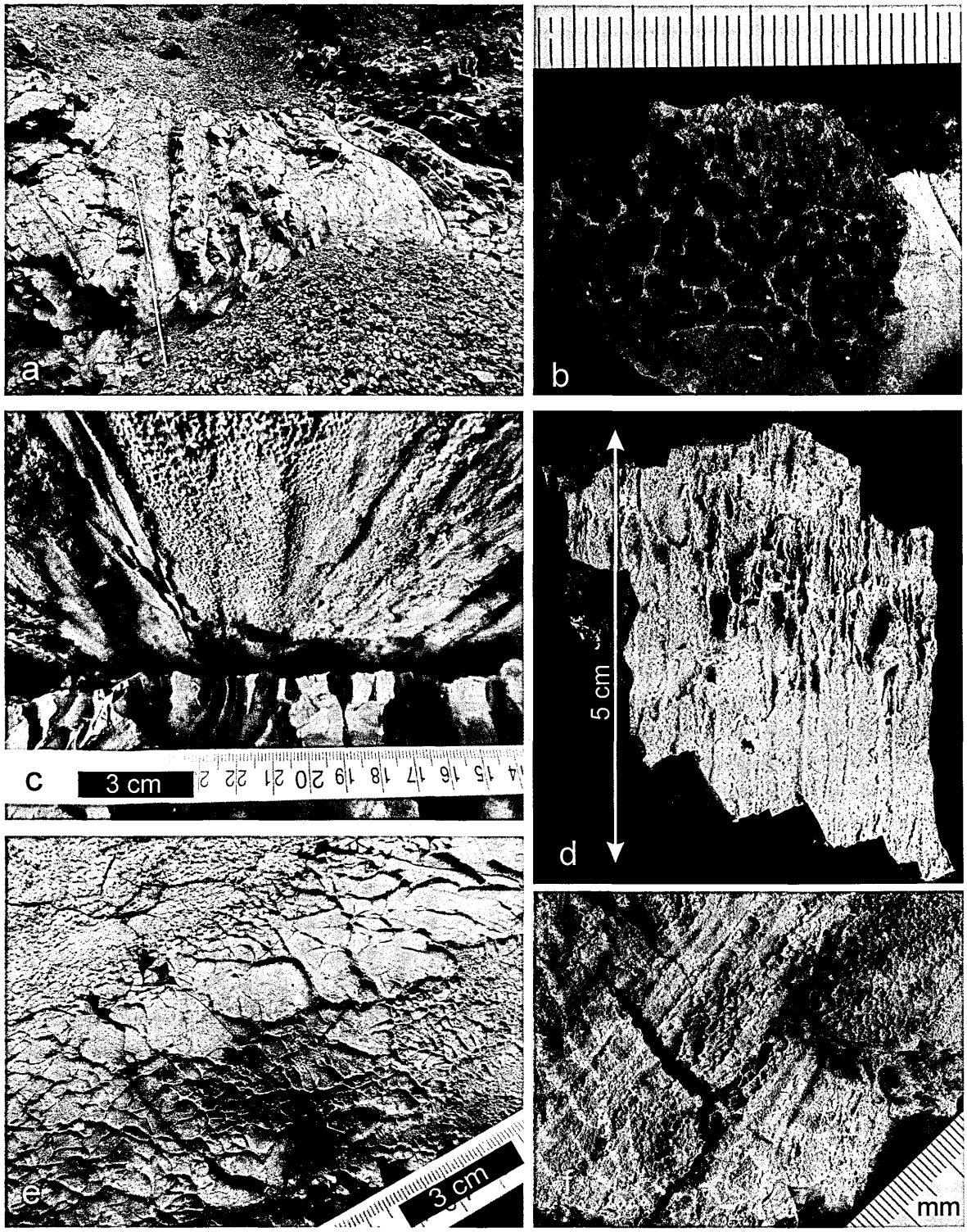

Fig. 2.4 Features of F-type master fractures: (a) Curviplanar set of F-type pseudopillow fracture systems, where each major fracture plane is an F-type master fracture. The master fractures follow the flow banding to produce this pattern. There is some paler alteration on the surface of the master fractures. Ruler on left is one metre long. (b) Close up photo of sub-circular dimpled texture on the surface of an F-type master fracture. The dimples are defined and separated by septa perpendicular to the master fracture surface. Scale is in millimetres. (c) F-type master fracture surface showing striations and lineations on the fracture surface (top), some dimpled texture can still be seen on this fracture surface. Below this the fracture surface of a subsidiary fracture can be seen with curved striae. (d) F-type master fracture where septa form linear ridges rather than sub-circular dimples. The ridges are aligned in the same orientation as the long planar subsidiary fractures. Some cavity-type features exist in the centre of the sample, these are elongate in the direction of the ridged septa. (e) F-type master fracture surface showing predominantly branching networks of septa but also some sub-circular dimples of varying size on the right hand side. Scale divisions are in millimetres. (f) F-type master fracture surface with aligned bands of sub-circular dimples. The septa here are not

perpendicular to the master fracture surface but are angled towards the bottom left hand corner of the image. Scale divisions are in millimetres.

The surface of F-type master fractures has a characteristic delicate dimpled texture (Fig. 2.4b), which is easily eroded in the sea shore environment. The dimples are in the order of a few millimetres in diameter but can have a range of sizes from 10 mm to < 1 mm, both on a single fracture surface and on different F-type master fracture surfaces. They are generally sub-circular and irregular, but occasionally show alignment (Fig. 2.4f). Each dimple is defined by a thin surrounding septum of lava up to a few mm high. Septa between dimples are generally perpendicular to the fracture surface but may be angled to show a preferred orientation (Fig. 2.4f).

A small minority of F-type master fractures do not show uniform dimples but instead have bands or striations, aligned dimples or vein-like patterns of septa across the fracture surface (Fig. 2.4c-e). The striations can occur in the same orientation as the long linear subsidiary fractures or perpendicular to them.

2.3.1.2 X-type master fractures

X-type master fractures (Fig. 2.5) cross-cut flow banding. They are typically sub-vertical and commonly occur between F-type master fractures, generally having a smaller surface area than F-type master fractures, they are up to 2 m across at their widest. Their surface texture is substantially different from the F-type master fractures, showing alternating smooth and rough textures on the same fracture surface and none of the dimples characteristic of F-type master fracture surfaces (Fig. 2.5a-b). The transition between the smooth and rough portions of the fracture is abrupt, and river lines (e.g. Pugh, 1967) can be seen at the junction on the smooth side (Fig. 2.5b). These are a series of steps on the fracture surface, with the same 'sign' or step direction, which commonly merge into one

another, forming larger steps. The surface shows an abrupt smooth-rough transition on one edge of the rough fracture surface area and a much more irregular transition at the other edge (Fig. 2.5a). The sharp transition usually occurs on the upper/higher part of the fracture.

Both F- and X-type fractures occur throughout the body of the lava, from the lava – flow top breccia boundary down to the subvertical columnar jointing at the base of the visible flow. X-type fractures also occur subvertically within the columnar-jointed lower section of the lava (Fig. 2.5c).

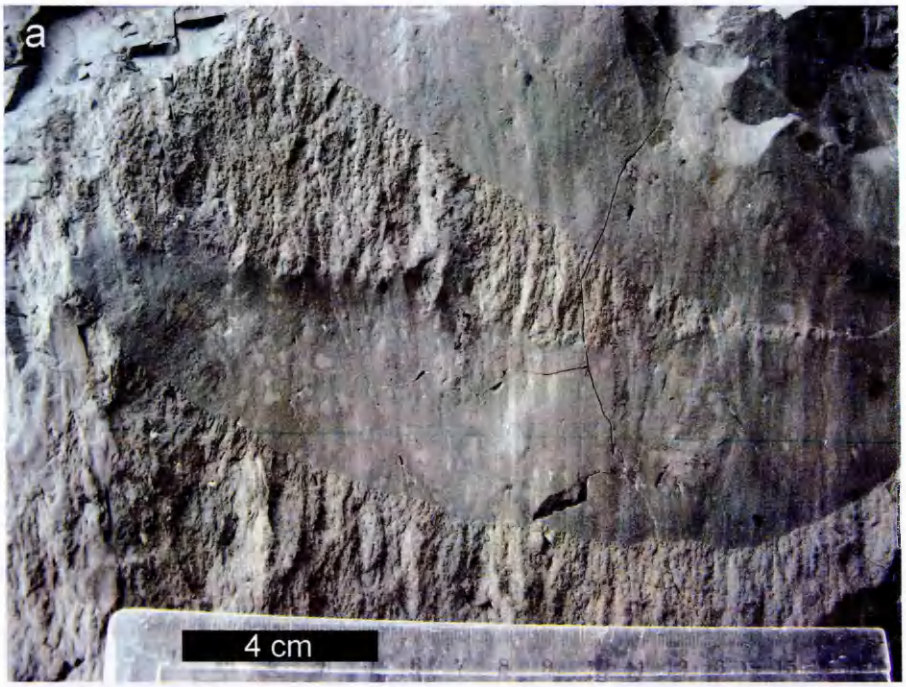

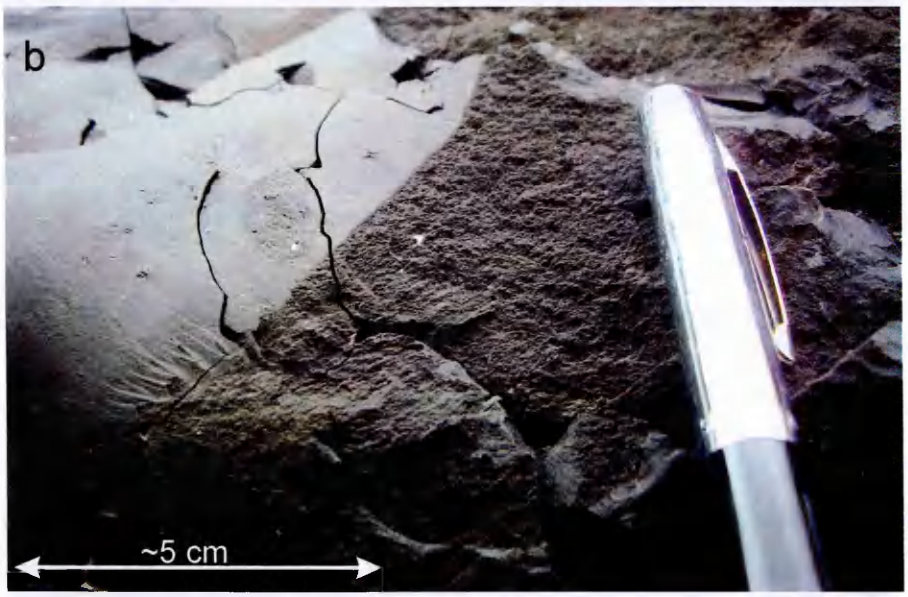

Fig. 2.5 Features of X-type master fractures: (a) X-type master fracture surface showing multiple smooth to rough transitions. From top to bottom of the fracture surface the transition from the smooth surface to the rough is sharp but from rough to smooth is highly irregular. Faint vertical bands across the fracture surface are flow bands. The ruler along the bottom of this image is 18 cm long. (b) Smooth to rough abrupt transition on an X-type master fracture surface. Below and left of centre are river lines on the smooth part of the fracture surface at the interface. They indicate fracture propagation direction towards the bottom right, i.e. from smooth to rough. Pen top for scale 5.4 cm long. (c) X-type pseudopillow fracture systems interacting with columnar jointing which has been pervasively fractured after columnar joint formation. Pseudopillow fractures can be distinguished by the high density of small subsidiary fractures perpendicular to a long master fracture e.g. in the top right and left corners.

2.3.1.3 G-type master fractures

G-type master fractures (Fig. 2.6) generally have a smaller surface area than either X- or F-type, typically being less than 1 m long and 25 cm wide. They can form either parallel to or cross-cutting the flow banding.

The master fracture surface is characterised by striae (Fig. 2.6a), often called chisel marks (e.g. Ryan and Sammis, 1978) spaced 0.5-1 mm apart; hackle (also called plumose structures; Ryan and Sammis, 1978; DeGraff and Aydin, 1987) are present on the surfaces of the striae. The striae are straight and long, sometimes curving slightly at the ends to meet the next stria, and form perpendicular to the long planar subsidiary fractures (see section 2.3.2.1 below).

Unlike F- and X-type master fractures, G-type master fractures do not occur throughout the lava, but are instead confined to horizontally oriented, laterally continuous horizons ≤ 2 m thick (Fig. 2.6b). Horizons containing G-type master fractures are characterised by more intense fracturing and darker, much glassier lava. The G-type master fractures can be in any orientation in these horizons and often form in pairs that define small bulbous or lenticular bodies of lava (Fig. 2.6c).

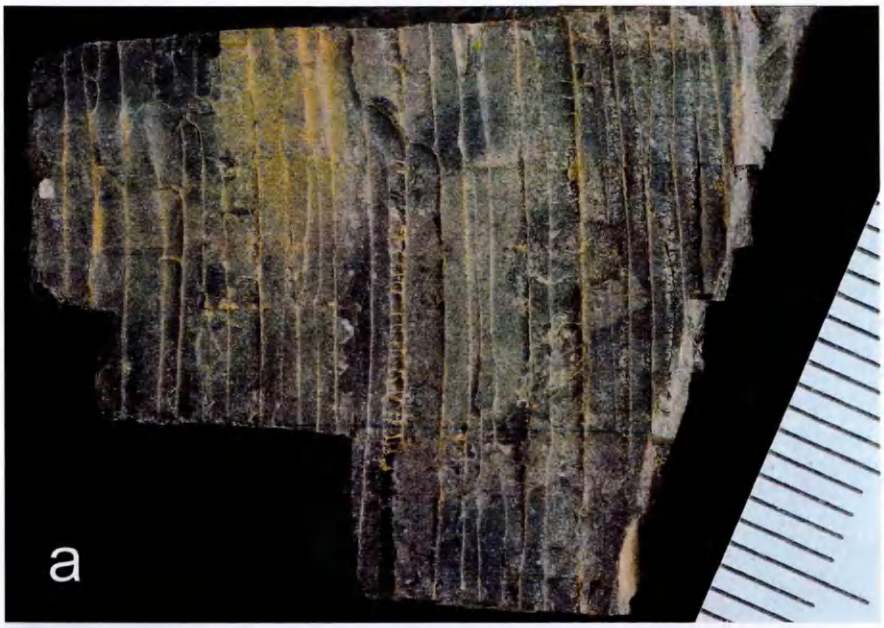

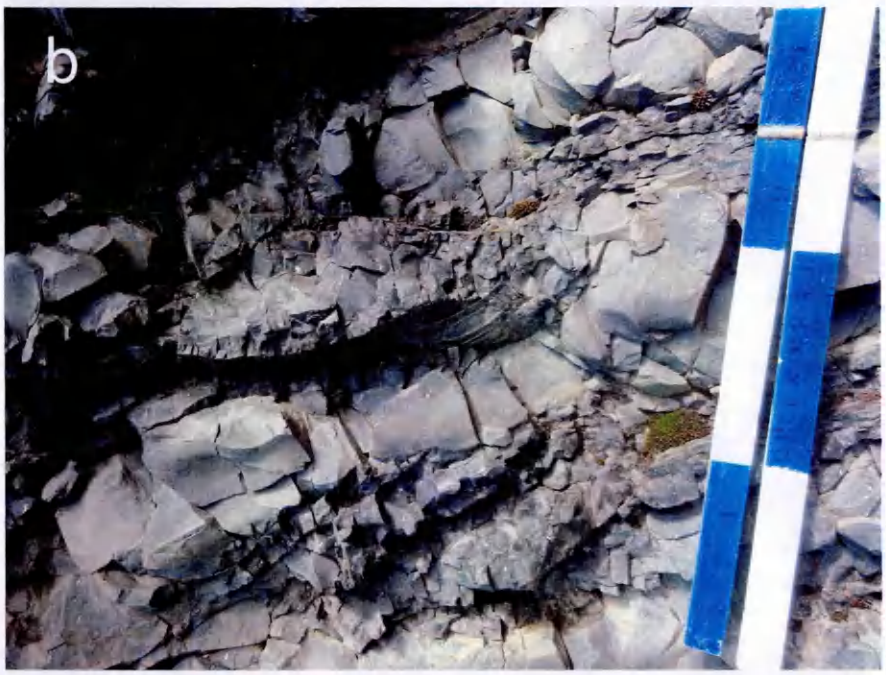

Fig. 2.6 Features of G-type master fractures: (a) Very closely spaced linear striae on a G-type master fracture surface. Hackle are present on some of the striae indicating a propagation direction from right to left. Long planar subsidiary fractures occur in this fracture system and are horizontal across this image, although their outlines are faint. Scale divisions are in millimetres. (b) Close up view of a lenticular body formed by two G-type pseudopillow fracture systems in the centre of the image. Striae on the lower G-type master surface can just be seen. Ruler is 30 cm long. (c) G-type pseudopillow fracture systems forming in a concentrated zone of this type of pseudopillow fracture system. They are subvertical, dipping towards the right in this image, forming elongate, lenticular bodies. Ruler is 0.5 m long.

2.3.2 Subsidiary fractures

Subsidiary fractures in pseudopillow fracture systems in the Tangahraun lava occur in two forms: more commonly in long planar parallel or fanning sets, and secondly as polygonal fracture arrays. The long planar type of subsidiary fractures (long and planar in comparison to polygonal subsidiary fractures) have not been documented previously in pseudopillow fracture systems, only polygonal subsidiary fractures have been previously described (see Table 2.1).

2.3.2.1 Long planar subsidiary fractures

Long planar subsidiary fractures (Fig. 2.7) often occur in parallel or fanning sets, which intersect the master fracture perpendicularly (Fig. 2.7a-b). They are generally spaced 0.5-5 cm apart, and extend up to 15 cm into the lava either side of the master fracture. Many of these subsidiary fractures stop a few centimetres depth into the lava while others extend further, so increasing the spacing of subsidiary fractures further from the master fracture. There can be more than one set of long planar subsidiary fractures fanning across a master fracture, causing intersection of the sets. This type of subsidiary fracture occurs in conjunction with all of X-, F- and G-type master fractures, however they tend to be less well formed in X-type, where they are less continuous and often have jagged edges (Fig. 2.7b). Fanning out of long planar subsidiary fractures is most common in association with F-type master fractures (Fig. 2.7a).

The long planar sets of subsidiary fractures show striae on the fracture surface. These striae differ notably from those on standard columnar joints and G-type master fractures, as they are curved (Fig. 2.7c-d). The striae meet the master fracture perpendicularly at the top of the subsidiary fracture and then curve further into the subsidiary fracture surface to become

almost parallel with the master fracture. Striae on subsidiary fractures are much more closely spaced on G-type master and subsidiary fractures, where they are normally < 1 mm, than on subsidiary fractures in F- and X-type systems where they are generally > 2 mm. The striae on G-type subsidiary fractures are less widely spaced than those on the master fracture surface, which have much more pronounced surface topography (Table 2.3; Fig. 2.7d). Striae are more widely spaced than the alternating dark grey and yellow stripes that occur across F-type master fractures.

Table 2.3 G-type pseudopillow fracture system striae from master and subsidiary fractures (mean values, see appendix 1 for details of number of measurements and error).

Sample	Mean master fracture striae /mm	Mean subsidiary fracture striae /mm
AF214	1.59	0.61
AF215	0.94	0.7

Hackle can sometimes be seen on the striae (Fig. 2.7d) which can give an indication of the propagation direction of the fracture (Ryan and Sammis, 1978 and DeGraff and Aydin, 1987 describe how to interpret hackle for fracture propagation direction). Some curved striae show a smooth to rough transition (Fig. 2.7c). This may be similar to the smooth-rough transition seen on striae in columnar jointing (Ryan and Sammis, 1978).

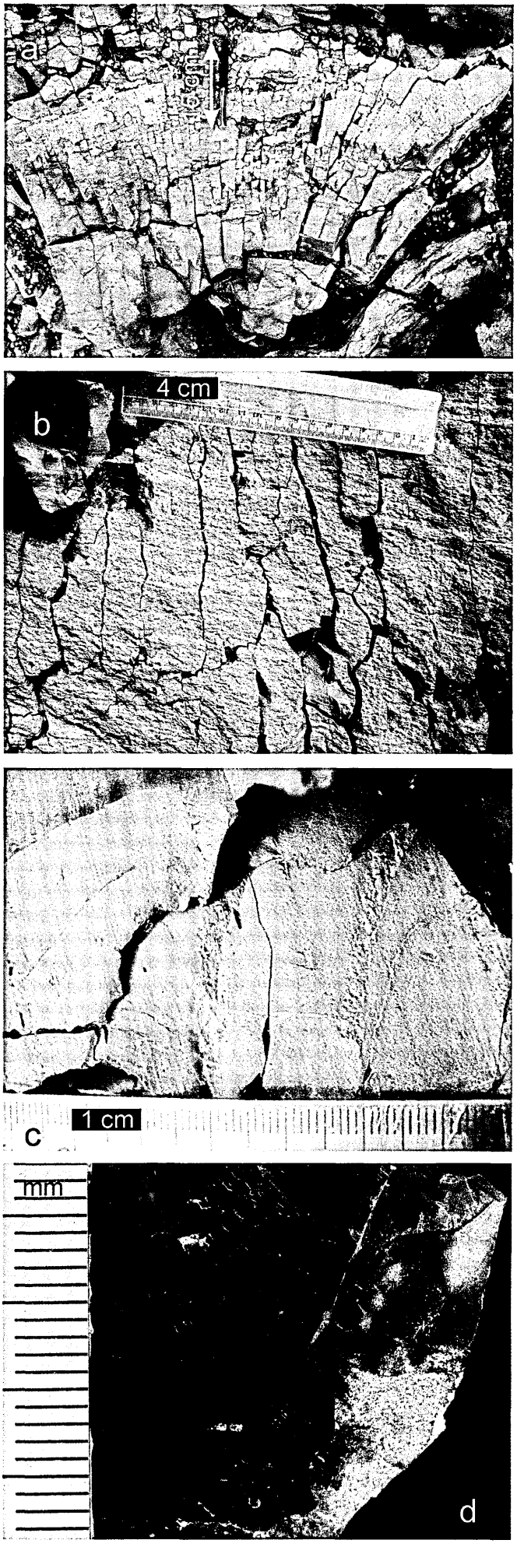

Fig. 2.7 Features of long planar subsidiary fractures (a) Partially-eroded F-type pseudopillow fracture system clearly showing fanning long planar subsidiary fractures. The paler colour is the eroded remains of the master fracture surface. Further down from the master fracture fewer subsidiary fractures extend into the lava and so the spacing of the subsidiary fractures becomes larger. (b) View of an X-type pseudopillow fracture system showing irregular long planar subsidiary fractures. Bands across the master fracture surface are flow bands. Ruler is 18 cm long. (c) Curved striae on a long planar subsidiary fracture from an X-type pseudopillow fracture system. The striae show a smooth to rough transition and are convex pointing towards the left, i.e. propagation direction is to the left. The smooth to rough transition is likely to be a change from brittle to ductile fracture, similar to that seen on striae from columnar joints. Scale divisions are in millimetres. (d) Very closely spaced curved striae on a long planar subsidiary fracture surface from a G-type pseudopillow fracture system. The left hand side of the sample clearly shows the exaggerated topography of the striae on the G-type master fracture surface. Scale divisions are in millimetres.

The fanning outwards direction of long planar subsidiary fracture traces on a master fracture surface always matches with the convex pointing direction of the curved striae on the subsidiary fracture surfaces (i.e. downwards in Fig. 2.7d) where both features can be observed. The abrupt transition from smooth to rough fracture surface on X-type master fractures (i.e. downwards in Fig. 2.5a) also matches with the convex pointing curved stria direction. The curved striae on the subsidiary fracture surfaces generally show convex direction pointing downwards where the fracture is other than horizontal.

2.3.2.2 Polygonal subsidiary fractures

A much smaller proportion of subsidiary fractures are polygonal, generally occurring only in association with X-type master fractures. This is particularly common on the smooth parts of X-type master fractures (Fig. 2.8a-b). The polygons are millimetres to centimetres in diameter, and are fairly irregular, with fractures generally meeting at approximately right angles. Where visible, striae tend to be straight and form parallel to the master fracture. Polygonal subsidiary jointing occasionally develops between long planar subsidiary fractures, so that both subsidiary fracture types are present in one pseudopillow fracture system. Some X-type master fractures do not show any subsidiary fracturing.

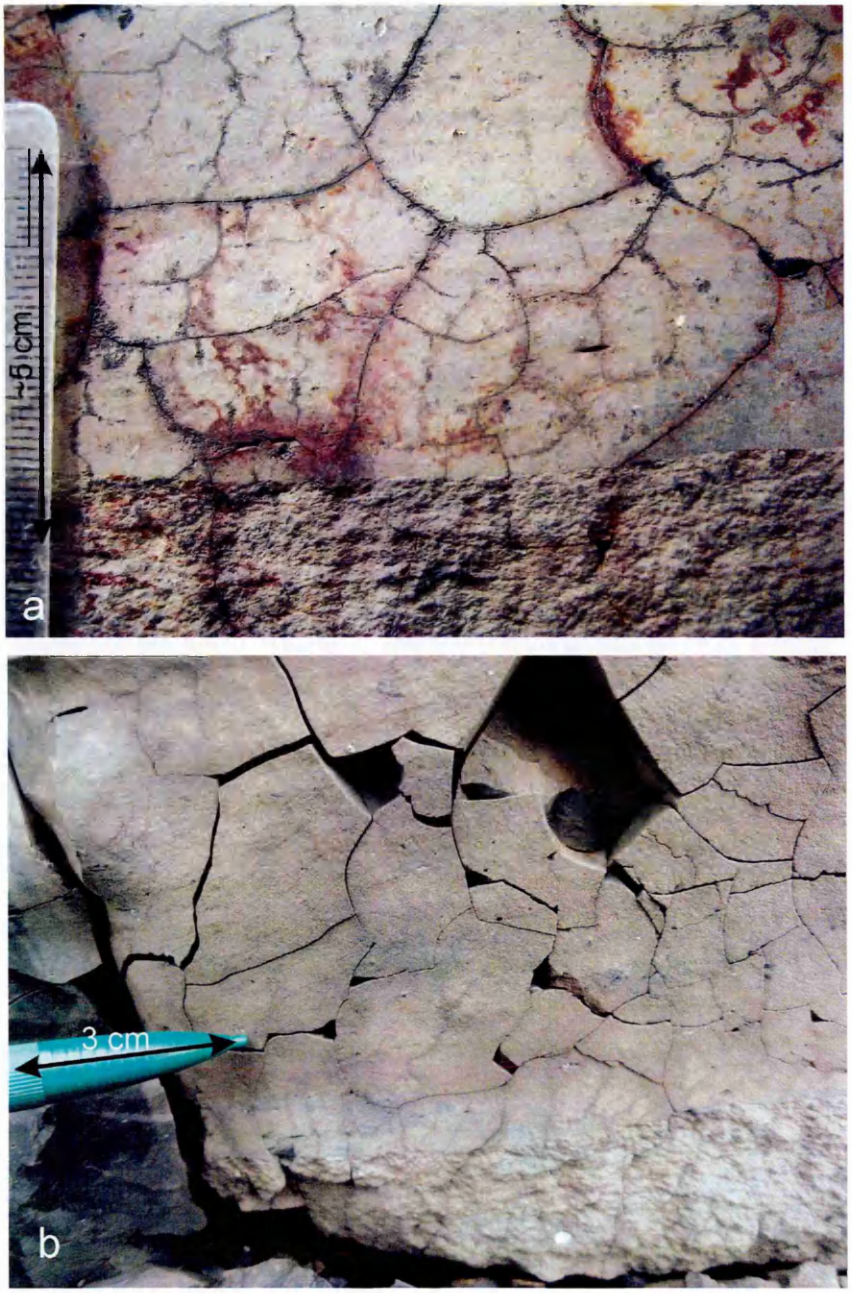

Fig. 2.8 (a) An X-type master fracture showing polygonal subsidiary fractures at the smooth-rough boundary on the master fracture surface. Scale divisions are in millimetres. (b) Well developed polygonal subsidiary fractures in an X-type pseudopillow fracture system at the smooth-rough boundary.

2.3.3 Measurements of long planar subsidiary fractures

Measurements of stria widths on long planar subsidiary fractures and measurements of subsidiary fracture spacing were collected from G-, X- and F-type pseudopillow fracture systems in the field and from photographs (Fig. 2.9). The data were collected using digital callipers in the field for X- and F-type pseudopillow fracture systems and from laboratory

photographs of samples for G-type systems. Precision of the digital callipers was 0.01 mm, however accuracy is more likely to be 0.1 mm, thus with measurement error of a similar magnitude. Striae were measured at the intersection with the master fracture. This data was not collected from G-type pseudopillow fracture systems in the field because the striae widths were too small to measure accurately and individually using callipers. Each data point in the graph is the average of up to 26 striae widths and up to 23 subsidiary fracture spacing widths from a single pseudopillow fracture system (see appendix 1 for data tables and Fig 2.9a for graphical representation).

Figure 2.9a shows a clear positive correlation between subsidiary fracture spacing and striae width. Data from X-type pseudopillow fracture systems tends to plot at larger striae widths and larger subsidiary fracture spacing than the data from F-type systems, although the data overlap. The data from G-type pseudopillow fracture systems plot at the smallest striae widths and subsidiary fracture spacing, but do still appear to correlate with the data from X- and F-types.

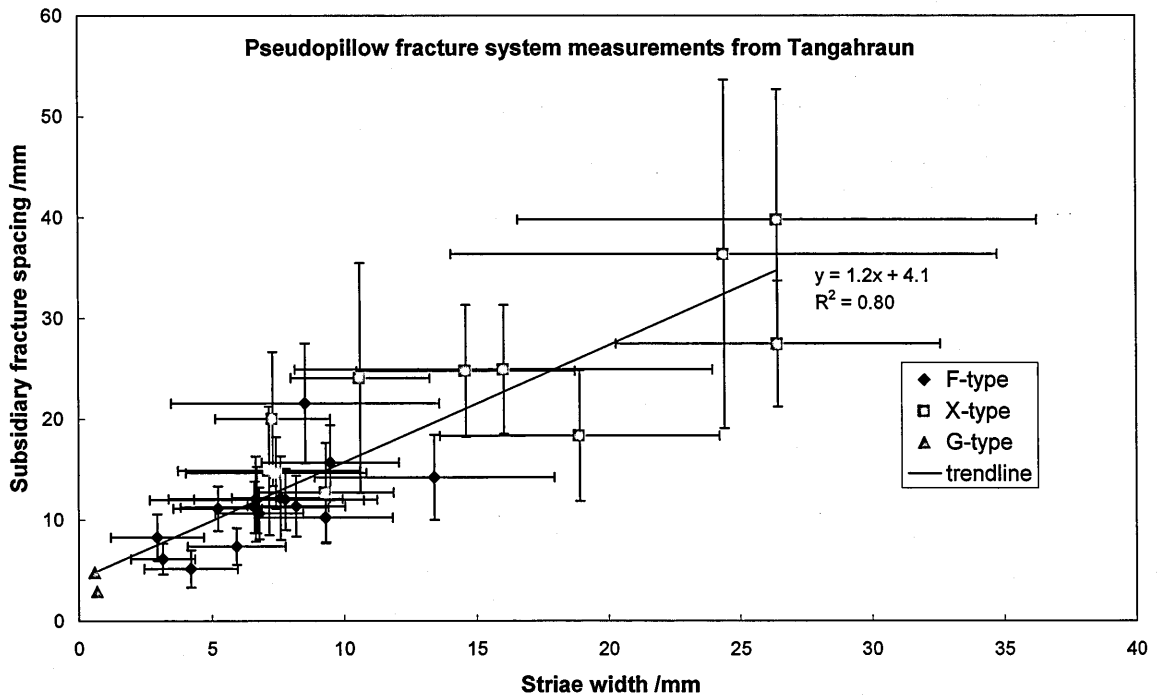

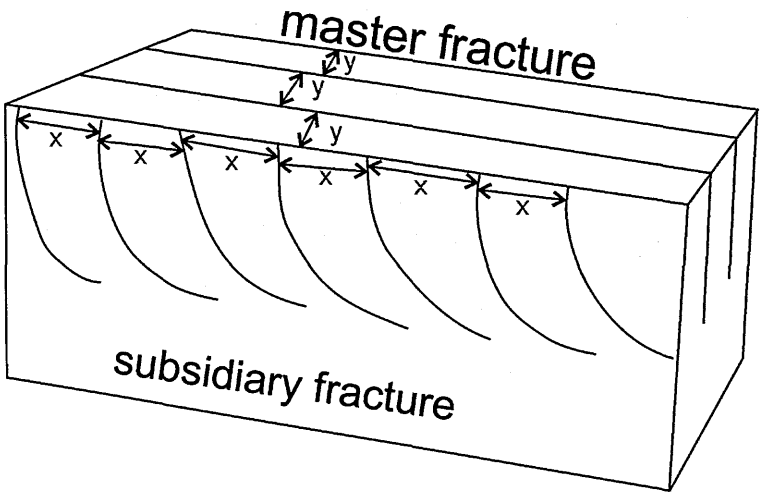

Fig. 2.9 a) Mean subsidiary fracture spacing plotted against mean striae width, differentiated according to the type of pseudopillow fracture system. Linear trend line is fitted to all the data. Error bars are ± 1σ. b) Simplified diagram of a pseudopillow fracture system. Subsidiary fracture spacing is measured on the master fracture surface, the measurements 'y' are averaged together to provide one y-axis measurement for 2.9a. Striae are measured on the subsidiary fracture surface, close to the master/subsidiary fracture junction. The measurements called 'x' are striae measurements and are averaged together (often from more than one subsidiary fracture in the same fracture system) to produce one, corresponding, x-axis measurement in Fig. 2.9a.

2.3.4 Fracture interaction

F- and X-type pseudopillow fracture systems commonly form together, with X-type systems often forming smaller fractures between parallel sets of F-type systems. X-type master fractures may start as F-type subsidiary fractures that then transform into X-type master fractures. When this occurs they show progressively increasing widths of smooth and rough fracture surface from widths characteristic of curved striae on subsidiary fractures to those of X-type master fractures. Larger X-type pseudopillow fracture systems not obviously bounded by F-type pseudopillow fracture systems also occur in the flow. G-type pseudopillow fracture systems occur without interacting extensively with other types of pseudopillow fracture systems or columnar joints.

In the lowest exposed part of the flow subvertical columnar jointing is the prominent type of fracturing. Column-bounding fractures occur with subvertical X-type pseudopillow fracture systems in this lower part of the lava (Fig. 2.5c). They form longer fractures (in the horizontal direction) than any individual column-bounding fracture, so that one X-type

pseudopillow fracture system forms a bounding fracture for several adjacent subvertical columns. In the columnar jointed part of the lava, where flow banding dips gently north / inland, no F-type pseudopillow fracture systems were observed. However they commonly occur above the columnar jointing, and some columns appear to truncate against them. As the columns occur at the most seaward part of the lava they are heavily eroded and striae cannot be seen on the column bounding fractures, so no direction of propagation can be inferred.

2.4 Interpretation of fracture mechanisms

The following contains the interpretation of the fracture mechanisms of all types of master and subsidiary fractures (summarised in Table 2.4), using the surface topography of these fractures. F- and X-type master fractures are discussed first, together with the process of ductile fracture in the lava flow. We then discuss G-type master fractures and subsidiary fractures, which are both brittle fractures displaying striae. Finally, we discuss the characteristics of possible environments within which pseudopillow fracture systems may form.

Table 2.4 Summary of fracture features in pseudopillow fracture systems.

Fracture type	Surface features	Fracture mechanism	Occurs with subsidiary fractures
Master			
F-type	Dimpled or vein textured	Cavitation ductile fracture	Long planar, rarely polygonal
X-type	Smooth & rough, river lines	Brittle to ductile transition	Long planar, polygonal & rarely none
G-type	Closely spaced striae	Brittle incremental fracture	Long planar only
Subsidiary			
Long planar	Curved striae	Brittle incremental fracture	-
Polygonal	Straight striae	Brittle incremental fracture	-

2.4.1 Formation of master fractures

2.4.1.1 Formation of F-type master fractures

The two defining features of F-type master fractures are the dimpled surface texture and their formation along flow bands. This dimpled texture is diagnostic of ductile fracture, seen commonly in metals (e.g. Tvergaard, 1997; Hull, 1999; Bron et al., 2004), and forms through the process of cavitation. During cavitation, ductile materials under tension start to nucleate holes or cavities on heterogeneities. The holes grow and coalesce to form a crack, which advances by nucleation and growth of holes at the crack tip. Bridging filaments (or septa) form between holes and each septum acts as a small tensile specimen, fracturing independently (Hull, 1999). Smaller holes may nucleate in the septa between already formed cavities thus creating a range of hole sizes (Bron et al., 2004). Cavitation is favoured in a plastic (ductile) layer embedded between two non-yielding (rigid) layers (Tvergaard, 1997), indicating that rheological differences between adjacent bands may influence the location of cavitation. It is likely that the position of cavitated bands is controlled by the occurrence of crystal-poor and vesicular flow bands, especially if they are sandwiched between two rigid bands of crystalline material (Tvergaard, 1997). We propose that the ingress of water or steam and rapid cooling effectively freezes the crack in place and stops lava septa entirely relaxing back into the fracture surface once they have broken; essentially the cavitation texture is frozen in by coolant infiltration and quenching to form a glass.

Cavitation in rocks has been described previously from the dacitic Unzen lava dome, Japan (Smith et al., 2001) and in combustion-altered siliceous mudstones (Eichhubl and Aydin, 2003). Smith et al. (2001) report irregular pore space, interpreted as resulting from cavitation (rather than vesiculation), however cavitation did not continue to the extent that

it formed a fracture plane. The authors observe that cavitation occurs in some bands and not others, as in F-type master fractures. Eichhubl and Aydin (2003) inferred that cavitation was not triggered by net extension, but from tensile stresses associated with partial melting reactions. The cavitation exploited previously-formed pores within the original mudstone.

Cavitation only occurs on fractures along flow bands, never across them (X-type master fractures do not show cavitation textures). This could be in part due to some flow bands having a higher concentration of vesicles causing them to be less viscous and so weaker (Bagdassarov and Dingwell, 1994). Weaker more vesicular bands would be more prone to fracture, the vesicles would promote cavitation as the initial holes/cavities are already formed within the flow band. Another possible cause of cavitation on particular flow bands is stress concentrated preferentially along some flow bands or in some areas of the flow. This strain localisation could cause viscous heating (e.g. Hess et al., 2008), and possibly vesiculation, leading to hotter weaker bands, which when sandwiched between more solid layers would increase the likelihood of cavitation (Tvergaard, 1997). Thus ductile fracture could occur preferentially along these bands.

The striations and linear ridges that occasionally form the surface of F-type master fractures (Fig. 4c-e) could form in two ways. These features could be due to shearing of the fracture surfaces past each other after the fracture has already formed. Alternatively they could be caused by mixed mode fracturing, whereby the fracture opens not only in tension (mode I) but also with an element of shearing in the direction of fracture propagation (mode II) or perpendicular to the direction of fracture propagation (mode III) (e.g. Tuffen and Dingwell, 2005; Fig. 2.10). Either of these mechanisms would likely be caused by movement of the flow, however we do not see any large open or gaping master fractures which might indicate large scale flow movement while the fractures were forming. The

striated master fracture surfaces (Fig. 2.4d) are more likely due to shearing while the two surfaces of the fracture are still hot and in contact (e.g. the 'hot slickenlines' of Varga et al., 1998; Cashman et al., 2008). The linear ridges and vein structure (Figs. 2.4c and 2.4e; Hull, 1999) are expected to form by shearing while the ductile fracture is forming, rather than after the fracture has already formed. This provides evidence that some minor mixed mode fracturing occurs, in the case of Fig. 2.4c this is mixed mode I/II fracturing as the ridges align with the subsidiary fractures that indicate the propagation direction. The vein structure does not give a clear indication of the type of mixed mode fracturing, it is generally localised on a fracture surface rather than occurring across the entire fracture. A small amount of mixed mode fracturing could possibly create the alignment of cavitation dimples which sometimes occur on F-type master fractures (Fig. 2.4f).

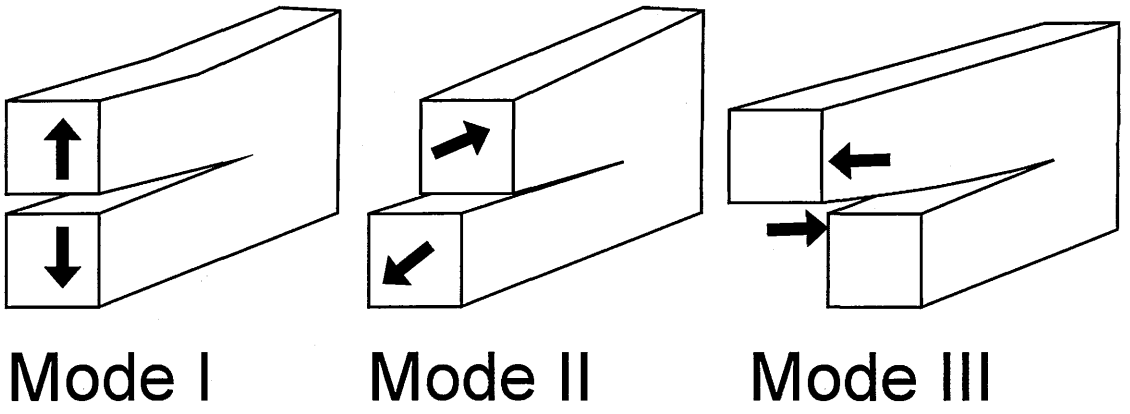

Fig. 2.10 Diagram showing the three modes of fracture. Mode I is opening in tension, mode II shows shear in the direction of fracture opening, and mode III shows shear perpendicular to the fracture propagation direction, in the plane of the fracture.

2.4.1.2 Formation of X-type master fractures

River lines (e.g. Pugh, 1967) at the smooth-rough boundary on X-type master fracture surfaces (Fig. 2.5b) show the propagation direction of the fracture from the smooth surface to the rough surface on the fracture plane. River lines form when brittle fracturing occurs under mixed mode I/III conditions, i.e. tensile opening (mode I) and shear movement perpendicular to the fracture propagation direction in the plane of the fracture (mode III;

Sommer, 1969; Hull, 1993, 1994; see also Fig. 2.10). They consist of a series of steps on the fracture surface aligned in the direction of crack propagation. All the steps are of the same 'sign' or direction of step; they form as a series of closely-spaced steps that merge to form larger steps, hence giving the direction of propagation. They effectively split the fracture plane into many smaller planes to overcome the twisting motion of the fracture.

The increase in surface roughening in the direction of fracture propagation on X-type master fractures could be formed in two ways: mirror, mist and hackle type brittle fracturing or by a change from a brittle to a ductile mode of fracturing. Mirror, mist and hackle is a type of brittle fracture showing an increasing surface roughness as the fracture progresses and accelerates (e.g. Johnson and Holloway, 1966; Hull, 1996, 1999). The features of mirror, mist and hackle fracturing are best observed in glass or glassy materials. Where the fracture initiates a 'mirror-smooth' often reflective region occurs. Beyond this a progressive roughening of the surface produces a 'mist' region, where the fracture surface is no longer smooth and reflective, which then transitions into a hackle region, where pronounced hackle (steps on the surface of the fracture) are clearly visible.

However, the transition from smooth to rough appears much too abrupt for mirror, mist and hackle, and the texture of rough portions of the fracture surface contain no visible hackle. It is considered more likely that the smooth to rough transition represents a transition from brittle to ductile fracturing. This also explains why the river lines do not propagate into the rough part of the fracture surface, because they are a feature of brittle fracture, and do not form in the ductile regime. A similar feature has been observed in striae on basaltic columnar jointing and on curved striae from subsidiary fractures from Tangahraun (Fig. 2.7c) where a propagating brittle fracture 'overshoots' into the ductile regime (Ryan and Sammis, 1978). This creates a characteristic rough texture, like that seen on X-type master fractures, on the surface of the stria fracture although much smaller in

extent in the fracture propagation direction than occurs on X-type master fractures. In X-type master fractures the rough surface texture is most likely an indication of sustained ductile fracturing, as in F-type master fractures. However there is a clear difference between the ductile fracture of X-type master fractures and that in column-bounding fractures. Something has caused sustained ductile fracturing in X-type master fractures and not striae. Two possible mechanisms could cause this: added coolant causing continued rapid contraction, or high stress due to flow in the lava continuing to tear the fracture apart, or more likely a combination of both processes.

2.4.1.3 Ductile fracture and the formation of F- and X-type master fractures

The cause of ductile fracturing in F- and X-type master fractures must involve high strain rates to enable tearing apart of the lava while it is above its glass transition temperature (Dingwell, 1996). The input of additional coolant into the lava is unlikely to be the cause of these high strain rates. High strain rates are more probably caused by flow stresses in the high viscosity lava and strain localisation (e.g. Gonnermann and Manga, 2003; Tuffen and Dingwell, 2005), and flow of the lava across an uneven or unstable base (possibly sand or gravel at the beach, or a basal breccia). High strain rates will be emphasised by the evolution of zones of strain localisation in melt-rich bands, where viscous heating would help to retard cooling and delay crystal growth. Once other zones became crystalline they will begin to "lock up", develop a yield strength and stop accommodating strain, leaving the remaining melt-rich zones with even more strain to accommodate.

However, we are not aware of large ductile fractures such as F- and X-type master fractures having been documented in lavas, so if ductile fractures are generally formed in lavas that experience high strain rates they are not commonly preserved (or observed). If cavitation fracturing occurred in a melt-rich material subjected to a load by overlying lava,

then complete healing is likely without the intervention of an external cooling agent. As the lava is still above its glass transition temperature the fracture is liable to anneal, leaving little evidence that it existed. Fracturing of silicic magma and subsequent annealing has been observed in natural silicic lavas (e.g. Tuffen et al., 2003; Tuffen and Dingwell, 2005), and recreated experimentally (e.g. Yoshimura and Nakamura, 2010). Fracturing of silicic magma under high strain rates at conduit walls may create transient pathways for escape of magmatic fluids (Gonnermann and Manga, 2003). Similarly at Tangahraun, ductile fracturing may have opened transient pathways that allowed the ingress of external water, which then quenched the fracture surface and preserved the delicate ductile cavitation textures. Steam or water that rapidly heats and expands may provide pressure to keep the fracture open, it will also cause cooling contraction necessary to produce the subsidiary fractures.

The ability of lava to maintain high stresses is likely related to its viscosity. Higher viscosity lavas are much more able to maintain stresses as the time it takes for the stress to relax is proportional to viscosity (e.g. Gottsmann et al., 2002). This may explain why pseudopillow fracture systems generally occur in lavas with higher silica content: andesites and dacites, they appear to be much rarer (or less commonly documented) in more mafic lavas. Note that this corresponds to the composition of lavas in which flow banding forms, which is generated through similar processes of strain localisation and ductile-brittle deformation (e.g. Tuffen et al., 2003).

Striations on fracture surfaces occur in the minority of cases of F-type master fractures but not at all on X-type master fractures. Cavitation dimples and smooth-rough fracture surfaces are more common and are exceptionally well preserved away from direct contact with the sea. As explained above, pseudopillow fracture systems are likely to form in a flow environment with high strain rates and strong shear stresses. Yet if this is the case,

shearing on fractures is massively under-represented in the fracture record at Tangahraun. We propose that this is due to movement taking place along fractures while the gap between the fracture surfaces is maintained. The gap between the fracture surfaces could be enhanced or maintained by high pressures as steam or water enters hot lava, rapidly heats and increases pressure. The gap could also be maintained by cooling contraction caused by the steam or water, allowing movement to take place along the fracture without causing grinding along fracture planes so that cavitation and smooth-rough textures are preserved.

We interpret the fractography of both X- and F-type master fractures as being produced by ductile fracture mechanisms, however they clearly show significantly different fracture surface textures. The cavitation in F-type master fractures may exploit or be caused by pre-existing features such as vesicles, concentrated in a particular melt-rich flow band undergoing high strain rates, as is the case for the ductile fracturing documented by Eichhubl and Aydin (2003). In contrast, for a master fracture cross-cutting the flow banding, the concentration of vesicles will be much lower and so cavitation is an unfavourable mechanism of ductile fracture in X-type master fractures.

2.4.1.4 Formation of G-type master fractures

Striae on the fracture surface of G-type master fractures indicate these are brittle fractures that formed incrementally (e.g. Ryan and Sammis, 1978; DeGraff and Aydin, 1987). More information can be extracted from these striae as the width of the striae give an idea of the temperature gradient and so the cooling rate when they formed. A stria initiates when lava cools and contracts sufficiently to overcome its tensile strength and start fracturing. This fracture progresses from cooler to hotter lava until it propagates into lava that is no longer under sufficient tension and is too hot and ductile to fracture, so the fracture stops and

cooling proceeds to rebuild contractional tension. Each cycle of this process creates a single stria on a fracture surface. A temperature is implied in both the initiation and termination of a stria producing cycle, whereby the lava will only start to fracture at a given temperature when it has cooled and contracted sufficiently; the fracture will stop once the lava it is propagating into becomes too hot to sustain brittle fracturing (Ryan and Sammis, 1978; DeGraff and Aydin, 1993; Goehring and Morris, 2008). This indicates that the extremely small striae on G-type master fractures (and their associated long planar subsidiary fractures) represent a large temperature gradient, and so a high cooling rate. The glassier nature of the lava associated with G-type pseudopillow fracture systems also indicates rapid cooling in these fracture systems.

We postulate that G-type master fractures experienced more rapid cooling during fracturing than F- or X-type. This more rapid cooling resulted in very closely spaced striae on both the master and subsidiary fractures and caused the lava to be much glassier. The lava was cooled sufficiently that it was below its brittle-ductile transition temperature as it fractured, resulting in brittle rather than ductile fracture. It is suggested therefore that these types of pseudopillow fracture systems have experienced more coolant (water/steam) in the system and were cooled more rapidly than other types.

2.4.2 Formation of subsidiary fractures

2.4.2.1 Formation of long planar subsidiary fractures

Long planar subsidiary fracture surfaces are characterised by curved striae, indicating brittle incremental fracturing (see above), which record the shape of the advancing crack tip. We are not aware that curved striae have previously been documented from any lava fracture. Hackle can sometimes be seen on the curved striae on long planar subsidiary

fractures, giving a direction of propagation with the convex side of the stria propagating forwards (Fig. 2.7d; Ryan and Sammis, 1978; DeGraff and Aydin, 1987). This indicates fracture propagation perpendicular to the master fracture at the intersection of the two fractures, changing to approximately parallel to the master fracture farther away from the master fracture (see Fig. 2.11).

Our model suggests that the long planar subsidiary fractures form while the master fracture is forming, causing the directionality and curvature in these striae. As a master fracture opens it enables coolant (water and/or steam) access to the hot lava, causing rapid cooling contraction. This triggers the formation of subsidiary fractures while the master fracture continues to propagate/open. Thus cooling at the master/subsidiary fracture interface is happening along the direction of master fracture opening and coolant ingress. However, further away from the master/subsidiary fracture interface this strong directionality is not felt. The master fracture simply acts as a cool outer surface, causing fracture propagation in the subsidiary fracture perpendicularly away from the master fracture; thus setting up a more standard cooling pattern whereby the fracture progresses from the cooler outer to the hotter inner. The striae follow the isotherms in the cooling lava and so can be taken to represent the position of successive isotherms. This preserves evidence of the shape and direction of progression of the isotherms, enabling us to see the complex cooling history that has occurred in this lava preserved in the curved striae.

This model predicts that the opening of master and subsidiary fractures will be in the same direction, one immediately following the other. This directional prediction holds true for X-type and G-type pseudopillow fracture systems. In F-type pseudopillow fracture systems where a master fracture propagation direction is not so easily identified, this model enables prediction of the master fracture propagation direction. Where the master fracture is other than entirely horizontal the curved striae on the subsidiary fracture surfaces almost always

show propagation of subsidiary fractures in a downwards direction. There are few instances where this is not the case, which may be explained by the curviplanar nature of the master fractures. This is interpreted as demonstrating that coolant entered at the top of the lava, which may aid identification of the type of coolant, i.e. it cannot be ground water or surficial snow. The coolant could be sea water, possibly precipitation or ice (i.e. a subglacial lava) causing coolant ingress from the top. However, the postglacial date and coastal position together with the observation that pseudopillow fracture systems only occur at the shore front of the lava flow make ice and rain water very unlikely coolants indeed, leaving sea water as the obvious coolant source.

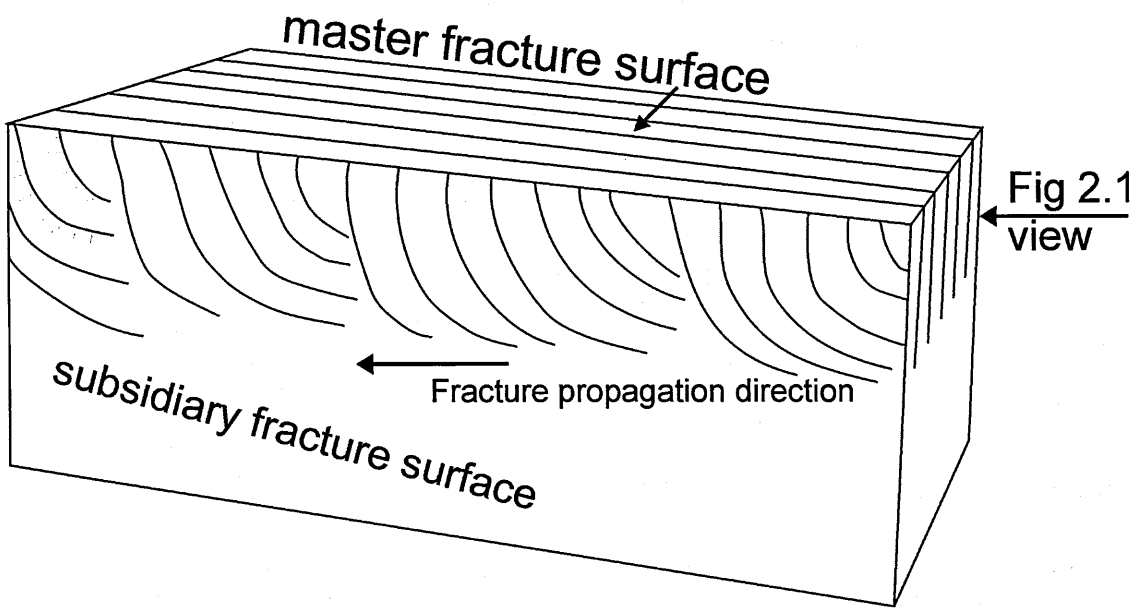

Fig. 2.11 Schematic summary diagram of a pseudopillow fracture system. The view from the right side is equivalent to the view of a pseudopillow fracture system in Fig. 2.1. At the top is the master fracture, the view from on top is equivalent to the views in Fig. 2.7a-b. At the front is the subsidiary fracture showing curved striae and some hackle on the left hand side. The propagation direction is from right to left, and striae reflect isotherms at the time of fracture. This view is equivalent to Fig. 2.7c-d.

2.4.2.2 Striae widths in G-type fracture systems

The master and subsidiary fracture surfaces in G-type pseudopillow fracture systems have differently spaced striae. If the two fractures experienced the same cooling rate conditions while they were forming they would be expected to have the same striae widths. However

the spacing of the striae on the master fracture surface is greater than that on the subsidiary fracture surfaces (see Table 2.3). Two possible explanations for this are: either the two fracture sets (master and subsidiary) formed at different times and so experienced different cooling rates, resulting in different striae widths; or they experienced different stress regimes which influenced the size of the striae on the different fracture surfaces.

The first suggestion implies higher cooling rates (higher temperature gradient) during the formation of the subsidiary fractures causing smaller striae spacing. However, it is probable that the master and subsidiary fractures formed together because of the geometry of the curved striae (see above) and so unlikely that the two fractures experienced different cooling rates. The size disparity of the striae could be caused by a larger strain rate pulling the lava apart to form the master fractures, whereas the subsidiary fractures form purely through cooling contraction fracturing and are associated with lower strain rates. High strain rates are proposed to be the cause of both F-and X-type master fractures and so might also be expected in the formation of G-type master fractures. If high strain rates were present during the opening of G-type master fractures this could cause fracture increments to continue propagating beyond the temperature where fracturing would usually have stopped. Fracturing stops because the lava is too ductile and/or there is not enough tension from the cooling contraction to exceed the material tensile strength and propagate the fracture any further. However the presence of high strain rates can cause fracturing where the lava would otherwise be too ductile to fracture (Dingwell, 1996). This increased fracture propagation distance per increment of fracturing may be the cause of the disparity between striae widths on the master and subsidiary fractures.

2.4.2.3 Long planar vs. polygonal subsidiary fractures

Subsidiary fractures are cooling contraction fractures, which are commonly polygonal in lava e.g. columnar jointing (Aydin and DeGraff, 1988). Contraction joints in other systems such as those caused by desiccation are also commonly polygonal, e.g. starch water mixtures and mud cracks (Müller, 1998a, b; Weinberger, 1999; Toramaru and Matsumoto, 2004; Goehring and Morris, 2005). It is therefore surprising that the dominant form of subsidiary fractures in pseudopillow fracture systems in Tangahraun are long planar parallel fractures rather than polygonal fractures. This strongly indicates that the lava is not under simple biaxial tension, as in the cases of polygonal contraction fracturing, but there is a stress field controlling the orientation and form of the subsidiary fractures.

When long planar and polygonal subsidiary fractures coincide the polygonal fractures are interpreted to have formed after the long planar set, as the polygons are bound by the long planar fractures. This may indicate two phases of cooling. The first phase occurs under high (flow-related) stress conditions when the master fracture and long planar fractures are forming. The second phase follows once this stress has relaxed, allowing normal polygonal cooling contraction to occur. Rarely, straight striae parallel to the master fracture are seen in this flow. These are attributed to polygonal subsidiary fractures, like those observed by Lescinsky and Fink (2000) and Lodge and Lescinsky (2009).

Our study is the first to document the type of long planar subsidiary fracture that is predominant at Tangahraun. All previous studies of pseudopillow fracture systems have instead described polygonal subsidiary fractures (Table 2.2). Either long planar subsidiary fractures were missed in previous studies, perhaps because polygonal fracturing had formed between long planar fracture sets so they were less obvious, or they were not present in the first place. If the latter were true this indicates that the Tangahraun flow was

under a greater amount of (flow-related) stress when the pseudopillow fracture systems formed in the lava. This stress field could not be relaxed by the formation of the master fractures alone, as it persisted while the subsidiary fractures were forming and altered their formation from the preferred polygonal orientation to long planar sets of fractures.

Polygonal subsidiary fracturing only occurs in X-type pseudopillow fracture systems (but may form in F-type when in conjunction with long planar subsidiary fracturing). This may indicate that X-type pseudopillow fracture systems can form under lower (background or flow-related) stress conditions than F-type. Polygonal subsidiary fracturing is particularly prevalent on the smooth parts of X-type master fractures.

Long planar subsidiary fractures present a problem when trying to understand how cooling contraction is accommodated by fracturing. They only release the stress associated with contraction in one direction (the direction perpendicular to the orientation of the long planar subsidiary fracture), whereas polygonal fracturing can release stress in both directions across the plane of the master fracture. It is unclear what happened to this unreleased stress, whether it remains unreleased, is released by another mechanism such as viscous relaxation (which seems unlikely given that the lava is cooling rapidly) or polygonal fracturing between the long planar subsidiary fractures. Perhaps fanning of long planar subsidiary fractures is an attempt to release the stress in the direction parallel with the long planar fractures. As the fractures fan outwards some portion of stress relief can be resolved in this direction.

2.4.2.4 Striae spacing on subsidiary fractures

The data show a positive correlation between striae width and subsidiary fracture spacing (Fig. 2.9). As stria width is controlled by the temperature gradient, and so the cooling rate,

(and possibly strain rate) at the time of formation, it is therefore likely that there is a link between cooling rate and subsidiary fracture spacing. Subsidiary fractures are likely controlled by the viscoelastic response of the lava to cooling. This relationship is comparable with columnar jointing where a strong link exists between stria width and column side width (a proxy for fracture spacing; DeGraff and Aydin, 1993; Grossenbacher and McDuffie, 1995; Goehring and Morris, 2008).

In a viscoelastic material (such as lava) stress accumulation only occurs when the rate of elastic stress accumulation exceeds the temperature- and composition-dependent rate of viscous relaxation (e.g. Dingwell, 1996). If the cooling rate/strain rate is slow enough then viscous relaxation can accommodate the thermal/contractional/flow-related stress accumulation. However, if the cooling rate/strain rate is more rapid then the rate of stress accumulation will exceed the rate of viscous relaxation and stress will accumulate. This accumulation of elastic stress will eventually lead to fracturing (Lore et al., 2000). Thus the faster the cooling rate the more elastic stress will accumulate (as less stress can relax viscously in the time) so requiring more closely spaced fracturing to relieve this build up of stress. This shows a strong link between the cooling rate of a lava and the fracture density, which results in the strong correlation between the striae widths and subsidiary fracture spacing. Scatter in the data may in part be caused by fanning of subsidiary fractures, which changes the subsidiary fracture spacing but does not appear to affect the striae spacing. As data were taken randomly (i.e. where exposure was good enough), the data are likely to include various stages of subsidiary fracture fanning so increasing scatter in the data.

In general X-type pseudopillow fracture systems appear to have experienced less rapid cooling than F-type, as X-type show large striae widths and wider spacing of subsidiary fractures. F-type have experienced less rapid cooling than G-type pseudopillow fracture

systems, which have even smaller striae widths and smaller subsidiary fracture spacing (Fig. 2.9a).

2.4.3 Columnar jointing and the two-tiered flow

The Tangahraun flow can be split into two tiers that show predominantly different styles of fracturing. The upper tier consists of pseudopillow fracture systems that propagate from the top downwards. The lower tier consists mainly of subvertical columnar joints with some subvertical X-type pseudopillow fracture systems. There are no preserved striae on the columns that can be used to obtain a fracture propagation direction from the lower tier. This poor fracture surface preservation is due to these fractures outcropping in an area where the tide regularly washes across and erodes them. The two tier effect, with much more closely-spaced fractures in the upper tier and colonnade-type columnar jointing in the lower tier, broadly resembles a colonnade and entablature type jointing pattern (e.g. Tomkeieff, 1940; Saemundsson, 1970; Long and Wood, 1986; Lyle, 2000).

The columnar joints in the lower tier do not enable the interpretation of a fracture propagation direction, however, by analogy with other documented occurrences it is reasonable to assume that these fractures propagated from the base of the flow upwards. The style of jointing is unlikely to change abruptly from dominantly pseudopillow fracture systems to columns in the same tier, as the formation of pseudopillow fracture systems appears to require a highly non-uniform stress field with high strain rates in places, whereas the formation of columnar joints requires a much simpler, uniform biaxial stress field. The columns are fairly large, with column side width of approximately 25 cm, comparable in size to other lower colonnade columns measured by Goehring and Morris (2008) in basalts, indicating that they have not been much influenced by additional coolant

that would act to make the columns smaller (by increasing the cooling rate; DeGraff and Aydin, 1993; Grossenbacher and McDuffie, 1995).

The X-type pseudopillow fracture systems that form in conjunction with the columnar joints are more perplexing. Again, there are no well-preserved fracture surfaces so direct measurement of the propagation direction is not possible. However, assuming that columns and pseudopillow fracture systems require significantly different stress fields in which to form, it is unlikely that they formed at the same time, in the lower tier of the flow. From field evidence showing long pseudopillow fracture systems with many individual columns forming along them we therefore suggest that the X-type pseudopillow fracture systems formed first. This is the expected order of fracture formation as pseudopillow fracture systems form at higher temperatures (as seen by the evidence of extensive ductile fracturing). They likely propagated from the top tier of the flow downwards, as there is little evidence of the coolant that appears necessary to form them (or at least preserve pseudopillow fracture systems) coming from the base.

2.4.4 Environmental implications of pseudopillow fracture systems

Anecdotally there appears to be a strong connection between the environment and the presence of pseudopillow fracture systems in a lava flow. They have only been documented in environments where additional coolant (ice, snow, water) has been observed or inferred (Table 2.1), but have never been reported from subaerial lava flows. There is evidence from the fractures in this study that supports this connection, such as glass associated with the fractures, the exceptionally small striae widths on both subsidiary and G-type master fracture surfaces, the preservation of cavitation fracture surfaces, and the curving of striae on long planar subsidiary fractures.

Striae on subsidiary fractures and G-type master fractures are very closely spaced (≤ 30 mm, in some cases < 1 mm), leading to the conclusion that this lava experienced high temperature gradients while the fractures were forming, i.e. high cooling rates. The temperatures of fracture initiation and termination that create striae are not known, though some authors have made estimates (e.g. Goehring and Morris, 2008). However a comparison with striae in other environments and lavas does give a relative indication of cooling rates. Goehring and Morris (2008) measured striae widths in subaerial columnar jointed basalts of the Columbia River Basalt. Widths range from 41-358 mm, clearly much larger than those found in the Tangahraun lava flow (<1-30 mm). The striae at Tangahraun are of a similar size to striae measured from columns in subglacially erupted rhyolite lavas, which range from 1-32 mm (see Chapter 3). Despite the unknown effect of composition on striae widths it is clear that the striae on subsidiary fractures and G-type master fractures record significantly higher cooling rates than the columns of Goehring and Morris (2008) and others. This idea of rapid cooling is further supported by the glassy nature of much of the lava, particularly around the G-type pseudopillow fracture systems.

Lodge and Lescinsky (2009) proposed that the occurrence of pseudopillow fracture systems in a lava indicates the presence of water surrounding the lava as it cools, essentially a subaqueous lava or part of the lava. While this seems likely when considering the lavas described by Tucker and Scott (2009) and Watanabe and Katsui (1976), both of which flowed into lakes, it appears not to be possible for the case described by Mee et al. (2006), where pseudopillow fracture systems occur above the level of the snow that produced the pseudopillow fracture systems in the lava they describe. It is also unlikely that water is the cause of pseudopillow fracture systems in lavas that interact with thin alpine glaciers on stratovolcanoes (e.g. Lescinsky and Fink, 2000) as melt water can rapidly drain through these relatively thin alpine glaciers and is unlikely to pond (Smellie,

2000). This strongly suggests that in general steam is the main coolant causing the formation of pseudopillow fracture systems in lava, rather than water.

This may not be the case for G-type pseudopillow fracture systems however. These are highly glassy and show evidence of extremely rapid cooling, substantially more rapid than other types of pseudopillow fracture systems in terms of striae widths on subsidiary fractures. This may be due to water, rather than steam infiltrating the lava, causing more rapid cooling in the limited areas where G-type pseudopillow fractures occur (as water is far more effective at removing heat than steam, due to its vastly higher density and the latent heat of vaporisation).

Pseudopillow fracture systems therefore appear to be a useful environmental indicator as they are the products of enhanced cooling and as such require the addition of coolant sourced from a range of possible environments containing ice, snow or water. However, simply demonstrating the presence of pseudopillow fracture systems in a lava cannot define the specific environment. Other evidence must be used, for example: the location of the lava (caldera lake, stratovolcano, coast etc.), confinement (if any), direction of propagation of the pseudopillow fracture systems (i.e. where did the coolant come from), presence of glassy lava, occurrence of other fracture types (e.g. columnar jointing, hackly jointing etc.) and their direction of propagation.

2.5 Fracture synthesis

Columnar jointing started forming from the base up, possibly above a zone of more closely space fractures where lava interacted with the wet seabed or beach. Meanwhile water and/or steam were infiltrating the main body of lava from the top, causing pseudopillow fracture systems to form in the lava, propagating from the top downwards. The cooling

from the top downwards being enhanced by water and steam almost certainly occurred more rapidly than the cooling from the base upwards, probably leading to the upper tier of the flow being thicker than the lower one. X-type pseudopillow fracture systems propagated down into the lower tier where columnar joints are the dominant fracture type. Columnar fractures forming from the base upwards often have one or more sides formed from a long X-type pseudopillow fracture system, and commonly truncate against horizontal F-type pseudopillow fracture systems above, at the interface of the two tiers.

Expansion fractures would be unlikely to form many metres deep, confined inside a flow, which is how pseudopillow fracture systems occur in the Tangahraun lava flow, suggesting that pseudopillow fracture systems do not occur as a result of expansion fracturing. We therefore suggest that F- and X-type master fractures form as a result of high stain rate fracturing of hot, ductile material and the fractures are preserved by the introduction of coolant and contraction related to rapid cooling, rather than forming as expansion fractures. Indeed, the brittle G-type master fractures, having striae on their master fracture surface, show classic evidence of cooling contraction fracturing. Some instability of the flow may result from the lava advancing across a beach where the ground is unconsolidated (i.e. pebbles as the beach is now, or possibly sand or basal breccia), this combined with flow of a viscous lava may result in high enough strain rates to produce the ductile fracturing observed.

Curved striae on subsidiary fractures demonstrate that the pseudopillow fracture systems in Tangahraun propagated from the top of the flow downwards. The source of coolant to form these fractures was from the top of the flow. Having eliminated ice and precipitation as possible coolant sources (see section 2.4.2.1. Formation of long planar subsidiary fractures above) we conclude that sea water is the likely coolant source. The exact age of this lava is unknown so relative sea level at its time of emplacement is not known. The history of sea

level in west Iceland through the Holocene has been complicated (e.g. Lloyd et al., 2009; Norðdahl and Pétursson, 2005). More than 2 ka relative sea level was probably a metre or so higher than today, a few thousand years before that if may have been on the order of tens of metres higher still (Lloyd et al., 2009). Higher relative sea level would obviously aid ingress of water into the top of the lava flow. However, if sea level were more similar to modern levels, it is more difficult to explain how the water infiltrated the top of the lava to form pseudopillow fracture systems.

One explanation may be that inflation of the flow provided an originally lower flow top that aided ingress of seawater. Inflation of a rubbly topped a'a flow has been described from Sierra Negra volcano in the Galapagos (Geist et al., 2008). The change from multiple lobes to a single thick flow which appears to be occurring at the flow front (see section 2 Geological setting) would likely occur by inflation of the flow front. However, we did not observe any evidence for the interaction of inflation and chilling / fracturing, but if this occurred then it may have happened in parts of the flow that have now been eroded further out to sea.

Current sea level is approximately 10-15 m below the top of the lava. It is possible that a storm and/or high tide could have provided water to the top of the flow. For example the storm that hit Iceland in January 1990 had a significant wave height (the mean wave height from trough to peak of the highest third of waves) of 16.8 m and a surge level about 80 cm higher than the estimated tidal level (Tomasson et al., 1997), this would have been more than sufficient to emplace significant amounts of water to the top of the lava flow. Perhaps a combination of the some or all of the above hypotheses might provide the best explanation of coolant ingress into the top of the lava flow.

2.6 Summary

This study has revealed a number of features of pseudopillow fracture systems in lavas for the first time, which are summarised below. Three different types of pseudopillow fracture systems have been recognised on the basis of master fracture fractography and orientation in relation to flow banding. F-type master fractures form parallel to the flow banding and have sub-circular dimples on their fracture surfaces; X-type master fractures cross-cut the flow banding and show smooth to rough transitions on their fracture surfaces; G-type master fractures have narrowly spaced straight striae across their master fracture surfaces and may be either flow banding parallel or cross-cutting.

Long planar subsidiary fractures have been identified in the Tangahraun flow, they are the dominant subsidiary fracture type and have curved striae on their fracture surfaces. Long planar subsidiary fractures can also occur in conjunction with polygonal subsidiary fracturing, particularly on X-type pseudopillow fracture systems. There is a clear correlation between long planar subsidiary fracture spacing and striae width. Both are larger on average in X-type than in F-type pseudopillow fracture systems, and G-type pseudopillow fracture systems have smaller striae widths and subsidiary fracture spacing than in either X- or F-type.

These new discoveries have led to enhanced understanding of pseudopillow fracture systems through interpretation of these findings and new data summarised below. Extensive ductile fracturing occurs in F- and X-type master fractures, in the case of F-type this ductile fracturing occurs by cavitation. Entirely brittle fracturing occurs in almost all subsidiary and G-type master fractures. Curved striae on subsidiary fracture surfaces indicate that subsidiary fractures formed as the master fracture was opening, giving a strong directionality to the isotherms in the lava either side of the master fracture. The

directionality associated with curved striae allows an interpretation of propagation direction of the whole pseudopillow fracture system. The cooling rate appears to be the major control on subsidiary fracture spacing as it correlates well with striae width, known to be dependent on temperature gradient and so cooling rate.

Rapid localised cooling occurs in conjunction with the opening and development of pseudopillow fracture systems, as indicated by often large amounts of glassy lava and very small striae widths. The high cooling rates in the Tangahraun lava are interpreted to be caused by ingress of large volumes of sea water while the lava was still very hot. This also enabled preservation of ductile fractures and formation of pseudopillow fracture systems and provides unique insights into the coupling between external water ingress and fracture propagation in a lava flow.

2.7 Highlights

- Three types of pseudopillow fracture system have been recognised based on their master fracture orientation and fractography: F-type, X-type and G-type.
- F- and X-type master fractures are partly or entirely ductile.
- G-type master fractures are brittle.
- Two types of subsidiary fractures have been recognised: polygonal and parallel arrays, both are brittle fractures.
- Fracture propagation can be deduced from striae or smooth-rough fracture surface transitions.
- Preservation of ductile fractures likely results from rapid cooling and freezing of the lava.

Chapter 3: Columnar jointing in subglacial rhyolite lavas

3.1 Introduction

Columnar jointing in felsic lavas is particularly associated with glacial environments and has been used as an indicator of lava-ice interaction (e.g. Lescinsky and Sisson, 1998; Lescinsky and Fink, 2000; Tuffen et al., 2001; Tuffen et al., 2002a; Stevenson et al., 2006). Columnar jointing may also form in lava-wet sediment subaqueous environments (e.g. Goto and McPhie, 1998; DeRita et al., 2001; Stewart and McPhie, 2003) and occurs rarely in purely subaqueous or subaerial settings (e.g. Fink, 1983; Scutter et al., 1998; DeRita et al., 2001; Gottsmann and Dingwell, 2001). Columns only appear to occur subaerially in very thick (up to 250 m!) rhyolite flows (Bonnichsen and Kauffman, 1987; Henry et al., 1990; Allen and McPhie, 2002). Columnar jointing develops normal to the cooling surfaces (DeGraff et al., 1989) and so may be used to identify the orientation of past lava-ice contact surfaces (Lescinsky and Sisson, 1998; Tuffen et al., 2001; Tuffen et al., 2002a).

Columnar jointing forms due to the cooling and contraction of lava. Fractures initiate in response to this contraction at the cooling surfaces of a body, with 'T' shaped junctions between fractures (Aydin and DeGraff, 1988). A fracture, once initiated, will stop propagating once the material it propagates into becomes too hot and ductile to fracture, and/or there is not enough contractional stress in the lava to continue fracture opening. Continued cooling deeper into the body will result in further contraction and fracturing. This incremental process of fracture initiation and termination will repeat continuously into the cooling lava body, perpendicularly away from the cooling face. As this process continues the right-angled 'T' junctions between fractures tend to form into 'Y' shaped

junctions (Aydin and DeGraff, 1988), with an ideal angle of 120° giving hexagonal rather than quadrilateral column shapes.

Each increment of fracture leaves behind a small topographical irregularity on the surface of the fracture, caused by plastic deformation and blunting of the crack tip during the pause between fracture events (Ryan and Sammis, 1978; DeGraff and Aydin, 1993). These form bands perpendicular to the column axis, called striae. The widths of striae, *S* (Fig. 3.1), represents a temperature gradient and so a cooling rate, as the fracture starts at one temperature and terminates at a higher temperature a certain measurable distance away. This process of brittle fracture may also leave hackle, or plumose structures, on the fracture surface that enable the direction of fracture propagation to be determined (Ryan and Sammis, 1978; DeGraff and Aydin, 1987).

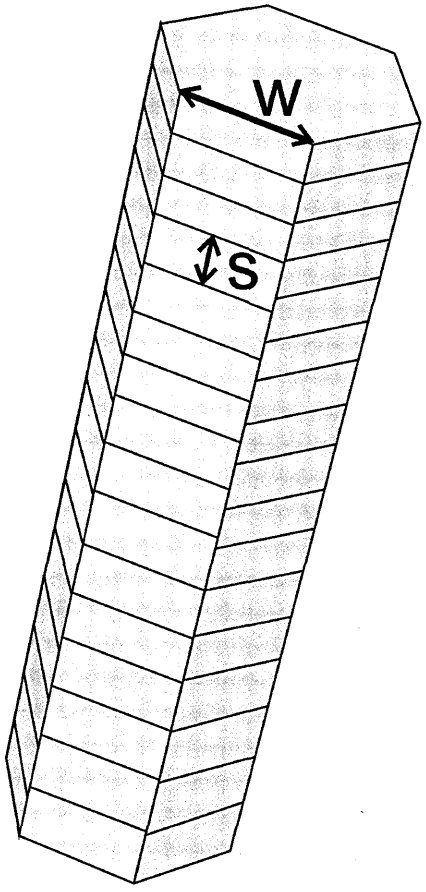

Fig. 3.1 Diagram of a column, with striae on its column bounding fractures, showing both *W* and *S*. This column has 6 sides.

Cooling rate controls the striae widths and it likewise controls the size of columns, usually measured as column side width, *W* (Fig. 3.1). In a viscoelastic material stress accumulation caused by cooling contraction is countered by viscous relaxation, this accumulation of elastic stress will eventually lead to fracturing (Lore et al., 2000). The more rapid the cooling rate the less stress can relax viscously, resulting in a build up of more stress, thus requiring more

fractures to release this stress. A denser array of fractures will lead to smaller columns and so smaller column side width, *W*.

Columnar jointing studies in rocks focus almost exclusively on basalt lava flows. Columnar jointing occurs in other materials including sandstone and coal due to thermal metamorphism (Spry and Solomon, 1964; Crelling and Dutcher, 1968; Young, 2008), in welded ignimbrites (e.g. Wright et al., 2011) and has been studied extensively in dried starch-water mixtures (Müller, 1998a, b; Toramaru and Matsumoto, 2004; Goehring et al., 2006). Much of our understanding of how columns form comes from studies of basalts and extensive measurements of column side width, striae height, and number of columns sides have been collected (Ryan and Sammis, 1978; DeGraff and Aydin, 1993; Grossenbacher and McDuffie, 1995; Goehring and Morris, 2008; Hetényi et al., 2012). Very little of this data has been collected from non-basaltic columns, and nothing more felsic than ~60 wt% SiO_2 (Hetényi et al., 2012).

These studies show that in basalt columnar jointing the ratio *W/S* has a range ~5-20, with a mean of approximately 7, i.e. column side width tends to be about 7 times larger than striae height (DeGraff and Aydin, 1993; Grossenbacher and McDuffie, 1995; Goehring and Morris, 2008). Basaltic columns tend to have 6 sides, although may occasionally show a preference for 5 sided columns (Beard, 1959; Goehring and Morris, 2008; Hetényi et al., 2012).

Columns in more felsic lavas have been previously observed to be slightly larger than those in basalt, perhaps due to a lower eruption temperature or due to the geometry of the flow, with more viscous lavas forming thicker, slower cooling flows, resulting in larger columns (Hetényi et al., 2012). However, this has only been observed in lavas up to ~60 wt% SiO_2 and this data does not include striae measurements (Hetényi et al., 2012).

There are no equivalent measurements of column side width, striae height, and number of column sides of rhyolite lavas in existence. One of the aims of this study is to compare previous basalt columnar jointing measurements with those of rhyolite columns, but the main focus of this study is to understand more about the environment of emplacement of rhyolitic lavas by using columnar jointing measurements. As the columnar jointing in this study comes from ice-interaction rhyolitic lavas, rather than subaerial basalts as in previous studies, some differences are expected. Whether these differences are due to lava composition or environment of eruption is critical to understanding more about columnar jointing and the environments of the rhyolite lavas in this study.

Five separate lava bodies were studied in order to understand columnar jointing processes in subglacial rhyolites. One of these lavas has been extensively studied in the past: Bláhnúkur, which was formed by a subglacial effusive rhyolite eruption, part of the Torfajökull central volcano (e.g. Furnes et al., 1980; Tuffen et al., 2001; Tuffen et al., 2002b; Owen et al., 2012). In contrast, columnar jointed rhyolite lavas in Hvalvörðugil valley on Goðafjall mountain, Öræfajökull, and an un-named flow in northern Rauðufossafjöll, also part of the Torfajökull central volcano, are little studied previously and will be described in some detail in this chapter, so that their columnar jointing can be understood in the context of their environment and the other fractures present in these flows.

3.2 Geological setting and flow descriptions

3.2.1 Bláhnúkur, Torfajökull

Much is known about this lava and its eruptive environment, so it is an ideal lava to study to understand the formation and environmental significance of columnar jointing in subglacial rhyolitic lavas. It is a ≥ 50 m thick deposit of fine grained fragmentary volcaniclastic material and protruding jointed lava lobes, blanketing an older rhyolitic hill (Tuffen et al., 2001; Fig. 3.2). It was probably emplaced some time in the last glacial period, 115-11 ka (Tuffen et al., 2001). The environment in which this deposit formed can be deduced from various forms of physical evidence for ice including perlitised obsidian, blocky ash shards, paleotopography/geography, columnar jointing patterns, and the ubiquitous presence of till (Tuffen et al., 2001). Fourier transform infrared (FTIR) analyses show elevated water concentrations in rhyolitic glass that indicate that the subglacial Bláhnúkur deposit was emplaced under ~400 m of ice (Owen et al., 2012). The lobes are generally polygonally jointed with joint axes perpendicular to the lobe sides. The lobes may have been intruded into ice, cavities within the glacier base or into wet tephra from an initial phreatomagmatic phase of the eruption, causing peperitic lobe margins (Tuffen et al., 2001; Owen et al., 2012).

Fig. 3.2 Overview of Bláhnúkur deposit morphologies on the western side looking east, view across to the far skyline is approx. 500m. This is a subglacial rhyolite, showing polygonally jointed lava lobes protruding from fragmental hyaloclastite.

Columnar jointing measurements were taken from two different lobes from this subglacial eruption (Fig. 3.3): one a lobe at the base of the mountain in the Grænagil valley (Fig. 3.4), the other at the very top of the mountain (Fig. 3.5). The many other lava lobes on Bláhnúkur that display polygonal-type jointing were deemed unsuitable for studies of rhyolite columnar jointing due to the abundant presence of other fracture types (Fig. 3.6), such as sheet-like fractures (Lodge and Lescinsky, 2009) and pseudopillow fracture systems (Watanabe and Katsui, 1976; Mee et al., 2006; Forbes et al., 2012).

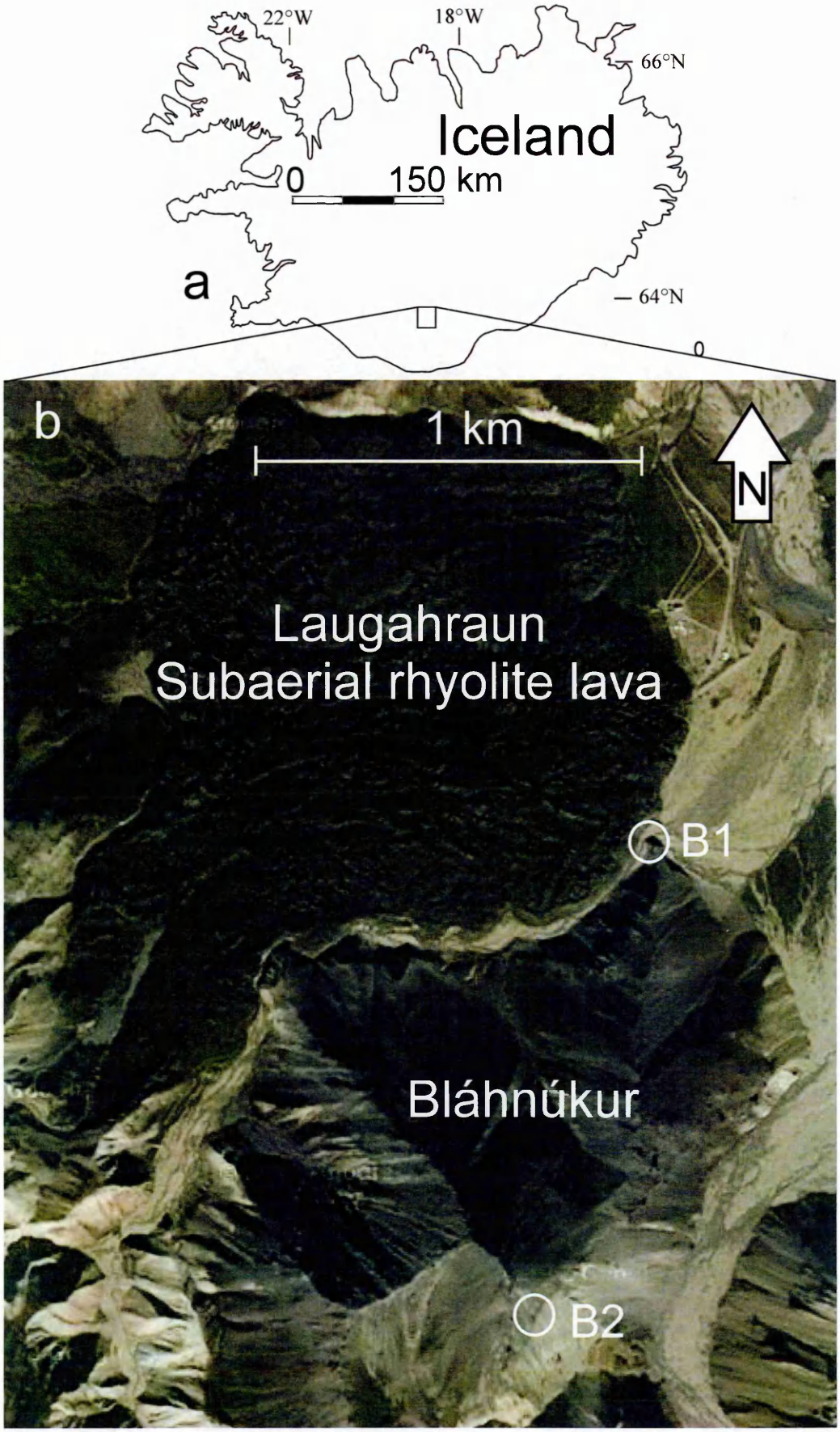

Fig. 3.3 Bláhnúkur and Laugahraun, Torfajökull, Iceland. Lobes B1 and B2 are circled. Bláhnúkur is a relatively thin subglacial volcanic deposit ~50 m thick, resting on an older rhyolite hill. Laugahraun is a recent, postglacial, subaerial rhyolite lava flow.

Fig. 3.4 Lobe B1 of Bláhnúkur, in Grænagil valley at the base of the mountain, looking east. It shows columnar jointing, but with some preferred orientation fractures present (e.g. just to the left of the scale person), such as pseudopillow fracture systems (one shown by the white arrow).

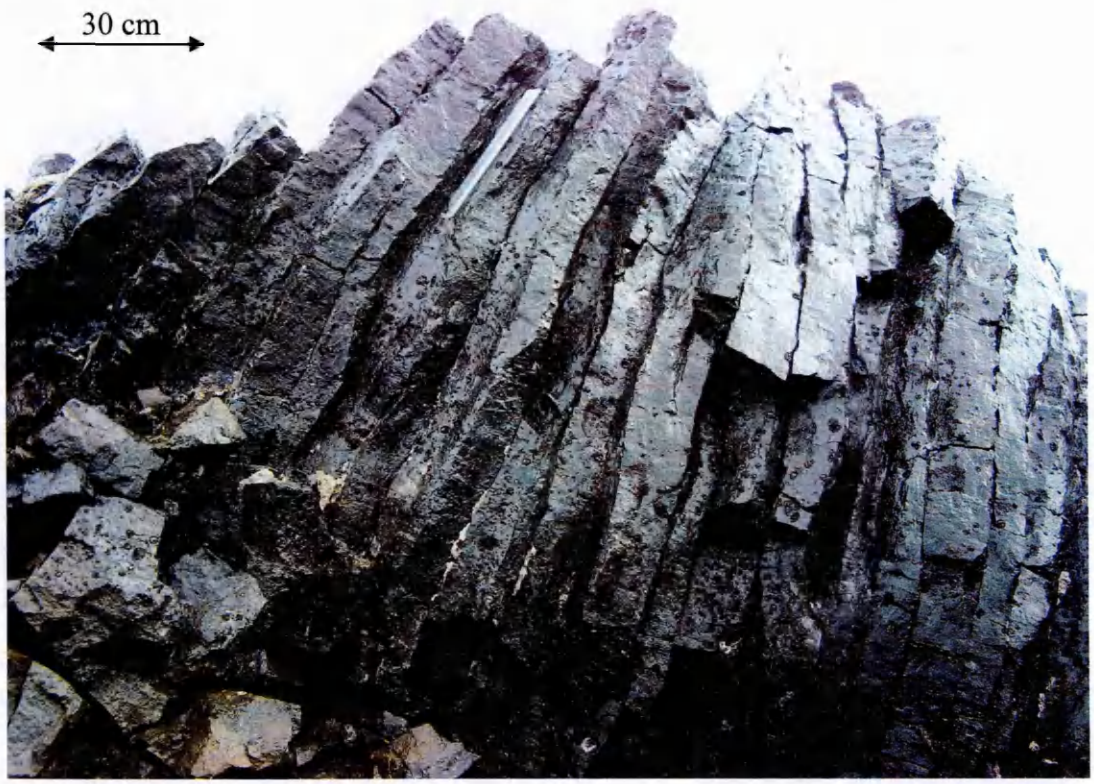

Fig. 3.5 Lobe B2 at the top of Bláhnúkur. These are glassy columns with clear striae in a small outcrop. Ruler is 30 cm for scale.

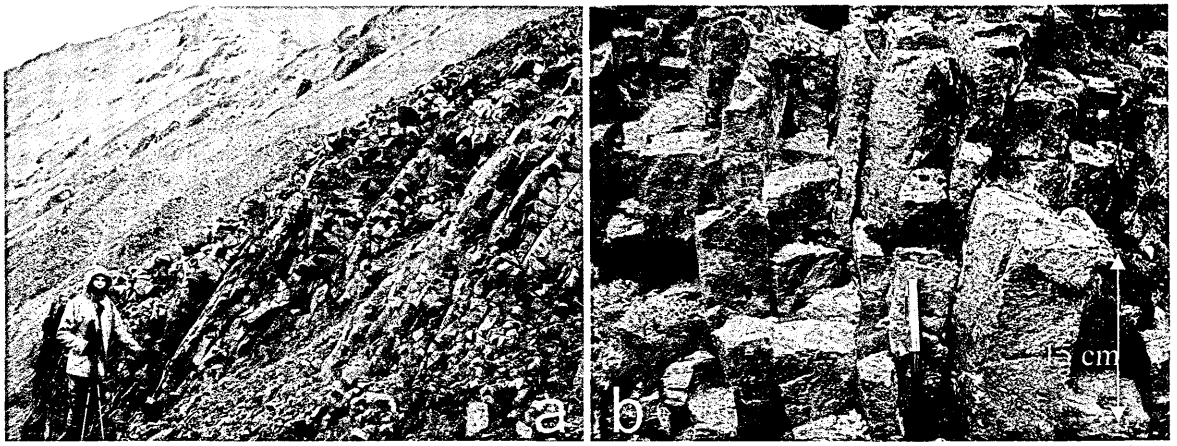

Fig. 3.6 Preferred orientation, or sheet-like, fractures from two different lobes on Bláhnúkur. a) A blocky jointed lobe with large fractures normal to the down slope direction. b) Closely spaced preferred orientation fractures in glassy rhyolite, with fractures forming perpendicularly between these resulting in crude 4 sided columns. Pen for scale.

The lobe in Grænagil valley (Fig. 3.4), termed B1 (Fig. 3.5; 63.986084, -19.061042), shows additional types of fractures besides columnar jointing. Pseudopillow fracture systems are present in this lobe, each consisting of a single, vertical, planar master fracture with straight subhorizontal striae across the fracture surface. The master fracture is cut by vertical subsidiary fractures on either side, formed perpendicular to it, which show narrow curved striae on their fracture surfaces (Fig. 3.6). The interaction of pseudopillow fracture systems and columnar jointing appears as polygonal-type fractures abutting a planar surface (Fig. 3.8). Columnar jointing measurements were made away from pseudopillow fracture systems where possible to give accurate column measurements. The columns here have a pale yellow staining.

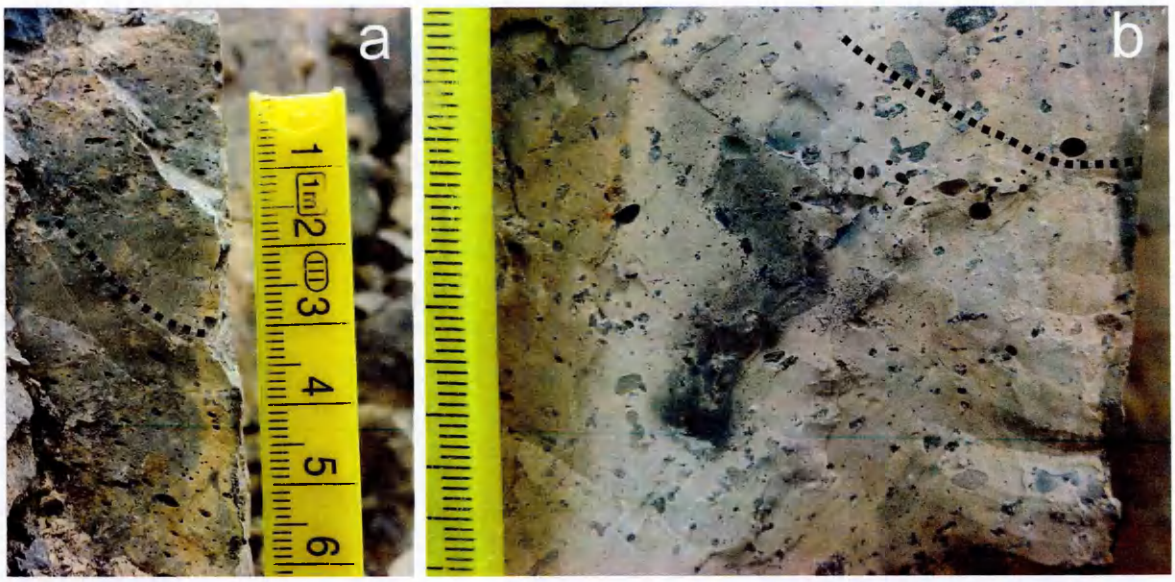

Fig. 3.7 Samples from the preferred orientation fractures at lobe B1. These are from pseudopillow fracture systems, the master fracture is perpendicular to the plane of the image on the right hand side, in both a) and b). The images show subsidiary fractures with curved striae, a curved stria is traced over in each image for clarity. Scale graduations are in mm, numbers are in cm.

Fig. 3.8 View looking downwards on a subvertical master fracture from a pseudopillow fracture system in lobe B1, Bláhnúkur. These preferred orientation fractures alter the way in which columnar jointing forms around them, tending to cause the formation of four sided columns. Ruler is 25 cm long.

The small lobe at the top of Bláhnúkur (Fig. 3.5), termed B2 (Fig. 3.8; 63.976690, -19.069107), appears to show only columnar jointing and no other fracture types. These columns are subvertical and glassy, showing clear striae.

3.2.2 Goðafjall, Öræfajökull

Two columnar jointed rhyolite lobes have been studied in Hvalvörðugil valley, on the southern side of Goðafjall Mountain at Öræfajökull. We have labelled these G1 (63.927015, -16.729098) and G2 (63.927632, -16.720888) as they have no official names (see Fig. 3.9 for a location map).

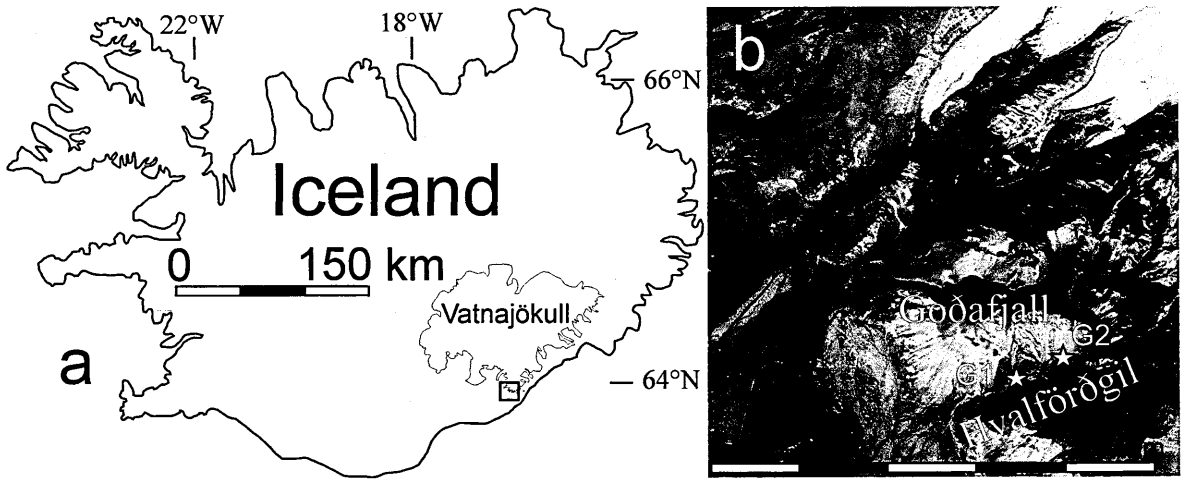

Fig. 3.9 a) Map of Iceland showing the Vatnajökull glacier. The box on the southern side is on the Öræfajökull glacier and is the area shown in b). b) Shows the location of lobes G1 and G2 in Hvalvörðugil valley on Goðafjall mountain at Öræfajökull. Scale divisions are in km.

The G1 exposure is approximately 100 m long striking roughly north-south, and 50 m wide, on a modern slope of approximately 30°, entirely surrounded by columnar rhyolite scree. The base of the flow is not visible. Bed rock (amygdaloidal basalt) is visible in contact with the flow on the south western corner and occurs on the east side approximately 10 m away from the last visible outcrop of the flow. Therefore the flow was

unlikely much wider than about 60 m. The cross section of the flow has an aspect ratio of approximately 1, it is only slightly wider than it is high (Fig. 3.10).

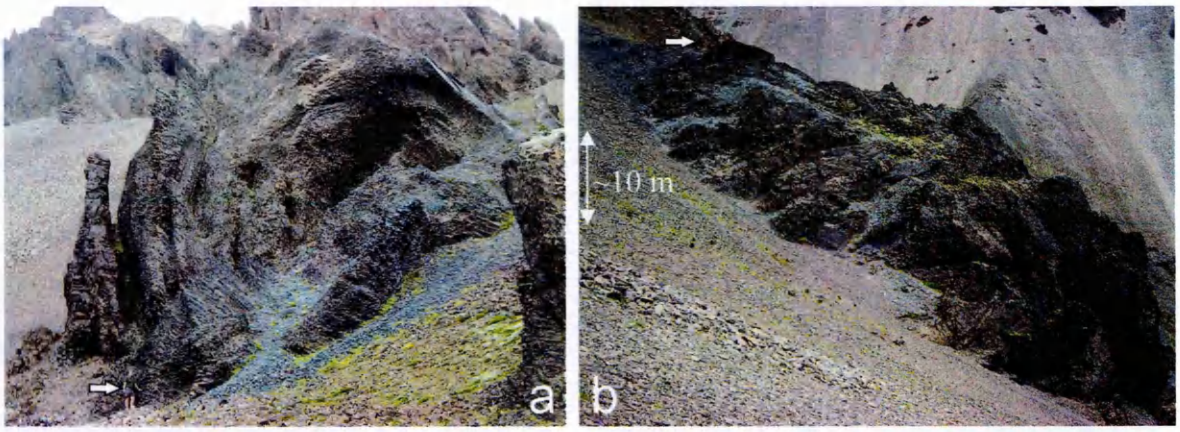

Fig. 3.10 a) Cross section through lobe G1 looking north. Columnar jointing is arranged radially around this lobe, glassy flow banding parallel surfaces give this lobe a distinctive onion-like layered appearance. b) View of G1 looking east, it is surrounded by columnar rhyolite scree. Arrows point to a person for scale in both images.

The visible flow is entirely columnar jointed, with columns arranged radially around the centre, so that columns are vertical in the centre and horizontal at the sides of the flow. The lava is strongly flow banded, with flow bands at a wide range of angles in relation to the columns, often occurring perpendicular to the columns but also at a high angle to the column axes in other areas. (Fig. 3.11)

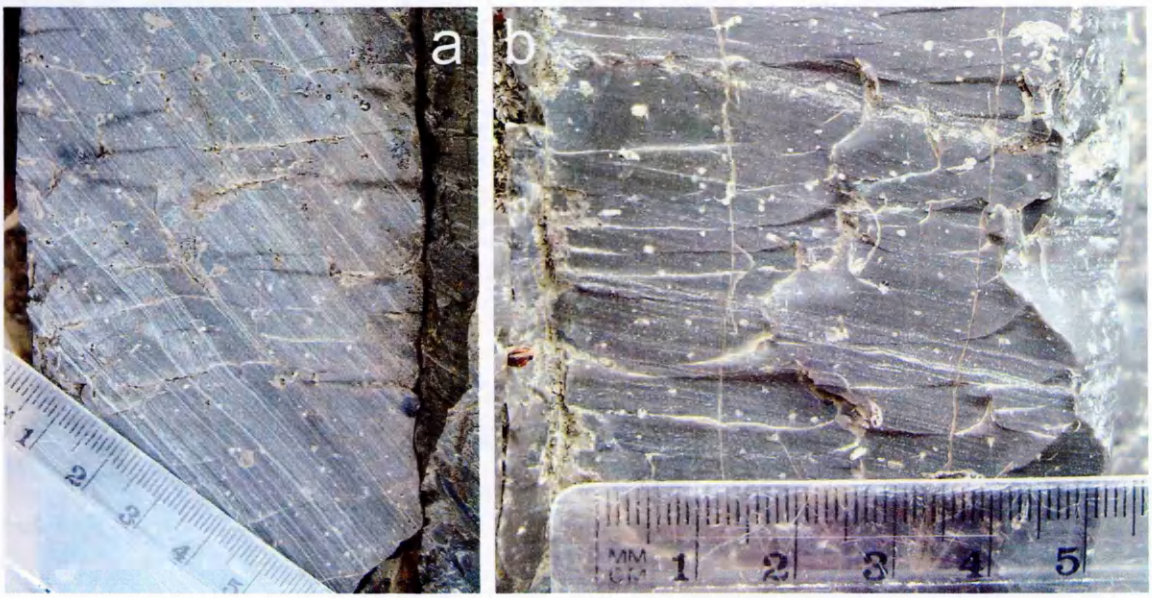

Fig. 3.11 Columns in G1 showing a) high and b) low angles between column axes and flow banding.

Large, laterally pervasive, flow banding-parallel, glassy surfaces (fractures?) occur throughout the flow, resulting in an 'onion'-like appearance with multiple layers occurring around the width of the flow (Fig. 3.12), perhaps similar to features that have been observed in a submarine endogenously grown dacite dome (Goto and McPhie, 1998). These have a number of different features and textures. The lava is glassier on the surfaces of these fracture planes, with the glassier zone extending down a few centimetres into the lava below. The surface of these large fractures may show crude columnar/polygonal jointing where fractures commonly meet at right angles, perhaps suggesting that the columnar jointing stops and reinitiates at these surfaces (Aydin and DeGraff, 1988). They may instead show a glassy scale-like textured pattern with small glass bead-like structures centimetre sized or smaller, reminiscent of perlite features. Some of these beads are highly elongate being 1 cm wide and up to 20 cm long. Small 'sprays' of bead-like forms also occasionally appear on the surface of these large fracture planes (Fig. 3.13).

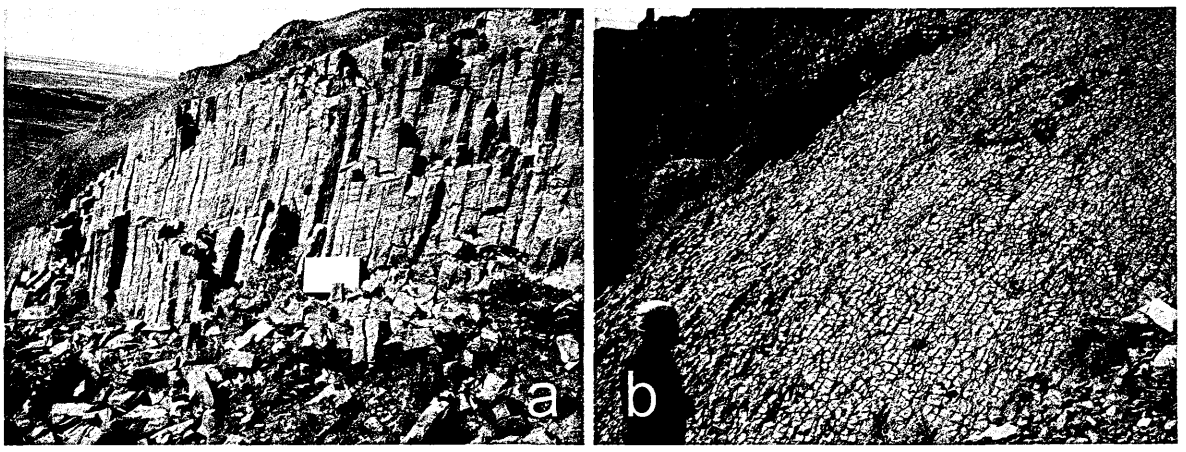

Fig. 3.12 Flow banding parallel glassy surfaces from lobe G1. a) The flow banding is clearly visible and the glassy surface is subhorizontal, sharply cutting off the top of these columns. Yellow notebook is 20 cm long for scale. b) This shows the surface of an extensive flow banding parallel glassy surface in G1. Polygonal jointing can be seen on the surface.

Fig. 3.13 Textures from large pervasive flowbanding parallel surfaces in lobe G1. a) Scale-like beads on a glassy surface. b) Elongate glassy beads and c) a spray or fan-like occurrence of finer glassy beads. These glassy beads are commonly associated with flow banding parallel glassy surfaces. Scale is in mm, with numbers in cm.

Generally the lava is glassy with acicular microlites and tiny black opaque oxides aligned in the flow bands. It also contains small, <3 mm long plagioclase phenocrysts and some smaller opaque oxide phenocrysts (Fig. 3.14a). The lava flow has an area of perlite and pale grey material forming in the south western corner adjacent to the residual bedrock outcrop and in the top central part of the flow, indicating hydration (e.g. Denton et al., 2009). Bands of perlite beads interspersed with bands of white to grey non-glassy material form within the flow banding here, some areas contain mixed perlitic beaded glass and grey material on a centimetre scale (Fig. 3.15a and b). The alternating perlitic and grey altered bands can clearly be seen defined by the flow banding where the flow bands are deformed, e.g. folded. So the type of alteration does not seem to relate to the proximity of the edge of the flow but to a particular flow band (Fig. 3.15c). Perlite beads in this area range in size from 1 mm to 1 cm. No vesicles have been observed anywhere in this flow.

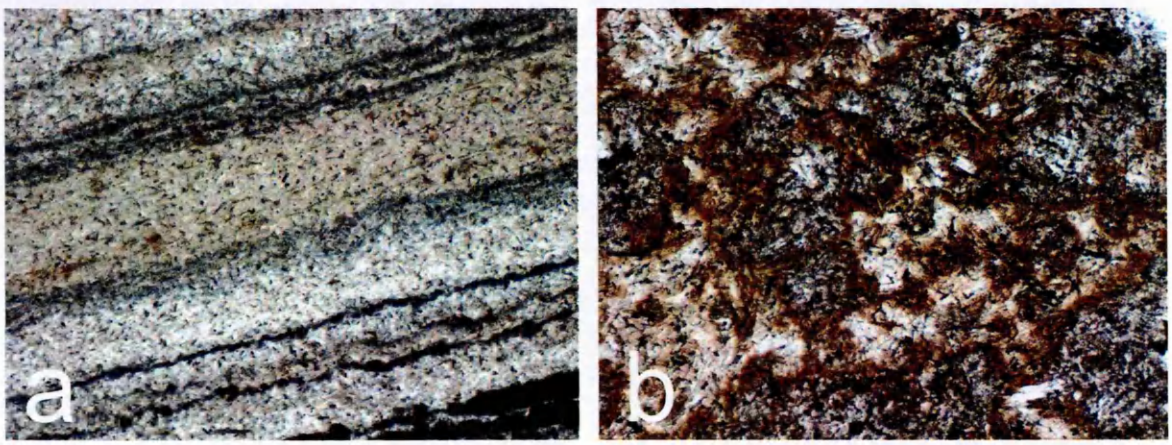

Fig. 3.14 Thin section images from a) G1 and b) G2. Field of view for both is ~1.5 x 1.0 mm. a) This image clearly shows the strong flow banding that occurs in lobe G1. b) Shows the more crystalline nature of this lava, this occurs as patchy areas of more and less crystal-rich lava. The red-brown material may be some type of weathering alteration.

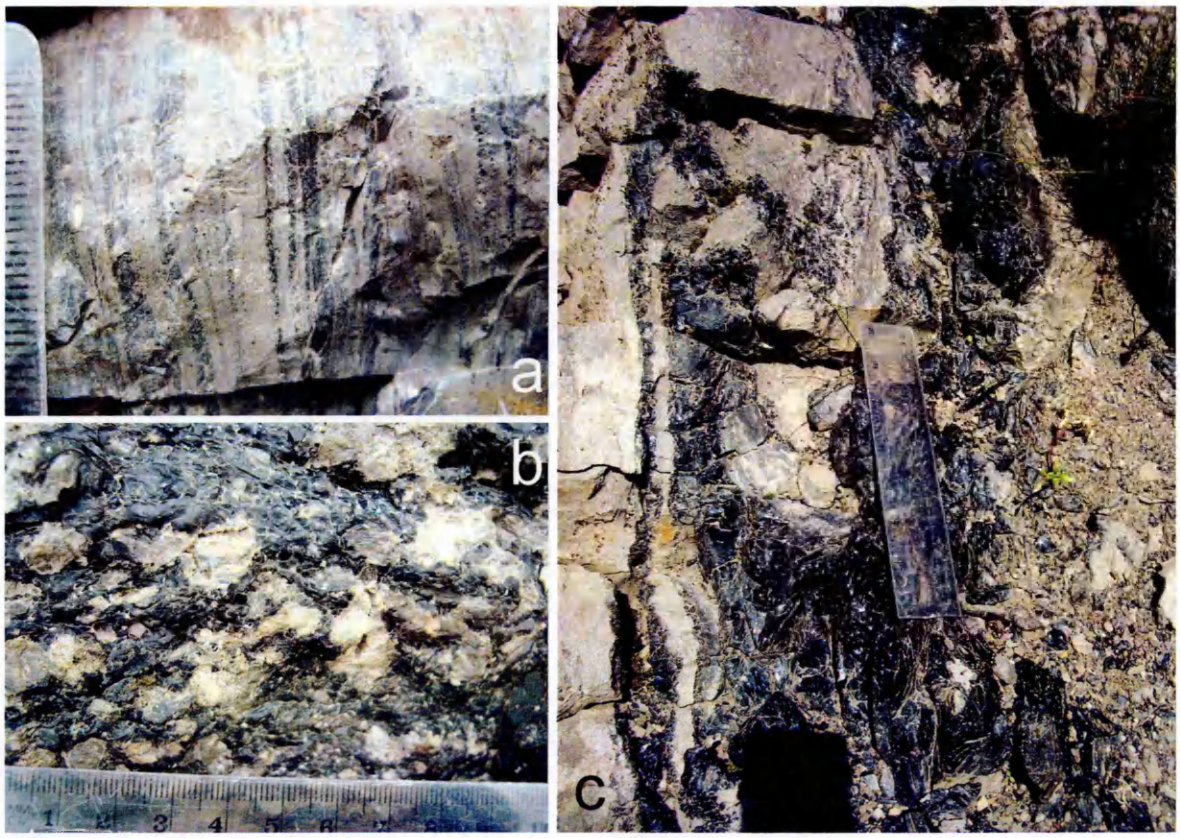

Fig. 3.15 Hydration textures from the south western corner of G1. a) Alternating bands of black glassy perlite beads and grey hydrated rhyolite, scale graduations in mm. b) Area of perlite beads and grey hydrated rhyolite which do not occur in bands, scale graduations in mm. c) Folded flow bands, some of which show grey hydrated rhyolite and others show black perlite beads, demonstrating that generally it is not the proximity to the flow edge that determines how hydrated areas are, but is somehow controlled by the small differences between flow bands. Ruler is 18 cm for scale.

Striae on G1 columns are much more varied across the lobe than on other rhyolite columnar joints studied, displaying features often not observed on other rhyolite column bounding fractures. Striae on the column bounding fractures here are highly variable in their morphology. Some are straight and regular, some are curved or very irregular and do not reach across a single column's side, others give the column face a shattered appearance while some form straight but at an angle across the column face (Fig. 3.16).

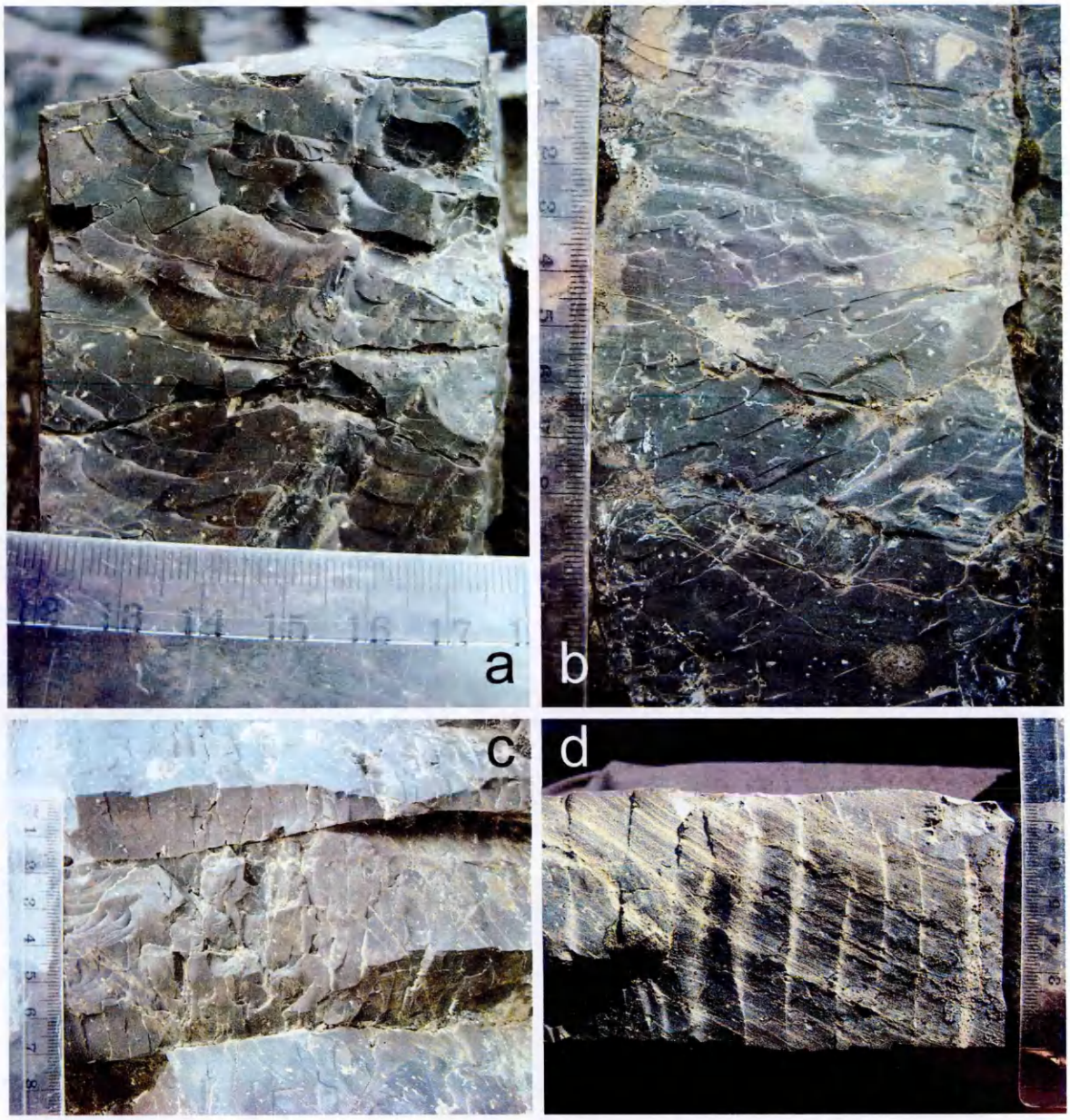

Fig. 3.16 Striae variations from lobe G1. a) Striae curve and are not continuous across the column side. They give the column side a shattered appearance. b) Striae are approximately perpendicular to the column side at the top of this image but abruptly become inclined (they straighten out again below this). c) Striae on this column almost disappear entirely as the column surface is so irregular and uneven. On the left hand side of the image striae appear to be forming parallel with the column sides. Approximately half way along this column side the column face splits into two column faces, thus increasing the number of sides on the column here. d) Very regular, widely spaced striae that are continuous across the column side, this is not a common occurrence at G1, the striae do not tend to form continuously across a column side. Column bounding fractures form at a high angle to the flow bands. In all images scale graduations are in mm and numbers are in cm.

Some of the columnar jointing in G1 shows a strong preferred orientation of fractures within the columnar jointing, causing continuous straight fractures and an alignment of columns, which often have 4 rather than 5 or 6 sides. They are not pseudopillow fracture systems as occurs in lobe B1, because fractures abutting the preferred orientation fractures

show straight striae across the column side, rather than curved striae like those in lobe B1. These preferred orientation fractures are particularly clear on the top central part of the flow where they are parallel with the elongate direction of the lobe G1, striking north-south, but they also occur on the lobe margins and elsewhere within the flow (Fig. 3.17). Striae on these preferred orientation fractures are often continuous across adjacent column bounding fractures.

Fig. 3.17 Preferred orientation fractures in G1. a) Preferred orientation fractures occur vertically in this image. Smaller fractures form between these long preferred orientation fractures resulting in generally four sided polygonal jointing. b) Side view of preferred orientation fractures (pointed out by the arrows, and red stippled surface) on the top northern part of G1, looking south east. Striae are continuous across these long straight fractures, and smaller fractures form cross cutting between the long preferred orientation fractures, forming crude four sided polygonal jointing.

G2 is approximately 500 m east of G1 in Hvalvörðugil valley. It shows well developed columnar jointing, and has the largest column sizes measured in this study. Columns in this lobe fan round, being subvertical at the top of the outcrop becoming subhorizontal towards the visible base and southern extent (away from the mountain) of this lobe (Fig. 3.18).

Fig. 3.18 Columnar jointing at G2. a) The southern side of the outcrop shows columns oriented subhorizontally, most of these columns are inaccessible for measurements. Person 1.65 m tall for scale. b) Columns above and north of the previous image show more vertical orientations fanning round to become more horizontal lower down. Columns are approximately 4 m long.

There is no obvious flow banding in G2 lobe, however large pervasive surfaces approximately perpendicular to the column axes, much like those parallel to flow banding in G1, do occur in this lobe (Fig. 3.19). These surfaces do not show the highly glassy textures of those in G1 lobe, however G2 is not as glassy as G1 in any part of the lobe. The lava contains small phenocrysts of plagioclase <3 mm long, and smaller phenocrysts of opaque oxides. It is much more crystal rich than G1 (being approximately 80% crystalline) and has a patchy texture showing more and less crystalline areas. The groundmass is commonly altered to a red-brown colour and is dominated by acicular microlites and opaques with a low percentage of glass (Fig. 3.14b).

Fig. 3.19 Pervasive surfaces, similar to the glassy flow banding surfaces in lobe G1 and the rest of the rhyolite in the Hvalvörðugil valley. These have a strong influence on the shape and appearance of the outcrop. Photo taken looking upwards from location of person in Fig. 3.18a, column diameters are approx. 25 cm. Scale bar on the left is ~3 m.

Striae are not easy to see or well preserved in this flow. Where they are visible they are straight, regular and widely spaced (Fig. 3.20).

Fig. 3.20 Striae on a column at lobe G2. They are fainter than those in G1 and considerably more widely spaced. The columns at G2 often have a red-brown colour, probably due to weathering alteration.

Hvalvörðugil valley, between lobes G1 and G2, is filled with polygonally jointed rhyolite. The lava appears to have flowed down Goðafjall Mountain on its eastern side, and is plastered to the side of the mountain (Fig. 3.21). Flow banding is subvertical in this rhyolite, parallel with the surfaces of the exposure and columnar jointing is approximately normal to the flow banding. This lava also forms large, flow banding parallel glassy surfaces as in G1 and G2. Columns commonly show preferred orientation fractures or very closely spaced flow banding parallel glassy surfaces that interfere with the formation of columnar jointing, and much of this lava is inaccessible. Therefore no column measurements could be obtained from this Hvalvörðugil valley rhyolite. The rhyolite in Hvalvörðugil valley has been shown to be a single eruptive unit geochemically and is dated at 116 ka ± 20 ka (Walker, 2011).

Fig. 3.21 The Hvalvörðugil valley rhyolite. It appears as a sheet flowing down the side of Goðafjall mountain, it was probably supported by a glacier when it was emplaced which would account for its orientation and columnar jointing orientations. It also has the large pervasive flow banding parallel surfaces, often more closely spaced than those in G1 and G2. Much of this lava is inaccessible for measurements.

3.2.3 Northern Rauðufossafjöll, Torfajökull

This un-named exposure, termed R1 (location 64.006554, -19.396168), is a small cap of rhyolite entirely columnar jointed, at the top of a subglacial volcanic edifice consisting of predominantly fragmental deposits (pumice, ash and obsidian). Other columnar jointed subglacial rhyolitic lavas have been studied at Rauðufossafjöll previously (Tuffen et al., 2002a). The columns in the lava cap are subvertical towards the bottom of the exposure changing abruptly to subhorizontal above (Fig. 3.22). No clear basal or top surfaces of this columnar jointed rhyolite body are exposed, so it is uncertain how much larger or what

shape this lava body may be or once have been. Hackle show that the upper tier of subhorizontal columns propagated inwards and downwards.

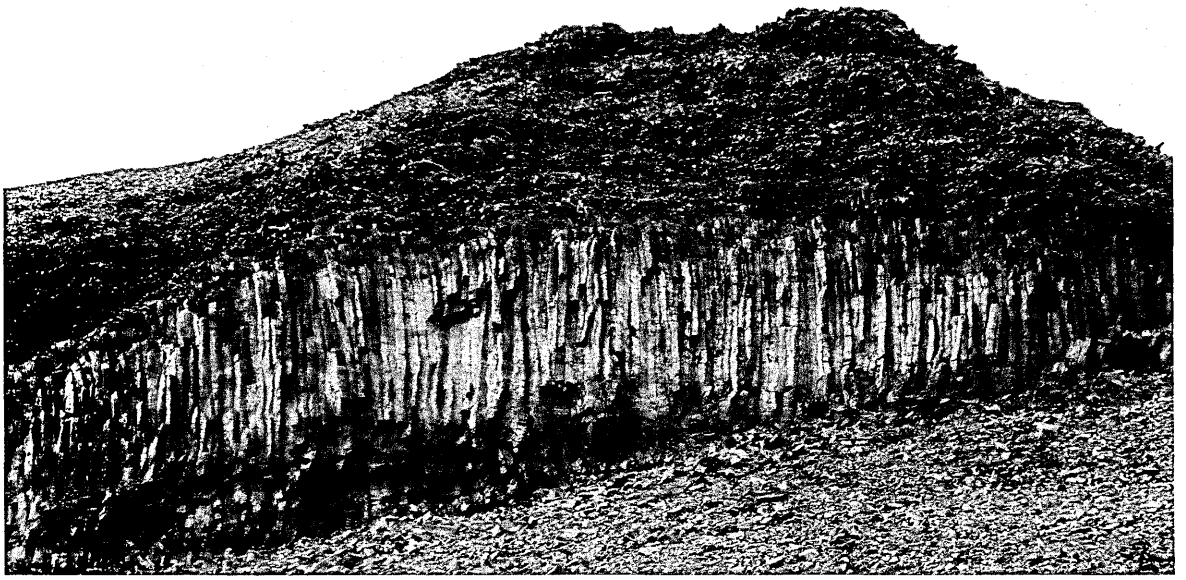

Fig. 3.22 Columns at R1, this outcrop of lava is approximately 8 m high. Columns at the base are subvertical and those on top and are subhorizontal, giving a two tiered affect.

The rhyolite is very glassy, commonly with a glassy sheen on the column bounding fractures. It contains copious tabular blocky phenocrysts of plagioclase up to 5 mm long and green clinopyroxene phenocrysts. The glassy groundmass contains very few acicular microlites and some tiny opaques (Fig. 3.23). Striae here are spaced 1-2 mm apart, the smallest measured of any rhyolite columns, and they have muted topography on the fracture surface, their hackle (plumose structures) are generally visible (Fig. 3.24). In plan view columns tend to be irregular with a large range of column side widths and shapes (Fig. 3.25). No fracture types other than columnar joints are seen at this outcrop.

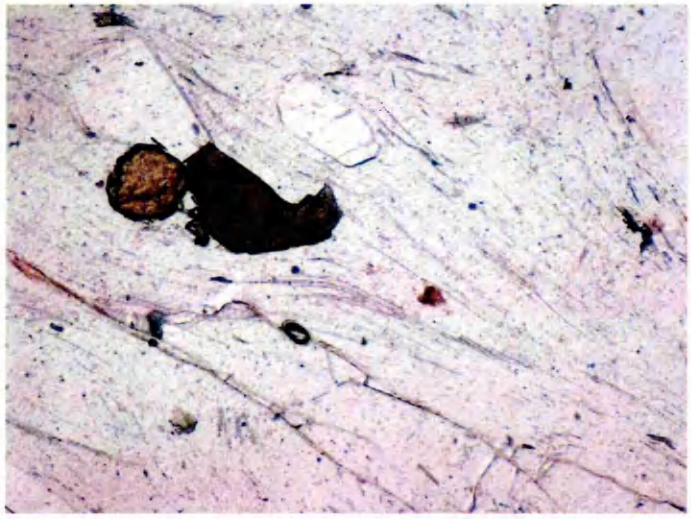

Fig. 3.23 Thin section of R1 lava has phenocrysts of plagioclase feldspar and green clinopyroxene. The glassy groundmass is very microlite poor, which links with the very glassy appearance of the lava in hand specimen. Field of view is ~1.5 x 1.0 mm.

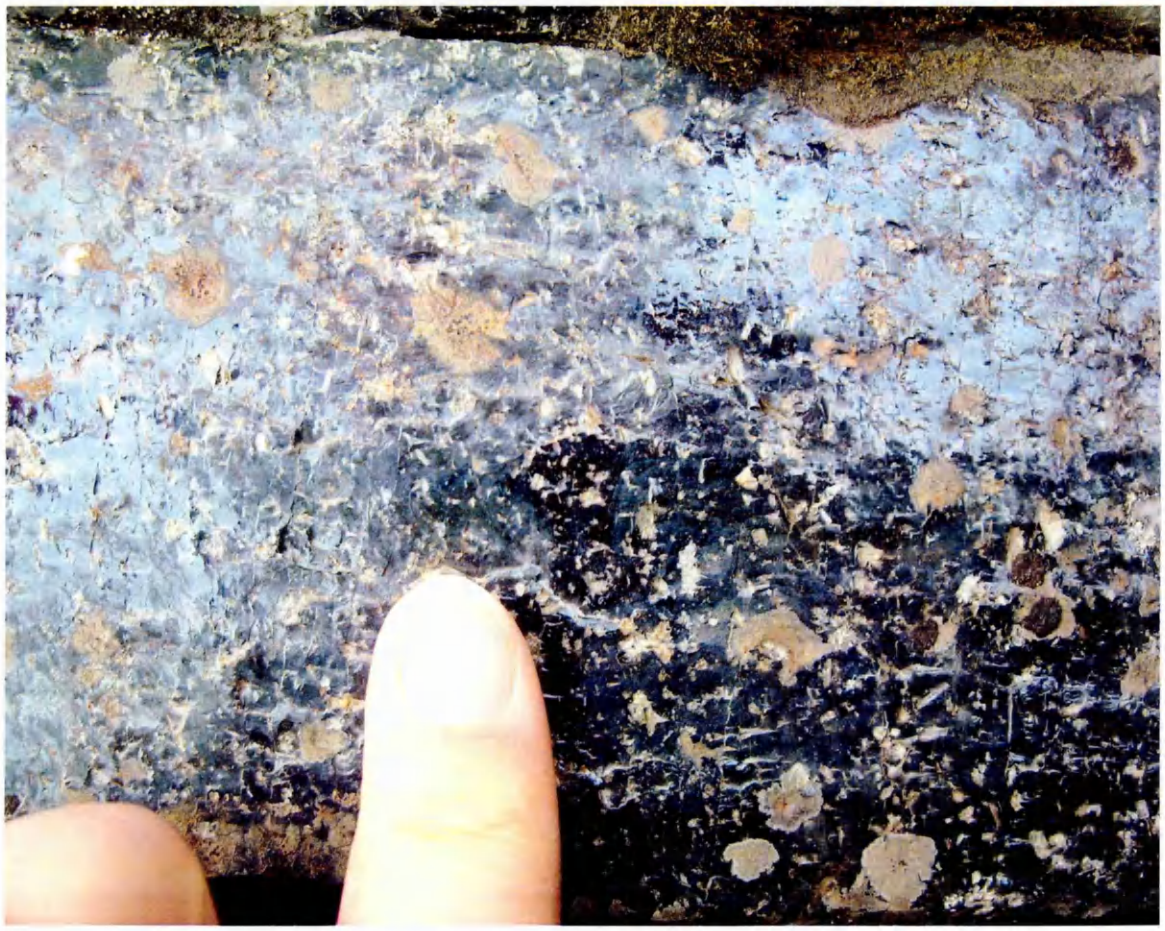

Fig. 3.24 Striae on a very glassy column at R1 (there is some lichen on the column surface). Striae are extremely closely spaced at R1, they are smaller than any others previously measured on columnar jointing. Hackle on the striae here show propagation from left to right. Finger for scale.

Fig. 3.25 Irregular end sections of columns from R1 subhorizontal columns (and some moss). Pen is 15 cm for scale.

3.2.4 XRF composition data

XRF major and trace element compositional data were obtained for G1, G2 and R1 (Table 3.1 and appendix 7). Samples selected were the most pristine and unhydrated that could be found at any outcrop / lava lobe. XRF data for a different lobe on Bláhnúkur were also obtained, but as Bláhnúkur appears to be compositionally very uniform (Owen et al., 2012) this is likely a good approximation for the lobes B1 and B2. Compositions for G1 and G2 are very similar and as they both occur within the same valley they have been classed as part of the same lava eruption previously (Walker, 2011).

Table 3.1 Major and trace XRF compositions of rhyolites in this study.

Sample:	Rauðfoss	Goðafjall		Bláhnúkur		
Wt.%	R1	G1	G2	B	Mean	±2σ
SiO_2	73.56	73.29	73.42	70.76	70.09	1.17
TiO_2	0.289	0.189	0.188	0.277	0.29	0.03
Al_2O_3	12.83	13.52	13.50	14.13	14.11	0.19
Fe_2O_3	3.27	2.55	2.51	3.31	3.35	0.21
MnO	0.123	0.067	0.063	0.085	0.08	0.00
MgO	0.10	0.14	0.16	0.22	0.32	0.21
CaO	0.70	0.88	0.87	0.94	0.97	0.31
Na_2O	5.48	5.10	4.94	5.77	5.57	0.19
K_2O	3.89	4.09	4.04	4.28	4.33	0.14
P_2O_5	0.022	0.026	0.026	0.037	0.03	0.00
LOI	0.28	0.46	0.87	0.90	0.72	0.77
Total	100.55	100.31	100.59	100.71	99.87	0.90

Sample:	Rauðfoss	Goðafjall		Bláhnúkur
ppm	R1	G1	G2	B
Rb	99	101	102	106
Sr	48	47	48	58
Y	118.2	90.3	96.7	86.6
Zr	851	441	437	807
Nb	162.6	70.4	69.0	119.9
Ba	483	694	686	471
Pb	11	9	11	9
Th	17	15	13	18
U	6	4	4	6
Sc	2	2	2	3
V	4	2	1	4
Cr	5	8	5	4
Co	1	1	0	1
Ni	6	4	3	4
Cu	4	10	9	8
Zn	186	98	100	127
Ga	33	25	25	30

XRF major and trace element data. 'Bláhnúkur mean' data is from Owen et al. (2012). It is a mean of 5 analyses and the 2σ values show the uniformity in composition of the lava lobes at Bláhnúkur.

3.2.5 FTIR data

Fourier transform infrared (FTIR) spectroscopic analyses were carried out on rhyolitic glass from G1 and R1 in order to determine water concentrations. Lava samples from G2 were too crumbly and crystalline to make into wafers for FTIR analysis. Extensive FTIR analyses have been carried out for Bláhnúkur previously (Owen et al., 2012). Analyses were performed on double polished glass wafers 154-587 μm thick (see appendix 3) using

a Thermo Nicolet FTIR with a Continuum Analytical microscope at The Open University. For each measurement 512 scans were collected to give good signal to noise, with a resolution of 4 cm^{-1}, which gives good resolution in the spectra without making the data gathering process overly long. Wafer thicknesses were measured using a Mitutoyo digital displacement gauge.

Total water content (the sum total of both OH and H_2O) was calculated using the peak at ~3550 cm^{-1} and molecular water content (H_2O_m) from the ~1630 cm^{-1} peak using the Beer-Lambert Law (Stolper, 1982; Leschik et al., 2004):

$$c = \frac{M \times Absorbance}{d\rho\varepsilon} \qquad (1)$$

where c is concentration in weight percent, M is the molecular weight of water (18.02 $gmol^{-1}$), Absorbance is absorbance peak of the FTIR spectrum (i.e. the measured peak height), d is the sample thickness (in centimetres), ρ is sample density (in grams per litre) and ε is the absorption coefficient (in litres per mole per centimetre).

H_2O_m data are subject to a larger error than total water data due to the highly sloping background of the spectra in the region of this peak resulting from alumino-silicate tetrahedral absorbance. When calculating water content from FTIR absorbance a density of 2300 kg m^{-3} was assumed for the glass, an absorbtivity of 80 l mol^{-1} cm^{-1} for the total water calculations (Leschik et al., 2004), and 55 l mol^{-1} cm^{-1} for the molecular water calculations (Newman et al., 1986). Data are presented in Table 3.2 (full data presented in appendix 3).

Some grey altered lava and glasses showing perlitic and hydrated textures from the southwest corner of lobe G1 show high total water concentrations with particularly high

H_2O_m (Table 3.2). These high water concentrations, and the elevated H_2O_m concentrations indicate hydration of these samples has occurred (Denton et al., 2009). Some of these hydrated glasses saturate the FTIR spectra, meaning that they do not reflect the true water concentrations but underestimate them.

Table 3.2 FTIR water concentration for samples from G1 and R1.

Sample	Location	H_2O total / wt%	H_2Om / wt%	OH / wt% *	Comments:
AF112	R1 column	0.20			Too noisy for 1630cm^{-1} peak
AF15	G1 column	0.20	0.14	0.06	
AF16	G1 column	0.19			Too noisy for 1630cm^{-1} peak
AF20	G1 column	0.29	0.14	0.16	
AF128	G1 grey material	1.55	1.58	-0.03	Saturated 3550cm^{-1} peak
AF132_1	G1 perlitised	0.29	0.16	0.14	
AF132_2	G1 perlitised	0.27	0.15	0.12	
AF132_3	G1 perlitised	0.52	0.46	0.06	
AF132_4	G1 perlitised	0.55	0.50	0.05	
AF132_5	G1 perlitised	0.60	0.61	-0.01	
AF132_6	G1 perlitised	0.62	0.69	-0.07	
AF132_7	G1 perlitised	1.10	1.27	-0.16	Saturated 3550cm^{-1} peak

Samples AF15, 16, 20, 128 and 112 are all averages of 5 data points from the same sample. Each of the measurements in AF132 are single measurements in different flow bands.
* OH calculated as H_2O - H_2Om

Results for G1 and R1 are presented in Table 3.3, with corresponding saturation pressures calculated using VolatileCalc (Newman and Lowenstern, 2002), assuming zero CO_2 content. Theoretical ice thicknesses are then calculated from these pressures (Table 3.3) assuming an ice density of 917 kg m^{-3} (Tuffen et al., 2010; Owen et al., 2012). Temperature is important when calculating pressures, as volatile solubility is affected by temperature. A lava temperature of 830 °C was assumed, as this was the lava temperature calculated for the 1362 AD Öræfajökull rhyolite eruption (Sharma et al., 2008) and a similar temperature is likely for the Öræfajökull rhyolites in this study. The same temperature was also used for the sample from Rauðufossafjöll as rhyolite eruption temperatures from Torfajökull can vary 750-950 °C (Owen et al., 2012) and the eruption temperature of R1 is unknown. An attempt was made to calculate the R1 eruption

temperature using the Fe-Ti oxides magnetite and ilmenite, however Mn-Mg ratios showed that these oxides were not in equilibrium with each other and so could not be used (Bacon and Hirschmann, 1988).

Table 3.3 Calculated pressures and ice thicknesses

Sample	Location	H_2O total / wt%	Pressure / bar	Ice thickness / m	Temperature / °C
AF112	R1 column	0.20	3	33	830
AF15	G1 column	0.20	3	33	830
AF16	G1 column	0.19	3	33	830
AF20	G1 column	0.29	7	78	830

3.3 Measurements on rhyolite columnar jointing

In situ field measurements of striae and column side widths, *W* and *S*, were made using digital callipers where possible, otherwise with a ruler or tape measure. The most comprehensive set of measurements from basaltic columnar jointing were made by Goehring and Morris (2008) and in order to directly compare these measurements their measurement strategy was replicated as far as possible. They made three measurements of each stria width, one in the column face centre and one at either edge of the column side. This was not possible for rhyolite columns in this study due to the irregularity and variations in striae widths across a column side (e.g. Fig. 3.16). Instead measurements were taken from the same distance from the nearest column edge, along the length of a column face. This ensures there is no bias in the measurements, as striae widths can vary laterally across a column side.

Where possible, ten striae measurements were taken per column side, and ten column sides worth of striae were measured per site (per data point on Fig. 3.26; see appendix 2). In general only one or two column sides were measured for striae, per column. If this number of striae measurements was not possible, then as many striae as possible were measured

(up to 100 striae measurements); as many column side widths (up to 46 measurements) were measured within an area usually smaller than 3×3 metres. If possible this was repeated elsewhere within a single flow / lobe depending on its size. The number of sides on columns within each area was also counted. See Table 3.4 for column measurements and Appendix 2 for full measurement details, including standard deviations and number of measurements per data point.

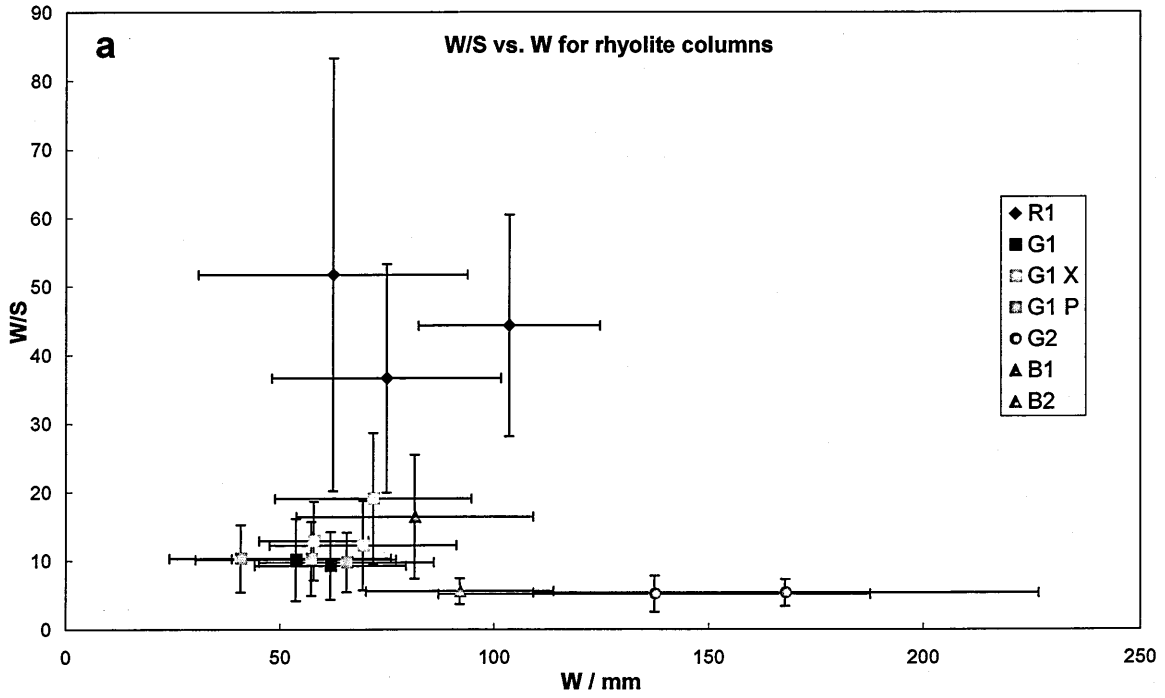

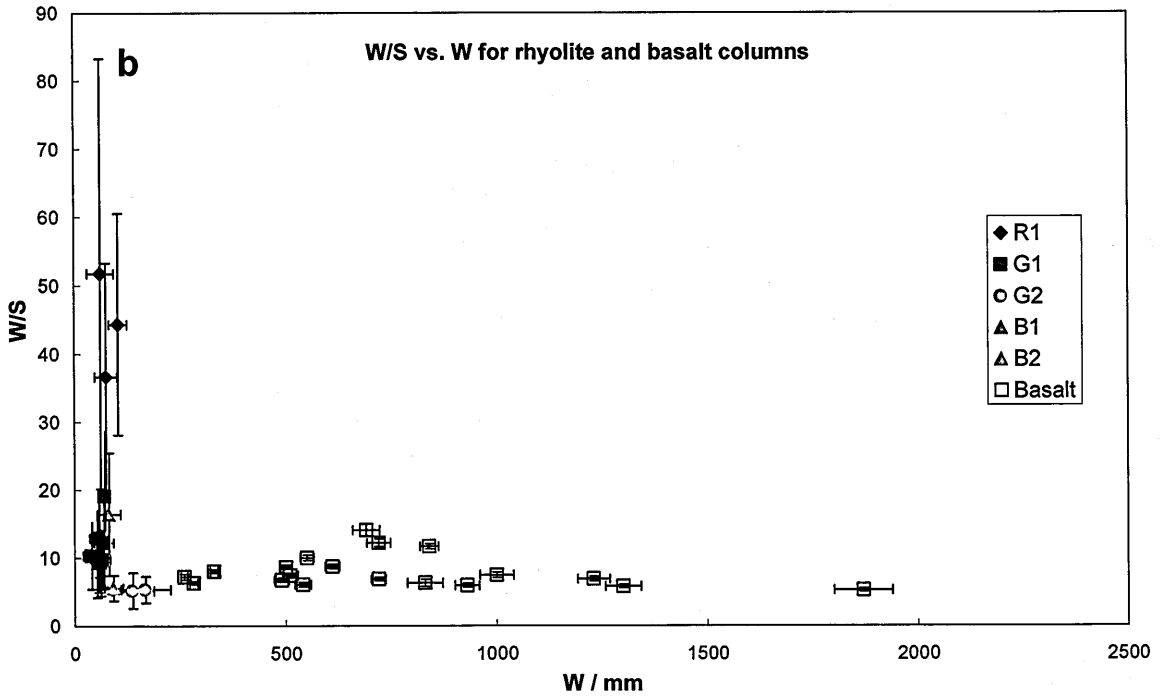
b
W/S vs. W for rhyolite and basalt columns
W/S
W / mm
R1
G1
G2
B1
B2
Basalt
0
10
20
30
40
50
60
70
80
90
0
500
1000
1500
2000
2500

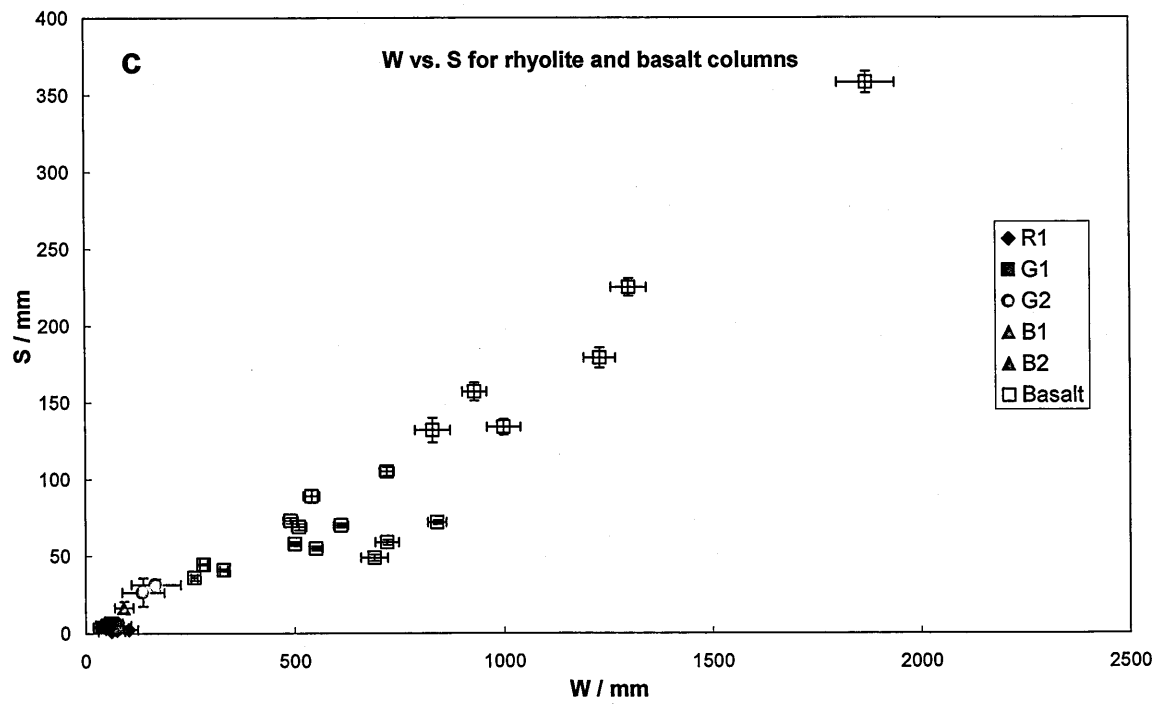
c
W vs. S for rhyolite and basalt columns
S / mm
W / mm
R1
G1
G2
B1
B2
Basalt
0
50
100
150
200
250
300
350
400
0
500
1000
1500
2000
2500

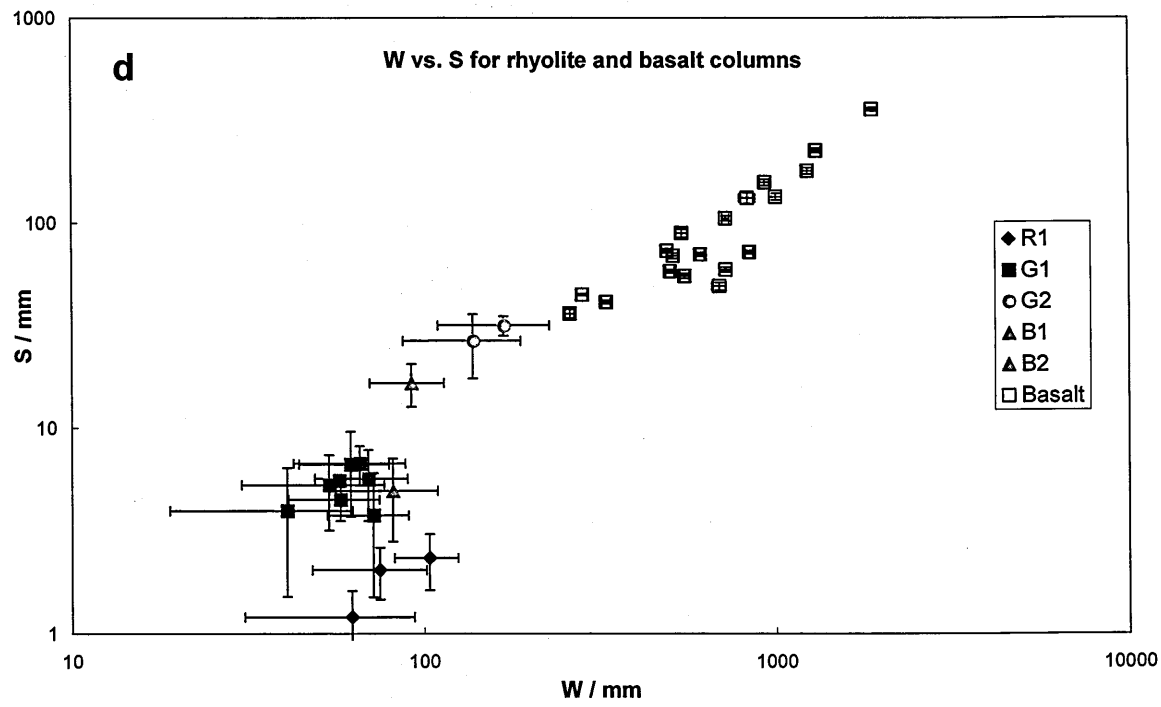

Fig. 3.26 Error bars are ± 1σ. a) *W/S* vs. *W* for rhyolite columns from this study (where *W* is column side width and *S* is striae height). The data naturally forms groups according to flow, and shows no correlation. b) *W/S* vs. *W* for rhyolite columns from this study and from basalt columns from the Columbia River Basalt Province (data of Goehring and Morris 2008). Rhyolite columns plot at much smaller *W* and a much wider range of *W/S* than the basalt column data of Goehring and Morris (2008). c) *W* vs. *S* for both rhyolite and basalt column data. This demonstrates how this plot may be confusing as it appears to show a good correlation indicating a fairly constant *W/S* value which is certainly not the case for the rhyolite column data from this study given a) and b). The data appear to show a minimum *W/S* ratio of approximately 5. d) This is a log-log version of c. It shows the rhyolite data more clearly.

In some cases columns align so that long planar, continuous fractures are present which cause a preferred fracture orientation within the columnar jointing (e.g. lobes B1 and G1; Figs. 3.7 and 3.17). This may occur as a result of another fracture type occurring with the columnar jointing, such as the pseudopillow fracture systems in lobe B1, but does not have to. Data were either not collected from the parts of the flow where continuous fractures cause a preferred fracture orientation within the columnar jointing (e.g. in lobe B1) or data were collected and logged separately from these areas (e.g. G1). In the case of G1 the data were separated between measurements along the preferred orientation fractures and those cross-cutting between the preferred orientation fractures. In general columns partly bound by preferred orientation fractures tend to have fewer sides, 4 rather than 5, and column

bounding fractures cross cutting between the long preferred orientation fractures tend to be longer, spanning the distance between one preferred orientation fracture and the next, causing slightly larger *W/S* values (Table 3.4).

Table 3.4 Column measurements in subglacial rhyolite

Flow	S / mm	W /mm	W/S	number of sides	
				mode	mean
R1	2.0	74.8	36.6	5	5.2
R1	2.3	103.4	44.3		
R1	1.2	62.3	51.8	5	5.1
R1		70.5		5	5.6
B1	4.9	81.3	16.4	4	4.6
B2	16.6	91.9	5.6	5	5.2
G1	6.6	61.7	9.3	5	4.9
G1	5.3	53.6	10.2	5	5.3
G1 X	4.5	57.8	12.9	5	4.8
G1 P	3.9	40.8	10.3	5	4.8
G1 X	5.7	69.3	12.2	4	4.8
G1 P	6.7	65.4	9.8	4	4.8
G1 X	3.8	71.7	19.1	4	4.5
G1 P	5.5	57.2	10.3	4	4.5
G2	26.5	137.3	5.2	5	5.4
G2	31.5	167.8	5.3		
G2		109.2		6	5.4

X indicates measurements on column sides cross-cutting between preferred orientation fractures. P indicates measurements on column sides parallel to preferred orientation fractures. These are listed in X-P pairs from the same area of measurements. Number of sides are the same for X and P measurements, as a columns cannot be formed without both these side types

Fig. 3.26a shows *W/S* ratio plotted against column side width, *W*. The data show clustering of *W/S* ratios depending on which flow they are from, with *W/S* ratios ranging from 5 to 52 and column side widths ranging from 54 to 168 mm wide. For comparison this is replotted in Fig. 3.26b to include the equivalent basalt columnar jointing data of (Goehring and Morris, 2008), to demonstrate the large differences between the data sets and the extreme values of *W/S* ratios that may occur in subglacial rhyolite columns. Fig. 3.26c and d show *W* vs. *S*, which in 3.26c appear to show a straight line with little variation, but in the log-log graph of 3.26d shows the true variation in the data. Each point in the basalt data set is also the mean of numerous measurements, as for the rhyolite data.

3.4 Interpretation of lava flow environments

The subglaical eruption environment of Bláhnúkur was established by Tuffen et al. (2001), Tuffen et al. (2002b) and Owen et al. (2012), and was outlined above. However, the interpretation of the eruption/emplacement environments at G1 and G2, Goðafjall, Öræfajökull, and R1, Rauðufossafjöll, were previously unknown and are discussed below.

Other than the presence of columnar jointing in lobe G1 a number of features indicate that this flow may have interacted with water or ice. The presence of perlite and grey hydrated rhyolite (see Table 3.2), particularly concentrated in the south western corner of this outcrop, demonstrate that water flowed around this lava while it was still hot (e.g. Denton et al., 2009). Water appears to have been able to drain away fairly rapidly from most of this flow, as throughout the rest of the lava perlite is not common. Water may have become trapped in the south western corner due to the presence of bedrock here which is not seen elsewhere beside the flow. The only other hydrated, perlite bearing area is at the southern, top centre part of the flow. Water could have been trapped or channelled here by the large flow banding parallel glassy surfaces or fractures.

Flow-banding parallel glassy surfaces are prominent in this lava, resulting in its onion-like layered appearance (Fig. 3.10). Polygonal jointing on these surfaces generally displays T-shaped junctions, indicating that columnar jointing re-initiates at these surfaces (Aydin and DeGraff, 1988). This, combined with the glassy textures and perlite-like features suggests that these surfaces may have channelled water through the flow. These surfaces may be flow-banding parallel fractures, perhaps caused by movement occurring on some flow bands due to stresses as the lava flows downhill while cooling from the outside, leading to fracturing along these flow bands.

The aspect ratio of the flow in cross-section is almost 1 and the flow shape can be approximately described as a hemi-cylinder (Fig. 3.10). Despite the high viscosity of rhyolite this is still an unexpectedly high aspect ratio for a flow, strongly suggesting confinement of the flow to produce this shape. Confinement could be caused by surrounding bedrock, although there appears to be very little of this. More probable is that most of the flow was confined by ice. The flow is columnar jointed in its entirety, with columns orientated in a radial pattern, indicating that the flow was likely sub-glacial rather than just ice-contact in setting (e.g. Lescinsky and Sisson, 1998). All striae in the flow indicate columnar jointing formation from the outside inwards, even in the lowest most central visible parts of the flow, demonstrating that enough coolant (melt water) came from the outer edges of the lava flow that a lower tier of columns did not form at the base of the flow. These features indicate that G1 was emplaced in a subglacial tunnel as an 'esker-like' flow (e.g. Lescinsky and Fink, 2000).

FTIR data indicate that water concentrations are low in G1, where the lava is not hydrated. This could be linked to ice thickness above G1 of ~30-80 m (Table 3.3), however it may instead indicate that the flow was degassed, thus it could be overlain by thicker ice but there would be no way to tell this from the FTIR data. There are no vesicles present in the lava flow; vesicles would be expected from a degassing flow under shallow ice conditions, as implied by the FTIR data. This suggests that either the lava was originally low in volatiles or it may have degassed higher up at the vent, before flowing down to its current position (e.g. Tuffen et al., 2010), and in either case we cannot determine a palaeo ice-thickness. The flow is more than 200 m above sea level on a steep mountain side where lake water could not pond, pointing to a subglacial origin.

G2 is the same composition as G1, and only 500 m west, so it likely erupted into the same or very similar environment. The orientation of columnar jointing here and throughout the valley would seem to indicate that a glacier filled the valley when this rhyolite flow was emplaced. Much of the lava in Hvalvörðugil valley, including the part that became lobe G2, appears to have flowed down the interface between the mountain and the glacier (Fig. 3.21; as G1 probably has, but the slope of the mountain here was shallower and the lava was likely confined to a tunnel). The glacier then supported the flow, causing columnar jointing to form perpendicular to this contact, horizontally at the base and vertically in the upper part, where there appears to be a bench or break in slope on the mountain.

The columns at G2 are much larger than those in G1, with wider spaced striae, indicating a slower cooling rate. This may be due to G2 representing the interior of a large flow so cooling more slowly, or having a smaller supply of melt water due to its orientation in relation to the glacier (or both?). The more crystalline nature of the lava at G2 would support a slower cooling regime.

The rhyolite that forms G1, G2 and the rest of the lava in Hvalvörðugil valley has been dated at 116 ka ± 20 ka, using the $^{40}Ar/^{39}Ar$ method (Walker, 2011). This time period was colder than the modern climate conditions and within this time a number of colder periods, associated with increases in the occurrence of ice-rafted debris in north Atlantic sediments, occurred (Chapman and Shackleton, 1999; Helmke et al., 2002). This may have resulted in the Vatnajökull glacier being larger than it is currently, filling Hvalvörðugil valley and providing a subglacial environment for the contemporary volcanism.

The evidence for the formation environment of R1 at Rauðufossafjöll comes partly from its location: it is high, >1000 m above sea level, and precipitous. The extremely small striae spacing, the smallest ever measured in columnar jointing, and extremely glassy nature of

the lava that forms these columns (Fig. 3.23) demonstrate very rapid cooling, likely related to ice-contact or subglacial cooling. No perlite or hydrated grey rhyolite has been found here indicating that melt water was able to escape soon after formation, probably due to the lava's precipitous location. Low volatile concentrations and lack of vesicles indicate either very thin ice conditions (~33 m thickness) or previously low volatile content lava. It is unlikely that the lava flowed from elsewhere to become emplaced here as it is perched on the top of a hill.

3.5 Interpretation of column measurements

All measurements from rhyolite columnar jointing differ significantly from those reported in studies of basaltic columnar jointing. Both *W* and *S* are significantly smaller than those measured in basalts and *W/S* ratios span a significantly wider range than in basaltic columnar jointing studies (Goehring and Morris, 2008; Fig. 3.26). Subglacial rhyolite columns more often have 5 than 6 sides, whereas those in basalts may have 5 but more commonly have 6 sides (Beard, 1959; Goehring and Morris, 2008).

These differences may be caused by either differences in composition or eruption environment. The aim of this study is to understand more about the eruption environment, but to do this it is vital to understand how different compositions may affect columnar jointing. Here we attempt to explain why there are such dramatic differences between subaerial basaltic and subglacial rhyolitic columnar jointing and what these differences might mean in terms of the columnar jointing process, the eruptive environment and lava composition.

All rhyolite columns have smaller *W* and *S* than in basalt columnar jointing. There are two probable causes of this: the first is the difference in environment as rhyolite lavas in this

study erupted or were emplaced subglacially, and so were surrounded by water and/or ice which caused rapid cooling. Previous studies of basalt columnar jointing are of subaerial flows or lower colonnades, which have not experienced inundation with water or other external cooling agent (e.g. Ryan and Sammis, 1978; DeGraff and Aydin, 1993; Grossenbacher and McDuffie, 1995; Goehring and Morris, 2008) and so will have cooled less rapidly. The second possible cause of the substantially different column measurements may be related to the different compositions, and so different physical and chemical properties of rhyolite and basalt, as both W and S can be changed by physical properties of the lava. All the properties that may affect W and S are listed in Table 3.5 and are discussed individually below. When thinking about how properties affect fracturing it is easier to understand how the density of fractures changes. This relates to W as a higher density of fractures causes smaller columns and so smaller W.

3.5.1 Factors affecting W

Lava is a visco-elastic material and as it cools stress accumulation is countered by viscous relaxation of the lava (e.g. Dingwell, 1996; Lore et al., 2000). Thermal stress caused by cooling shrinkage of lava is given by:

$$\sigma_{therm} = \frac{E\alpha\,\Delta T}{(1-\nu)}, \qquad (2)$$

where σ_{therm} is the thermal stress, E is Young's modulus, ν is the Poisson's ratio, α is the coefficient of thermal expansion and ΔT is the temperature interval over which thermal stress accumulates (Spry, 1962; Fink, 1983).

This build up of stress from contraction is countered by viscous relaxation of the lava with time:

$$\sigma = \sigma_i \exp(-Et/2\eta), \qquad (3)$$

where η is the lava viscosity, t is the time over which the relaxation occurs and σ_i is the initial stress in the material that relaxes over time (Lore et al., 2000). Thus stress will build up over a temperature step ΔT (eq. 2), some of this stress will relax over the time it takes for the lava to cool by ΔT (eq. 3). The faster the cooling rate the less time it will take for the lava to cool by ΔT and so the less time, t, there will be for stress relaxation (eq. 3) and more stress will build up. So for faster cooling rates more stress will build up over a cooling step (as less stress will be relaxed) requiring more closely spaced fracturing to relieve this build-up of stress, resulting in smaller W values. Fracture will occur when the accumulated contractional stress becomes greater than the tensile strength of the lava (Lore et al., 2000). This demonstrates how W is affected by cooling rate.

Another result that becomes clear from Eq. 3 is that lava with a higher viscosity takes more time to relax a certain amount of stress. Viscosity of lava is strongly composition and temperature dependent and differs drastically between rhyolite and basalt (but is also affected by crystallinity, bubbles/vesicularity and water concentration). For a given cooling rate, and so stress accumulation rate due to thermal contraction, more stress will accumulate in a more viscous lava. This will cause more fracturing in order to release this larger stress accumulation. Thus lava with a higher viscosity will have more closely spaced fractures, and so smaller W, at a given cooling rate.

Related to the cooling rate is the property of thermal diffusivity, the ability of a material to lose heat by conduction. Rhyolite has slightly higher thermal diffusivity than basalt, ranging 0.5-12 $\times 10^{-6}$ m^2s^{-1} in basalt and is 1.0×10^{-6} m^2s^{-1} in rhyolite (Hanley et al., 1978; Bagdassarov and Dingwell, 1994; Keszthelyi, 1994; Mostafa et al., 2004; Whittington et al., 2009) i.e. rhyolite is able to lose heat slightly faster. Higher thermal diffusivity will cause faster cooling rates and so smaller W in rhyolite. As the difference in thermal diffusivity is small it may not have a noticeable effect on sizes of columns, especially when compared to large differences in externally forced cooling rates. There is no obvious difference in thermal expansivity values for differing lava compositions (ranging 4.5-9.5×10^{-6} $°C^{-1}$), and so little effect on W (e.g. Ryan and Sammis, 1981; Bagdassarov and Dingwell, 1992; Alidibirov et al., 1997; Goehring and Morris, 2008).

Eq. 2 shows that both Young's modulus and Poisson's ratio will directly affect the amount of thermal stress that will accumulate in the lava during cooling, thus affecting the density of fractures and so W. There is some disagreement in the columnar jointing literature as to the extent of variation of Young's modulus and Poisson's ratio between mafic and felsic lavas (e.g. Lescinsky and Fink, 2000; Hetényi et al., 2012). There are few measurements of these physical properties of lavas and they almost exclusively concentrate on basalt, however, some comparison may be possible. Poisson's ratio is generally measured or calculated as 0.2 and Young's modulus is given as 50-78 GPa in basalt (Kulhawy, 1975; Schultz, 1993; Schultz, 1995; Lore et al., 2000; Goehring and Morris, 2008). Young's modulus and Poisson's ratio calculated from compressional and shear wave velocities for glassy dacite give similar values (79 GPa and 0.22 respectively) to those of basalt (Alidibirov et al., 1997). Similarly, measurements of Young's modulus and Poisson's ratio on soda-lime-glass (window glass) give very similar values (73 GPa and 0.23 respectively) to those from basalt (Rouxel and Sanglebœuf, 2000), which although a rather different composition from rhyolite (similar SiO_2 content but higher Na_2O and CaO and lower

Al_2O_3, Fe_2O_3 and K_2O than rhyolite) hints that there may be little difference in these values between mafic and felsic lavas. However a value of just 20 ± 4 GPa was measured for the Young's modulus of a porphyritic crystalline andesite (Smith et al., 2009).

The tensile strength of the lava is also an important parameter controlling the spacing of fractures. Once the accumulated stress due to cooling contraction reaches the tensile strength of the lava it will fracture. This releases the strain which then proceeds to build up again. With lower tensile strength more fractures will be needed to release the stress build up, and so lava with lower tensile strength will display closer spaced fractures, and thus smaller *W*. However, there appears to be no published measurements of the tensile strength of glassy rhyolite. There appears to be little difference between basalt and granite in terms of tensile strength at about 8 MPa (Heuze, 1983; Schultz, 1993; Lore et al., 2000; Vásárhelyi et al., 2000; Goehring and Morris, 2008; Yan et al., 2012), but it is not certain that this would also be the case for glassy rhyolite.

Crystallisation may have some small bearing on the density of fracture spacing. It causes a volume decrease with respect to the same mass of glassy lava and would likely increase fracture density, and thus decrease *W*. The combined effect of cooling contraction and crystallisation contraction is -12% in the interval 0–91% crystals, 1,200–800°C (Mattsson et al., 2011), and just 0.28% contraction will be due to thermal contraction. There is also a release of latent heat associated with crystallisation, this would buffer the cooling rate, causing a slower cooling rate which is known to increase *W*.

Crack widths, the space between two opposing column faces formed by the same fracture event, may also have some bearing on *W*. Larger fracture spacing will accommodate more contraction and so will result in fewer fractures needed to relieve the stress due to contraction. It is not clear what might control crack width, but it could be related to the

elastic layer thickness below the advancing crack tip, which may depend on the temperature gradient. Crack width has not been measured in this study or reported in previous studies, and may be affected by any post emplacement movement or collapse of the lava flow.

3.5.2 Factors affecting *S*

The main factor affecting striae spacing, *S*, is cooling rate. A fracture initiates at one temperature and terminates at a higher temperature. The faster the cooling rate the higher the temperature gradient and so the closer these two temperatures will be physically, resulting in smaller striae spacing, *S*.

These temperatures of fracture initiation and termination are unknown for both basalt and rhyolite although there have been previous estimates and guesses. Goehring and Morris (2008) assumed that the temperature gap between fracture initiation and termination in basalts was constant and estimated this as 11 ± 4 °C based on the increasing of *S* near the margins of flows and a model of conductive cooling of the lava. This same method cannot be applied in this study, as the modern preserved margins are not the original flow margins. They also postulated that fracture initiation occurs at T_g, given as 750°C. It may be more likely that Tg represents fracture termination (e.g. Budkewitsch and Robin, 1994; Hetényi et al., 2012), i.e. the point at which the lava undergoes the transformation from solid, brittle behaviour to more liquid/melt-like ductile behaviour.

It is probable that fracture initiation and termination temperatures are not fixed but affected by both the cooling rate and the lava composition. Fracture initiation temperatures may be affected by the cooling rate, as a slower cooling rate will lead to more viscous relaxation, thus contraction will not build up sufficiently to initiate a fracture until a lower

temperature, lowering the fracture initiation temperature. Lore et al. (2000) show that this change in fracture initiation temperature could be more than 150 °C in basalt for modelled cooling rates in an 8.7 m thick flow (depending on the tensile strength of the lava), with fracture initiation temperatures ranging ~600-760 °C.

The tensile strength of the lava may also affect the fracture initiation temperature. A higher tensile strength would mean more cooling must take place before stress builds up sufficiently to cause fracture initiation, so higher tensile strength would result in lower fracture initiation temperatures and thus larger *S*, if the fracture termination temperature were unaffected.

Fracture termination is postulated to occur at Tg, this means that anything affecting Tg may affect the fracture termination temperature. Tg will vary with composition, being higher in rhyolite than basalt (Giordano et al., 2008); and volatile content, with higher volatile content lowering Tg (Giordano et al., 2005). A faster cooling rate will result in higher Tg (Dingwell, 1996) and so a higher fracture termination temperature.

Thus faster cooling rates will result in higher temperatures for both fracture initiation and termination, which may go some way towards balancing out the effect of cooling rate on the temperature interval that *S* represents. However, compositional differences may also cause changes in fracture initiation temperature due differences in tensile strength (although we don't know if there is a difference, or what it might be) and changes in fracture termination temperature, Tg, due to composition and dissolved volatile content.

Within a narrow compositional range *S* may be a very useful comparative indicator of cooling rate, but it may not be applicable when comparing across a wide range of lava

compositions. It must also be noted that it will only indicate the temperature gradient (and so cooling rate) across the probably narrow, and unknown, temperature range of fracture.

Table 3.5 Properties that affect *W* and *S*. The third column shows how *W* or *S* are affected if the factor in the first column is increased.

Factor	Rhyolite vs. Basalt	How property affects *W* or *S* if factor increased
Cooling rate	Environment dependent	Decreases *W* and *S*
Viscosity	Higher in rhyolite	Decreases *W*
Thermal expansivity	Similar	Decreases *W*
Thermal diffusivity	Slightly higher in rhyolite	Decreases *W*
Tensile strength	Possibly similar?	Increase *W*; may increase *S*
Crystallisation	More in basalt	Decreases *W*, but latent heat released may increase *W*
Young's modulus	Similar	Decreases *W*
Poisson's ratio	Similar	Decreases *W*

3.5.3 Modelling of cooling and stress accumulation

In order to understand more quantitatively how composition-dependent physical factors (viscosity and thermal diffusivity) may affect *W* some simple numerical modelling was undertaken, using Microsoft Excel. In order to eliminate the environmental aspect of cooling on columnar joint formation, and understand the changes in fracture density, and so *W*, due only to differences in composition, a simple conductive cooling model was used. This treats the lava flow as an infinite half-space, ignoring the complicating factors of the base upwards cooling, and models the cooling at seven different depths within the lava flow: 0.1, 0.5, 1.0, 2.0, 3.0, 4.0 and 5.0 m.

The equation used to model this was one of simple conductive cooling from Goehring and Morris (2008), their equation 3:

$$T = T_0 + (T_i - T_0)\, erf\left[\frac{z}{\sqrt{4\kappa t}}\right] \qquad (5)$$

where T is temperature, T_i is the initial or eruption temperature of the lava flow, T_0 is the fixed temperature of the upper boundary of the half space (i.e. at $z = 0$), z is the depth in metres, t is the absolute time in seconds and κ is the thermal diffusivity. No effect of latent heat is taken into account in this cooling equation. The change in properties with temperature, other than viscosity, i.e. thermal diffusivity (Ryan and Sammis, 1981) and the coefficient of expansion, are likely small and are not compensated for.

For the rhyolite viscosity was calculated as a function of temperature, using the composition of the G1 rhyolite lobe from Hvalvörðugil valley (Table 3.1). The rhyolite lavas are glassy and have low crystallinity throughout, indicating that cooling did not cause crystallisation. The viscosity of rhyolite was therefore calculated from the whole rock composition with the empirical model of melt viscosity of Giordano et al. (2008). This model is calibrated up to viscosities of 10^{14} Pa s, but is used at viscosities exceeding this value.

For basalt, unlike the glassy rhyolites, cooling does cause an increase in crystallinity. Crystals increase viscosity, and at a critical proportion of crystallinity, usually estimated at around 40-50% volume of crystals, the viscosity vastly increases (e.g. Marsh, 1981; Costa, 2005). For this reason the relative viscosity model for crystal bearing magmas of Caricchi et al. (2007) was used for the basalt composition:

$$\eta_r = \eta_{app} / \eta_{melt} \qquad (6)$$

where η_r is the relative viscosity, calculated using the model of Caricchi et al. (2007), η_{app} is the apparent viscosity and η_{melt} is the melt viscosity. The basalt composition used is that of the Hreppar lava (Mattsson et al., 2011) and the temperature-crystallinity relation calculated by Mattsson et al. (2011) for this composition was used to input into the equations of Caricchi et al. (2007). η_{melt} was calculated using the viscosity model of Giordano et al. (2008) using the residual melt compositions due to crystallisation as calculated by Mattsson et al. (2011).

The model of Caricchi et al. (2007) is only valid up to 80% crystallinity, however at higher crystallinities the basalt will effectively become solid. At this point it will deform by diffusion creep, rather than viscous flow. A viscosity based on diffusion creep is used (Jull and Keleman, 2001) for higher crystallinities:

$$\eta = 0.5A^{-1/n} \exp\left(\frac{Q}{nRT}\right) \qquad (7)$$

where A is the pre-exponential factor, Q is the activation energy, n is the creep exponent (n= 1 for diffusion creep), R is the universal gas constant and T is the absolute temperature. The transition is taken as the cross-over point between the two models (see Fig. 3.27a). This occurs at a temperature of 1085 °C and a crystallinity of 74.8 %. Grain size is important in diffusion creep, this is not taken into account in equation 7, and is a limiting factor in this study.

Q, A and n were calculated by combining separate values from fine grained anorthite (Wang et al., 1996) and diopside (Dimanov et al., 2007) aggregates using the equations of Tullis et al. (1991), with a 60:40 clinopyroxene:plagioclase ratio:

$$n_a = 10^{(f_1 \log n_1 - f_2 \log n_2)} \quad (8)$$

$$Q_a = \frac{Q_2(n_a - n_1) - Q_1(n_a - n_2)}{(n_2 - n_1)} \quad (9)$$

$$A_a = 10^{[\log A_2(n_a - n_{11}) - \log A_1(n_a - n_2)]/[n_2 - n_1]} \quad (10)$$

Where A is the pre-exponential factor, Q is the activation energy, n is the creep exponent, f is the volume fraction, the subscripts a , 1, and 2 are for the aggregate, phase 1, and phase 2, respectively. This was necessary as no studies for diffusion creep on basalt could be found, and due to the importance of grain size in creep studies on diabase/ dolerite were not suitable (e.g. Mackwell et al., 1998). The calculated and individual values of Q, A and n used in the modelling are shown below in Table 3.6.

Table 3.6 Values used to calculate and the calculated values of A, Q and n for diffusion creep viscosity.

Phase	A	Q	n	f	Source
Anorthite	3.80E+10	4.20E+05	1.3	0.4	Wang et al., 1996
Diopside	1.15E-01	2.90E+05	1	0.6	Dimanov et al., 2007
Calculated combined	2.04E+03	3.38E+05	1.11065		Tullis et al., 1991

The temperature-viscosity relations calculated above were then used in the discretised visco-elastic stress equation of Lore et al., (2000), their equation 16:

$$\sigma_{t \geq t_i} = \left[\sigma_i + \varepsilon_i\left(\frac{E}{1-\nu}\right)\right] \exp\left[\frac{-E(t-t_i)}{(1-\nu)\eta_i}\right] \quad (11)$$

where σ_t is the stress at time t, $(t\text{-}t_i)$ is the time step of the discretised stress equation, υ is Poisson's ratio, E is Young's modulus, η is the viscosity, and ε is strain, where, $\varepsilon = \alpha\, \Delta T$, where α is the coefficient of thermal expansion and ΔT is the change in temperature over time $(t\text{-}t_i)$.

To take account of the contraction caused by crystallisation in basalts α is increased to 2.0×10^{-3} m^2s^{-1} for the temperature interval 1150-1075 °C before becoming 6.5×10^{-7} m^2s^{-1} at temperatures below 1075 °C. This reflects a 15% volume decrease over this temperature interval (Mattsson et al,. 2011). However, no stress builds up in this temperature interval, so this has no effect on the stress accumulation model (see Fig. 3.27b below).

The input parameters: E, υ, α, η, Ti and κ, can be changed to quantitatively determine how these affect the build up of stress in the lava flow, and so how these will affect W and even S. However, E, υ, were not changed as they are constant regardless of composition, only the variation in η, and κ with composition were tested.

The results from equation 8 can be dependent on the size of the time steps, $(t\text{-}t_i)$, with larger time steps resulting in build-up of stresses at lower temperatures. However, at increasingly smaller time steps the models converge, so the smallest feasible time steps were used in the creation of the cooling model for rhyolite. This involved experimenting with various time steps until the results were independent of the time step. Full details of cooling steps used in the models can be found in appendix 4. For the basalt viscosity model 1°C intervals were used, this sets the size of the time interval, using the inverse of equation 5 to calculate time taken to reach a given temperature. These time steps are generally of a similar magnitude, though slightly larger, as those that are shown to converge in experiments, and so give a good approximation.

Table 3.7 Physical properties of lavas used to model cooling and stress.

Property	Basalt	Rhyolite	References
K	2.0×10^{-3} m^2s^{-1} 6.5×10^{-7} m^2s^{-1}	1.0×10^{-6} m^2s^{-1}	Goehring and Morris (2008); Whittington et al. (2009)
Ti	1150 °C	900 °C	
H	Hreppar composition	G1 composition	Mattsson et al. (2011) and this study
A	7.0×10^{-6} $°C^{-1}$		Goehring and Morris (2008)
E	68 GPa		Lore et al. (2000)
N	0.2		Goehring and Morris (2008); Lore et al. (2000)
η model	Crystallinity-dependent viscosity, and creep	Melt viscosity	Caricchi et al. (2007); Jull and Keleman (2001); Giordano et al. (2008) See text for discussion.

The first stress accumulation model is that of a basalt (Fig. 3.27b) with the properties outlined in Table 3.7 above. Stress starts to build up once temperature has fallen sufficiently and this temperature of stress build up decreases with increasing depth. This is because deeper parts of the lava cool more slowly and therefore build stress more slowly as there is more time for viscous relaxation of the stresses. These stress models continue building up stress indefinitely, however, in reality the lava will fracture once the stress build-up reaches the tensile strength of the lava, around 8-10 MPa (e.g. Lore et al., 2000; Goehring and Morris, 2008). Stress reaches values similar to tensile strength (10 MPa) at approximately 640 °C for z = 0.1 m, and 550°C at z = 5 m depth.

The next graph (Figs. 3.27c) shows how the basalt stress accumulation model responds if κ is changed to the rhyolite value. The higher thermal diffusivity, as in rhyolite, causes the lava to cool more rapidly which causes stress to build up at slightly higher temperatures. Stress reaches 10 MPa at approximately 650 °C for z = 0.1 m, and 555°C at z = 5 m depth, showing a small but measureable difference.

Figure 3.27d is the stress model for rhyolite using the properties outlined in Table 3.7. Here stresses builds up at significantly lower temperatures compared with the basalt stress accumulation model. Stress reaches 10 MPa at approximately 605 °C for z = 0.1 m, and 505°C at z = 5 m depth. The major difference between the basalt (Fig. 3.27b) and rhyolite

(Fig. 3.27d) stress models is caused by the difference in viscosity, with thermal diffusivity having little effect by comparison in the resulting stress models.

The viscosity of rhyolite is higher than that of basalt above 1090 °C, but at lower temperatures rhyolite is less viscous that basalt. This is because the basalt will crystallise and starts to become a solid (i.e. extremely high viscosity) at temperatures where non-crystalline rhyolite will still act as a liquid. This is demonstrated by the temperatures measured in basalt lava lake crusts, which may be higher than the liquidus of rhyolite, but the basalt is solid at these temperatures (e.g. Peck and Minakami, 1968; Wright and Okamura, 1977).

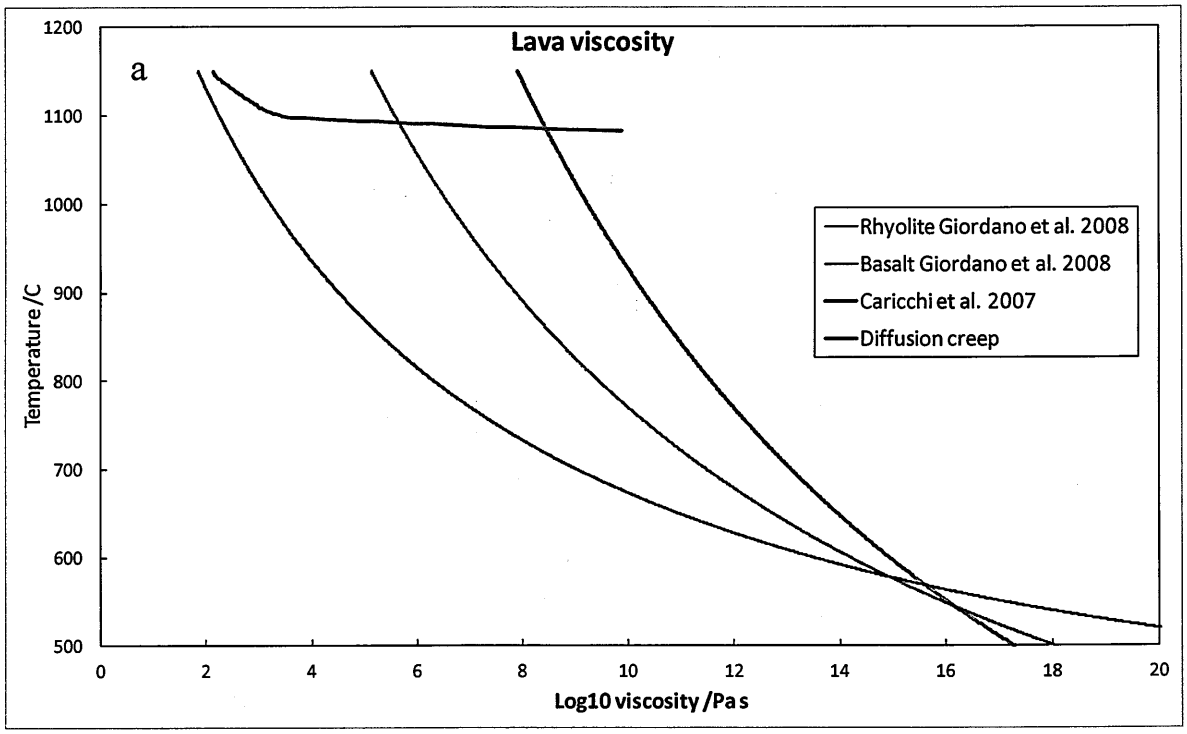

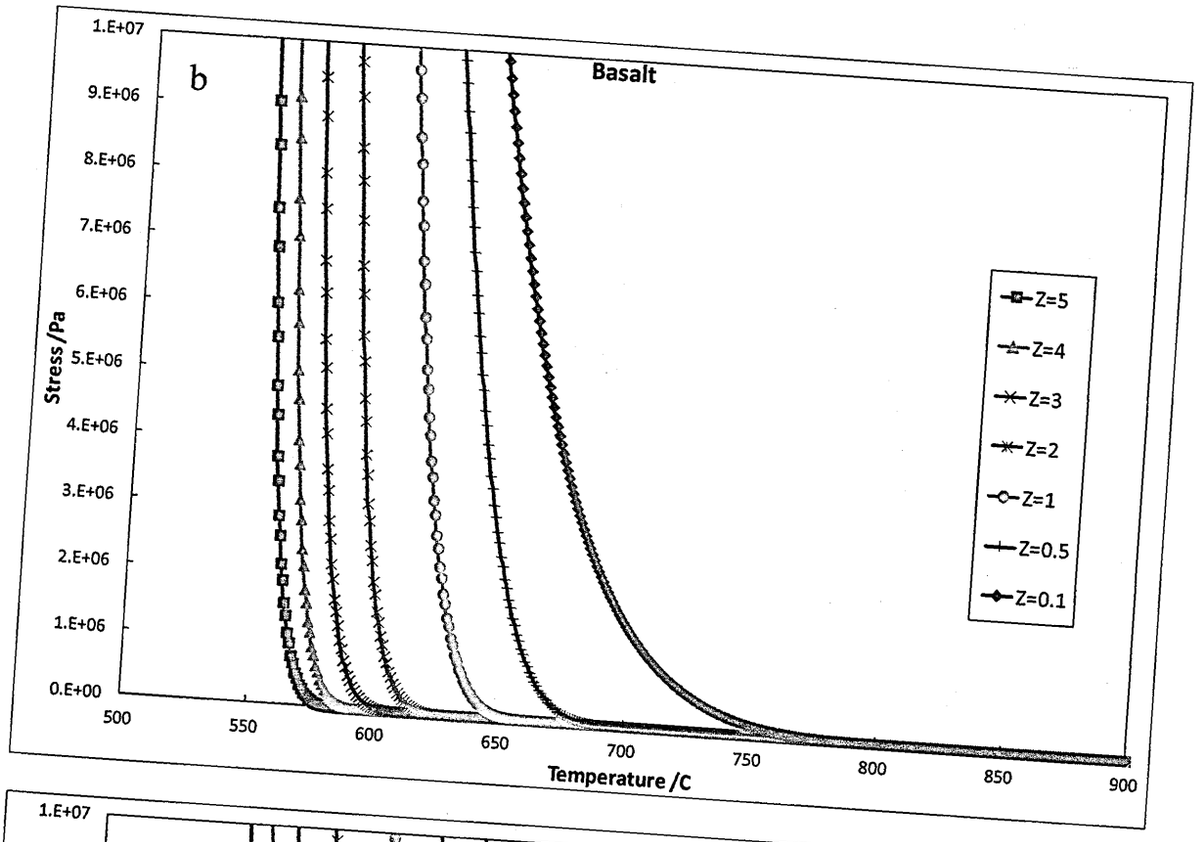
b
Basalt
Stress /Pa
Temperature /C
1.E+07
9.E+06
8.E+06
7.E+06
6.E+06
5.E+06
4.E+06
3.E+06
2.E+06
1.E+06
0.E+00
500
550
600
650
700
750
800
850
900
Z=5
Z=4
Z=3
Z=2
Z=1
Z=0.5
Z=0.1

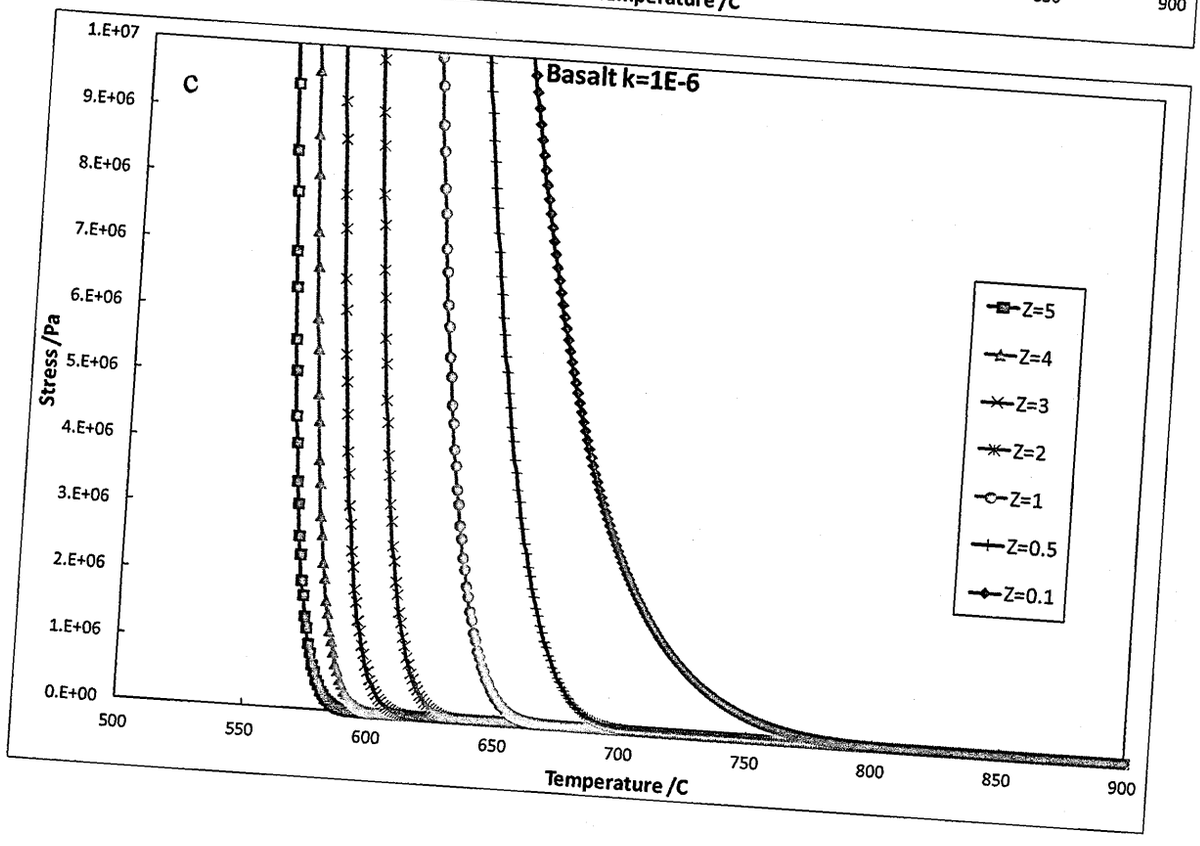
c
Basalt k=1E-6
Stress /Pa
Temperature /C
1.E+07
9.E+06
8.E+06
7.E+06
6.E+06
5.E+06
4.E+06
3.E+06
2.E+06
1.E+06
0.E+00
500
550
600
650
700
750
800
850
900
Z=5
Z=4
Z=3
Z=2
Z=1
Z=0.5
Z=0.1

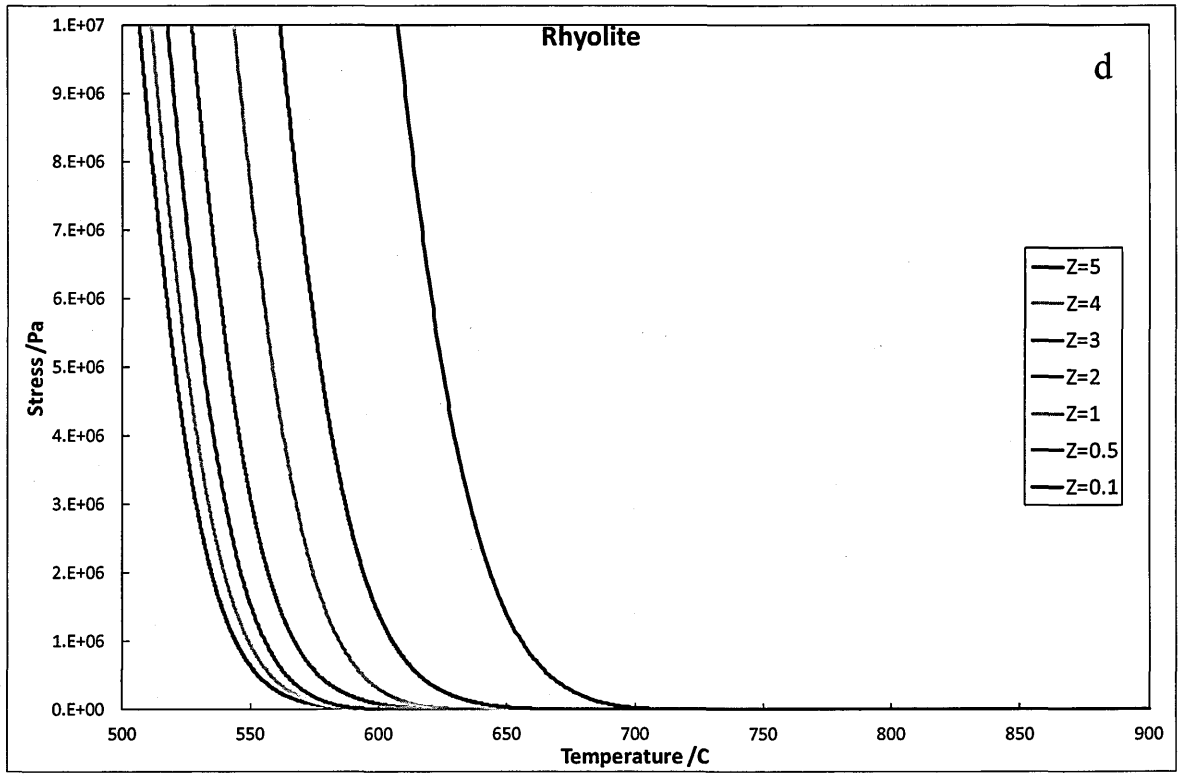

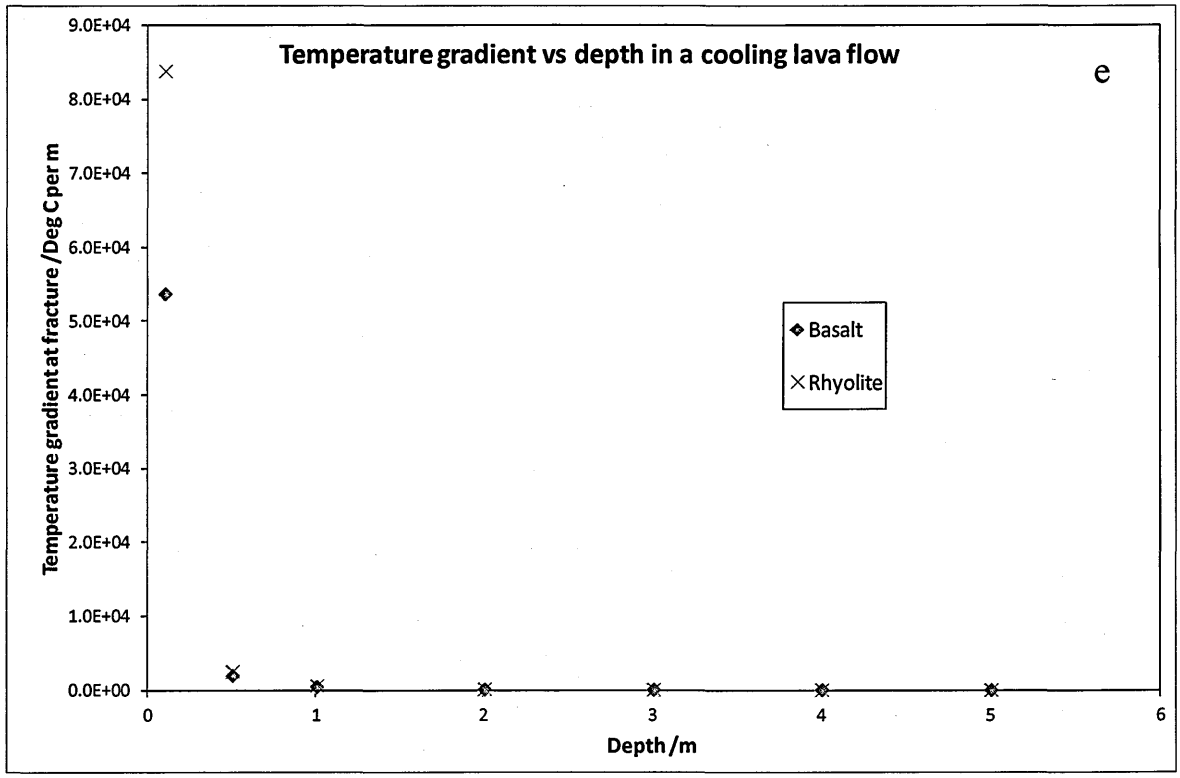

Fig. 3.27 Graphs of viscosity and stress accumulation versus temperature for various depths (in metres), z, within the lava flow. a) Viscosity of rhyolite (pink line) and basalt (various models as discussed in main text, blue and green lines) with temperature. Below approximately 1090°C basalt becomes more viscous than rhyolite for a given temperature, due to its crystallinity. b) Stress accumulation model using basalt properties of thermal diffusivity, eruption temperature and viscosity. c) Changing thermal diffusivity to the rhyolite value, this causes stresses to build up at slightly higher temperatures. d) Using a rhyolite viscosity model and properties to model stress accumulation, causes stress accumulation at lower temperatures than in the basalt model. e) A graph of temperature gradient at the time of fracture (when stress has accumulated to 10 MPa), versus depth in the lava flow, for both the rhyolite and basalt models. Both show that in the outer parts of the lava flow

temperature gradients are significantly larger and so striae heights will be much smaller, whereas below 1 m depth the temperature gradient and so the striae will be more uniform in size.

The stress accumulation models show that fracture initiation occurs at a range of temperatures spanning 100 °C for just the first 5 m of a lava flow. This is contrary to the assumption of Goehring and Morris (2008) that fracture initiation in basalt occurs at a single temperature of 750 °C. In fact the stress accumulation models show that stress is only just beginning to build up at temperatures of 750 °C in the shallowest parts of the basalt flow, so this may be a significant overestimate of the fracture initiation temperature.

This shows that the initiation temperature of striae forming fracture cycles is strongly controlled by cooling rate, as postulated above in section 3.5.2 (Factors affecting *S*). Unless the fracture termination temperature is similarly affected by the cooling rate, so that striae represent a fixed ΔT, then striae heights might not be a reliable way to study changes in cooling rates or temperature gradients even within a single lava flow. Furthermore as a fixed temperature isotherm migrates into the lava in proportion to the square root of time, these results show that the fracture front actually migrates more slowly than that.

Fig.3.27e shows the temperature gradient at the time of fracture plotted against depth in the lava flow. At shallow depths in the lava flow, for both basalt and rhyolite, large temperature gradients dominate. This will result in small striae heights, but below about 1m there is a relatively constant temperature gradient by comparison, which would result in more constant larger striae. This links well with the observations that striae heights are considerably smaller in the outer 1m of a lava flow but become much more uniform in size inside of this (Goehring and Morris, 2008).

The stress accumulation models clearly show that visco-elastic stress build up in cooling lavas is significantly different in basalt and rhyolite. This is due to the difference in viscosity between the two lava compositions, as changing the thermal diffusivity makes little difference to the stress accumulation model.

The viscosity difference of basalt and rhyolite is perhaps slightly counter-intuitive at first, as generally rhyolite is regarded as more viscous than basalt, which is true at their eruption temperatures. This higher viscosity in basalt than rhyolite at temperatures relevant to stress build-up and fracture will result in more stress building up in basalt (less stress relaxation, see eq. 3). This will result in more dense fracturing in basalt to relieve this stress and so smaller W in basalt for a given cooling rate i.e. at a given cooling rate rhyolite columns should be larger in diameter than basalt columns (for the same cooling environment). This therefore enables us to explain the observations of Hetényi et al. (2012) who find a correlation between composition and column side width. They expected that more felsic columns should have smaller W, but they observed the opposite. They explained this by 1) more felsic lavas having a lower eruption temperature (which likely only has a small effect on the stress build-up in the lava), and 2) more felsic lavas generally forming thicker flows because of their higher viscosity when erupted, so having slower cooling rates. The models from this study (Fig. 3.27) show that the viscosity is probably the controlling factor in altering W, but it causes larger columns in more felsic lavas not smaller. This is due to higher viscosities in basalt than rhyolite at temperatures relevant to stress accumulation and fracture (Fig. 3.27a).

It is important to note that the crystallisation in basalt, which causes a significant volume shrinkage in the lava, does not affect the stress accumulation. Crystallisation might cause a considerable build up of stresses, however it occurs at high temperatures, where the lava is

able to viscously relax these stresses. Thus the crystallisation of basalt lava has no impact on the spacing of columnar joints.

3.5.4 *W*, *S* and *W/S* in rhyolite columnar jointing

W and *S* in all the rhyolite columns from this study are significantly smaller than those from the basalt columnar jointing data of Goehring and Morris (2008). Despite the many factors that might affect these (see above) the main cause of this difference is likely to be the much higher cooling rates in the rhyolite columns from this study resulting from their environment. An investigation of subaerial rhyolite columnar jointing might confirm how much other properties might affect *W* and *S*, with the main property other than cooling rate affecting *W* likely being viscosity, but this will act to make rhyolite columns larger due to its larger viscosity at temperature of fracture formation.

The ratios of *W/S* differ significantly between basaltic and rhyolitic columnar jointing. *W/S* ranges 5.2 – 14.1 from the data of Goehring and Morris (2008) and is suggested to range between 5 – 20 by Grossenbacher and McDuffie (1995). In rhyolite this ratio spans 5.2 – 51.8, but individual flows have fairly constant *W/S* ratios even where they show a range of column sizes (e.g. G1 and G2, Fig 3.26). *W/S* is unlikely related solely to compositional effects, or properties dependent on composition, as G1 and G2 (and in fact all the rhyolites in this study) have extremely similar compositions (see Table 3.1) therefore it must be related to changes in cooling rate, i.e. environment.

W/S ratios in most of the rhyolite columns in fact overlap with basalt values except for those from lobe R1 which have the most extreme *W/S* values. These have a wide range of *W/S* values of 36.6 – 51.8, much wider than for any other flow, but still distinctly different. Column sizes, *W*, here are similar to those in G1, B1 and B2 yet striae heights are very

much smaller. One possible reason for this is that the cooling rate is sufficiently rapid and viscosity so high that most of the rhyolite columns (with the exception of G2) have reached their minimum possible column size, i.e. there is very little or no viscous relaxation of stress so only equation 2 (section 3.5.1) is relevant in this case. Smaller columns than these could still be formed but would then need to have smaller crack spacing i.e. the distance between two opposite column faces formed in the same fracture event would need to be smaller.

3.5.5 Number of column sides

In basaltic columnar jointed lava flows there are generally more 6 sided columns than 5 or 7 sided ones, although there are cases of flows with more 5 sided columns (Beard, 1959; Goehring and Morris, 2008; Hetényi et al., 2012). However, in 4 out of 5 flows from this study the rhyolite columns have more 5 sided than 6 sided columns, excluding measurements from areas with preferred orientation fractures which are discussed below (section 3.4).

Hexagonal 6 sided columns reduce the fracture surface energy needed to accommodate contraction fracturing (e.g. Jagla and Rojo, 2002). Therefore columns would form into hexagons if they were not limited in some way, however, this is clearly not the case for the columns in rhyolite from this study. In general columns tend to have fewer than 6 sides on average even if their modal number of sides is 6 (e.g. Hetényi et al., 2012). This may be related to the way in which columnar jointing initiates with T-shaped fracture junctions which then change into Y-shaped fracture junctions deeper into the flow, as the fractures propagate inwards from the cooling edge (Aydin and DeGraff, 1988). The T-shaped junctions form initially because a fracture initiating under bi-axial tension will interact with other already formed fractures, once it gets close enough, and will curve to meet a pre-

existing fracture at right angles. In brittle materials the fractures intersect at a right angle because there is no tensile component of the stress field normal to the free surface of a fracture, so the maximum tensile stress is parallel to the pre-existing fracture and thus causes the new fracture to curve round to open perpendicular to the pre-existing fracture (Hull, 1999).

As the fractures initiate with 90° intersections they will form roughly tetragonal columns which change to form hexagonal columns with 120° column side intersection angles. However, it appears that this process is somehow retarded in at least 4 of the 5 rhyolite flows of this study. This is unlikely related to chemical or physical properties of the lava, e.g. viscosity, as G1 and G2 show different column side numbers, but have exactly the same composition. In fact all the rhyolites in this study have very similar compositions (see Table 3.1). Instead it is more likely related to cooling rates in these rhyolite flows. G2 has the largest column sizes and striae heights of all the flows studied, thus indicating it had a slower cooling rate than the other flows. This slower cooling may have allowed more time for the column sides to change and adjust to a more efficient organisation, thus creating more 6 sided columns. However Hetényi et al., (2012) did not find any correlation between W and mean number of sides in their data, although they compared mean rather than modal number of sides. Averaged across all their measurements from all lava flows they found the modal number of column sides was 6.

3.6 Preferred orientations in columns

Preferred orientations of fractures occur in two of the columnar jointed lobes, G1 and B1 These alter the way in which the columns form when associated with them. In lobe B1 the preferred fracture orientation is formed by pseudopillow fracture systems (e.g. Watanabe and Katsui, 1976; Lescinsky and Fink, 2000; Mee et al., 2006; Forbes et al., 2012) with

striae-bearing master fractures forming the large preferred orientation fractures and subsidiary fractures with curved striae forming vertically and perpendicularly to the master fracture. Columns that form abutting a pseudopillow fracture system are generally 4 sided with two of the sides being subsidiary fractures and one being part of the master fracture (Fig. 3.7).

In G1 preferred orientation fractures occur in various places throughout the flow. They are prominent on the top central part of the flow, parallel with the sides of the lobe striking approximately north-south (Fig. 3.17). They can also be seen on the sides of the lobe perpendicular to the elongate direction of the flow, striking roughly east-west. These fractures are not pseudopillow fracture systems as in B1, they are less planar than master fractures and do not show curved striae on the column sides normal to these preferred orientation fractures. They have separate column faces related by angles close to 180° and continuous striae across separate columns and are probably the same as or similar to sheet-like fractures described by Lodge and Lescinsky (2009).

Columnar jointed lava showing preferred orientations of fractures within it indicates that the stress field is not purely bi-axial, there is some non-uniformity in the stress field. This seems particularly true for G1 where multiple, parallel, preferred orientation fractures occur together. Flow-related stresses may be the cause of these fractures. For G1 their location and orientation can be linked to collapse of ice supporting walls leading to the formation of the preferred fracture orientations at the top centre of the flow, and down slope flow stresses leading to preferred fracture orientations at the edges of the flow lobe.

A notable feature of the preferred orientation fractures at G1 is how they affect *W* and so *W/S*. Column side widths for cross cutting fractures are always larger than those that form along the preferred orientation fracture. This is probably due to cross cutting fractures

simply forming between two preferred orientation fractures, so their length is determined partly by the spacing of these preferred orientation fractures rather than purely by environmental and physical properties of the lava. The larger *W* values in turn result in larger *W/S* values. Columns associated with preferred orientation fractures in both G1 and B1 tend to have 4 or 5 sided columns.

The majority of lobes on Bláhnúkur show preferred orientations of fractures, these have also been called sheet-like fractures (Lescinsky and Fink, 2000; Lodge and Lescinsky, 2009; Fig 2). These are likely related to the steep emplacement slope of these lobes, and mean that although many of the lobes on Bláhnúkur appear polygonally jointed they do not show true columnar jointing. These types of fractures appear common in subglacial rhyolite (e.g. Fig 8 of McGarvie et al., 2007) and other felsic and intermediate lavas (Lescinsky and Fink, 2000; Lodge and Lescinsky, 2009) and yet previously unobserved in basalt. This is likely related to the higher viscosity of rhyolite at its eruption temperature allowing the stresses to be maintained rather than relaxed or the lava to freely flow downhill.

3.7 Differences between columnar jointing in rhyolitic and basaltic lava flows

There are a number of key differences between rhyolite and basalt lava cooling fractures and their development. These are discussed below and can be summarised in terms of differences in entablature formation, ductile fracture, and the general lack of columnar jointing in subaerial rhyolite lava flows.

Entablature, a common feature in basaltic lava flows that interact with water, does not appear to occur in rhyolite lavas from similar environments (e.g. Sæmundsson, 1970; Long and Wood, 1986; Lyle, 2000). In basalt the interaction of pseudopillow fracture systems and columnar jointing produces some shapes commonly associated with entablature, such as chevron fracture patterns. They also produce an irregularity in the orientations of columns and contribute to cube-jointing (see chapter 4). These chevron fracture patterns and other irregularly oriented columns do not occur in rhyolite, possibly because the curved striae on the subsidiary fractures do not extend more than a few centimetres from the master fracture (Fig. 3.6). These show the relative influence of two different cooling directions, one downward and the other normal to the master fracture, which cause the inclined columns to form against master fractures in entablature in basalt (see chapter 4, sections 4.3.1.3 and 4.4.3.2). In rhyolite, the downward cooling dominates, forming vertical columns abutting vertical pseudopillow fracture systems. Other patterns observed in entablature such as fans, rosettes etc. (e.g. Spry, 1962; DeGraff and Aydin, 1987) also do not occur in rhyolite-water interaction settings, perhaps due to the influence that upper colonnade fractures have in basalt but not in rhyolite (e.g. Fig. 16 of DeGraff and Aydin, 1987).

Ductile fracture has not been observed in any of the column-bounding fracture surfaces in rhyolite from this study. This is a common feature in basaltic columnar jointing, occurring as rough portions of the striae (Ryan and Sammis, 1978), and also on master fractures in pseudopillow fracture systems (Forbes et al., 2012; see also chapters 2 and 5, sections 2.3.1 and 5.3.1). This may be related to the high viscosity or lower temperatures of rhyolite.

Columnar jointing is not common in subaerial rhyolite lava and only appears to occur in very thick rhyolite lava flows (e.g. Bonnichsen and Kauffman, 1987; Allen and McPhie, 2002). Incremental cooling contraction fractures do occur in subaerial rhyolite but as

individual planar fractures rather than columnar jointing (see Fig. 3.28). This indicates stresses in the lava flow that are not due purely to cooling contraction, rather like those that form the preferred orientation fractures. Slow emplacement coupled with cooling will result in a non-uniform, high stress environment during the cooling of a rhyolite flow, which will not be conducive to columnar joint formation. Rhyolite may only stay hot enough to relax these flow emplacement stresses in the centres of very thick flows such as those described by Bonnichsen and Kauffman (1987), (see their Fig. 5).

Fig. 3.28 Striae on a planar fracture from a subaerial rhyolite flow, Laugahraun, Landmannalaugar, Iceland. This flow has many striae, indicating brittle incremental fracture, but no columnar jointing. Some hackle to the right of the hammer indicate fracture propagation from left to right.

This then leads to questions about how and why columnar jointing forms in small subglacial rhyolite flows. These cool faster and so should not be able to relax their flow stresses in the timescales of cooling and this does appear to be true in some cases such as the preferred orientation fractures in some of the Bláhnúkur lobes. It may be that the

confinement and support of the ice in subglacial settings reduces flow stresses and allows columns to form. Dacites showing columnar jointing also often occur in confined settings, such as those intruded into wet sediment (e.g. Goto and McPhie, 1998; Stewart and McPhie, 2003) or supported by ice (e.g. Lescinsky and Fink, 2000). Purely subaqueous rhyolite does not commonly form columnar jointing (e.g. Scutter et al., 1998) but those intruded into wet sediment may do (DeRita et al., 2001).

3.8 Conclusions

In summary, a number of factors will affect column side width, *W*, these include cooling rate as well as physical properties that vary between different lava compositions. Cooling rate is the main factor causing the large difference between subaerial basalt and subglacial rhyolite column sizes. The lower viscosity in rhyolite at temperatures relevant to stress build-up will cause larger column sizes than in basalt, for a given cooling rate. Therefore the considerably smaller *W* values for rhyolite columns are very strongly influenced by high cooling rates.

Striae height, *S*, is also affected by physical properties of lava, they may affect the temperature interval over which *S* occurs, thus complicating the interpretation of *S* values between different lavas and even different cooling rates. It appears that for subglacial rhyolite columns *W* does not vary greatly and *S* may be a more reliable way to compare relative cooling rates in lava flows of similar composition.

Some interesting environmental information may be shown by *W*/*S* variations. The range in *W*/*S* ratio may be related to a change in *S* due to more rapid cooling, without a change in *W* as the minimum column side may have formed for most of the rhyolite columns.

Columns in rhyolite in this study tend to have fewer sides than those from basalt columnar jointing studies. This is possibly due to the more rapid cooling that formed these rhyolite columns not allowing the normal transition from tetragonal to hexagonal columns.

Preferred orientation fractures that sometimes occur with rhyolite columnar jointing may be caused by pseudopillow fracture systems or by stresses in the lava related to flow or melting of supporting ice. These are caused both by the environment of emplacement and by the differing physical properties of rhyolite, in particular its higher viscosity.

Columnar jointing may only form in rhyolite that is either supported in some way, e.g. by ice or sediment, or that can cool slowly and relax its flow stresses before it cools through the temperature region where columnar jointing starts to form.

3.9 Highlights

- Cooling rate is the main factor causing the large difference between subaerial basalt and subglacial rhyolite column sizes.
- The lower viscosity in rhyolite, at temperatures of stress build-up, will cause larger column sizes than in basalt, for a given cooling rate.
- Columns in rhyolite in this study have fewer sides than those from basalt columnar jointing studies, possibly due to more rapid cooling.
- Columnar jointing may only form in rhyolite that is supported in some way or can relax its flow stresses.

Chapter 4: Entablature

Abstract

Entablature is the term used to describe zones or tiers of irregular jointing in basaltic lava flows. It has previously been linked to lava-water interaction and forms when water from rivers dammed by the lava inundates the lava flow surface, or from lava-water interaction in subglacial settings. There has been no previous in-depth study of the different types of fractures present in entablature tiers or the detailed mechanisms of how they form, and these are the focus for this chapter.

A number of different fracture types have been recognised in entablature outcrops from the Búrfell lava and older lava flows in Þjórsádalur, southwest Iceland. These are striae bearing column bounding fractures and pseudopillow fracture systems that themselves consist of two different fracture types: master fractures with dimpled surface textures and subsidiary fractures with curved striae. The interaction of pseudopillow fracture systems and columnar jointing in the entablature causes chevron fracture patterns commonly observed in entablature. Cube-jointing is a more densely fractured version of entablature, which likely forms when more coolant enters the hot lava. The entablature is generally flanked by both an upper and lower colonnade of straight, regular, vertical columns.

Closely narrow striae widths and dendritic crystal textures in the entablature tier indicate rapid cooling. Master fracture surfaces show a thin band with an evolved composition, mineral textures in this band show evidence of quenching of this material. We interpret this as gas-driven filter pressing of late stage residual melt. This segregation melt percolates into an area of low pressure prior to the formation of a master fracture. This melt is then

quenched by an influx of water and/or steam when the master fracture fully opens. Master fractures appear to be the main conduit for coolant entering the lava flow during entablature formation.

4.1 Introduction

Entablature is a term first used by Tomkeieff (1940) to describe the zones or tiers of irregular jointing that occur in the upper parts of some basalt lava flows from the Giant's Causeway area of Northern Ireland. Long and Wood (1986) describe entablature as part of a flow that exhibits smaller column diameters and more irregular fracture patterns than those of the colonnade. Tomkeieff (1940) divided entablature bearing flows into entablature and colonnade, splitting entablature into pseudocolumnar above and curvicolumnar below. However, we use the nomenclature of Spry (1962) and Long and Wood (1986) to divide flows into an upper and lower colonnade and central entablature (Fig. 4.1).

Entablature jointing consists of irregularly orientated columnar joints or hackly/cube-jointing, generally sandwiched between two tiers of regular colonnade columns (e.g. Fig. 4.1). Entablature is found in basaltic lava flows all over the world, and has been studied in the Columbia River Basalt province (Swanson 1967; Long and Wood 1986; DeGraff et al. 1989), Iceland (Sæmundsson, 1970; Lyle, 2000), British Tertiary Igneous province (Tomkeieff, 1940; Lyle, 2000) and India (Sen and Sabale, 2011), among other locations.

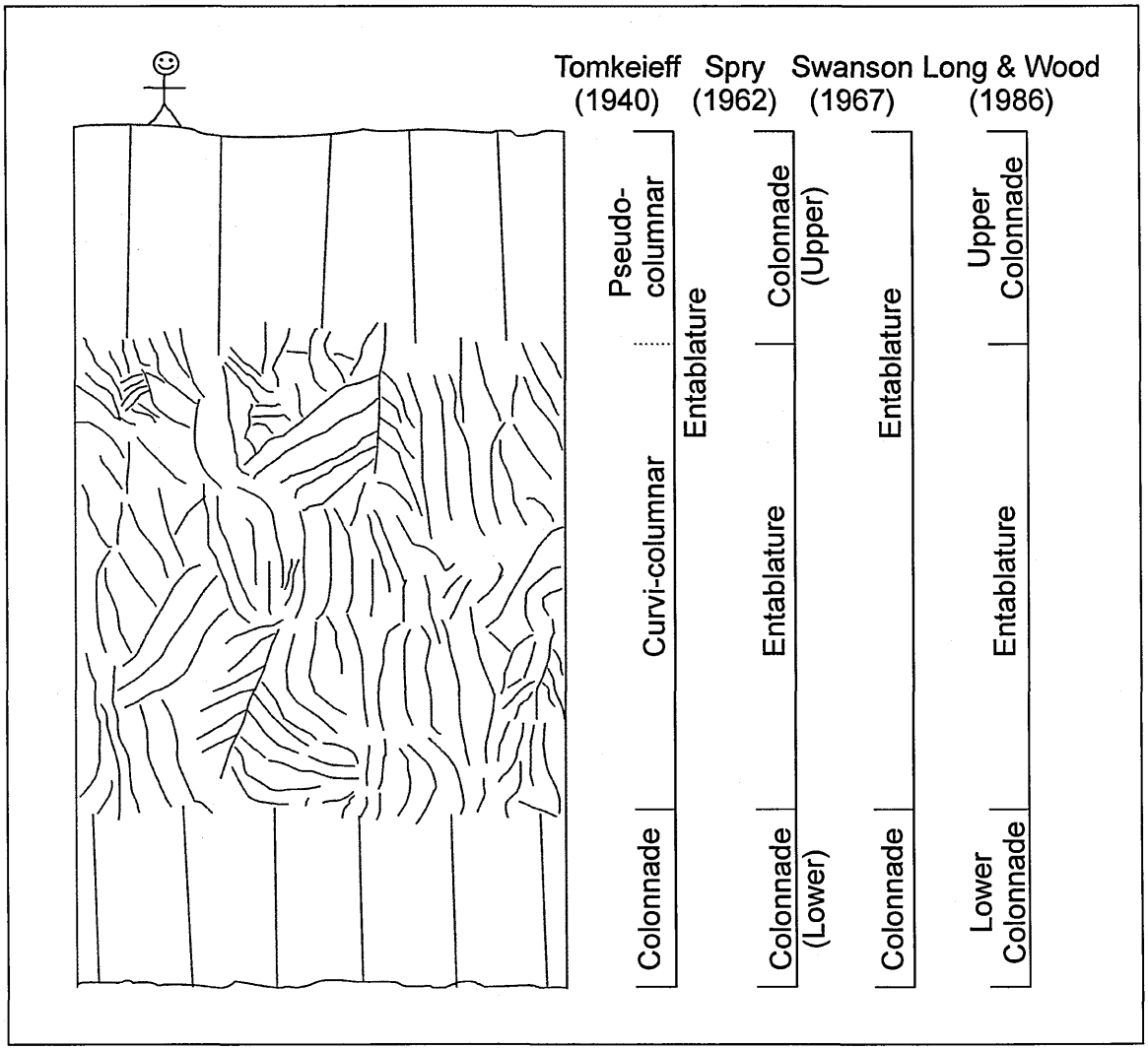

Fig. 4.1 Entablature sketch diagram showing nomenclature and how it has changed. We use the nomenclature of Spry (1962) and Long and Wood (1986). Person not to scale.

Evidence from petrographic studies suggests entablature is formed during rapid cooling of hot lava. Dendritic oxides and glassy mesostasis in entablature indicate rapid cooling (Long and Wood, 1986; DeGraff et al., 1989; Lyle, 2000). Conversely in lower colonnades, glassy mesostasis is scarce or absent and dendritic oxides are not observed, indicating a much slower rate of cooling (Swanson, 1967; Long and Wood, 1986). This rapid cooling in entablature is interpreted as the product of water interacting with ponded lava, most likely from damming of rivers by the lava flows and subsequent flooding of the lava flow surface by this dammed river water (Sæmundsson, 1970; Long and Wood, 1986; Lyle, 2000). Cooling in entablature has been demonstrated to occur from the top downwards, using striae (chisel mark) propagation directions (DeGraff and Aydin, 1987;

DeGraff et al., 1989). Palaeoenvironmental and palaeoclimatic evidence suggest wet conditions, and palaeotopography shows evidence of conditions that were conducive to ponding of lavas, in places where entablature commonly forms (Lyle, 2000), as entablature is typically formed in water-rich environments that encourage ponding of lava, such as river valleys. Entablature tiers also appear to be a common feature of subglacial basaltic lava flows (e.g. Smellie et al., 2006; Smellie, 2008), further supporting the link to a lava-water interaction origin.

However, no previous work on entablature has provided an in-depth study of fractures and fracture mechanisms in the entablature tiers of lava flows. Some reference is made to the presence of 'master' fractures (Spry 1962; DeGraff et al. 1989; Lyle 2000), early formed fractures from which columns appear to sprout, forming patterns of entablature columns. The type and formation mechanisms of these master fractures are not known, but they appear to have a strong influence on the fracture patterns formed in entablature, such as chevron and fan patterns (e.g. Spry, 1962; DeGraff and Aydin, 1987). Data that can help with understanding cooling rates, such as column side width or striae spacing, is lacking from entablature due to difficulties in finding striae on entablature columns, despite a wealth of equivalent data from colonnade columns (e.g. DeGraff and Aydin, 1993; Grossenbacher and McDuffie, 1995; Goehring and Morris, 2008).

This study aims to investigate the fracture types in entablature more fully, linking these with key features that enable a more insightful understanding of entablature-type jointing and its environment of formation.

4.2 Geological setting

Two sets of basaltic lava flows are studied, the first are those described and mapped by Sæmundsson (1970, his Fig. 1) as the entablature of interglacial lavas in the Hreppar area, southwest Iceland (Fig. 4.2 and 3). The other are two outcrops of the tholeiitic Búrfellshraun-Þjórsárdalshraun lava (referred to as 'Búrfell lava' in the following), at Hjálparfoss and Gjáin, in the Þjórsádalur valley, southwest Iceland (Vilmundardóttir et al., 1985; Lyle, 2000; Thordarson and Höskuldsson, 2002; Fig. 4.3). Table 4.1 contains XRF compositional data for all the flows studied. All display prominent entablature tiers and a lower colonnade, whereas outcrops of the Búrfell lava also display well-developed upper colonnades. The entablature tier dominates all the flows studied, being at least half of the thickness of the flow.

Table 4.1 XRF composition data for basalts from the Búrfell and the localities of Sæmundsson (1970). In each case a single representative sample was used. The negative LOI (loss on ignition) likely results from the iron in these relatively young, fresh lavas oxidising.

Sample	Búrfell		Galtafell						
wt. %	Hjálparfoss	Gjáin	Flow 4	Flow 3	Flow 2	Sheepfold	Þjorsaholt	Miðfell	Skarðsfjall
SiO_2	49.25	49.89	49.17	49.63	49.36	50.76	51.52	49.03	50.74
TiO_2	1.800	1.536	3.467	3.454	2.896	3.265	3.204	2.846	3.161
Al_2O_3	14.53	14.90	13.00	13.14	13.36	13.23	13.06	13.32	13.12
Fe_2O_3	12.45	12.22	16.15	16.20	15.46	15.46	15.12	15.30	15.03
MnO	0.194	0.191	0.233	0.230	0.227	0.225	0.227	0.221	0.226
MgO	7.37	7.73	5.26	5.39	6.06	5.09	4.79	6.06	4.86
CaO	12.34	12.80	9.67	9.82	10.63	9.36	9.02	10.51	9.03
Na_2O	2.20	2.03	2.53	2.59	2.43	2.69	2.79	2.41	2.72
K_2O	0.23	0.14	0.59	0.59	0.38	0.67	0.75	0.39	0.71
P_2O_5	0.265	0.144	0.410	0.424	0.293	0.402	0.402	0.281	0.386
LOI	-0.55	-0.75	-0.61	-0.38	-0.34	-0.32	-0.40	-0.56	-0.14
Total	100.08	100.83	99.87	101.09	100.76	100.83	100.47	99.82	99.83

We focus our study particularly on the Búrfell lava (Fig. 4.2 and 3). This is a spectacularly well exposed, well preserved post-glacial flow (3500 years old; Thordarson and Höskuldsson, 2002), which allows ideal access to cooling fractures and their fractography, without the interference of later post-cooling fractures. We also describe the fractures of

cube-jointing style entablature tiers (Fig. 4.7) from the sites of Sæmundsson, 1970. Although these are not as well preserved as those from the Búrfell lava they give insight into the different types of entablature.

The Búrfell lava in the Þjórsádalur valley is part of the Tungnaá lavas from the Veiðivötn fissure system at Barðabunga central volcano. It is a very large flow with a volume of 6.5 km^3, it flowed about 70 km from its source (Thordarson and Höskuldsson, 2002). The outcrops at Hjálparfoss and Gjáin are at in the distal parts of this flow (Halldorsson et al., 2008; their Fig. 1). The Búrfell lava features a large field of rootless cones, or pseudocraters, which occur at and to the north of Hjálparfoss, either side of road 32 (Thordarson and Höskuldsson, 2002; see Fig. 4.4). Rootless cones form when lava flows over wet or marshy ground interacting with the water producing explosive interactions and accumulating cones of spatter and scoria (e.g. Greeley and Fagents, 2001), indicating the whole area was wet when this lava flow was emplaced.

Fig. 4.2 Section through the Búrfell lava at Gjáin. The vesicular upper part of the lava contains an upper colonnade, the lowest visible part of the lava shows a lower colonnade. The majority of the flow in dominated by an entablature tier between these two colonnades. Yellow metre rule for scale.

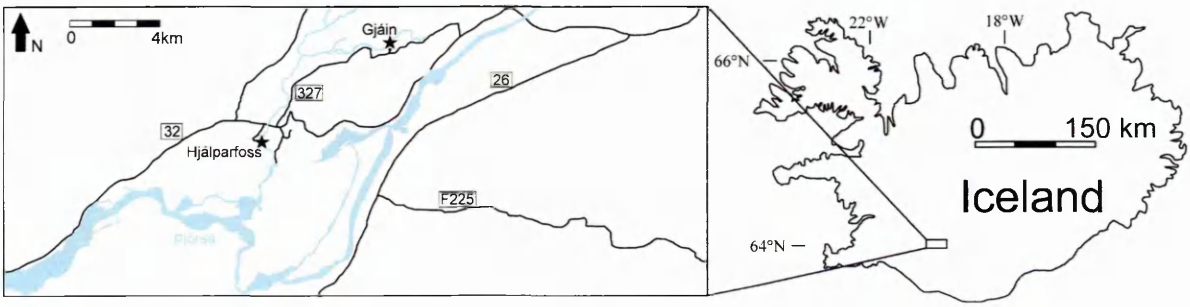

Fig. 4.3 Map of field locations in the Búrfell lava, Þjórsádalur valley, Iceland, showing Hjálparfoss and Gjáin marked by stars. Numbers in boxes are road numbers.

Fig. 4.4 Pseudocraters or rootless cones near Hjálparfoss, either side of road 32. North is to the right.

At Gjáin there are numerous older flows showing clear colonnade and entablature jointing tiers, demonstrating that lavas have a history of interacting with water, probably older incarnations of the river Rauðá, at this point (Fig. 4.5). At Gjáin and approximately 250 m upstream (north) of Gjáin the Búrfell flow has been eroded by the river and the lava flow can be seen to flow into a palaeo-valley and thicken out (Fig. 4.6). Where the lava is thinnest the upper and lower colonnades meet in the centre of the flow, however where the lava thickens out an entablature tier appears between the two colonnades, eventually becoming the thickest tier where the flow is at full thickness.

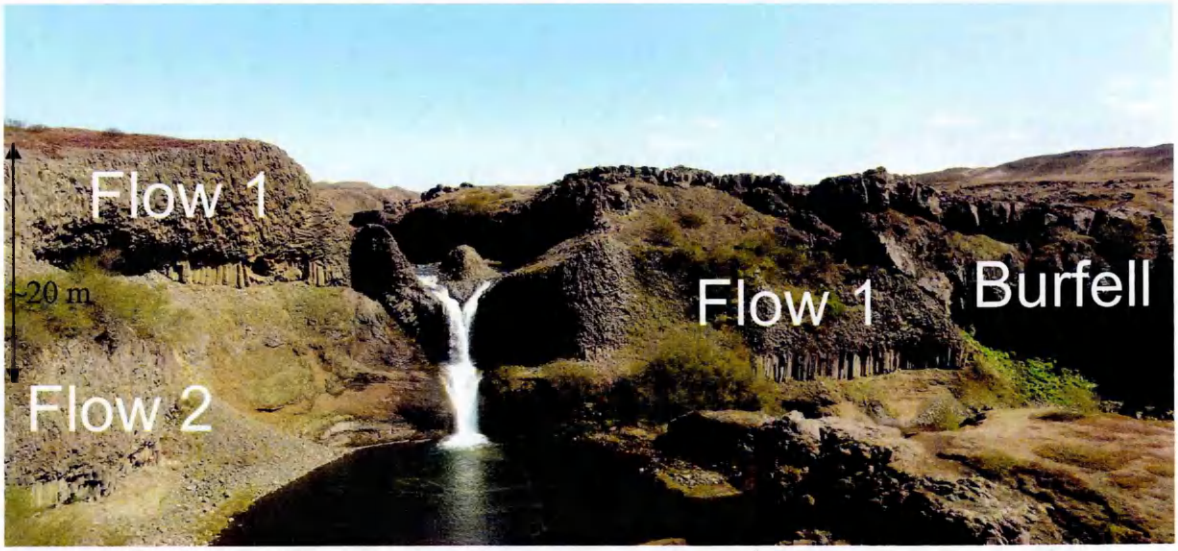

Fig. 4.5 Gjáin, showing older entablature bearing flows and the Búrfell lava. Both flow 1 and the Búrfell lava can be seen flowing into palaeovalleys, Fig. 4.6 gives a close up of this.

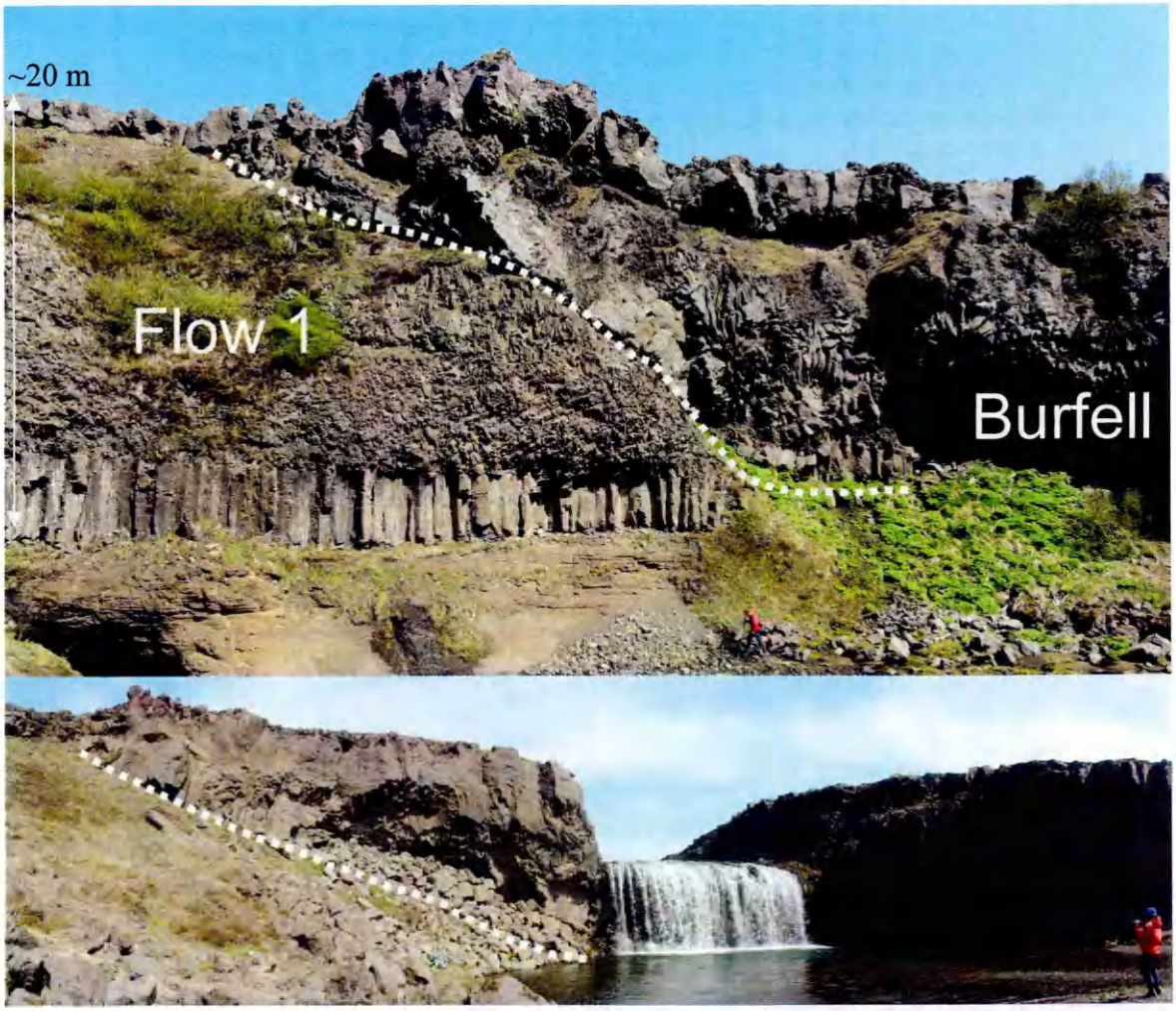

Fig. 4.6 Búrfell lava thickening into valleys both at Gjáin and approx. 250 m upstream of Gjáin. Person for scale is 2 m.

Little environmental evidence can be gained from the sites described by Sæmundsson (1970) as they are old, and eroded into mountains/hills/cliffs, preserving none of their original surroundings. The best exposed examples (Fig. 4.7) of cube-jointing visited are at Galtafell near Fluðir, Iceland (see Fig. 1 of Sæmundsson, 1970). This outcrop consists of 5 flows numbered 1-5 from the base upwards, 4 of which (flows 1-4) show an upper tier of cube-jointing style entablature. Large pillows occur at the base of flow 4 in one area, indicating this part of the flow entered a wet environment. However, in general there is usually no pillow-palagonite complex at the base of flows, which might show they flowed into ponded water, such as occurs in the Columbia River Basalt Province (Swanson, 1967; Long and Wood, 1986).

Fig. 4.7 Cube-jointing style of entablature from flow 4 at Galtafell, near Fluðir, southwest Iceland. No clear 'columns' can be seen in this type of entablature jointing as blocks are too densely fractured, but the same fracture types exist in this style of entablature as those in Fig. 4.1 entablature, i.e. column bounding fractures with striae and pseudopillow fracture systems. This image is from the centre of the entablature tier. Yellow metre rule for scale.

4.3 Results

4.3.1 Fractures in entablature and their fractography

Two fracture types have been consistently observed in entablature exposures documented for this study: column-bounding fractures (e.g. Ryan and Sammis, 1978; DeGraff and Aydin, 1987), and pseudopillow fracture systems (e.g. Watanabe and Katsui, 1976; Lescinsky and Fink, 2000; Forbes et al., 2012). They commonly interact, forming together into chevron-type geometric patterns in the Búrfell outcrops. Fractures were studied and differentiated from one another predominantly by their fractography – their fracture surface textures, descriptions of which follow below.

4.3.1.1 Pseudopillow fracture systems

Pseudopillow fracture systems in entablature consist of a large metre-scale master fracture and many subsidiary fractures with centimetre-scale spacing formed perpendicular to the master fracture (Forbes et al., 2012, chapter 2). Master fracture surfaces generally appear glassy in hand specimen, showing a glassy-looking selvage up to 2 mm thick. This is characterised by a rough surface texture typically consisting of sub-millimetre dimples separated by tiny septa of glassy material and less commonly by millimetre-scale glassy bulbous shapes. These fracture surface textures can be seen in both hand specimen and thin section (Fig. 4.8).

Subsidiary fractures in entablature form as a set of planar subparallel fractures perpendicular to the master fracture (Fig. 4.9; cf. Forbes et al., 2012). A set of subsidiary fractures occurs on both sides of a master fracture, propagating up to ~0.5 m away from the master fracture. Where master fractures are vertical, as is typical in the Búrfell outcrops,

subsidiary fractures also form vertically, breaking the lava into long vertical slabs either side of the master fracture (Fig. 4.9). Subsidiary fractures have curving striae on their surfaces, the direction of striae curvature on pseudopillow fracture systems with vertical master fractures is always in the same orientation in entablature. Striae are horizontal at the master/subsidiary fracture junction and curve upwards further away from the master fracture (Fig. 4.9).

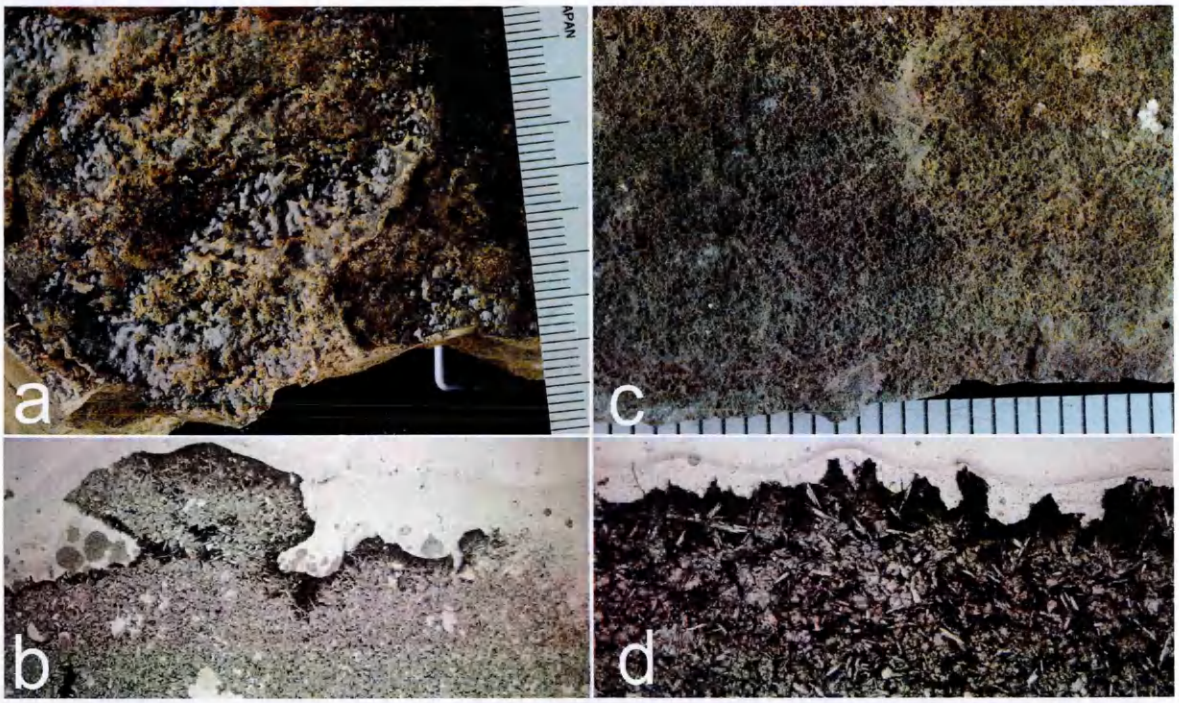

Fig. 4.8 a) and b) show the 'bulbous' master fracture surface texture in hand specimen and thin section respectively. c) and d) show the more common dimpled master fracture surface texture, thin septa of material separating the individual dimples are visible in d). Samples a and b are from the Búrfell lava at Hjálparfoss and samples c and d are from the Búrfell lava at Gjáin. The master fracture surface is darker glassy in appearance in a) and c) which corresponds to the dark finer grained areas in b) and d). b) and d) are plain polarised light thin sections normal to the fracture surfaces. a) and c) scale graduations are in mm, b) field of view ~8 mm across, d) field of view 2.8 mm across.

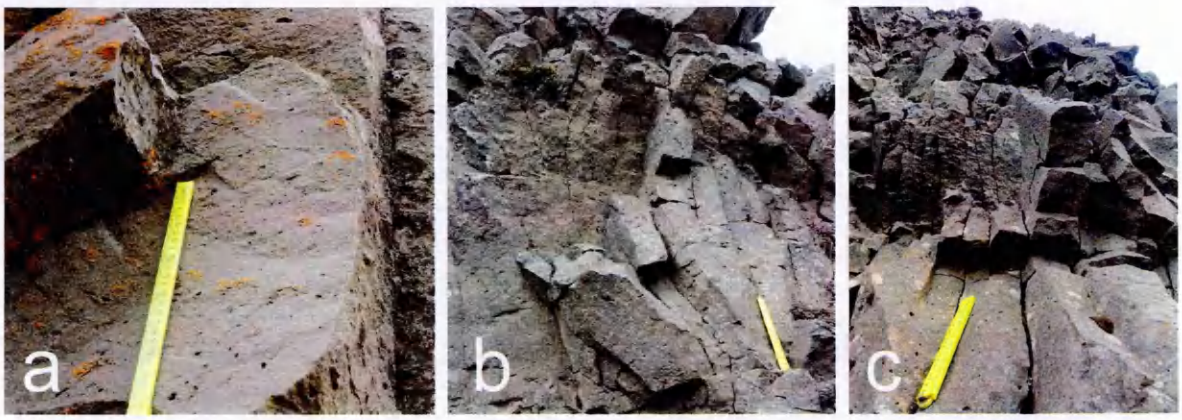

Fig. 4.9 Pseudopillow fracture systems: a) curved striae on the subsidiary fracture surface, master fracture is the vertical fracture at right hand side of image. Ruler is 25 cm long. b) and c) Pseudopillow fracture system with vertical master and subsidiary fractures. Images from the Búrfell lava at Gjáin. The master fracture, in the plane of the image, is cut by the subsidiary fractures which are

perpendicular to it. In c) in the right centre of the image three columns have formed bound by two subsidiary fractures. These columns bound by subsidiary fractures form the chevron shapes shown in Fig.7. Ruler is 25 cm long.

4.3.1.2 Column-bounding fractures

Column-bounding fractures occur throughout the entablature tier, forming irregularly oriented columns of decimetre to metre length. They may show centimetre-scale spacing of striae on their fracture surfaces, but often striae are not visible. There is much less topography on striae on column-bounding fractures in entablature than on column-bounding fractures of lower colonnade columns from the same flow (Fig. 4.10).

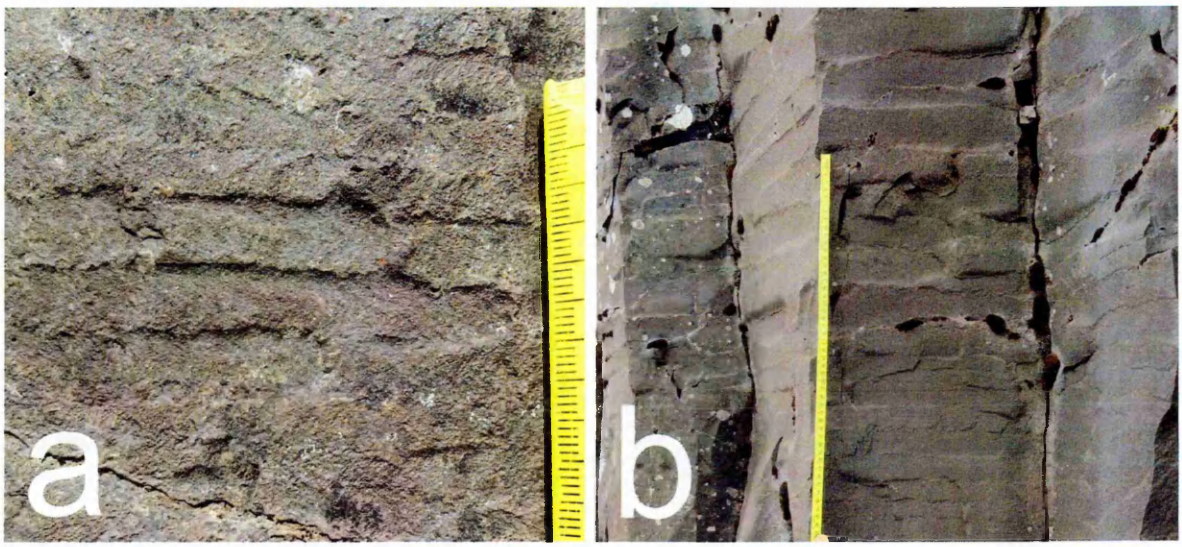

Fig. 4.10 Striae in a) entablature and b) lower colonnade from the Búrfell lava. Topography on the striae is much less on column bounding fractures in entablature than in colonnades and striae are much closer spaced in entablature, indicating more rapid cooling and fracturing. Scale graduations in mm in a) and scale is 0.5 m in b).

Column side widths and striae heights were measured, using a tape measure and digital callipers respectively, in outcrops of the Búrfell lava at Gjáin and Hjálparfoss. Measurements were generally taken only where pseudopillow fracture systems were absent from the immediate vicinity in the entablature so that only 'true' column-bounding fracture widths and their striae were measured. These measurements (Table 4.2) were taken from both entablature and colonnade column-bounding fractures. Mean stria width and mean

column side width are always smaller on entablature than on colonnade column-bounding fractures (e.g. Fig. 4.10).

Table 4.2 Striae widths. See appendix 5 for number of measurements and standard deviations.

		Mean	
Description	**Location**	**Striae /mm**	**Side /mm**
Colonnade	Gjain	27.9	385.3
Colonnade, northern, top of columns	Hjalparfoss	31.2	282.6
Colonnade, northern, base of columns	Hjalparfoss	15.7	271.5
Colonnade, southern	Hjalparfoss	31.0	420.3
Entablature	Gjain	13.0	118.1
Entablature	Hjalparfoss	26.2	221.8
Entablature near waterfall	Hjalparfoss	14.7	248.1
Entablature near waterfall 2	Hjalparfoss	16.2	269.3
Entablature, southern	Hjalparfoss	13.5	171.1
Subsidiary fracture measurements	Hjalparfoss	10.7	-
Cube-jointed entablature, flow 4	Galtafell	13.0	69.5
Cube-jointed entablature, flow 2	Galtafell	10.7	109.0
Cube-jointed entablature	Sheepfold	11.7	-
Colonnade, flow 4	Galtafell	58.5	372.4

4.3.1.3 Fracture interaction

In the Búrfell lava at Gjáin and Hjálparfoss vertically orientated pseudopillow fracture systems form in the entablature, with both master and subsidiary fractures forming vertically, the subsidiary fractures perpendicular to the master fractures. This results in slabs of rock up to ~10 cm wide either side of the master fracture. These slabs of rock are then fractured into 4 or 5 sided 'columns' with column-axes at 30-45° to the master fracture/vertical, measured upwards from the vertical master fracture. This creates the characteristic upward pointing chevron shape commonly seen here and in other entablature tiers (Figs. 4.9 and 4.11; e.g. Spry, 1962).

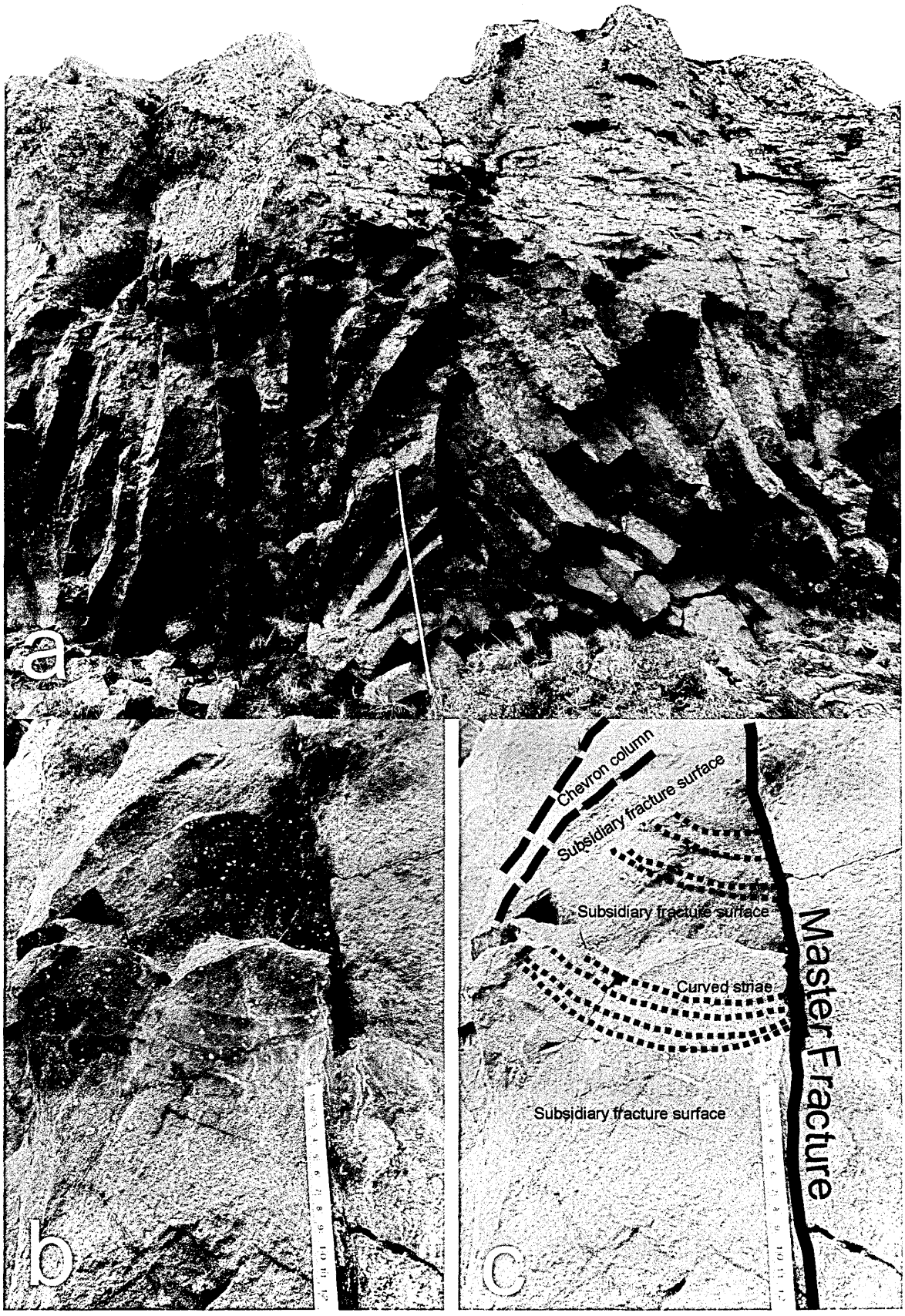

Fig. 4.11 Chevron fracture pattern from the interaction of columnar jointing and a pseudopillow fracture system, from the Búrfell lava at Gjáin. The vertical master fracture is in the centre of the images, perpendicular to the plane of the image, the subsidiary fractures are also vertical but parallel to the plane of the images. Sets of columns form between the subsidiary fractures at ~30 - 45° to the vertical causing the chevron pattern with b) and c) showing the curved chisel marks on the subsidiary fractures. Metre rule for scale.

4.3.2 Cube-jointing

Cube-jointing is a type of entablature that has the same fracture types as the entablature tiers described from the Búrfell lava, pseudopillow fracture systems and column bounding fractures, but has a different appearance. No 'columns' exist is this type of entablature, as fracture-bound blocks generally have an aspect ratio of about 1, due to a considerably higher fracture density in cube-jointing. This means that the chevron fracture patterns that form the Búrfell entablature do not occur in cube-jointing. Fractures bounding blocks may show centimetre spacing of striae, but striae are generally absent as in other entablature exposures in this study.

Kubbaberg, which is sometimes translated as *cube-jointing*, is the Icelandic name for entablature (e.g. Sæmundsson, 1970; Bergh and Sigvaldason, 1991; Smellie, 2008) but has also been used as a term for a more densely fractured type of entablature (Walker, 1993; Tucker and Scott, 2009). Here we use cube-jointing to indicate this more densely fractured type of entablature, to avoid confusion. Cube-jointing is studied predominantly in the exposures at Galtafell. Generally fracture surfaces are not as well preserved in these older lavas and may be covered in lichens and mosses.

Column bounding fractures and pseudopillow fracture systems are common in all cube-jointed outcrops visited. Master fractures form in all orientations and typically have a smaller surface area than those in the Búrfell lava. Master fractures may show rough or dimpled surface textures, although generally fracture surfaces are not well preserved. Subsidiary fractures here also form as sets of long planar parallel fractures, perpendicular to the master fracture, they may show curved striae on their fracture surfaces. Subsidiary fractures sometimes fan outwards rather than occurring as strictly parallel sets of fractures, (seen previously in pseudopillow fracture systems by Forbes et al., 2012, chapter 2); they

are commonly closer spaced than in the entablature of the Búrfell outcrops. In general pseudopillow fracture systems in cube-jointed entablature appear to form in an identical way to those in the Búrfell lava, but with smaller area master fractures that occur in more varied orientations.

4.3.3 Petrographic textures at fracture edges

Crystal textures at fracture edges have been examined in thin section and back-scatter electron images from lower and upper colonnades, entablature column bounding fractures and master fractures of pseudopillow fracture systems. Fracture edges are very well preserved in thin sections but much less well preserved in microprobe sections due to extra polishing involved in preparing these samples damaging the delicate fracture edges.

4.3.3.1 Master fractures

The dark glassy-looking material in hand specimen that forms at the fracture edge on master fractures contains some glass but also copious fine grained dendritic Fe-Ti oxides and dendritic and lath-shaped clinopyroxene and plagioclase crystals (Figs. 4.4 and 4.8). Dendritic oxides only occur in large quantities clustered at few millimetres from the master fracture edge, otherwise oxides form as small isolated dendritic and blocky crystals throughout the section. Plagioclase and clinopyroxene crystal shapes and sizes are highly uniform across a section away from the master fracture edge. Rounded olivines are found in all samples but not in the oxide-rich material immediately adjacent to the fracture edge of master fractures.

The fracture edge itself is characterised by a dimpled or ragged surface, with thin septa of the same dark, dendrite filled material forming dimples up to 1 mm across (Fig. 4.8). One

sample has a master fracture surface formed of glassy-looking bulbous shapes, which are visible in both thin section and hand specimen (Fig. 4.8). Each bulbous shape extends from the fracture surface on a thin neck of material, the outer part and the thin neck are formed from the dark dendrite rich lava and occurs at the master fracture edge on other fracture samples.

Features that appear like linked vesicle chains are visible in some samples occurring a few millimetres behind the master fracture edge. They have similar, but less abundant, dark oxide-rich material typical of the master fracture surfaces coating their surfaces. Vesicle chains often occur behind the main master fracture (Fig. 4.12b and g) and are generally parallel to the master fracture.

4.3.3.2 Entablature column-bounding fractures

Column-bounding fracture edges in entablature do not show any glassy-looking, oxide-rich material or spherulitic splays of plagioclase and clinopyroxene found at master fractures. Crystals are slightly finer grained up to 0.5 mm from the fracture edge but then become uniform in size throughout the section (Fig. 4.12). Small dendritic oxides occur throughout the entire section (up to 3 cm from the fracture edge) but are more abundant closer to the fracture edge. Slightly rounded olivines occur throughout the sections.

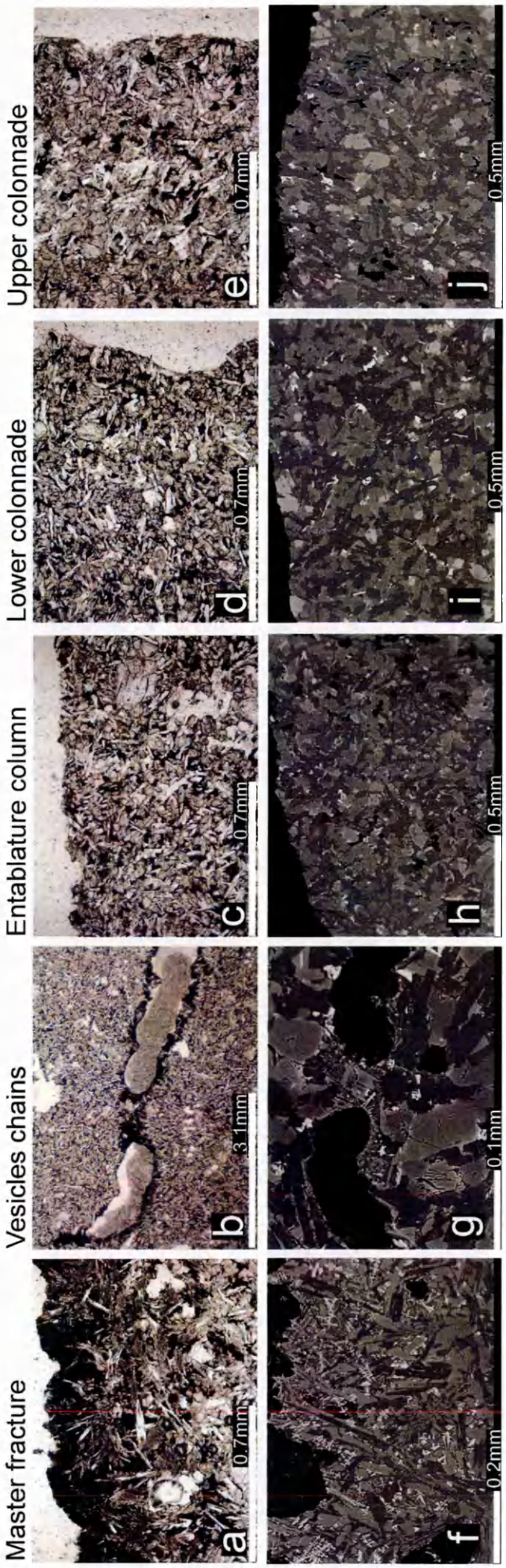

Fig. 4.12 Photomicrographs (a-e) and backscatter images (f-j) of different types of fractures that occur in entablature bearing lava flows. Fracture edges are at, or just beyond, the top of the images in all cases except d) and e) where the fracture edge is at the right hand side. Master fractures show finer grained dendritic oxide enriched material at the fracture. Vesicle chains near the master fracture edge also show this fine grained oxide rich material. Entablature column fractures show some dendritic oxides and are slightly finer grained than those in the colonnades.

4.3.3.3 Colonnade column-bounding fractures

Fracture edges of column-bounding fractures from upper and lower colonnades do not show any glassy or oxide-rich material or dendritic crystal textures. They have uniform crystal size over the whole of a section from the fracture edge inwards (3 cm) and no discernible differences between the two colonnade column types (Fig. 4.12). Crystals are a similar size and habit to those in entablature and master fractures away from the fracture edges (with the exception of the dendritic oxides in these). Slightly rounded olivines occur throughout these sections.

4.3.4 Mineral compositions

Individual crystals (plagioclase, clinopyroxene and olivine) from lower and upper colonnades, entablature column bounding fractures and master fractures were analysed using a Cameca SX 100 electron microprobe at the Open University. Element maps for Ti, Al, Ca, Fe, K, Mg, Mn, Na and Si of an area from the best preserved master fracture edge were also acquired (Fig. 4.13).

Mean values of individually probed minerals do not show significant or systematic variations between different areas or fracture types. The mineral compositions are highly varied, and often anomalous, likely due to the small size of the crystals making individual spot measurements difficult.

Element maps of a well preserved master fracture show significant, systematic variation in all the elements (Fig. 4.13). In these element maps warm colours show high concentrations and cool colours show lower concentrations but no absolute values can be attributed to these colours.

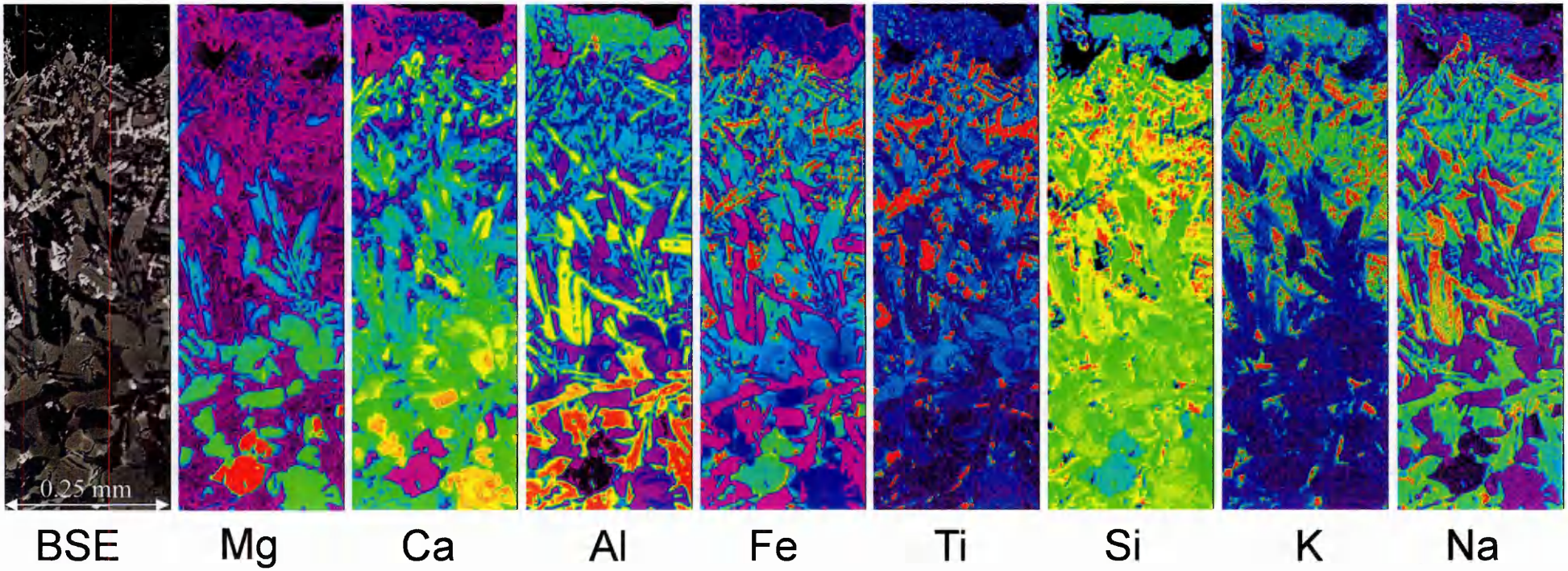

Fig. 4.13 Back scatter electron (BSE) image and element maps of the same area of a master fracture from the Búrfell lava at Gjáin for Mg, Ca, Al, Fe, Ti, Si, K and Na. Warm colours denote relative enrichment, cool colours relative depletion and black an absence of an element. No absolute values can be attached to these element maps. Mg and Ca are depleted at the fracture edge and Fe, Ti, Si, K and Na are enriched. This enrichment corresponds to the darker finer grained material in Fig. 12a. Images are 0.25 mm across.

Fig. 4.13 shows a clear transition in mineral abundances and crystal textures at the master fracture area. Much higher concentrations of Fe-Ti oxides occur near the fracture, all of which are dendritic. There is a greater abundance of plagioclase in the material next to the master fracture, a decrease in the amount of clinopyroxene and olivine is absent. Clinopyroxene occurs as smaller crystals or dendrites and plagioclase crystals are small and acicular or occur intricately mingled with dendritic clinopyroxene. The small area of dark grey, speckled material just above the fracture edge is detrital grains that have accreted at the fracture edge as a result of sample preparation and is ignored hereafter.

Clinopyroxene near the master fracture shows higher concentrations of Fe and Ti and lower concentrations of Mg and Ca, with little variations shown in the very minor constituents such as Na and K. Plagioclase shows higher Fe, Ti, Na, K and Si near the master fracture and lower Ca and Al concentrations. The composition of the Fe-Ti oxides does not appear to vary, only their abundance. Overall the fracture edge is relatively enriched in Fe, Ti, K, Na and Si, and depleted in Mg and Ca (and Al in plagioclase) compared to the rest of the basalt.

Some areas of the section have corresponding high concentration of Si, K and Na, intermediate concentrations (light blue) of Al, and are an intermediate grey on the backscatter image (i.e. not easy to identify as clinopyroxene, plagioclase, olivine or oxides). These are concentrated near the fracture edge but also occur more sparsely away from the fracture edge, usually on grain boundaries. These are likely to be glass.

4.4 Discussion

4.4.1 Environmental evidence

Crystal textures, fracture types and surface textures in entablature all relate to the rapid cooling environment of entablature, and enable us to demonstrate that different fracture types have different cooling rates, refining our understanding of exactly how entablature forms.

4.4.1.1 Fractures

The presence of pseudopillow fracture systems in lava is taken to indicate lava-coolant interaction has occurred (Watanabe and Katsui, 1976; Lescinsky and Fink, 2000; Mee et al., 2006; Lodge and Lescinsky, 2009; Tucker and Scott, 2009). The coolant can be steam (Mee et al., 2006; Forbes et al., 2012) or liquid water (Watanabe and Katsui, 1976; Tucker and Scott, 2009; Forbes et al., 2012), which may ultimately come from ice, snow or liquid water (Watanabe and Katsui, 1976; Lescinsky and Fink, 2000; Mee et al., 2006; Tucker and Scott, 2009). The ubiquitous presence of pseudopillow fracture systems in entablature provides good evidence in support of the lava-water interaction origin of entablature.

Comparison of column side width and striae height measurements from lower colonnade and entablature column-bounding fractures give a good indication of the relative cooling rates. Column side width (an easily reproducible way of measuring column 'size' or fracture spacing) is controlled by the visco-elastic response of the lava to cooling rate (Spry, 1962; Lore et al., 2000) resulting in more rapidly cooled columns being smaller, such as those in the entablature. Column side width is 2-3 times larger in the colonnade

than the entablature, suggesting significantly faster cooling rates in the entablature portion of the flow to produce these smaller columns.

Striae are formed by cyclical fracture propagation and termination. The fracture initiates at a certain temperature when the lava has cooled and contracted sufficiently to overcome its tensile strength. Fracture propagation will stop when the material the fracture is propagating into becomes too hot to sustain brittle fracturing (Ryan and Sammis, 1978; DeGraff and Aydin, 1993; Goehring and Morris, 2008), and so a temperature is implied in both the initiation and termination of a fracture cycle. Thus the size of striae gives an indication of temperature gradients, and so cooling rates, in the colonnade and entablature column-bounding fractures, with smaller striae indicating faster cooling. Striae height in entablature is approximately half that on colonnade column bounding fractures (e.g. Fig. 4.10), suggesting that the temperature gradient was significantly larger in the colonnade than the entablature column bounding fractures, providing fracture initiation and termination temperatures were the same for both, or at least that the temperature interval of striae formation was the same.

Topography of striae is much less on entablature column-bounding fractures than on colonnade fractures (Fig. 4.10). In many cases striae are not visible at all on columns in entablature, whereas they are typically easily observable in colonnades. Striae topography is caused by the blunting of the crack tip due to plastic deformation in the hot lava between fracture propagation cycles (Ryan and Sammis, 1978; Goehring and Morris, 2008). When fracture propagation starts the next fracture cycle this blunting causes the fracture to propagate in a slightly different direction, resulting in the striae topography. The contrast in rapidity of formation of these two different column bounding fractures may relate to the striae topography. Both the fractography and petrology indicate faster cooling and so faster fracture formation in entablature. Faster cooling would result in a shorter pause between

individual fracture propagations, less blunting of the crack tip and so smaller striae topography. If fracture propagation were sufficiently rapid then deformation would be minimal, leading to little evidence of striae due to the lack of striae topography. This could also be caused by rapid quenching of the plastic zone immediately after fracture formation due to cooling effects of water or steam infiltrating the entablature, stopping the crack tip from blunting.

An upper colonnade of 1-5 m thick is present in the Búrfell lava both at Gjáin and Hjálparfoss. This indicates that there was a significant time gap between the emplacement of the flow and the cooling event that caused the formation of the entablature, to allow time for an upper colonnade to form. Damming of the river valley by a lava flow and subsequent flooding/overtopping of the river (e.g. Sæmundsson, 1970; Lyle, 2000) may allow time for this upper colonnade to form. This is a likely source of coolant causing the formation of pseudopillow fracture systems and high cooling rates needed for the formation of entablature. Damming of the river may have occurred at Gjáin, where the Búrfell lava can be seen thickening into a valley (Fig. 4.6).

4.4.1.2 Petrography and its implications

Crystal textures show strong evidence of rapid cooling at master fracture edges in pseudopillow fracture systems. Collections of dendritic oxides and dendritic sprays of clinopyroxene and plagioclase demonstrate high cooling rates (e.g. Long and Wood, 1986; Lyle, 2000). Away from the fracture edge the crystal sizes are similar to those found in the colonnade and entablature columnar jointing samples, although dendritic oxides are still present throughout (up to at least 3 cm from the master fracture edge), indicating fairly rapid cooling occurred throughout.

Column-bounding fractures in the entablature do not show such strong evidence of rapid cooling. A slight decrease in crystal size very close to the fracture edge and some dendritic oxides provide evidence for their rapid formation (Fig. 4.12). These fractures have not experienced the extremes of cooling rate that occurred at the master fractures. This suggests master fractures are the main conduits bringing steam and/or water into the entablature, rather than the column bounding fractures in the entablature.

Column-bounding fractures in both the upper and lower colonnades contain uniform crystal size throughout. They are lacking in dendritic oxides and do not show any evidence of chilled fracture edges. Their cooling rates at the time of crystal formation do not appear to have been significantly affected by water, unlike the master fractures and column-bounding fractures in the entablature.

4.4.2 Composition at the master fracture

The area adjacent to the master fracture edge shows an enrichment in Fe, Ti, K, Na and Si, and depletion in Mg and Ca. It also shows higher proportions of plagioclase feldspar and Fe-Ti oxides, a lower abundance of clinopyroxene and a lack of olivine. These observations indicate a more evolved composition at the master fracture that is not seen elsewhere in the lava, which correlates with the dark glassy material seen in hand specimen at the master fracture.

More evolved material commonly occurs in basaltic lava flows in the form of segregation vesicles, vertical cylinders and horizontal sheets (e.g. Anderson et al. 1984; Rogan et al. 1996; Hartley and Thordarson 2009). These may occur as finer grained (e.g. Anderson et al., 1984) or coarser grained (pegmatitic) (e.g. Rogan et al., 1996) bodies within the lava. They are formed through a process of gas-driven filter pressing whereby crystallisation of

the lava forms a permeable but rigid network of crystals and leaves the residual melt enriched in incompatible elements and volatiles. Crystallisation causes volatiles to exolve from the residual melt, resulting in vesicular evolved segregation material at higher pressure (Anderson et al., 1984; Sisson and Bacon, 1999). This forces the residual liquid into lower pressure regions such as pre-existing vesicles and may cause it to rise buoyantly through the lava flow forming cylinders as it rises and horizontal sheets where it ponds, resulting in all the geometries of segregation material mentioned above.

4.4.3 Pseudopillow fracture systems in entablature

Some workers have discussed the influence of large first formed fractures, often termed 'master fractures' (e.g. Spry 1962; DeGraff *et al.* 1989; Lyle 2000), on the styles of columnar jointing in entablature tiers, however, these have not been recognised as part of a pseudopillow fracture system. The evidence for the formation mechanisms of the master fractures and their associated subsidiary fractures lies in their fracture surface textures.

4.4.3.1 Formation mechanisms

Master fractures have been linked with non-uniform high stress regimes in lava (e.g. Mee et al., 2006; Forbes et al., 2012). Stresses in the lava may result from the weight and movement of water on top of the lava flow. These stresses will create areas of compression and areas of tension, which result in lower pressure areas within the lava flow. This will cause migration of late stage melt into these areas of low pressure and tension. Areas of tension are likely to become the focus of master fracture formation, provided the stress in these parts of the lava overcomes the tensile strength of the material there. Late stage segregation melt that migrates into low pressure areas is likely to be vesicular, particularly if its movement results from gas-driven filter pressing. Small amounts of enriched residual

glass are present trapped at grain boundaries in the lava (e.g. Fig. 4.13), leaving evidence of the movement of enriched residual liquid through the crystal framework, which may happen rapidly (e.g. Schipper et al., 2012).

This collection of vesicular, enriched material eventually fractures in tension causing ductile cavitation fracture (see below in this section), resulting in the dimpled master fracture textures. This segregation material is then quenched by the influx of coolant once the lava fractures, causing the very fine grained and dendritic textures and glass, rather than the pegmatitic textures often observed in segregation material and preserving the delicate dimpled fracture surface textures. Shear is an unlikely mechanism for master fracture formation here because of the equant, well formed dimples on the master fracture surfaces. Ductile fractures opening in shear result in vein patterns, which do occur on some of the F-type master fractures in the Tangahraun lava (Chapter 2), but not at all in these basalt entablature exposures, so tension/extension stress is probably the best explanation for the master fracture formation.

Textures on the master fracture surface (e.g. Fig. 4.4c and d) seem to indicate that it is the segregated melt that is forming the cavitation dimples, i.e. it is that evolved melt that is being fractured, which points to the accumulation of this melt before fracture. Therefore they are unlike the segregation veins that have been observed to form in sub-horizontal and inclined tension fractures in Hawaiian lava lakes (Wright and Fiske, 1971; Wright and Okamura, 1977). These vein fills have been described as relatively coarse grained and vesicular and are thought to form by enriched material seeping out into the tension fracture after fracture has occurred.

Residual melt at master fractures is not always vesicular, although it may once have been. Bands of vesicles are thought to enhance the ability of lava to undergo ductile cavitation

fracture (see Chapter 2 discussion and this section below), so the original vesicles from this melt have probably been converted into the cavitation dimples of the ductile fracture. More information may be gathered from the chains of vesicles behind and generally parallel to the master fracture surface, which also show the presence of this enriched residual melt around the outside, but not filling or breaking into the vesicles (Fig. 4.8b and g). If these were earlier formed vesicles then with cooling of the lava they would represent low pressure areas and should fill with the residual melt (Anderson et al., 1984). As they are not filled with segregation melt they are more likely the failed attempts at master fracture formation in the same vicinity, i.e. within areas of low pressure in the lava, which stopped forming further once one main master fracture surface became dominant. That they are not filled with late stage melt demonstrates that they are higher pressure vesicles formed with the segregation melt, rather than vesicles within the lava that had formed prior to the invasion of later stage melt in these areas.

The dimpled surface texture of the master fractures is typical of ductile cavitation fracture (Fig. 4.8; e.g. Tvergaard, 1997; Hull, 1999; Bron et al., 2004). Cavitation occurs when a ductile material, in this case hot lava, is under tension. Holes nucleate on heterogeneities, which grow and coalesce to form the fracture surface (Hull, 1999). Cavitation appears uncommon as a fracture mechanism in lava or hot rock but has been documented from the dacitic Unzen lava dome, Japan (Smith et al., 2001) and in combustion-altered siliceous mudstones (Eichhubl and Aydin, 2003) and a larger scale version (1-10 mm vs. sub-millimetre diameter dimples) of this cavitation surface has been observed previously on pseudopillow fracture system master fractures in a trachyandesite lava flow (Forbes et al., 2012; Chapter 2). The presence of vesicles or void space in rock appears to encourage cavitation fracturing to occur (Eichhubl and Aydin, 2003; Forbes et al., 2012), and indeed the ductility of a material is strongly influenced by the volume fraction of inclusions or voids it contains (Le Roy et al., 1981). Such a case is likely for the master fractures in

entablature as they draw residual melt into the fracture area, which is typically enriched in volatiles and more vesicular than the surrounding lava. The cavitation dimple size difference between these and previously studied master fractures may be related to the density of heterogeneities that holes can nucleate on (more vesicles and crystals in basalt), or the size of the vesicles present in the fracturing plane.

The bulbous master fracture surface texture (Fig. 4.8) has been observed only once, whereas the cavitation dimpled texture is much more common, identifiable on almost every other well preserved master fracture surface. This texture may have formed due to the septa of material surrounding cavitation holes relaxing back into the fracture surface before being frozen in place by water or steam infiltrating the master fracture. This would imply that freezing of cavitation surfaces occurs extremely rapidly after their formation to preserve the dimpled texture; but in the case of the bulbous surface texture a small hiatus between fracture formation and water ingress may have occurred allowing septa of material between the cavitation dimples to relax back into the fracture surface.

Curved striae on the surfaces of subsidiary fractures show hackle (plumose structures; Ryan and Sammis, 1978; DeGraff and Aydin, 1987), which indicate general downward propagation of the subsidiary fractures, and by comparison with other pseudopillow fracture systems the downward propagation of the entire fracture system (Forbes et al., 2012; Chapter 2). Striae mirror isotherms in the cooling lava and are a good indicator of how the flow is cooling. Curved striae are likely caused by a strong directionality of cooling, as coolant (water or steam) infiltrates the master fracture from above and causes a downwards direction of cooling in the subsidiary fractures immediately adjacent to the master fracture. Further away from the master fracture the directionality of coolant ingress is not felt as strongly and so the striae curve round, trending towards forming parallel to the trace of the master fracture (i.e. subvertical), mirroring the isotherms in the system.

4.4.3.2 Pseudopillow fracture system-columnar jointing interaction

The interaction of pseudopillow fracture systems and columnar jointing in entablature produces upward pointing chevron-shaped fracture patterns (Fig. 4.11 and 4.14). Columns that form between the subsidiary fractures do not occur horizontally with their long axes perpendicular to the master fracture. This orientation would be expected if cooling from the master fracture horizontally outwards were the dominant process, as the master fracture acts as a cooler plane in the entablature. Instead the columns form at an angle of about 30-45° to the master fracture and curve to become slightly steeper further away from the master fracture. The subsidiary fractures likewise propagate at an angle to the master fracture, shown by the curved striae. These inclined columns can then be linked to the directional ingress of coolant just as the curved striae are linked to the directional ingress of water and so cooling.

Two different cooling directions are acting on the lava surrounding the master fracture: the master fracture is a conduit for coolant entering the lava and causes a cooler plane in the hot lava, so isotherms would be parallel to the plane (i.e. vertical); the coolant enters from the top of the lava and filters downwards through the master fracture plane, causing cooling to progress in a downward direction which would produce horizontal isotherms perpendicular to the master fracture. The columns respond to these two cooling directions by forming at 30-45° to the master fracture, i.e. half way between. Further away from the temperature disturbance caused by the coolant ingress at the master fracture the regular cooling field of the lava flow becomes more important and the columns start to respond to the overall cooling direction (i.e. from the top downwards) and so become more vertical.

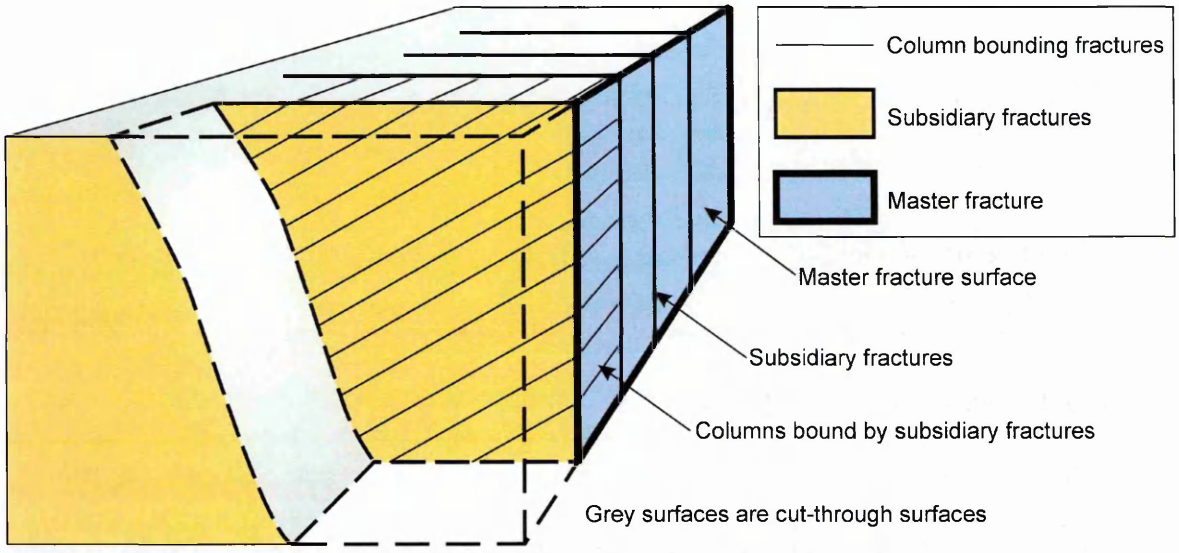

Fig. 4.14 A cut-through sketch diagram of a pseudopillow fracture system. Crude columnar joints have formed at an inclined angle to the master fracture, these are bound by subsidiary fractures. The master fracture is the blue plane, the subsidiary fractures are the yellow surfaces and the fractures behind and parallel to these. The columnar joints are marked between only one pair of subsidiary fractures, although they occur in between all the subsidiary fractures.

4.4.3.3 Cube-jointing

We define cube-jointing as a more densely fractured end member type of entablature, the other end member being column bearing entablature. A number of lines of evidence suggest that cube-jointing is caused by larger amounts of coolant entering the hot lava flow than in the Búrfell-type entablature. The higher fracture density is likely due to a larger amount of coolant infiltrating the lava while it is cooling. More varied orientations of pseudopillow fracture systems in cube-jointed entablature also contribute to this denser network of fractures. These may also be caused by more coolant in the system that can percolate down into the rock and so may go on to form horizontal pseudopillow fracture systems. Striae appear to be generally smaller in cube-jointing compared to column bearing entablature (Table 4.2), indicating more rapid cooling. However, we have few measurements due to the scarcity of striae in cube-jointing. Subsidiary fracture spacing in cube-jointing is also generally closer than that observed in entablature of the Búrfell lava. Subparallel planar subsidiary fracture spacing has been linked to striae spacing and so to

cooling rate, with closer spacing indicating faster cooling (Forbes et al., 2012; Chapters 2 and 5), so it is likely more coolant entered the lava flow to cause this faster cooling rate.

4.5 Conclusion

A number of new observations and interpretations of fractures that form in entablature jointed tiers are summarised below.

The presence of pseudopillow fracture systems in entablature strengthens their link to lava-water interaction, especially given their association with crystal textures which relate to rapid cooling. They explain the occurrence of chevron fracture patterns commonly seen in entablature.

Pseudopillow fracture systems are likely the main conduit for coolant entering the entablature tier, shown by crystal textures demonstrating most rapid cooling occurring at the master fracture.

The low pressure associated with master fracture formation causes gas-driven filter pressing of evolved residual melt into the region where the master fracture will form. Cavitation ductile fracture occurs within this residual liquid at the master fracture edge, probably encouraged by vesicles in the residual melt, followed by rapid quenching of the fracture and its surroundings by the influx of water and/or steam.

Cooling rate in entablature, as demonstrated by the presence and abundance of dendritic oxides and glassy mesostasis, is most rapid at master fractures of pseudopillow fracture systems and less rapid in columns in entablature. Cooling rates in entablature are higher than in either upper or lower colonnade columns.

Entablature broadly has two end members: cube-jointing and column forming entablature. Cube-jointing forms due to more coolant infiltrating the hot lava than in column forming entablature tiers.

4.6 Highlights

- Pseudopillow fracture systems in entablature strengthen the lava-water interaction hypothesis.
- Pseudopillow fracture systems help to form chevron fracture patterns commonly seen in entablature.
- Low pressure associated with master fracture formation causes gas-driven filter pressing of evolved residual melt into the region where the master fracture will form.
- Cavitation ductile fracture occurs within residual liquid at the master fracture edge.
- Evolved melt at the master fracture is rapidly cooled.
- Pseudopillow fracture systems are probably the main conduit for coolant entering the entablature tier.

Chapter 5: The Slaga lava flow

5.1 Introduction

The aims of this chapter are two fold: firstly to describe in detail a lava flow and its features related to cooling and emplacement and secondly to use knowledge gained through the study of cooling fractures, such as columnar jointing and pseudopillow fracture systems, to interpret the environment this lava flow was emplaced/erupted into. This is a 'proof of concept' study demonstrating that detailed investigations of cooling fractures can give pertinent information about the environments of lava flows.

Past studies have linked some cooling fracture types to particular environments containing ice, snow or water, such as columnar jointing in felsic lavas (Lescinsky, 1999; Lescinsky and Fink, 2000; Tuffen et al., 2001; Tuffen et al., 2002; Stevenson et al., 2009) and pseudopillow fracture systems (Watanabe and Katsui, 1976; Lescinsky and Fink, 2000; Mee et al., 2006; Lodge and Lescinsky, 2009; Tucker and Scott, 2009; Forbes et al., 2012). A previous advantage of using columnar jointing to interpret lava environment was that fracture propagation directions can be easily deduced from striae (chisel marks) and these have been understood for some time (Ryan and Sammis, 1978; DeGraff and Aydin, 1987), this had not been true for pseudopillow fracture systems until recently (see Chapter 2).

5.2 Geology of the Slaga lava flow

The lava flow in this study is located on the south western flanks of the Öræfajökull central volcano, Iceland (Fig. 5.1). It has no name that we can discern but occurs on the north eastern edge of a hill called Slaga so the flow has been informally named Slaga or the

Slaga lava flow. XRF data (Table 5.1) shows the flow to be a trachyandesite. The lava is highly fractured, displaying pseudopillow fracture systems (e.g. Watanabe and Katsui, 1976; Lescinsky and Fink, 2000; Mee et al., 2006), curved platy fractures and some columnar jointing.

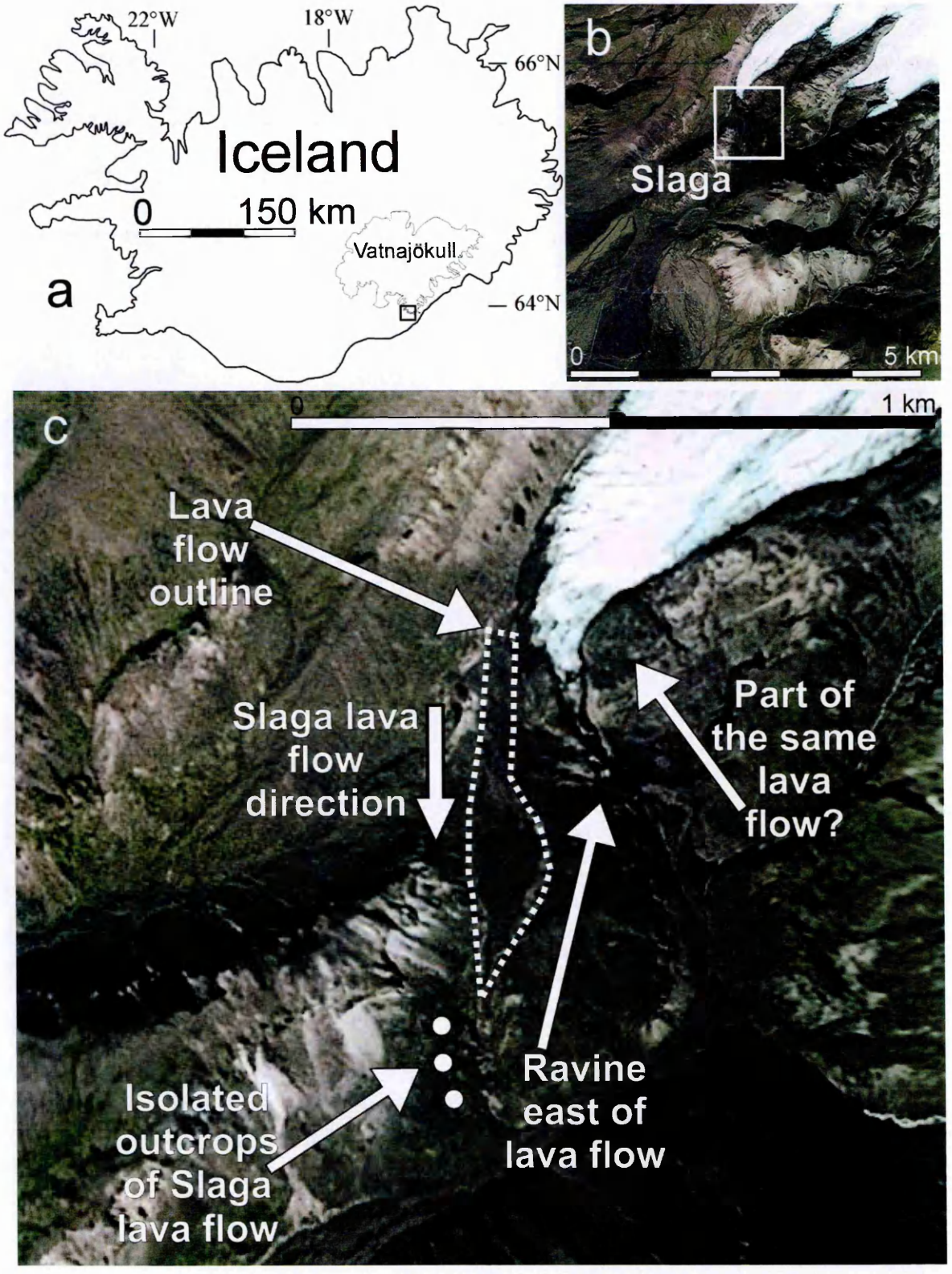

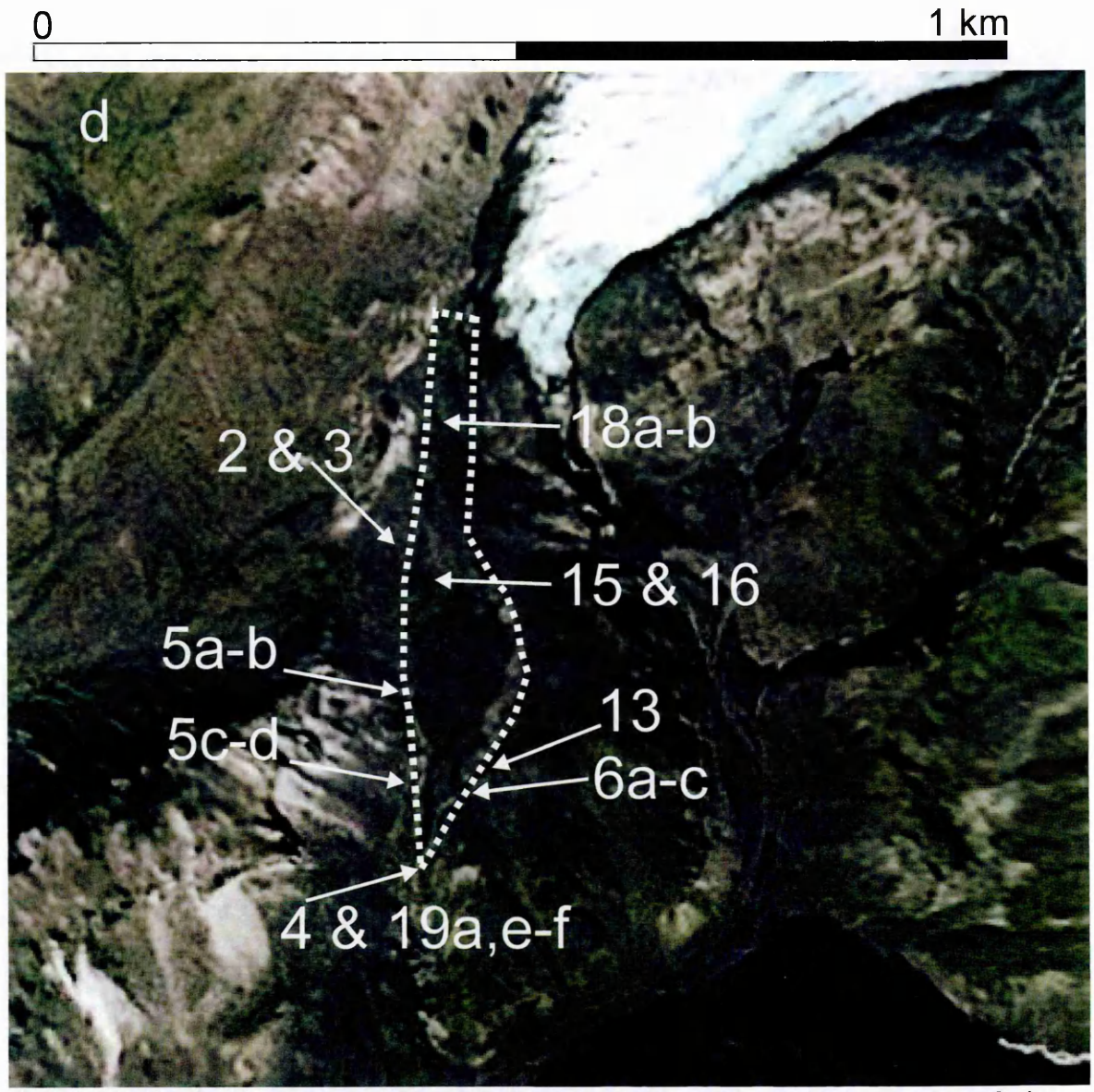

Fig. 5.1 a) Iceland with outline of the Vatnajökull glacier, the box on the southern side of the glacier (over the Öræfajökull glacier) expands to figure 1b. b) Area of the lava flow, Slaga hill is named and pale coloured mountains to the south are subglacial rhyolites. Boxed area expands to figure 1c. c) Dotted lines show the mapped lava area, spots to the south show isolated outcrops of the Slaga lava flow. Flow direction is southwards. d) Enlarged version of Fig.1c showing the location of subsequent figures in this chapter, numbers refer to figure numbers. The glacier is Kotárjökull, part of the Vatnajökull glacier.

Table 5.1 XRF composition data for the Slaga lava flow

wt. %	Slaga
SiO_2	57.04
TiO_2	1.598
Al_2O_3	14.02
Fe_2O_3	14.08
MnO	0.331
MgO	1.49
CaO	5.53
Na_2O	5.00
K_2O	1.65
P_2O_5	0.588
LOI	-0.34
Total	100.98

The extent of the flow is difficult to determine as a glacier tongue to the north and a very large ravine to the east appear to cut across it, and limit the study area. It is poorly exposed, as scree and glacially deposited debris, including large glacially striated boulders, are scattered across the top of the flow (Fig. 5.2). This can sometimes make it difficult to study the lava, in particular the tops of lobes, as it is not certain how much material has been removed. However, this glacial scouring has also resulted in lobe interiors that are well exposed at the edges of the mapped flow (Fig. 5.1), enabling the detailed study of flow lobes from centre to edge.

Fig. 5.2 From the northwest side of the outline mapped Slaga lava flow looking south east (see Fig. 1d for location). The lava is covered by glacially deposited boulders and scree formed by the break up of the lava flow. The mountains in the distance are behind the ravine that runs left-right in this image.

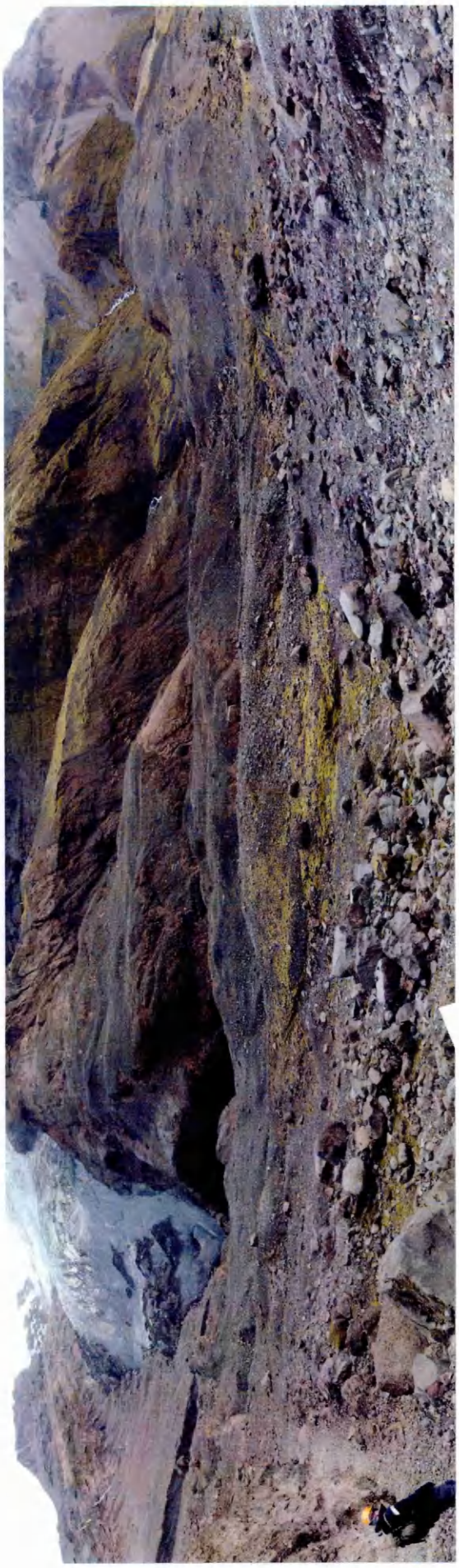

Fig. 5.3 180° panorama of the Slaga lava flow, north is to the left of the figure and south to the right. In the centre, just to the right of the glacier across the ravine, is lava with a very similar appearance to the Slaga flow, with similar looking eroded lobes of lava. The characteristic green moss that colonises this flow appears on some similar coloured rock just to the right (and behind) this, as well as in the foreground of the figure.

The Slaga lava flow sits on now lithified polymict sediment, which was probably glacially deposited. No vents were found during this study, but as the lava appears to flow downhill away from the glacier (flow direction determined by the topography) it is likely that the vent is currently somewhere under the glacier. The lava occurs as multiple lobes across a shallow area and is mapped as approximately 130 m wide at its widest measurable point, but is likely wider, with similar lava deposits occurring on the ravine's western edge and east of the ravine (Fig. 5.3; these were not visited). Because the flow is composed of multiple lobes its thickness across the mapped area varies greatly. Single lobes may be up to 5 m thick, or less than metre thick, but in general the flow is not more than ~2-3 m thick on average, across the area. Lobe widths are more difficult to gauge due to the preservation and erosions problems of this flow, but they appear to be generally $\leq$ 6 m across. Crystallinity also varies greatly, with areas of lobes being holocrystalline (particularly the central parts) and other areas being extremely glassy.

The flow is funnelled into a channel defined by the polymict sediment at the downslope most mapped part of the lava flow, becoming just ~2 m wide (Fig. 5.4). The flow is cut through at this point revealing a cross section of a lava lobe. Only a few isolated outcrops are preserved downhill (southeast) of this point, demonstrating that the flow continued beyond this point. These isolated outcrops occur where the slope becomes much steeper, with outcrops significantly below the last visible occurrences of the flow. This steeper slope may be the cause of their poor preservation.

Fig. 5.4 Looking north at the end section of southern most mapped lava lobe. It shows the inner platy core (eroded away in the closest part of the image) and the pseudopillow fractured outer carapace below (and above and to the sides further back in the image). This flow shows an aspect ratio of approximately 1.This lobes in the flow appear to have an aspect ratio of approximately 1 (e.g. Fig 5.4), although this can be difficult to ascertain as most lobes are eroded and/or scree covered.

The trachyandesite lava that forms these lobes is variably vesicular, with thinner lobes tending to be more vesicular and larger lobes usually having a vesicle-free outer carapace of fractured lava, vesicles range from spherical to highly elongate. Lobes are generally seen piled on top of one another (Fig. 5.5), but can also be observed to have flowed over and around each other (Fig. 5.5). The flow has been colonised by a particular type of bright green moss that occurs preferentially on the lava and less commonly on the surrounding rock (e.g. Figs. 5.2 and 5.5), that can make features in the exposures difficult to see. The flow may once have been continuous or had flowed independently down the area across the ravine to the east, as identical coloured material with a comparable morphology, sometimes showing a similar coloured moss, occurs there at a comparable elevation (Fig.

5.3), indicating that the flow may originally have been considerably larger than its present accessible exposure.

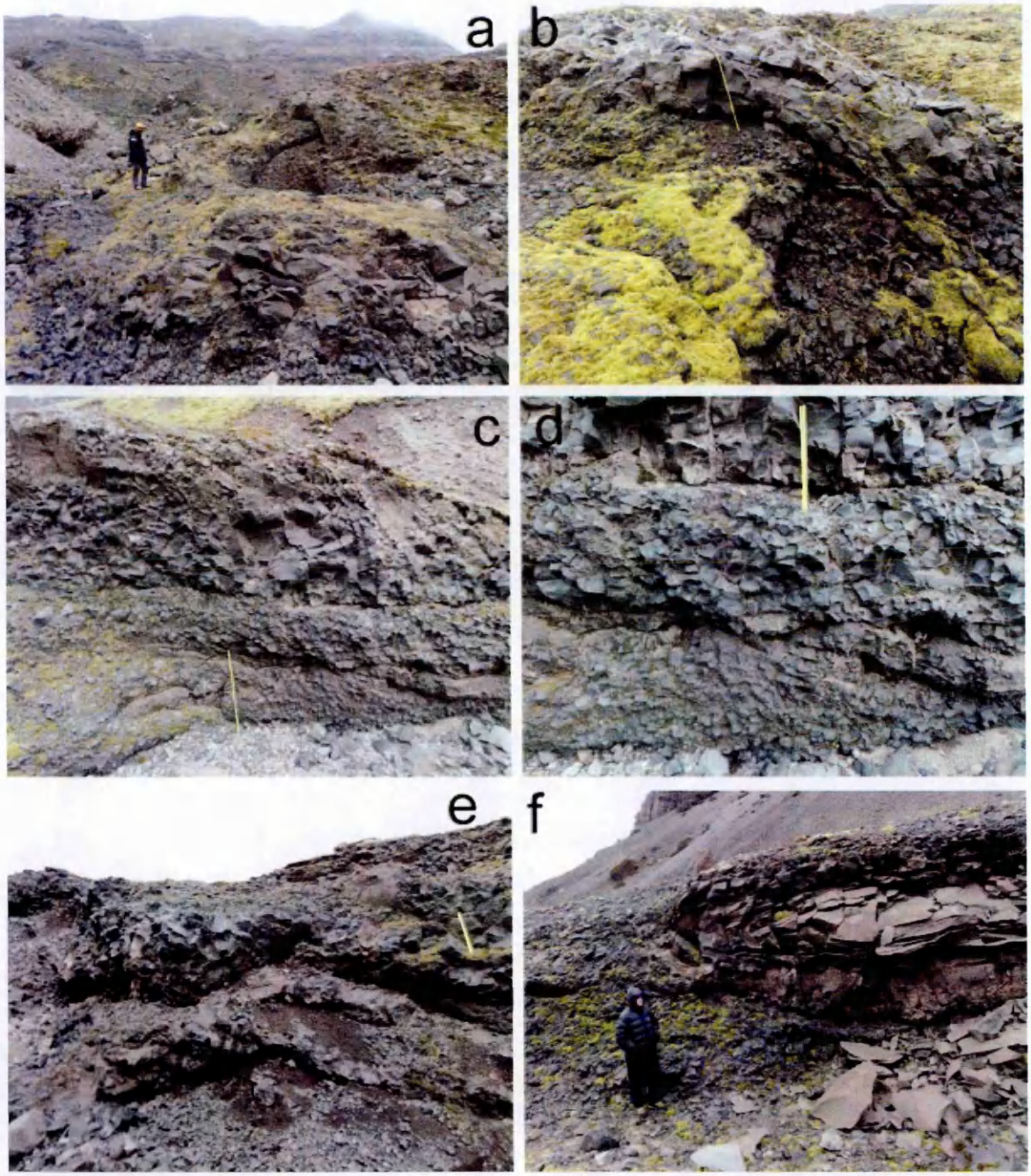

Fig. 5.5 a) Upper lobe flowing over lower lobe (person standing on the lower lobe). b) Close up of 15a where the upper lobe flows over the lower one, ruler 1 m. c) Three lobes stacked on top of one another, two thinner more densely fractured lobes at the base and a larger lobe on top, ruler 1 m. d) Close up of 15c showing lower more densely fractured lobes and basal crude columns on upper lobe. Ruler 50 cm. e) Complicated and poorly exposed piling up of lobes, ruler 50 cm for scale. f) Eroded lobe emplaced on top of another. The lobe on top clearly shows platy fractured interior, and also crude columnar jointing with some X-type pseudopillow fracture systems at the base and fractured upper.

5.2.1 Generalised lobe description

Having studied all accessible outcrops of this lava flow a number of features occur in most lobes and it is possible to give a generalised description of the features and fractures within a lobe:

X-type pseudopillow fracture systems (described in detail in the next section) generally occur, usually in non-vesicular lava, around the outer margins of lobes and in smaller lobes they occur throughout the entire lobe. By using fracture propagation directions from both master and subsidiary fractures, pseudopillow fracture systems generally propagate in towards the centre of the lobes in a radial fashion, whereby they propagate up from the base, inwards from the sides and downwards from the top. The thickness of the pseudopillow fractured outer carapace of a lobe varies, it is generally thinner on the top where the pseudopillow fracture systems propagate downwards, usually only a few tens of centimetres thick and is occasionally absent (although it is unknown what affect erosion may have had on this thickness). At the sides and towards the base the pseudopillow fractured outer carapace is considerably thicker, up to 1 m thick, surrounding the platy fractured lobe core (e.g. Fig. 5.4). The outer fractured carapace on lobes tends to be quite glassy but not uniformly so, with more and less glassy patches.

G-type pseudopillow fractures systems (described in detail in the next section) are not found in all lobes but where they do occur they form at the base of a lobe. Where many lobes have formed piled on top of one another the G-type pseudopillow fracture systems form in largest quantities in the lower lobes and tend to be entirely absent in the upper lobes. They only form in very glassy lava, and fracture propagation directions from hackle on master and subsidiary fractures demonstrate that they propagated inwards, and sometimes upwards, from the base. Columnar jointing does not occur in all lobes but is

more common at the base of upper lobes, it may transform into a region of X-type pseudopillow fracture systems or curved platy jointing above.

Curved platy fractures form in the cores of the larger lobes in lava that is more crystalline than the outer pseudopillow fractured carapace. They are often associated with highly vesicular lava in their upper portions and may be dissected by earlier formed X-type master fractures.

5.2.3 Other lobe features

A number of other features occur at the base of flows, in patches or areas but not uniformly across the whole lava flow. One such feature are large rounded pillow-like lobes ≤ 1 m in diameter, these generally have glassy, vesicular margins (Fig 5.6). They may occur directly beneath a platy fractured lobe centre or beneath pseudopillow fractured lava. Peperite is commonly associated with these pillow-like lobes and often occurs beneath them (Fig. 5.7d).

Other, smaller lobate bodies also occur at the base of flow lobes (e.g. Fig. 5.7a-c). These are distinctly different from the larger pillow-like lobes (Fig. 5.6) as they do not show vesicular or extensive glassy textures. Some are fingers of lava that can be seen intruding into the underlying sediment (polymict), these show chilled margins (Fig. 5.7). Other small lobate bodies were observed beneath one of the lobes, set in a coarse breccia with a fine grained muddy matrix (Fig. 5.7c). The coarse material in this breccia is composed of small blocks of the lava generally < 10 cm across. This may represent a basal flow breccia, a coarse peperite-type facies or perhaps a mixture of both, formed by the interaction of the basal polymict sediment and the lava.

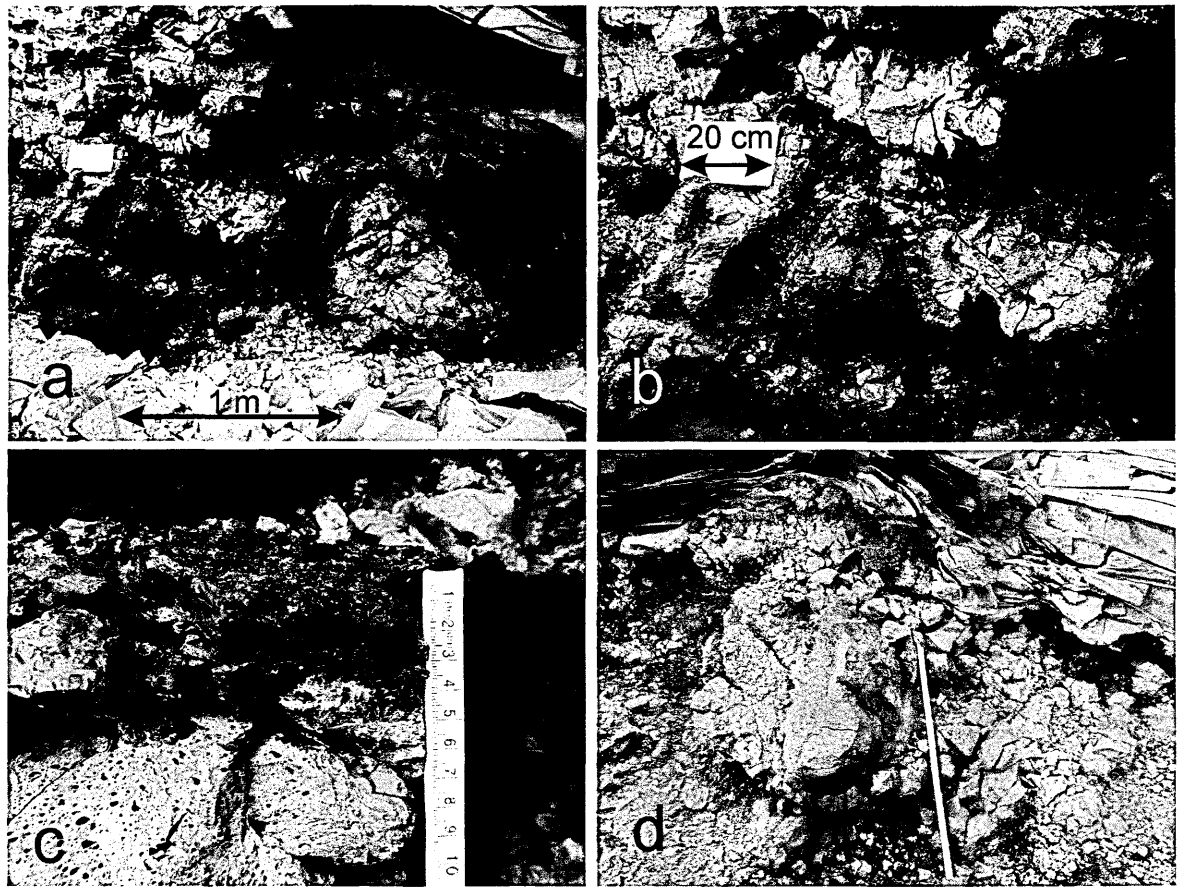

Fig. 5.6 a) Large rounded lobate pillow-like bodies with glassy and vesicular margins at the base of a lava lobe, note book 20 cm for scale. b) Close up of these same lobate features, note book 20 cm for scale. c) Glassy and vesicular margin of rounded lobate pillow-like body. d) Entirely vesicular, isolated large rounded lobate pillow-like body at the base of a lobe, ruler 50 cm.

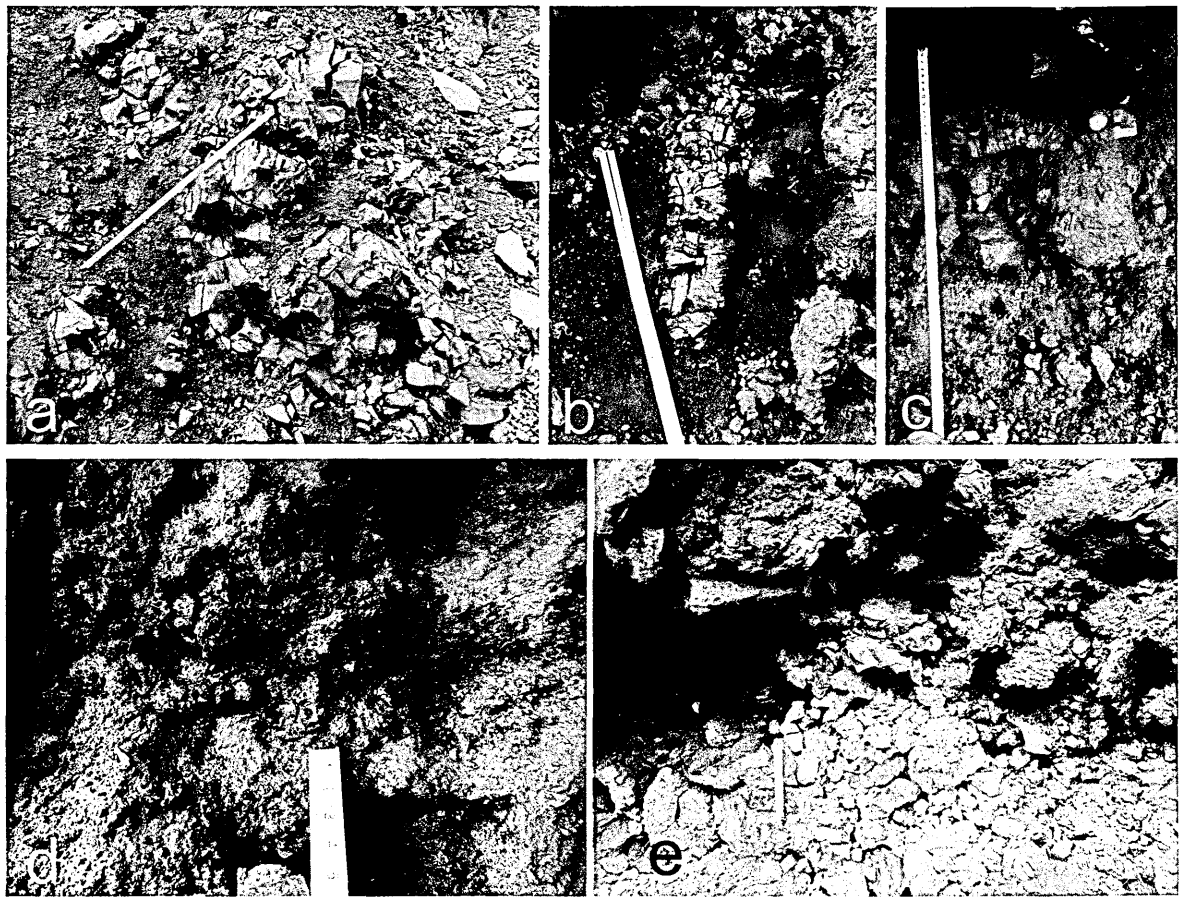

Fig. 5.7 a) Curved lobe intruded into, probably unlithified, polymict bedrock, ruler 50 cm. b) Lobe

intruded into polymict bedrock from the base of a lava lobe, ruler is 50 cm. c) Small pillow-like bodies in breccia or peperite at the base of a flow lobe, ruler is 50 cm. d) Peperite, fragments of glassy lava in sediment (polymict bedrock) at the base of a flow lobe, ruler 5 cm long. e) Basal flow breccia, consisting of a deposit of blocks of lava at the flow base, ruler is 25 cm.

Extensive deposits of blocks of lava ≤ 15 cm diameter, probably a flow breccia, were observed at the base of some lobes (Fig. 5.6d and 5.7d). Exposures of flow base breccia may be patchy either because flow breccia was not commonly produced in this flow or due to difficulties in recognising flow breccia in this highly broken up, eroded and scree covered lava. However flow base/top lava is generally absent where multiple lobes are piled on top of one another. Lescinsky and Fink (2000) also observe basal breccias to be either thin or absent in ice-interaction lavas of intermediate to silicic compositions. Vesicular frothy textures and vesicular features that appear to be ductile tearing of the lava occur in various places around the base and sides of lobes (Fig. 5.8). These are not linked with any particular type of fracturing.

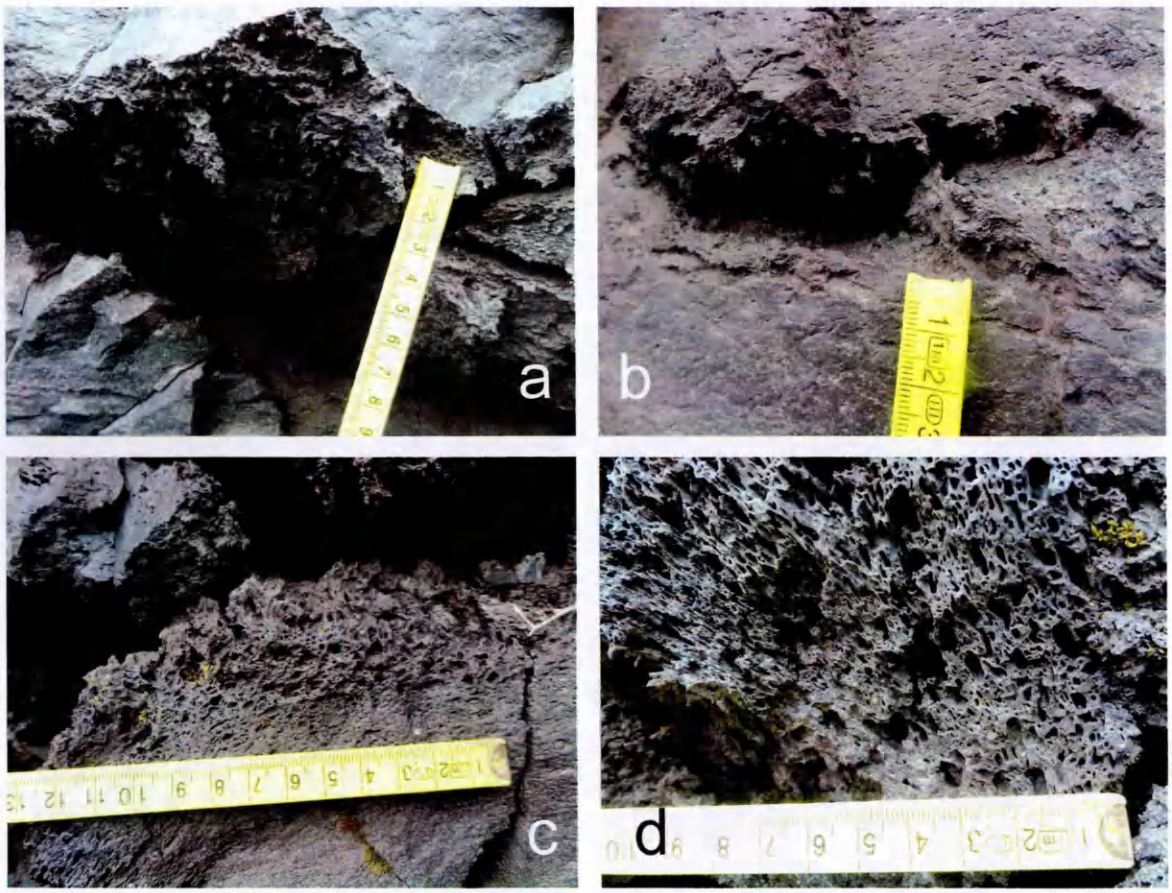

Fig. 5.8 a) and b) Ductile drooping and/or tearing textures. c) and d) Frothy vesicular textures.

In some lobes highly fractured lateral zones are sometimes observed, consisting of more densely fractured, glassier lava within the fractured outer carapace (Fig 5.9). These fracture zones may show extremely glassy selvages on the lava, ≤ 1 cm thickness (Fig. 5.9b-c), and usually have densely fractured, almost brecciated, curved shapes within them (Fig. 5.9d-f). The fractures in the lava surrounding these features, generally X-type pseudopillow fracture systems but also crude columnar joints, always propagate away from these areas and so may propagate contrary to the overall expected propagation directions (Fig. 5.9a). This demonstrates a local perturbation of the cooling regime with substantially more rapid cooling in these regions. These may perhaps be caused by ice-blocks becoming entrained within the flow (e.g. Lescinsky and Fink, 2000; Skilling, 2009; Graettinger et al., 2012).

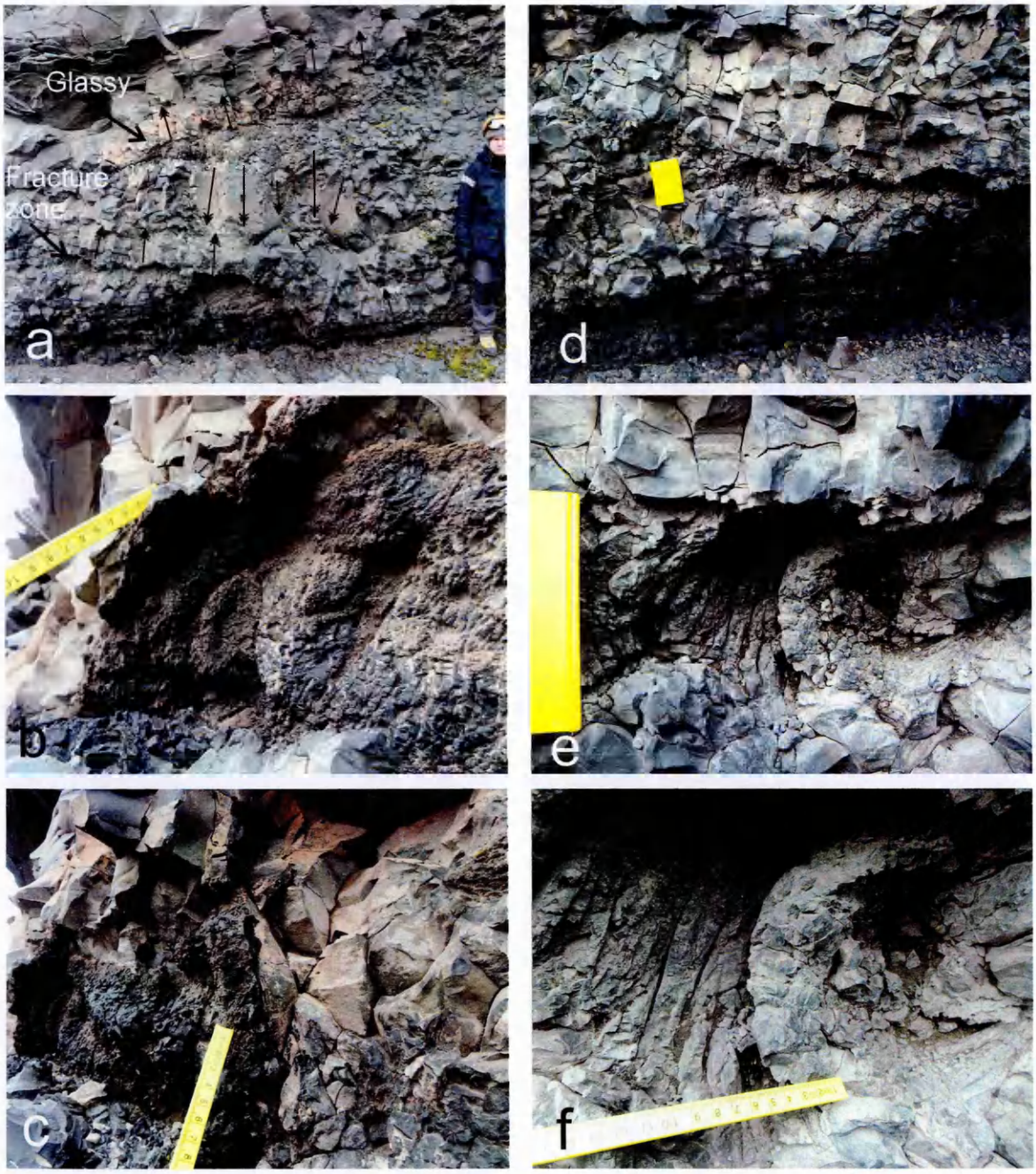

Fig. 5.9 a) Side of a lava lobe showing pseudopillow fractured outer carapace and some platy fracturing at the top. There are two interesting areas in this figure, one higher up shows extremely glassy selvages in an area of highly fracture lava (marked as 'glassy') the other below this shows a lateral fracture zone of highly fractured, almost brecciated, lava containing curved lobe shapes. Double headed arrows show fracture propagation directions, which are perturbed by these features and are always away from these areas. These are interpreted as ice entrainment features. b) and c) Close up from the glassy area, showing selvages of glass on the lava. d-f) Progressive close ups of the lateral fracture zone, showing the extreme fracturing and curved shaped within this zone. Note book is 20 cm in d) and e).

5.3 Description of fracture systems at Slaga

This flow is extensively fractured with almost every part of each flow lobe displaying some type of fracture. There are a variety of different fracture types in this flow which are described below. They can be summarised as X- and G-type pseudopillow fracture systems, columnar jointing and curved platy fractures. In order to understand what these fractures and their arrangement might tell us about the cooling regime of the lava flow it is important to understand how they form and where they fit into the structure of the flow.

5.3.1 Pseudopillow fracture systems in Slaga

Pseudopillow fracture systems are an association of two fracture types: each system comprises a single curviplanar master fracture and multiple subsidiary fractures that form perpendicular to the master fracture (e.g. Watanabe and Katsui, 1976; Lescinsky and Fink, 2000; Forbes et al., 2012). Subsidiary fractures can occur as either polygonal joint sets or as long planar subparallel collections of fractures (Fig 5.10). Pseudopillow fracture systems are present throughout much of the observable lava flow at Slaga, and have previously been linked to the presence of an additional coolant in the emplacement environment, either ice, snow or liquid water (Watanabe and Katsui, 1976; Lescinsky and Fink, 2000; Mee et al., 2006; Lodge and Lescinsky, 2009; Tucker and Scott, 2009; Forbes et al., 2012).

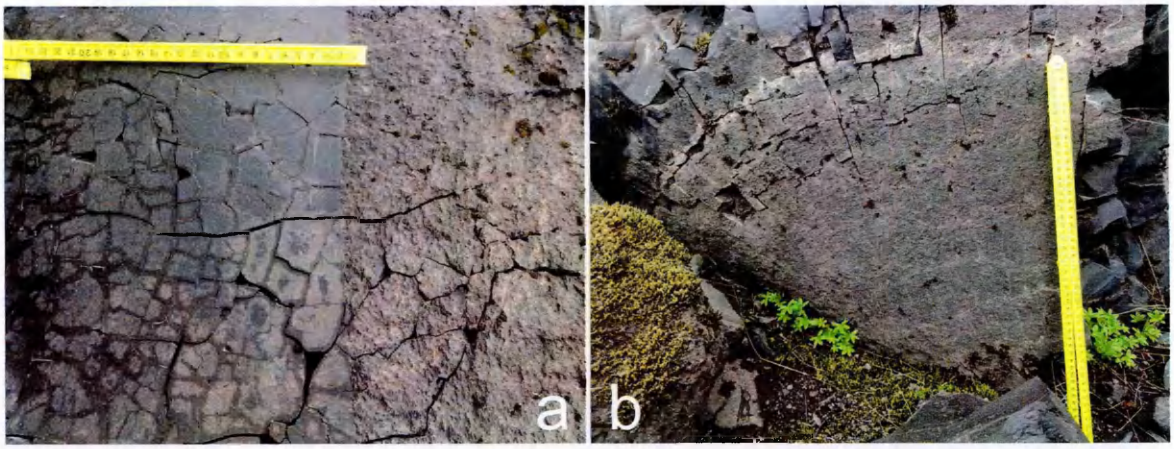

Fig. 5.10 a) Polygonal subsidiary fractures, with a very clear smooth to rough transition on the master fracture face indicating propagation from left to right. Ruler is 25 cm long. b) Long planar subsidiary fractures fanning outwards in an upwards direction, the master fracture here has a rough surface texture. Ruler is 50 cm long, top is to the right. Both of these are from the outer pseudopillow fractured carapace.

Pseudopillow fracture systems have been previously studied in trachyandesite lava of a very similar composition to that of the Slaga lava flow (Forbes et al., 2012; Chapter 2). Here pseudopillow fracture systems were divided into 3 types based on their master fractures: F-type have master fractures that form parallel to flow banding, X-type have master fractures that cross-cut flow banding, G-type have closely spaced striae across the master fracture surfaces, and so are not defined by their association with flow banding. In the Slaga lava flow banding is very faint and rarely visible so that X- and F-type are not useful or usable in the way in which they were originally defined. However, in the Tangahraun lava flow F-type master fractures showed a dimpled surface texture and X-type master fractures showed smooth and rough surface textures (see Figs. 2.4 and 2.5 in Chapter 2). There are two types of pseudopillow fracture systems in the Slaga flow: G-type and a type that have the smooth-rough master fracture surface textures and so are called X-type here. These X-type pseudopillow fracture systems are defined on the basis of master fracture texture rather than the orientation of the master fracture with respect to flow banding.

5.3.1.1 X- type pseudopillow fracture systems

X-type pseudopillow fracture systems occur in all the lobes of this flow. Master fractures from these fracture systems have a characteristic surface texture displaying both smooth and rough parts of the fracture surface. There is a sharp transition between the two surface textures, with river lines (e.g. Pugh, 1967) commonly occurring at the interface on the smooth part of the fracture surface. River lines occur as a result of mixed mode I and III fracture and can be used to demonstrate a fracture propagation direction (e.g. Hull, 1993), which in all cases observed at Slaga and Tangahraun (Chapter 2) is from the smooth to the rough part of the fracture (Forbes et al., 2012). These terminate abruptly against the rough portion of the fracture surface (Fig. 5.11). River lines are a feature of brittle fracture, so the fact that they terminate abruptly at the smooth-rough boundary indicates that the rough portion of the master fracture may be formed by ductile fracture as postulated previously (Forbes et al., 2012). The master fracture itself may be either fairly planar or strongly undulatory and may intersect with other master fractures. Glassier zones a few centimetres thick sometimes form either side of master fracture (Fig. 5.12) demonstrating more rapid cooling along the plane of the master fracture.

Fragmentary material, composed of mm-sized clasts of juvenile and other lithic material and a small amount of clay, is commonly seen trapped in X-type master fractures, this has been observed previously in master fractures (Lescinsky and Fink, 2000; Mee et al., 2006). In this case the trapped material may either be caused by fluxing of particle-bearing coolant during master fracture formation or may result from later deposition of glacial clays and gravels during glacier retreat and melting.

Fig. 5.11 River lines on an X-type master fractures at the smooth-rough boundary. River lines start as small closely spaced steps on the fracture surface and merge to form fewer larger steps. They show fracture propagation downwards here.

Fig. 5.12 Subhorizontal X-type master fracture at the bottom of the figure. The lava at the master fracture is very glassy and becomes less glassy within a few centimetres. Closely spaced striae propagating upwards from the master fracture can be seen on some of the subsidiary fractures.

The subsidiary fractures that form in conjunction with X-type master fractures occur in two distinct geometries: polygonal arrays of fractures and long planar subparallel or fanning fracture sets (Fig. 5.10). Both types of subsidiary fractures form normal to the master fracture on each side and propagate a similar distance from the master fracture. In a cross section of a pseudopillow fracture system taken normal to both the master and subsidiary fractures the two subsidiary fracture types are indistinguishable (Fig. 5.13). Both subsidiary fracture types are common in X-type pseudopillow fracture systems in this flow.

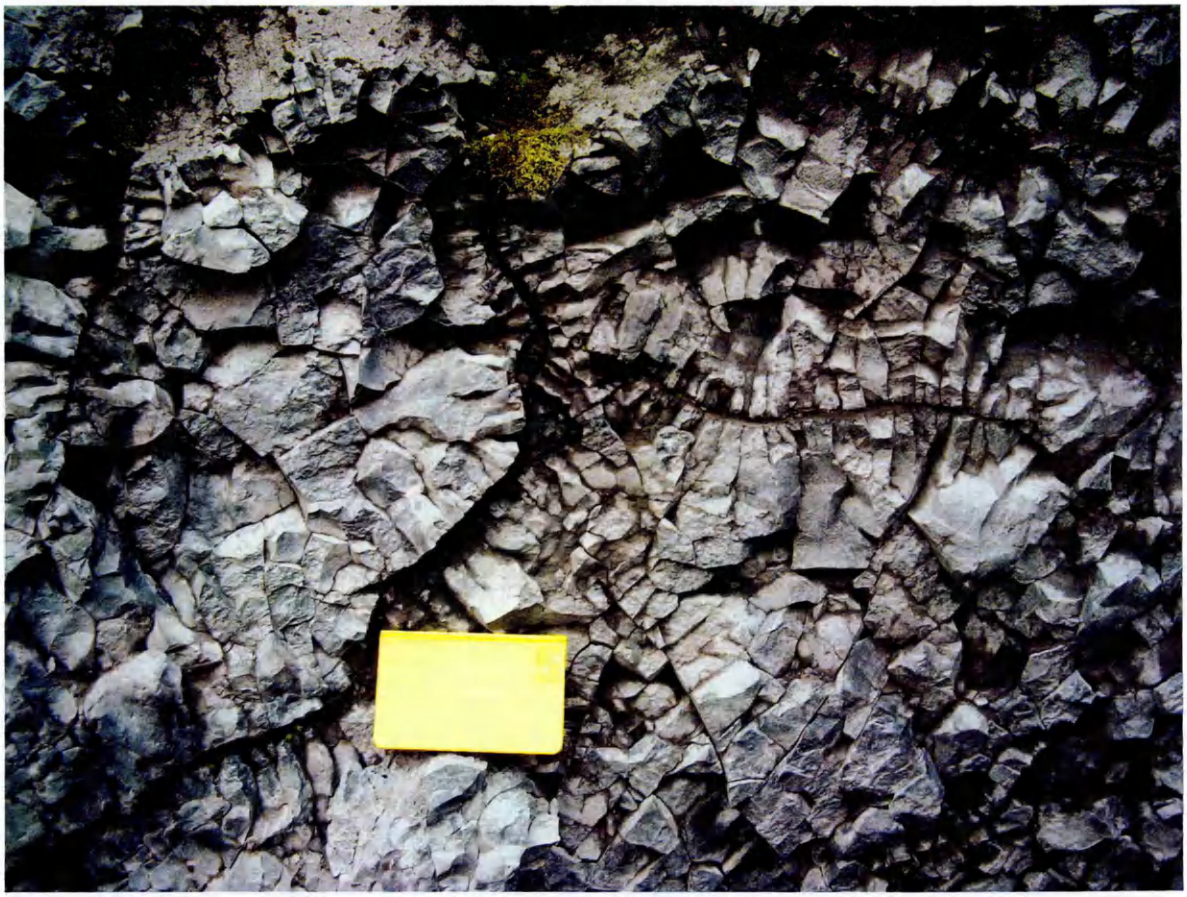

Fig. 5.13 Pseudopillow fracture system dominated outer carapace, showing curving and intersecting pseudopillow fracture systems in cross section. It is impossible to tell the type of subsidiary fractures (polygonal or subparallel) in cross section. Note book is 20 cm long.

Long planar subparallel subsidiary fractures display striae on their fracture surfaces demonstrating their formation by incremental advance of brittle fracturing (Ryan and Sammis, 1978; DeGraff and Aydin, 1987). The striae on these subsidiary fractures are

curved which appears to be a common feature on subsidiary fracture surfaces in pseudopillow fracture systems from all compositions of lava (Forbes et al., 2012; Chapters 2, 3 and 4; Fig. 5.14). Hackle (plumose structures), a common feature on striae and other brittle fractures (e.g. Ryan and Sammis, 1978; DeGraff and Aydin, 1987), show fracture propagation direction in a convex forward direction as previously (Forbes et al., 2012; Chapter 2).

As both master and subsidiary fractures show propagation directions, always in the same direction, general fracture forming directions can be deduced from both. They show that X-type pseudopillow fracture systems generally propagate upwards from the base, downwards from the top and inwards from the sides of flow lobes. In other words they always propagate in towards the centre of a flow lobe.

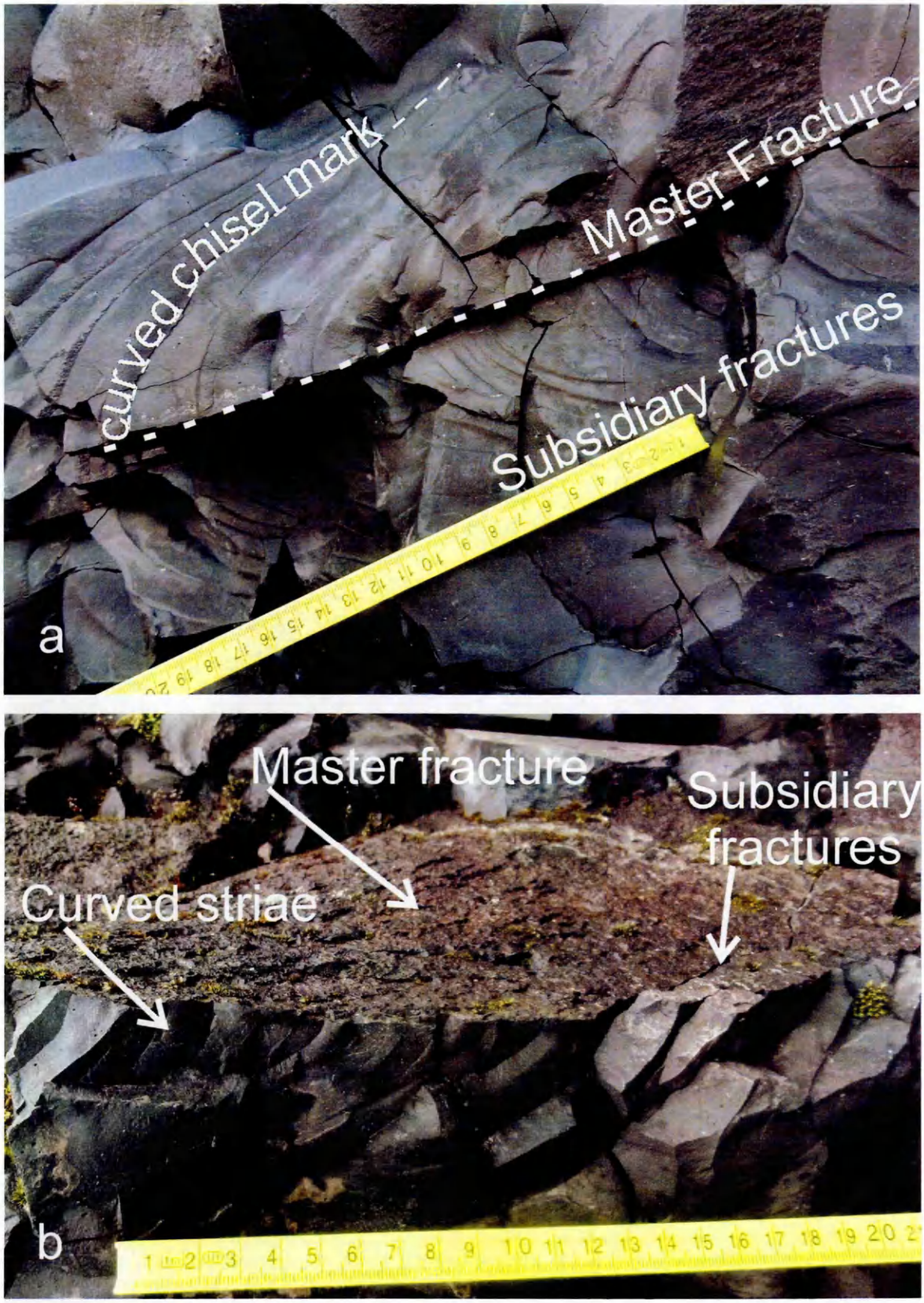

Fig. 5.14 a) Pseudopillow fracture system showing face-on subsidiary fractures with curved striae on subsidiary fractures. The master fracture of this pseudopillow fracture system is marked across the centre of the figure. b) X-type master fracture and subsidiary fractures with curved striae.

5.3.1.2 G-type pseudopillow fracture systems

G-type master fractures are characterised by very closely spaced, < 1 mm, striae across the master fracture surface (Fig. 5.15) and are identical to those described in Chapter 2. Subsidiary fractures in G-type pseudopillow fracture systems in this flow are always of the subparallel type. G-type pseudopillow fracture systems do not occur in every lobe, they feature only in very glassy parts of lobes and always at the base. G-type master fractures occur together in pairs, or as single curved fractures that form elongate lobate, or sausage-like, bodies at the base of some lobes (e.g. Mee et al., 2006; Fig. 5.11), and just once were observed on the side of a lobe, propagating inwards. Where G-type master fractures occur in pairs to form lobate bodies they appear to form as pull apart structures, with the two surfaces of the master fracture pulling away from each other, causing an open gape not generally seen on X-type master fractures (Fig. 5.16). G-type master fractures occasionally transform into X-type master fractures as they propagate inwards into the flow (Fig. 5.16).

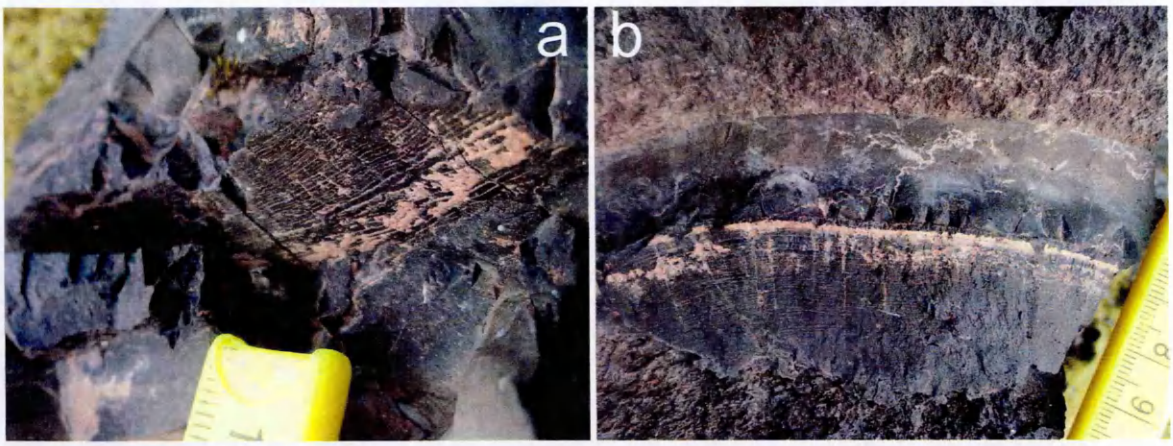

Fig. 5.15 a) G-type master fractures showing straight, very closely spaced striae on the fracture surface, indicating rapid brittle incremental fracture. b) G-type master fracture at the bottom of the figure with closely spaced striae, subsidiary fractures are picked out by pale pink fine material. This transforms into an X-type master fracture showing a smooth to rough transition, at the top of the image.

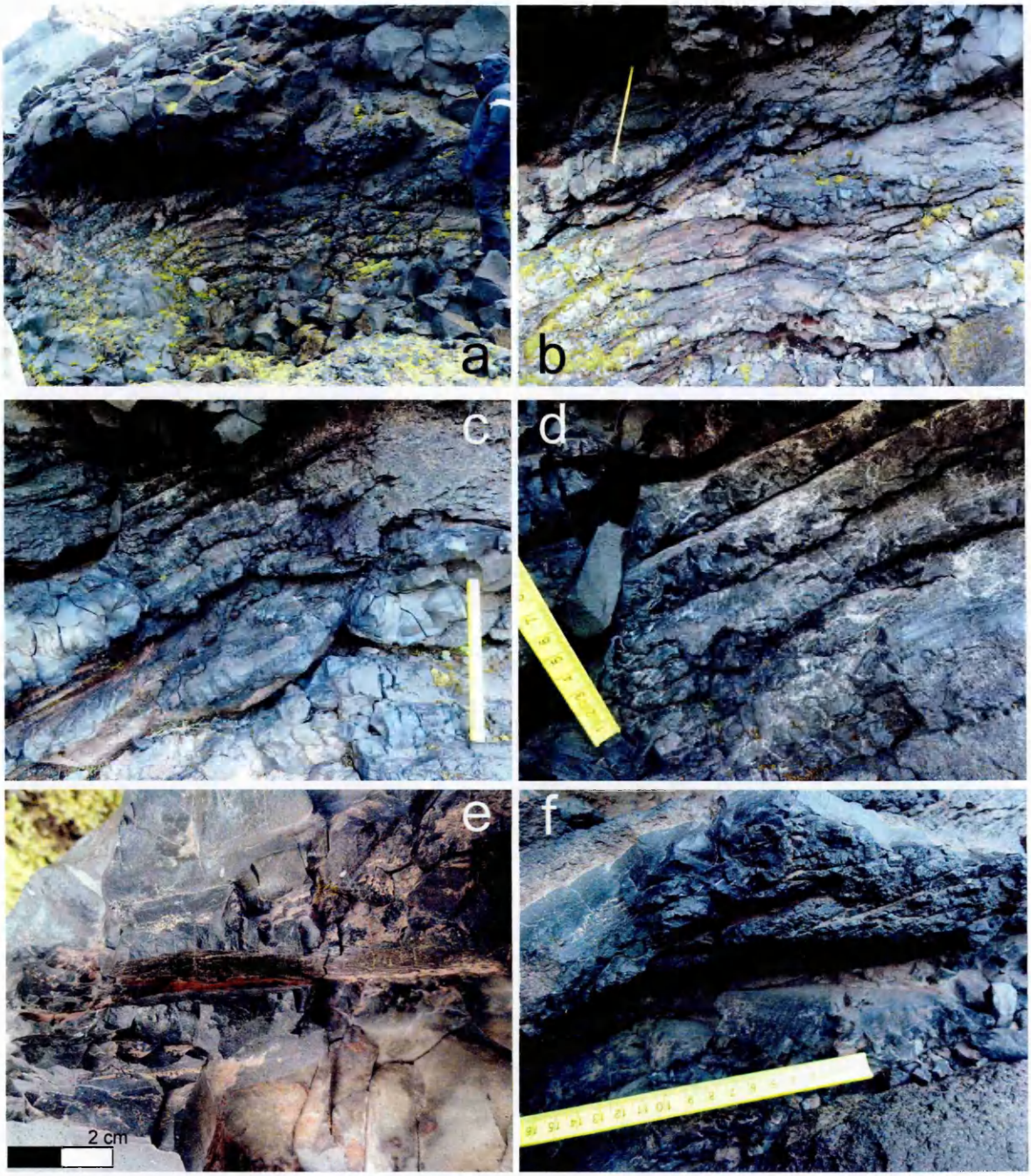

Fig. 5.16 a) G-type master fractures in elongate lobate forms at the base of a lava lobe. 16b-f are all close-ups of features in 16a. b) Close up view of G-type lobate forms, ruler is 50 cm. c) Closer view of G-type lobate forms with glassy margins, ruler is 25 cm. d) Glassy G-type master fractures forming elongate lobes. e) Pull apart structure formed by a G-type master fracture, notice the large gape across the master fracture, which is not observed in X-type master fractures. f) Multiple pull apart structures composed of G-type master fractures frozen in the process of formation, ruler is 16 cm.

The striae on G-type master fracture surfaces show hackle indicating fracture propagation generally inwards from the outside of the lobe. Striae on G-type subsidiary fractures are curved, like those in X-type systems. They are also very closely spaced, ≤ 1 mm apart, like those on G-type master fractures. Hackle that occur on these curved striae indicate the same direction of fracture propagation in relation to the shape of curved striae as in X-type

pseudopillow fracture systems and in G-type systems is always inwards and upwards from the base of lobes.

5.3.1.3 Measurements from long planar subsidiary fractures

Curved striae widths and subsidiary fracture spacing were measured from X-type pseudopillow fracture systems at various locations around the entire flow. The spacing of curved striae was measured as close to the master fracture as possible, for consistency within these results and for comparing them to measurements from the Tangahraun flow (see also Fig 2.9b for measurement methodology). These measurements were not obtained for G-type systems as striae were too small to measure accurately with callipers in the field. These data (Fig. 5.17a) show a positive correlation between subsidiary fracture spacing and striae widths. These are replotted (Fig. 5.17b) to include similar measurements from the Tangahraun lava (see Chapter 2), they plot in the same area as this previous data, showing a similar correlation.

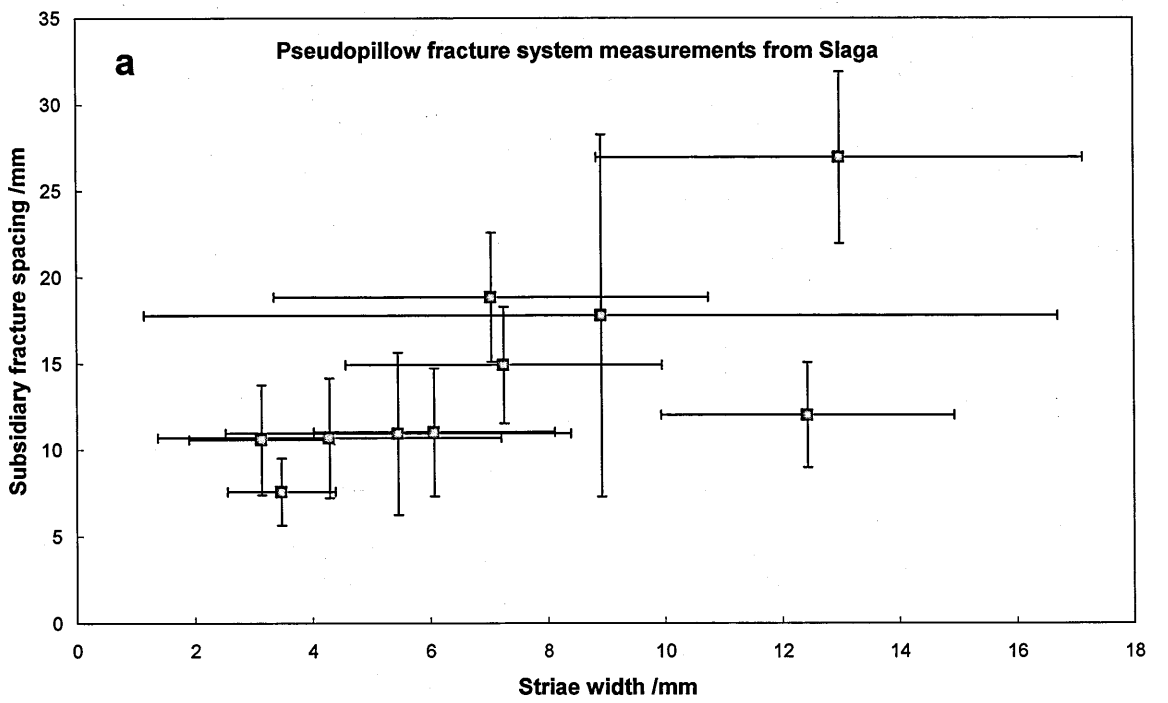

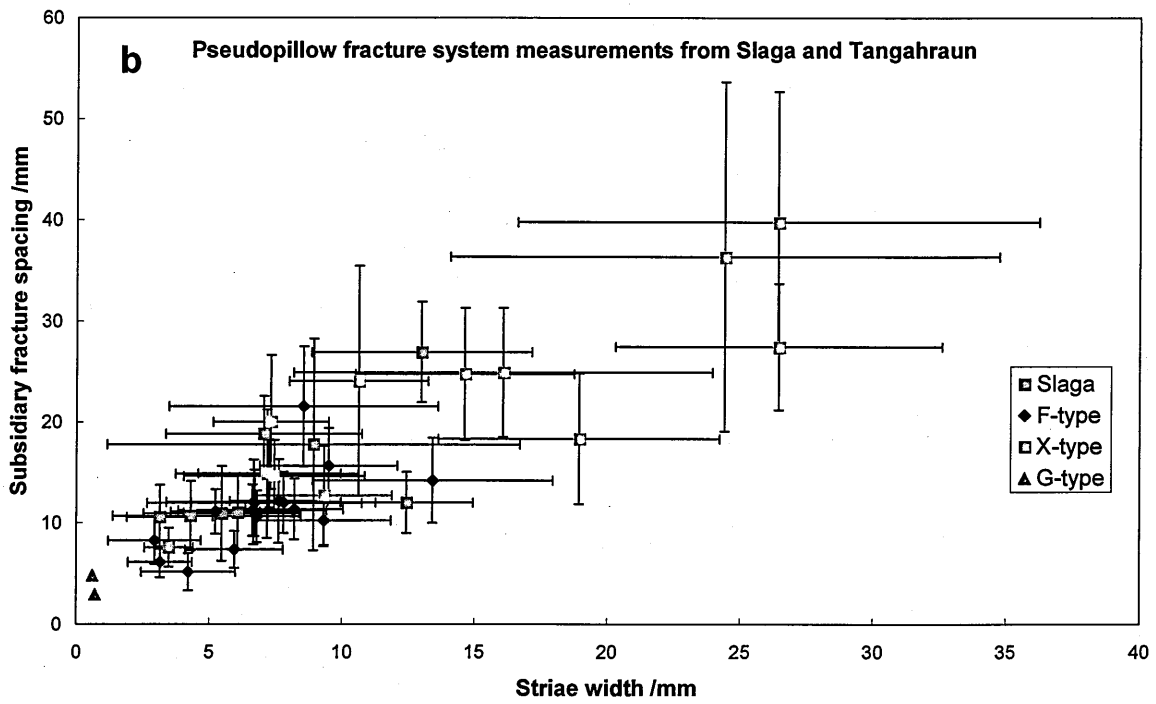

Fig. 5.17 a) Graph of subsidiary fracture spacing and striae widths from X-type pseudopillow fracture systems from the Slaga lava flow. They show a positive correlation. b) Slaga pseudopillow fracture system data replotted to include Tangahraun data (labelled as F-type, X-type and G-type). There is a very close overlap in the data from pseudopillow fractures systems in these two different lava flows. Error bars are ± 1σ.

5.3.2 Columnar jointing

Crude stubby columnar jointing or polygonally arranged fractures occur at the base of some lobes (Fig. 5.18). These tend to form in conjunction with upward propagating X-type master fractures so that subhorizontal striae can be seen on some fracture surfaces and smooth-rough transitions are seen on others. Columnar jointing often forms at the base of lava emplaced on top of older lobes, the top of the lobe with a columnar jointed base will commonly have downward propagating pseudopillow fracture systems (Figs. 5.18d and 5.5f).

In some larger lobes columns may be pervasively cut by subhorizontal platy fractures after the columns have formed (Fig. 5.18a-c). These fractured column zones then transition upwards into zones dominated by pseudopillow fracture systems and irregular blocky

jointing (Fig. 5.18a). This type of columnar jointing, cut by platy, fractures occurs more commonly in the northern part of the Slaga flow.

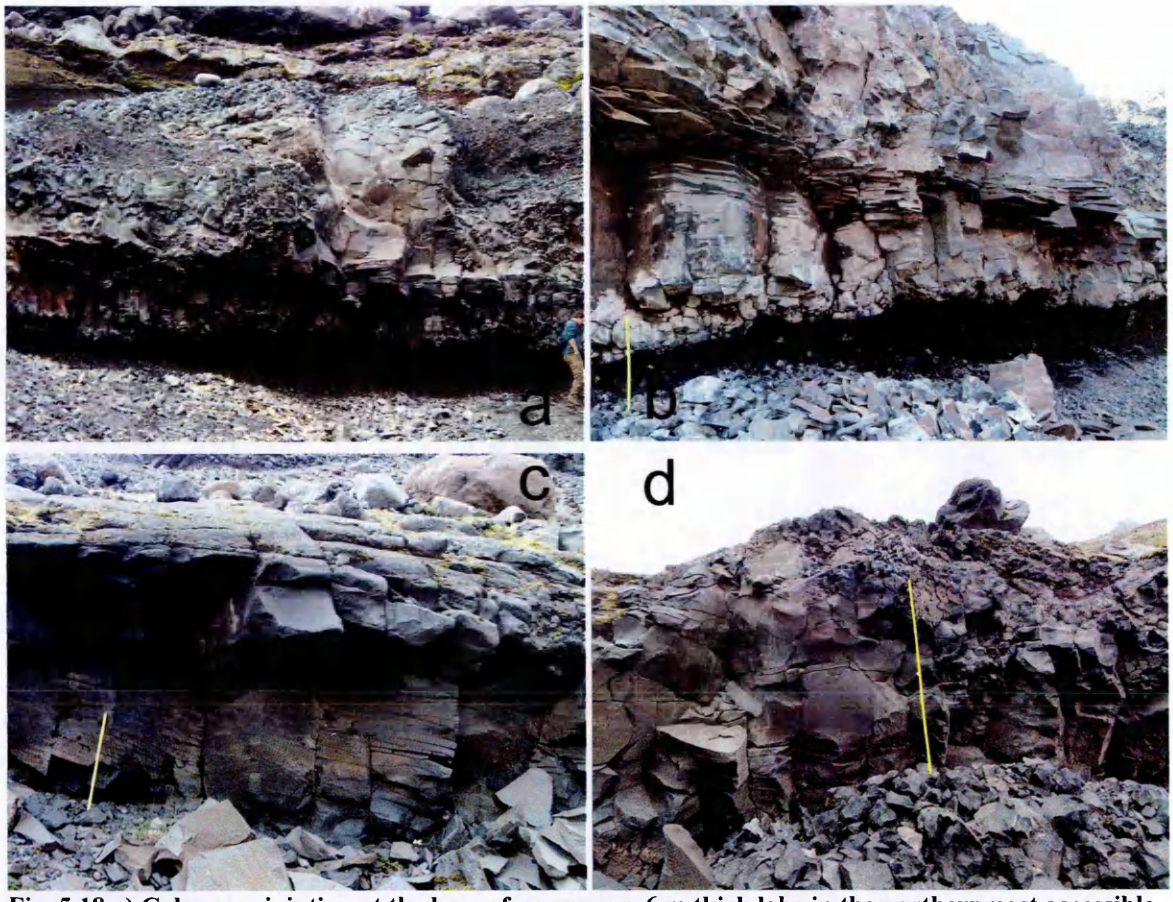

Fig. 5.18 a) Columnar jointing at the base of an approx. 6 m thick lobe in the northernmost accessible part of the flow. b) Close up of columnar jointing from the lobe in 13a. The columns are cross cut by platy fractures. Ruler is 75 cm. c) Columnar jointing cross cut by platy fractures at the base of an eroded lobe. Ruler is 50 cm. d) Columns with clear striae at the base of a lobe that rests on top of another lobe from this same flow. Ruler is 1 m.

5.3.3 Curved interior fractures

The centres of larger lobes are commonly dominated by more massive lava with curved platy joints spaced 1-10 cm apart (Fig. 5.19). Smaller lobes do not show this platy jointed interior. The platy joints form concentric layers in the centre of lobes, they curve round so that they are always approximately parallel with the edges of the lobe. Their fracture surfaces usually show extensive river lines spread across the surface of the joint (Fig. 5.19), indicating these were brittle fractures. River lines here are much more pronounced and expansive than those seen in X-type master fractures.

Fig. 5.19 a) End on view of concentric curved platy fractures in the centre of a lava lobe. Note book is 20 cm. b) Oblique view of curved platy fractures in the centre of a large lobe, surrounded by pseudopillow fractured outer carapace. c) and d) River lines on a platy fracture from the centre of a lobe. Notice how they merge and their topography become larger from right to left, indicating propagation from right to left. e) Vesicles collecting in the upper part of the central platy fracture core of a lobe (close up of 14a). The vesicles are mostly visible as darker spots in the lava. Note book is 20 cm for scale. f) Close up of large stretched vesicles from the top of a platy fractured interior from e), ruler is 20 cm.

Platy jointed lava in the centres of lobes is less glassy and coarser grained than the lava in the rest of the lobe. The centre is sometimes highly vesicular in the upper and outer parts of the platy jointing, with large, elongate, stretched vesicles (Fig. 5.19). Platy jointed lava generally has a reddish-brown colour rather than the black or dark-grey associated with the

outer part of lobes. These curved platy fractures are very much like those described by Mee et al. (2006) from the zone 2 andesite lavas of upper Santa Gertrudis valley, at Nevados de Chillán volcano, Chile.

A few X-type master fractures propagate from the base upwards, into the interior parts of large flows. They do not have any subsidiary fractures associated with them. These are later cross-cut by the curved platy fractures in the centre of the lobe, so must form before the platy fractures.

5.4 Discussion

The observations above are discussed in this section, demonstrating how they enable a detailed interpretation of the environment of this lava flow.

5.4.1 Pseudopillow fracture systems – bearers of environmental information

X-type pseudopillow fracture systems are the dominant fracture type in the Slaga lava flow. They occur in every lobe in the outer fractured, glassier carapace and X-type master fractures propagate upwards into the central portions of lobes. Their propagation directions taken from both master and subsidiary fractures indicate a coolant source entirely surrounding the lobes, which would indicate either a subaqueous or a subglacial eruption environment. Although, a subaqueous eruption or ponding of water at the glacier base might be expected to form pillow lavas (e.g. Lescinsky and Fink, 2000).

X-type pseudopillow fracture systems commonly have glassy zones either side of the master fracture which extend a few centimetres into adjacent the lava (Fig. 5.12). This demonstrates that X-type master fractures are acting as pathways to transport coolant

(water or steam) through the fractured lava from the outer into the deeper parts of the lava flow enabling these to be cooled, whilst causing rapid cooling of the lava surrounding the master fracture.

In a previously studied trachyandesite lava flow, Tangahraun, three types of pseudopillow fracture system were identified which included F-type pseudopillow fracture systems. This type of pseudopillow fracture system was defined as having a master fracture parallel to the flow banding. F-type master fractures have a characteristic dimpled surface texture resulting from cavitation ductile fracture (Forbes et al., 2012; Chapter 2). However, flow banding is rarely seen in the Slaga flow and so master fractures here are defined by fracture surface textures. No master fractures of the dimpled F-type are observed in Slaga, which may be related to the lack of vesicles in the parts of the flow where pseudopillow fracture systems form. In particular there is a lack of bands of vesicles which might induce cavitation ductile fracturing (e.g. Eichhubl and Aydin, 2003) rather than the type of ductile fracture seen on X-type master fractures.

G-type pseudopillow fracture systems are indicative of very rapid cooling of lava as demonstrated by their glassy nature and extremely narrow striae and therefore may reflect water rather than steam as a cooling agent (Forbes et al., 2012). The G-type pseudopillow fracture system link to water rather than steam as a coolant may be strengthened from studies of this flow. These fractures only occur at the base of lobes, where meltwater would preferentially collect or flow downhill as streams, and they generally do not occur throughout the rest of the flow. G-type pseudopillow fractures systems are also concentrated at the base of the lowermost lobes where many lobes occur together piled directly on top of each other. This may indicate some type of drying upwards sequence, whereby water could easily pond at the lava-sediment interface and would therefore affect only the base of the lowermost lobe and not the lobes higher up in the pile.

A subaqueous lava flow might be expected to show G-type pseudopillow fracture systems around the entire of the flow rather solely at the bases of lobes. This implies that the supply of coolant was not uniform which strongly suggests that the flow may have been subglacial rather than subaqueous.

5.4.1.1 Subsidiary fractures and striae widths

Striae widths on subsidiary fractures in this flow correlate well with spacing of long planar subparallel subsidiary fractures, which demonstrates that subsidiary fracture spacing is probably linked to cooling rate (e.g. Forbes et al., 2012; Chapter 2). Interestingly the relationship between stria width and subsidiary fracture spacing is exactly the same as that from the Tangahraun lava. This may be because the same fracture type was measured (i.e. pseudopillow fracture systems), or it may be caused by the extremely similar compositions of these two lava flows, resulting in similar physical properties. Stirae widths and subsidiary fracture spacings all plot in the smaller half of the graph Figure 5.12b, with X-type Slaga data plotting in the same space as F-type Tangahraun data, rather than with X-type Tangahraun data. This demonstrates more rapid cooling in the Slaga flow compared to the Tangahraun flow, as there are no data that plot in the slower cooling (larger striae and subsidiary fracture spacing) part of the graph.

5.4.2 Curved platy fractures

Platy fracturing has been observed previously in lava flows that have interacted with ice (e.g. Lescinsky and Sisson, 1998; Mee et al., 2006; Spörli and Rowland, 2006). The curved platy fractures in the Slaga flow appear to be identical in morphology and occurrence to those described by Mee et al. (2006), including their absence in the smaller lobes.

Curved platy fractures form in the much more coarsely crystalline central part of the flow, with none of the glassy areas or pseudopillow fracture systems that characterise the other parts of the flow lobes. This may be caused by an inability of coolant to infiltrate into the central parts of larger flow lobes, resulting in much slower cooling and a 'dry' environment. This could result from another lobe emplaced on top of the cooling lobe, blocking off its supply of coolant to the top of the lobe beneath, or by a gap melted above the flow into the ice retarding coolant supply to the top of the flow.

Spörli and Rowland (2006) suggested that platy fractures may be formed by detachment of the outer from the inner parts of the flow due to deflation. If this were the case then deflation would need to have occurred before the formation of the X-type master fractures which cut through the centre of the flow prior to the formation of curved platy joints. These X-type master fractures are undeformed and fairly planar indicating that they have not been affected by continued flow of the lava.

X-type master fractures form in lava that is still very hot, resulting in ductile fracture textures across their surfaces (Forbes et al., 2012; Chapter 2). The flow interior would then have had to cool further before the curved brittle fractures could form, without deforming or flowing away. Therefore the curved platy fractures are unlikely to be related to stresses from continued flow of the central portions of flow lobes and deflation because of the presence of X-type master fractures. For the same reason platy fractures are also unlikely due to late stage shear of the lava flow (Bonnichsen and Kauffman, 1987).

Degassing of the central portions of these flows is a slower less dynamic process that may have led to volume contraction and formation of curved platy fractures. In the central parts of lobes it is generally only the upper parts that are vesicular, indicating that the lower part

of the central portions of the lobe may have degassed. This degassing would be associated with a decrease in volume in the central part of the flow perhaps resulting in the curved platy fractures. Otherwise these curved platy fractures may be caused by microlite alignment orientation (Walker, 1993).

River lines are very prominent on these fracture surfaces. River lines result from mixed mode I/III fracturing and consist of a series of steps on the fracture surface aligned in the direction of crack propagation (e.g. Pugh, 1967; Sommer, 1969). All the steps are of the same 'sign' and they nucleate as a series of closely spaced steps that merge to form larger, more widely separated steps. They are caused by the crack trying to overcome its inability to twist, so forming steps which function as individual crack planes, with a very small rotation of the fracture plane across the boundary (Hull, 1999). The river lines likely form due to the strongly curved nature of these fractures, as they allow the fracture plane to effectively twist.

5.4.3 Columnar jointing

Columns at the base of a flow lobe demonstrate fairly even cooling from the base upwards in a uniform stress environment. Columns may form with or without the addition of some type of coolant (e.g. Lyle, 2000; Goehring and Morris, 2008; Chapters 3 and 4). In some cases columnar jointing occurs in this lava flow in lobes emplaced on top of others (e.g. Figs. 5.13d and 5.15f). This may result in a dryer, more slowly and evenly cooled flow base as coolant cannot collect on a porous fractured lava flow, and may be the cause of columnar jointing at some flow bases. These columns may occur in a flow that has pseudopillow fracture systems propagating downwards from the top of the flow, indicating a coolant supply to the upper parts of the flow.

In some cases striae bearing column bounding fractures occur in conjunction with X-type master fractures. This has also been observed in the Tangahraun trachyandesite flow (Chapter 2) and may indicate some coolant and/or non-uniformity in the stress field where this occurs. Columnar jointing sometimes transforms upwards into pseudopillow fractured lava. This may indicate an increase in the input of coolant to the cooling lava flow and possibly a related increase in the rate of cooling.

5.4.4. Environmental implications of fractures and flow morphology

The rapid radial cooling of lobes in this flow implies that the lobes were surrounded by coolant. A number of lines of evidence suggest that this was ice rather than water. The high aspect ratio of lobes strongly suggests confinement of this flow, probably by ice. The piling up of successive lobes on top of one another may also relate to their emplacement under ice, as it is easier for a lobe to flow along a path previously melted into the ice that create a new one. Glassier flow bases combined with G-type pseudopillow fracture systems only occurring in these glassy lobe bases of many flow lobes demonstrates the uneven nature of cooling of lobes. Coolant, probably water, runs along the base of the flow but has less influence on lobes higher up in the pile. The uneven nature of cooling in this flow, such as G-type pseudopillow fracture systems at the base of lobes, curved platy fractures in slower cooled lava in the centre of lobes, and a general lack of pillow lava suggests a subglacial rather than subaqueous lava flow environment.

The very vesicular frothy textures in this flow might indicate a sudden release of pressure, perhaps by fracturing of the ice above the flow, or due to fairly thin ice conditions, or both. The flow and drainage of water shown by the glassy lobe bases would also suggest that the ice here was thin, probably an alpine-type glacier $\leq$100-150 m thick (Smellie, 2000).

The interior portions of larger lobes are more slowly cooled than the rest of the flow, possibly because not enough coolant was produced to reach the centre of these large lobes. Thicker outer fracture carapace at the base indicates that much more cooling was progressing from the base upwards than from the top downwards. If the lava flow melted sufficient ice to result in a cavity between the lava upper surface and the ice this would cause retarded cooling at the top of the flow, melt water will be channelled to the base of the flow. Melting a cavity beneath ice has been shown to be possible for basaltic but not rhyolitic lavas, given an 80% heat transfer efficiency (Höskuldsson and Sparks, 1997). Pseudopillow fracture systems result in a large fracture surface area in a given volume of lava, likely resulting in efficient transfer of heat. The calculations of Höskuldsson and Sparks (1997) are based on a closed system with no escape of melt water, but the more rapidly cooled flow base indicates that this is probably not true for the Slaga flow. In which case the flow may have been able to melt a cavity above the lava. The insulated interior parts of larger lobes may also be explained by successive lobes emplaced on top, blocking coolant access to the lobe below from above.

Tunnels, formed by meltwater from the first incursion of the lava flow in the glacier closer to the vent(s), may be small. This could cause the flow to split into several lobes, if the flow becomes retarded flowing through a small space while being cooled rapidly. This may result in avulsion of the lava flow, splitting it into lobes which utilise other tunnels, cavities or areas of fractures and weakness at the glacier base.

A synopsis of the processes and evolution of the Slaga lava flow is outlined: the flow was emplaced as a series of lobes beneath thin ice, probably an alpine/valley type glacier. The lava flowed over, and sometimes interacted with, a probably soft, unlithified polymict sediment. It was cooled rapidly on all sides and lobes were probably confined by ice while they were being emplaced. Water flowed along the base of the lava causing particularly

rapid cooling there. The flow may have melted a cavity in the ice above, or successive lobes were emplaced on top of earlier ones fairly rapidly. The lava flow has since been eroded and glacially deposited debris has collected on top of the flow.

5.4.5 Slaga and Tangahraun: a brief comparison

These two lava flows, Slaga and Tangahraun, are very similar in composition and in fracture content, containing copious pseudopillow fracture systems and columnar jointing. However, they have very different flow morphologies, which may be related to their emplacement environments or flow properties and dynamics.

Tangahraun, where it is exposed at the shore, occurs as a single massive, rubble topped, flow ~15 m thick, although the flow base is not visible and it is likely that the flow is thicker than this. Further inland however, the lava has a more lobate form where individual lobes can be discerned within the lava, and ribbons of coherent lava form in the flow top breccia. Further south the lava is commonly thicker than the solid lava that forms the lobes in the cliff at the north of the beach. As the Tangahraun lava flowed towards the sea it has likely increased in thickness and lobes have amalgamated/coalesced to create a thicker body of lava. This may be a result of the lava entering the sea or coming into contact with sea water, slowing the flow down causing it to back up, while the flow was inflating. The gradient near the shore may have been fairly shallow, slowing down the lava flow, allowing it to thicken. Nearer to its source on Snæfellsjökull, where the terrain is much steeper, it appears to be composed of multiple lobes (see Fig. 2.2)

Slaga occurs as multiple lobes, much like those described by Mee et al., (2006) and seemingly similar to the 'pillow-lobes' described by Lescinsky and Fink (2000). It is a considerably thinner lava flow than Tangahraun and much smaller in visible extent. Its

lobate form may be due to the steeper slope it has flowed down, a slower effusion rate (e.g. Walker, 1971), or perhaps due to its subglacial environment and the affect small of meltwater channels at the glacier base causing the lava flow to split into multiple separate lobes.

5.5 Summary

This study demonstrates that cooling fractures in lavas, particularly pseudopillow fracture systems, can be an important information source when trying to establish and understand the eruption environments of lava flows. A number of conclusions can be drawn from the cooling fracture in this study: this lava likely flowed subglacially, being confined and cooled rapidly from all sides. The environment is probably a thin alpine-type glacier with ice < 150 m thick. This study has strengthened the link between G-type pseudopillow fracture systems and water (rather than steam) as a coolant, due to their formation only at the base of lobes.

An improved understanding of cooling fractures, such as pseudopillow fracture systems, has enabled the use of cooling fractures to derive information on the emplacement environment of this lava flow, thus demonstrating that this is a practical method when studying lavas of unknown environment. However it is important to gather all relevant observations relating to a lava body as presence of absence of any fracture type can only provide limited information in itself.

5.6 Highlights

- Demonstration of cooling fractures in lavas as a source of information when attempting to understand lava flow eruption environments.
- This is only possible due to advances in the understanding of relevant fracture mechanisms.
- The lava flowed under thin ice conditions and was particularly wet at its base.

Chapter 6: Conclusions

6.1 Introduction

The aim of this study was to enable a better understanding of the cooling environments of lavas from the fractures formed in lava flows, in particular pseudopillow fracture systems, columnar jointing in rhyolite, and entablature in basalt. In previous studies these fracture types were specifically related to the (interpreted) lava environment in which they are found, and yet there was little understanding of why they formed only in these environments, containing either ice, snow or water, and in some cases how they formed. The questions set out at the beginning of this thesis were: 1) how do pseudopillow fracture systems form and 2) why do they only form in 'wet' environments? 3) Why is columnar jointing so common in subglacial rhyolite and 4) what information can these columns give us about the cooling environment? 5) What fracture types occur in entablature in basalt and 6) how do they form? Below is a summary of the main results and conclusions from this study, followed by a brief discussion on the results of this work.

6.2 Summary of new findings

6.2.1 How do pseudopillow fracture systems form?

Pseudopillow fracture systems have been found in lavas ranging in composition from basalt to rhyolite, that have interacted with ice, water and steam in this study. Pseudopillow fracture systems consist of a single large curvi-planar master fracture, and many subsidiary fractures formed normal to the master fracture, that propagate away from the master fracture. The fracture type and formation mechanism of the master fracture was

previously unknown. This study shows there are three types of master fracture, termed F-, X- and G-type. F- and X-type are the most common (except in rhyolite) and were originally defined on the basis of their orientation to flow banding but subsequently on the basis of master fracture fractography where no flow banding exists in the lava flow. G-type were originally defined on the basis of master fracture surface texture and have continued to be so.

F-type master fractures form by cavitation ductile fracture. Holes, which may nucleate and/or be present previously as bubbles in the lava, grow and coalesce to form the master fracture surface which shows a characteristic dimpled texture resulting from the preservation of half cavities. F-type master fractures have been observed in flow banding parallel master fractures in the trachyandesite Tangahraun lava flow (Chapter 2) and in the master fractures in entablature (Chapter 4). However, they are not present in the Slaga flow, a lava flow with a very similar composition to the Tangahraun lava flow in which pseudopillow fracture systems are widespread. F-type master fractures are thought to only form where pre-existing holes or bubbles are already present, although cavities could nucleate spontaneously on inhomogeneities such as crystals in the lava. In the Tangahraun flow F-type master fractures are postulated to form in vesicle rich flow bands that occur in the lava, and in entablature they are thought to form within vesicle rich late stage segregation melt. The Slaga lava, which is highly vesicular in places, has no concentrations of vesicles in bands as in the two cases above, which may explain its lack of F-type master fractures.

X-type master fractures are also formed partly by ductile fracture, not by cavitation like F-type master fractures, but a type of ductile fracture which results in a rough surface texture, that is also observed on striae on columnar joints (Ryan and Sammis, 1978). X-

type master fractures show an abrupt transition in fracture surface texture from smooth to rough, commonly with river lines at the junction between these two textures. River lines only form on the smooth part of the fracture surface and are diagnostic of brittle fracture; they show fracture propagation from the smooth towards the rough fracture surface texture. The river lines terminate at the smooth-rough junction, suggesting that the rough fracture texture is not the result of brittle fracture (i.e. it is a ductile fracture). The smooth-rough fracture surface textures are useful as they can be used to demonstrate a fracture propagation direction, from smooth to rough – i.e. the fracture changes from brittle to ductile as it propagates into hotter lava.

G-type master fractures are formed entirely by brittle fracture, shown by striae on the fracture surface. These form in both the trachyandesite lava flows Tangahraun and Slaga (Chapters 2 and 5) in the very glassiest parts of these lava flows, and display extremely narrow striae, ≤ 1 mm. This is evidence of rapid cooling, and this master fracture type is thought to form during more rapid cooling than either F- or X-types. Cooling was so rapid during their formation that the lava was cooled below its brittle–ductile transition temperature as it fractured, resulting in brittle rather than ductile fracture. These types of pseudopillow fracture systems experienced more coolant (water/steam) in the system to cause more rapid cooling than in F- and X-types, and may be formed by lava-water cooling whereas F- and X-types are probably formed by lava-steam interaction (e.g. Mee et al., 2006). The striae on the master fracture surface can be used to demonstrate a fracture propagation direction using the hackle present on striae.

G-type master fractures are the only type that form in rhyolite (Chapter 3). Rhyolites in this study have not demonstrated any ductile fracture textures at all. This may be because rhyolite is too viscous and G-type master fracture form at too high strain rate to cause

ductile fracture in rhyolite. This could mean that any inferences about steam versus water cooling may not be valid for rhyolite, as they may only form G-type pseudopillow fracture systems, whatever the coolant. However, that other master fracture types or ductile fracturing were not seen during this study does not conclusively prove that they do not or cannot occur in rhyolite. As the only rhyolite lavas studied are subglacial they might be expected to cool more rapidly due to inundation with water, which is exactly the situation in which G-type master fractures are thought to form.

Two distinctly different morphologies of subsidiary fractures have been recognised in this study: the previously observed polygonal subsidiary fractures and the long subparallel sets of subsidiary fractures. Polygonal subsidiary fractures tend to have straight striae on their fracture surfaces showing propagation away from the master fracture, as described by Lescinsky and Fink (2000). They are very much like columnar joints and are caused by simple cooling contraction of the lava either side of the master fracture. Long parallel subsidiary fractures have not been documented previously and yet they appear to be the most common subsidiary fracture type. They form in all lava compositions studied (basalt, trachyandesite and rhyolite) and all display curved striae on their fracture surfaces.

Curved striae are also previously undocumented. Striae mirror the isotherms at the time of fracture, demonstrating cooling and fracture propagations directions normal to the isotherms and so normal to the striae. The curvature of isotherms is probably caused by the directional ingress of coolant along the master fracture, causing cooling both in the direction of master fracture advance and perpendicularly away from the master fracture. The radius of curvature of striae may be affected by cooling rate, with faster cooling causing a smaller radius of curvature as both G-type subsidiary fracture striae in Tangahraun/Slaga and in subglacial rhyolite from Bláhnúkur show a very tight curvature

whereas striae in basalt are much more broadly spaced and are more gently curving, with a larger radius of curvature. The spacing of long subparallel subsidiary fractures correlates well with striae widths. As striae widths are controlled by cooling rate so subsidiary fracture spacing is also, given this close correlation. Curved striae can be used to demonstrate a fracture propagation direction. They have always been observed to propagate in the same direction in relation to their curvature, and so their morphology can be used to infer propagation direction in examples where hackle are not preserved.

Perhaps less is understood about subsidiary fractures than was previously thought. When they were all thought to be polygonal fractures (e.g. Watanabe and Katsui, 1976; Yamagishi et al., 1989; Yamagishi, 1991; Lescinsky and Fink, 2000) their formation was easily explained by cooling contraction. Long subparallel sets of subsidiary fractures are less easily explained by cooling contraction alone, due to their preferred formation direction. However, the striae on their fracture surfaces indicate that the same fracture mechanism (incremental brittle fracture) occurred. Stresses in the lava likely cause the preferred orientation of subsidiary fractures. Although the subsidiary fractures are not able to relieve biaxial stresses due to cooling contraction, yet we know they are strongly controlled by cooling and cooling rate. They occur perpendicular to the master fracture but propagate in the same direction, possibly the combination of these two orthogonal fractures relieves the broader scale stress, or perhaps the fanning out of subsidiary fractures relieves some of the stress in the direction parallel with the long planar fractures. As the fractures fan outwards some portion of stress relief can be resolved perpendicular to the fracture. As subsidiary fracture types are almost impossible to determine without a direct view, subsidiary fractures may have been presumed to be polygonal when they were the subparallel type.

6.2.2 Why do pseudopillow fracture systems only form in 'wet' environments?

It is important to understand why pseudopillow fracture systems only form in wet environments if they are to be used as an indicator of the lava emplacement environment. Abundant evidence for these environments is seen in pseudopillow fracture systems in the form of glassy lava associated with these fractures and narrow striae, the ultimate example of this being G-type pseudopillow fracture systems. G-type pseudopillow fracture systems must form in environments with high cooling rates. The preservation of ductile master fractures may be key evidence for why F- and X- type pseudopillow fracture systems form only in these wet environments. Ductile fractures that form due to high strain rates in typical subaerial lava flows are likely to close and anneal soon after formation, leaving little evidence that they were ever there. At the very least the delicate ductile fracture textures will relax back into the fracture surface, leaving little evidence that any fracture was a ductile fracture. However in environments containing water or steam that can access the lava these ductile fractures will be cooled as soon as they open thus preserving them and their fracture textures. If this is true then ductile fractures may form more commonly than is appreciated in subaerial lava flows, which promptly anneal or lose their surface textures. If annealed fractures form along flow bands they will be impossible to identify. However if they do not form along flow bands then they might be identifiable in lava flows, particularly in the case of annealed master fractures in basalt which may occur as planes of late stage residual melt.

6.2.3 Why is columnar jointing so common in subglacial rhyolite?

The formation of columns in rhyolite is likely related to the stress environment rather than the cooling environment. Flows where stresses can be relaxed before the lava cools, such

as large flows or supported flows (intrusive or ice supported) can form columns. However, smaller-volume subaerial flows cannot form columns due to the non-uniform (anisotropic) stresses in the cooling environment.

6.2.4 What information can rhyolite columns give about the cooling environment?

One major contribution in this study was the presentation of a data set from rhyolite columns of subglacial origin (see appendix 2 for full data set). Column side width, *W*, striae widths, *S*, and the number of column sides were measured. This has contributed to both the understanding of columnar jointing and to our knowledge of subglacial rhyolite lava. Some factors affecting *W*, thermal diffusivity, eruption temperature and viscosity, were analysed and it was concluded that viscosity variations between basalt and rhyolite have the most significant effect on *W*, causing larger columns in rhyolite for a given cooling rate. Thermal diffusivity and eruption temperature only have minor effects on the build up of stress, by comparison. *W* and *S* from different compositions of lava are unlikely to be comparable due to differences in the physical properties of lavas of different compositions, but can be used to compare lavas of the same compositions.

Subglacial rhyolite columns tend to have fewer column sides on average, which may be related to rapid cooling, with a high cooling rate not allowing time for the columns to form into their equilibrium shape. Column size does not vary much between different outcrops meaning that it may not be a good indicator of the cooling environment. This may result from a minimum column size having formed due to rapid cooling rates. However, striae widths varies greatly between different rhyolite column bodies, meaning that striae may be a better way to compare and understand cooling environments. This leads to a large *W/S*

range, much larger than previously found in subaerial basalt columnar jointing measurements.

6.2.5 What fracture types occur in entablature in basalt?

Entablature tiers are dominated by two fracture types: columnar joints and pseudopillow fracture systems, which were previously unrecognised in entablature. The interaction of these two fracture types has been observed to form chevron fracture patterns, previously documented but unexplained in entablature tiers. The long, first formed fractures previously observed in entablature are master fracture of pseudopillow fracture systems and their presence strengthens the interpretation of a lava-coolant interaction origin of entablature.

Two end member types of entablature were identified: 1) more densely fractured cube-jointing, and 2) column forming entablature. Both contain pseudopillow fracture systems. The differences between these two end members probably relate to the amount of coolant infiltrating the lava, with cube-jointing forming due to more rapid cooling, shown by smaller relative striae widths and a denser fracture network.

6.2.6 How do pseudopillow fracture systems form in entablature?

Master fractures in entablature have a thin glassy band or selvage of material that is more evolved than the rest of the lava, and they have dimpled fracture surfaces. This more evolved material is formed by gas-driven filter pressing of late stage residual melt in the lava flow, into areas of low pressure caused by stresses in the lava flow, leading to master fracture formation. The stresses which enable master fracture formation may be caused by

movement of water on top of the lava flow. The evolved selvage of material at the master fracture shows strong evidence of rapid cooling with dendritic textures in Fe-Ti oxides, clinopyroxene and plagioclase and a higher concentration of glassy mesostasis in this part of the lava. The dimpled texture is likely the result of cavitation ductile fracture enabled by vesicles formed in a band in the residual melt, followed by rapid quenching of the fracture and its surroundings by the influx of water and/or steam.

Cooling in entablature is most rapid in the evolved material of the master fracture and occurs less rapidly in columns in entablature showing only a few dendritic oxides here. This demonstrates that master fractures are likely the main conduit for coolant entering entablature. There are no dendritic oxides in either the upper or lower colonnade columns, demonstrating that these cooled still slower than those in the entablature tier.

6.3 Discussion of results

Fractures can be extremely useful in interpreting lava flow environments. Both pseudopillow fracture systems and columnar jointing can provide fracture propagation directions allowing interpretation of the cooling direction. They also provide basic interpretations of the environment by simply being present in a lava flow: pseudopillow fracture systems are only found in 'wet' environments. Likewise entablature jointing, which commonly contains pseudopillow fracture systems as part of its fracture assemblage, only forms in 'wet' environments. Columnar jointing in rhyolite has been linked to subglacial environments, although caution is needed as columns may form in rhyolite in non-subglacial environments under the right conditions where their flow stresses can be relaxed.

However, it is important to note that a very detailed environmental description cannot be deduced from the presence of certain types of fractures alone. A number of other features must be used to enable an environmental determination, such as: perlite (in rhyolite), peperite, confinement of a lava flow causing large height to width aspect ratios, the locality of a lava flow (e.g. the coast, stratovolcano, caldera lake etc. versus a desert), the presence of glassy lava, dissolved volatile concentrations in the lava, the widths of striae, any indicative geological formations below or surrounding the lava e.g. glacial till, lake sediments, fluvial deposits.

It is not just the cooling environment that determines the fracture types that forms in a lava but also the stress environment. A uniform stress regime during cooling, caused by cooling contraction, will produce columnar jointing in almost any environment in almost any lava composition, at almost any cooling rate, except possibly for extremes of cooling rate (e.g. Toramaru and Matsumoto, 2004). So pseudopillow fracture systems may only form in 'wet' environments where there is an anisotropic stress regime and a sufficiently high strain rate to cause fracturing of lava near its brittle-ductile transition temperature.

The composition of lava is important to consider when trying to understand the stress environment as more viscous, silica-rich lavas are better able to retain flow related stresses, whereas mafic lavas can relax these stresses much more rapidly. This is likely the reason why columnar jointing does not form commonly in subaerial rhyolite lava but does in subaerial basalt. Flow related stresses relax much more rapidly in basalt leaving a uniform stress environment dominated almost solely by cooling contraction stresses. However, in subaerial rhyolite, the dominant stress regime is that of the flow stresses, with an additional, smaller component of cooling contraction.

A 2-dimensional parameter space can be envisioned where the amount of anisotropy in the stress field plots against the composition of the lava flow (Fig. 6.1). Different fracture types will form in varying parts of this parameter space and so different lava bodies (or parts of lava bodies) can be plotted within this parameter space, and has been done for lavas in this study (see Fig. 6.1). In the case of this study, at low anisotropy of stress columnar jointing will form and at larger anisotropic stresses pseudopillow fracture systems will form. In between low and high non-uniform stresses hybrid fracture types may form, such as columnar jointing with some preferred orientation of the columns. At even higher values of stress anisotropy a stress-field with a strong preferred orientation is present. This may produce sheet-like fractures like those seen in many of the Bláhnúkur lobes, rather than the more randomly oriented pseudopillow fracture systems formed in other lava flows. Higher stress environments often appear to accompany higher anisotropic stresses and may often have fractures formed at higher strain rates, such as pseudopillow fracture systems.

In subaerial environments this parameter space will be populated with different fracture types because other fracture types will form in the pseudopillow fracture system parameter space, as these do not form in 'dry' environments. At the rhyolite end these may be populated by fractures such as those that occur in subaerial rhyolite lava flows (e.g. Fig. 3.28). However, whether wet or dry the low non-uniform stress columnar jointing field is unlikely to change. It is uncertain how the larger anisotropic stress field in basalt might be populated, perhaps by pseudopillow fracture systems and subsequently by sheet-like fractures in wet environments but in dry environments it is not clear. Perhaps a certain amount can be learnt from fractures such as those that occur in tumuli (e.g. Hon et al., 1994) which are clearly non-uniform stress environments and form a single large striae-bearing fracture.

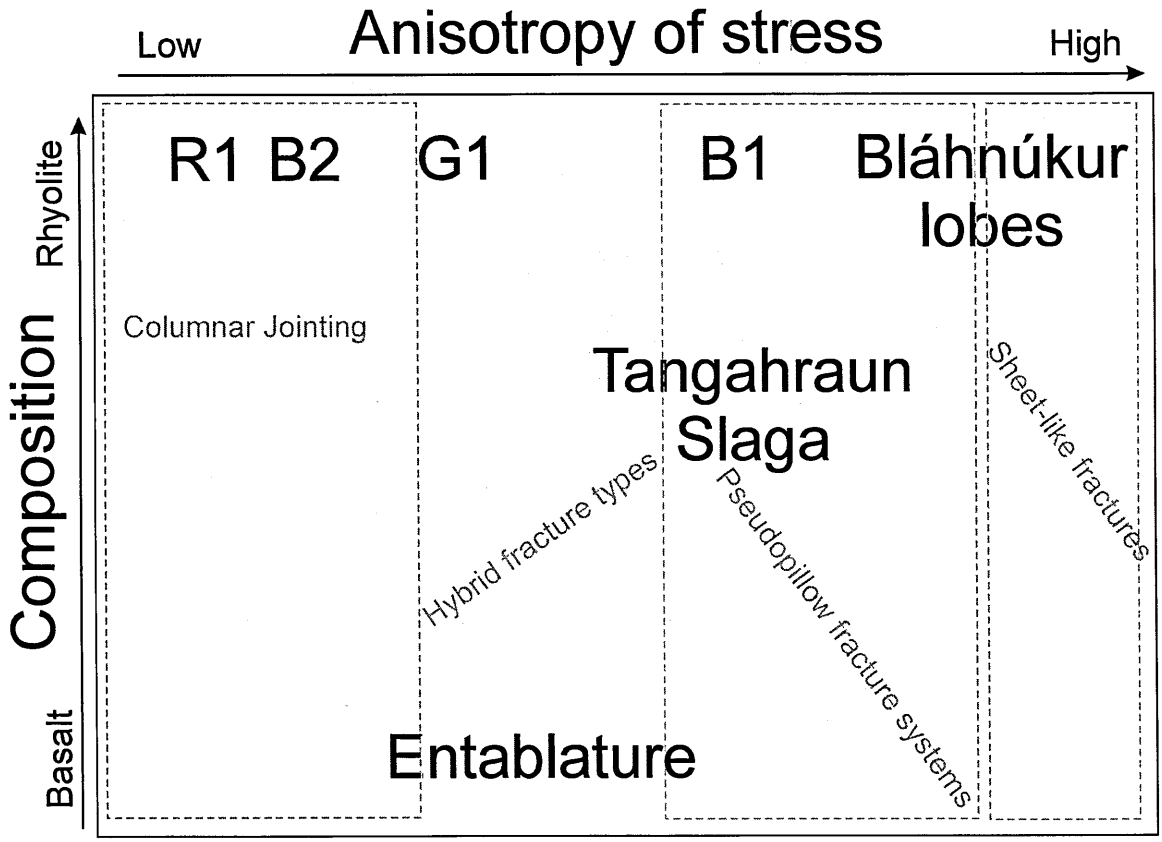

Fig. 6.1 Generalised parameter space diagram for lavas in environments containing any type of water-based coolant for a range of lava compositions on the x-axis and for anisotropy of stress on the y-axis. The left hand side of the diagram shows the area of columnar jointing formation, this grades into pseudopillow fracture systems and finally into sheet-like fractures at the highest anisotropic stresses. R1 is the columnar jointed rhyolite body from Rauðufossafjöll, G1 and G2 are columnar jointed rhyolite bodies from Goðafjall, Öræfajökull, B1 and B2 are columnar jointed rhyolite bodies from Bláhnúkur, Torfajökull. R1, G2 and B2 show only well formed columns and so are plotted at the low stress anisotropy end. G1 shows some preferred orientations and so has experienced some stress anisotropy while cooling and B1 contains preferred orientations and pseudopillow fracture systems and so experienced higher stress anisotropy. The entablature exposures of the Búrfell studied generally showed subvertical columns with pseudopillow fracture systems interspersed in the flow, this shows that there were areas of both higher and lower stress anisotropy in the lava flow.

6.4 Further work

Further work could usefully populate the parameter space of composition versus non-uniformity of the stress field in both 'wet' and 'dry' environments. This would involve the study of subaerial columnar jointing in both rhyolitic and intermediate lava flows, and the study of basaltic and intermediate composition columnar jointing from environments

containing some form of additional coolant. In basalt however this may be rather difficult as striae are faint or non-existent, at least in entablature. The high anisotropy of stress end of the subaerial version of the parameter space could be easily studied using subaerial rhyolite flows, but the basaltic part of this diagram may be harder to fill in. Better constraints on physical properties of lavas, particularly tensile strength, would be useful for further studies of lava fractures.

6.4.1 Pseudopillow fracture systems and ductile fracture

The studies of pseudopillow fracture systems in this thesis demonstrate the common occurrence of ductile fracture in lava in master fractures, in a range of compositions (basalt and trachyandesite). The hypothesis for pseudopillow fracture system formation does not require the presence of coolant to form ductile master fractures, only to preserve them. The driver of master fracture formation is instead thought to be caused by stress in the lava flow and high strain rates, resulting from flow-related stress of the lava or from the stresses caused by the weight of lava (particularly solidified lava) above where master fractures form. These stresses should also occur in lava flows that do not interact with some type of additional water-based coolant and so ductile master fractures may be expected to form in subaerial lava flows.

These types of fractures have never been documented in subaerial lavas so either they do not form or they do form but may be less visible, perhaps as a result of annealing of the fracture. Hot lava, above its glass transition temperature, is well known to have the ability anneal. If ductile master fractures anneal soon after their formation they may not leave any evidence of their existence, especially in master fractures that occur parallel to flow banding within a lava flow. In lavas where there is no flow banding or master fractures

also occur cross cutting flow banding closed master fractures may be visible as semi-annealed fractures, perhaps showing something akin to vesicularity along the annealed fracture plane. In glassy lavas annealed fractures may appear like annealed bubbles which show bubble 'ghosts' where annealing of bubbles occurred (e.g. Rust et al. 2004; Rust and Cashman 2007), or may show a mis-match in the flow banding for master fractures that fracture across flow banding.

However, in basaltic lava flows there may be a clearer way to determine the presence of annealed or semi-formed master fractures. Studies in entablature (chapter 4) show that master fractures form in conjunction with evolved residual melt. In subaerial lava flows these may appear as thin vertical bands / planes in the lava flow, distinct perhaps from cylinders and horizontal planes of evolved segregation material found more commonly in basalt lava flows. These vertical planes of segregation material may be pegmatitic rather than appearing as the fine grained dendritic and glass-rich material associated with master fractures in rapidly cooled lava flows in wet environments.

It is important that we look for and understand how and if master fractures form in subaerial lava flows. If they do not occur then a re-think of the original pseudopillow fracture system formation hypothesis is necessary, as clearly in this case an additional aqueous coolant is an important factor in their formation mechanism. However, if master fractures do occur in subaerial lavas they may give additional information about lava flows and their emplacement, and can tell us more about the stress state of lava flows while they are still hot and perhaps still being emplaced.

6.4.2 Columnar jointing

To better understand columnar jointing in rhyolite, and in general, a study of subaerial rhyolite columnar jointing would be beneficial. This may enable confirmation of the causes of the differences observed between basalt and rhyolite columnar jointing in this study in terms of *W*, *S* and number of column sides. *W/S* might be expected to be lower than subglacial rhyolite column values as the column sides measured may be the minimum possible, so columns should be larger. *W* would certainly be expected to be larger, due to slower cooling, however *W* may be larger than in comparable thickness basalt flows due to lower viscosity in rhyolite at the temperatures of stress build-up. *W* in subaerial rhyolite would be expected to be larger than in subaerial basalt lava flows of similar thickness.

Further studies of subglacial rhyolite, and other felsic lavas, e.g. dacite and andesite columns (both subglacial and subaerial), would enable the further study of compositional effects on columnar jointing and the environmental effects on columnar jointing. For example, is *W* actually showing a minimum possible value due to rapid cooling and no viscous relaxation in the lava, or might *W/S* ratio be giving information about the eruption environment?

Estimates of cooling rate from relaxation geospeedometry, carried out using differential scanning calormetry (DSC), on well preserved glass (e.g. Gottsmann and Dingwell, 2001) would be valuable in the study of subglacial rhyolite columnar jointing. This technique enables the cooling rate of the glass to be determined which would allow for an interesting comparison between DSC calculated cooling rates and striae measurements. These should correlate, which would allow for the development of a striae-based cooling rate calculator, providing that enough data can be gathered in order to establish a strong base-line

correlation. This would be an extremely powerful tool enabling the field measurements of striae to be easily and instantly transformed into a cooling rate. Some DSC data already exists from Icelandic subglacial rhyolites (Wilding et al., 2004), however, most of the samples chosen for this study were altered, usually by low temperature hydration by meteoric water (sourced from the subglacial eruption), a major feature in subglacial rhyolite lavas. This alters the glass from its original structure, which preserves the original cooling rate, to a structure that results in a much lower cooling rate. Only the most well preserved and least altered/hydrated samples would be useful in such measurements, such as those from lobe R1 at Rauðufossafjöll.

A similar method would not be feasible in basaltic columnar jointed lava flows as no glass is preserved in any significant quantities. Even during rapid cooling such as during the formation of entablature there is little or no basaltic glass formed. However, a novel method of measuring cooling rates has recently been developed by Holness et al. (2012) which uses dihedral angle (the angle between minerals) to infer a cooling rate. The median dihedral angle of plagioclase- plagioclase-clinopyroxene junctions evolves towards 120°, the equilibrium dihedral angle, the longer a lava body hot. For flows that cool quickly no evolution towards this equilibrium angle occurs. Thus the progression of the dihedral angle will record the cooling rate. There are limitations associated with this method as flows that cool too quickly tend to have plagioclase- plagioclase-glass junctions instead, rather than plagioclase- plagioclase-clinopyroxene junctions that are necessary for this method, or they show no evolution towards a higher dihedral angle. If this method could be correlated with measurements of striae on basaltic columnar joints in thick flows this would allow a similar striae-based cooling rate calculator to that proposed for subglacial rhyolite columnar jointing. However, for smaller striae measurements this method would need to be extrapolated significantly. An interesting comparison might be made between striae and

cooling rates in basalt and rhyolite, to judge whether a given stria width in rhyolite records the same cooling rate as the same stria width in basalt.

Some measurements of physical properties of rhyolite (and possibly basalt), such as tensile strength and Young's modulus, might also enable us to better understand how much these influence columnar jointing. Currently it appears that cooling rate and viscosity may be the main controls on the differences between these two types of columnar jointing, but better constrained physical properties, particularly tensile strength, of these lava types might shed further light on this topic.

Appendix 1: Tangahraun pseudopillow fracture system measurements in full

The following tables contain the full set of data collected from pseudopillow fracture systems in the Tangahraun lava flow, where σ is the standard deviation of the measurements for an individual fracture system (either the mean striae width or mean subsidiary fracture spacing), and # measurements is the number of measurements that produce the mean or standard deviation value. The data gathering method is presented in chapter 2, section 2.3.3 'Measurements of long planar subsidiary fractures'.

Table A1.1: Data from F-type pseudopillow fracture systems

Mean striae width /mm	σ	2σ	# measurements	Mean subsidiary fracture spacing /mm	σ	2σ	# measurements
2.9	1.7	3.5	3	8.3	2.3	4.6	11
9.3	2.5	5.1	13	10.2	2.6	5.1	13
7.6	1.9	3.7	6	12.2	4.1	8.3	15
8.5	5.1	10.1	16	21.6	5.9	11.9	12
7.8	3.5	6.9	10	12.0	3.1	6.1	10
5.9	1.8	3.7	8	7.4	1.8	3.7	12
6.8	1.7	3.3	15	10.7	2.6	5.1	14
6.7	3.3	6.6	13	12.1	4.2	8.4	20
13.4	4.5	9.1	20	14.2	4.2	8.4	9
6.7	4.0	8.1	14	12.0	3.3	6.6	12
6.6	2.8	5.6	12	11.3	2.5	5.1	10
4.2	1.8	3.5	12	5.2	1.8	3.7	13
9.5	2.6	5.2	16	15.7	3.7	7.4	10
3.2	1.2	2.4	26	6.1	1.5	3.1	21
8.2	1.8	3.7	12	11.4	3.0	6.0	9
5.2	1.7	3.4	14	11.1	2.2	4.4	23

Table A1.2: Data from X-type pseudopillow fracture systems

Mean striae width /mm	σ	2σ	# measurements	Mean subsidiary fracture spacing /mm	σ	2σ	# measurements
16.1	7.9	15.8	13	24.9	6.4	12.8	14
24.4	10.3	20.7	9	36.4	17.3	34.6	9
26.4	9.8	19.7	6	39.8	12.9	25.8	4
18.9	5.3	10.6	10	18.3	6.5	13.0	6
7.3	2.2	4.3	11	20.0	6.6	13.3	9
7.4	3.4	6.8	16	14.7	3.6	7.1	12
14.6	4.1	8.2	10	24.8	6.5	13.1	6
26.4	6.1	12.3	10	27.5	6.3	12.5	6
7.2	3.4	6.9	12	14.9	6.4	12.8	6
9.3	2.6	5.1	7	12.7	4.9	9.8	18
10.6	2.6	5.2	7	24.1	11.4	22.8	11

Table A1.3 Data from G-type pseudopillow fracture systems

Mean striae width /mm	σ	2σ	# measurements	Mean subsidiary fracture spacing /mm	σ	2σ	# measurements
0.6			37	4.8			3
0.7			9	2.9			11

Appendix 2: Rhyolite columnar jointing measurements in full

The following tables contain the full set of data collected from columnar joints in subglacial rhyolites, where S is mean striae width, σS is the standard deviation of the striae widths, # S measured is the number of striae widths measured to produce S, W is column side width, σW is the standard deviation of the column side widths, # W measured is the number of column side widths measured to produce W, W/S is the ratio of W:S, W/S error is the error on W/S measurement calculated as:

$$W/S\ error = W/S \times \sqrt{\left(\frac{\sigma S}{S}\right)^2 + \left(\frac{\sigma W}{W}\right)^2}$$

X indicates measurements on column sides cross cutting preferred orientation fractures and P indicates measurements on column sides of preferred orientation fractures. These are listed in X-P pairs from the same area of measurements. R1 is a lobe from Rauðufossafjöll, Torfajökull; B1 and B2 are lobes from Bláhnúkur, Torfajökull; G1 and G2 are lobes from Goðafjall, Öræfajökull, see section 3.2 'Geological setting and flow descriptions'.

The data gathering method is presented in chapter 3, section 3.3 'Measurements on rhyolite columnar jointing'.

Table A2.1: Rhyolite columnar jointing measurements

Flow	S / mm	σ S /mm	#S measured	W /mm	σ W /mm	#W measured	W/S	W/S error	number of sides: mode	mean	# measured
R1	2.0	0.6	53	74.8	26.7	35	36.6	16.7	5	5.2	27
R1	2.3	0.7	70	103.4	21.2	31	44.3	15.2			
R1	1.2	0.4	22	62.3	31.4	39	51.8	31.6			
R1				70.5	32.5	37					
B1	4.9	2.1	39	81.3	27.5	32	16.4	1.9	4	5.1	31
B2	16.6	3.9	27	91.9	21.9	15	5.6	9.0	5	5.6	27
G1	6.6	2.9	100	61.7	17.7	50	9.3	4.9	4	4.5	20
G1	5.3	2.1	100	53.5	23.4	36	10.2	6.0	5	5.2	13
G1 X	4.5	1.7	50	57.8	12.7	25	12.9	5.7	5	4.9	35
G1 p.	3.9	1.0	50	40.8	16.7	25	10.3	4.9	5	5.3	25
G1 X	5.7	2.4	50	69.3	21.8	25	12.2	6.5	4	4.8	49
G1 p.	6.7	2.1	50	65.4	20.4	25	9.8	4.4	4	4.8	49
G1 X	3.8	1.5	50	71.7	22.9	25	19.1	9.5	4	4.8	24
G1 p.	5.5	2.3	50	57.2	18.5	25	10.3	5.4	4	4.5	24
G2	26.5	9.2	36	137.3	50.3	44	5.2	2.5	5	5.4	31
G2	31.5	3.4	6	167.8	58.7	6	5.3	1.9	6	5.4	31
G2				109.2	39.3	36					15
											28

Table A2.2: Basalt columnar jointing data from Goehring and Morris (2008)

Site name	S / mm	σ S /mm	#S measured	W /mm	σ W /mm	#W measured	W/S	W/S error
Banks Lake I	58	1.2	103	500	14	12	8.6	0.3
Banks Lake II	55	1.5	80	550	16	30	10.0	0.4
Banks Lake gravel pit	134	5.1	46	1000	40	13	7.5	0.4
Park Lake	105	2.9	104	720	17	14	6.9	0.2
Tucannon River	89	4.1	163	540	19	52	6.1	0.4
Lyon Ferry Railway	59	1.6	114	720	28	25	12.2	0.6
Little Goose Dam	157	5.8	24	930	29	9	5.9	0.3
Chief Timothy I	41	0.8	63	329	9.2	24	8.0	0.3
Clarkston I	132	8.1	57	830	42	8	6.3	0.5
Clarkston II	36	1.8	63	259	7.8	30	7.2	0.4
Snake River Road	70	1.5	57	610	17	30	8.7	0.3
Asotin Creek	72	1.3	12	840	22	9	11.7	0.4
McCoy Canyon North	73	1.8	50	480	17	17	6.7	0.3
Devil's Canyon Pyramid	44.6	0.4	82	281	9.3	73	6.3	0.2
Rock River Road	49	2.1	44	690	32	9	14.1	0.9
Dell Road	69	2.1	43	510	18	14	7.4	0.3
Dalles Dam	358	7.0	50	1870	69	22	5.2	0.2
Dechutes Park I	179	6.6	25	1230	38	6	6.9	0.3
Dechutes Park II	225	5.7	39	1300	42	14	5.8	0.2

Appendix 3: Rhyolite FTIR data in full

The following tables contain the full set of data collected from FTIR analyses of subglacial rhyolites, where H_2O total is the mean total water content (H_2O plus OH) in wt. %, σ H_2O total is the standard deviation in the data of the mean total water content, H_2Om is the molecular water content (H_2O only) in wt. %, σ H_2Om the standard deviation in the mean molecular water content, OH is the OH content and is calculated as H_2O total minus H_2Om (i.e. OH = H_2O total - H_2Om), # measurements is the number of measurements taken for each mean value.

H_2O total is measured using the peak at ~3550cm^{-1} and H_2Om is measured using the peak at ~1630cm^{-1}. The method is included in chapter 3, section 3.2.5 'FTIR data'.

Table A3.1: FTIR rhyolite data

Sample	Location	Wafer thickness /mm	H_2O total / wt%	σ H_2O total	H_2Om / wt%	σ H_2Om	OH / wt% *	# measurements	Comments:
AF112	R1 column	0.519	0.20	0.001				5	Too noisy for 1630cm^{-1} peak
AF15	G1 column	0.394	0.20	0.003	0.14	0.004	0.06	5	
AF16	G1 column	0.587	0.19	0.007				5	Too noisy for 1630cm^{-1} peak
AF20	G1 column	0.394	0.29	0.015	0.14	0.011	0.16	5	
AF128	G1 grey material	0.154	1.55	0.105	1.58	0.044	-0.03	5	Saturated 3550cm^{-1} peak
AF132_1	G1 perlitised	0.186	0.29		0.16		0.14	1	
AF132_2	G1 perlitised	0.186	0.27		0.15		0.12	1	
AF132_3	G1 perlitised	0.186	0.52		0.46		0.06	1	
AF132_4	G1 perlitised	0.186	0.55		0.50		0.05	1	
AF132_5	G1 perlitised	0.186	0.60		0.61		-0.01	1	
AF132_6	G1 perlitised	0.186	0.62		0.69		-0.07	1	
AF132_7	G1 perlitised	0.186	1.10		1.27		-0.16	1	Saturated 3550cm^{-1} peak

* OH calculated as H_2O total - H_2Om

Appendix 2: Cooling and stress models

Table A4.1: Rhyolite cooling model, where K is thermal diffusivity, T_0 is the surface temperature, T_i is the eruption temperature, z is the depth and η is viscosity.

	A	B	C	D	E	F	G	H
1	K /m^2s^{-1}	T_0 /C	T_i /C	z /m	time /s	Temperature /C	Temp in K	Log10 (η) /Pa s
2	1.0E-06	20	900	5	0	900.00	1173.15	7.84
3	1.0E-06	20	900	5	1	900.00	1173.15	7.84
4	1.0E-06	20	900	5	10	900.00	1173.15	7.84
5	1.0E-06	20	900	5	100	900.00	1173.15	7.84
6	1.0E-06	20	900	5	1000000	899.64	1172.79	7.85
7	1.0E-06	20	900	5	1010000	899.62	1172.77	7.85
8	1.0E-06	20	900	5	1020000	899.59	1172.74	7.85
9	1.0E-06	20	900	5	1030000	899.56	1172.71	7.85
10	1.0E-06	20	900	5	1040000	899.54	1172.69	7.85
11	1.0E-06	20	900	5	1050000	899.51	1172.66	7.85
12	1.0E-06	20	900	5	1060000	899.48	1172.63	7.85
13	1.0E-06	20	900	5	1070000	899.44	1172.59	7.85
14	1.0E-06	20	900	5	1080000	899.41	1172.56	7.85
15	1.0E-06	20	900	5	1090000	899.38	1172.53	7.85
16	1.0E-06	20	900	5	1100000	899.34	1172.49	7.85
17	1.0E-06	20	900	5	1110000	899.30	1172.45	7.85
18	1.0E-06	20	900	5	1120000	899.26	1172.41	7.85
19	1.0E-06	20	900	5	1130000	899.22	1172.37	7.85
20	1.0E-06	20	900	5	1140000	899.18	1172.33	7.85
21	1.0E-06	20	900	5	1150000	899.14	1172.29	7.85
22	1.0E-06	20	900	5	1160000	899.10	1172.25	7.85
23	1.0E-06	20	900	5	1170000	899.05	1172.20	7.85
24	1.0E-06	20	900	5	1180000	899.00	1172.15	7.86
25	1.0E-06	20	900	5	1190000	898.95	1172.10	7.86
26	1.0E-06	20	900	5	1200000	898.90	1172.05	7.86
27	1.0E-06	20	900	5	1210000	898.85	1172.00	7.86
28	1.0E-06	20	900	5	1220000	898.79	1171.94	7.86
29	1.0E-06	20	900	5	1230000	898.74	1171.89	7.86
30	1.0E-06	20	900	5	1240000	898.68	1171.83	7.86

Table A4.2: Rhyolite cooling and stress model time steps at various depths

Depth	Time step
z = 0.1 m	10 s
z = 0.5 m	100 s
z = 1 m	1000 s
z = 2 m	1000 s
z = 3 m	10,000 s
z = 4 m	10,000 s
z = 5 m	10,000 s

Table A4.3: Rhyolite cooling model showing full formulae, where K is thermal diffusivity, T_0 is the surface temperature, T_i is the eruption temperature, z is the depth and η is viscosity.

	A	B	C	D	E	F	G	H
1	K /m^{2}s^{-1}	T_{0} /C	T_{i} /C	z /m	time /s	Temperature /C	Temp in K	Log10 (η) /Pa s
2	0.000001	20	900	5	0	=C2	=F2+273.15	=$O$25 + $O$26/(G2-$O$27)
3	0.000001	20	900	5	1	=C3	=F3+273.15	=$O$25 + $O$26/(G3-$O$27)
4	0.000001	20	900	5	10	=C4	=F4+273.15	=$O$25 + $O$26/(G4-$O$27)
5	0.000001	20	900	5	100	=C5	=F5+273.15	=$O$25 + $O$26/(G5-$O$27)
6	0.000001	20	900	5	1000000	=B6+(ERF(D6/(SQRT(4*A6*E6))))*(C6-B6)	=F6+273.15	=$O$25 + $O$26/(G6-$O$27)
7	0.000001	20	900	5	1010000	=B7+(ERF(D7/(SQRT(4*A7*E7))))*(C7-B7)	=F7+273.15	=$O$25 + $O$26/(G7-$O$27)
8	0.000001	20	900	5	1020000	=B8+(ERF(D8/(SQRT(4*A8*E8))))*(C8-B8)	=F8+273.15	=$O$25 + $O$26/(G8-$O$27)
9	0.000001	20	900	5	1030000	=B9+(ERF(D9/(SQRT(4*A9*E9))))*(C9-B9)	=F9+273.15	=$O$25 + $O$26/(G9-$O$27)
10	0.000001	20	900	5	1040000	=B10+(ERF(D10/(SQRT(4*A10*E10))))*(C10-B10)	=F10+273.15	=$O$25 + $O$26/(G10-$O$27)
11	0.000001	20	900	5	1050000	=B11+(ERF(D11/(SQRT(4*A11*E11))))*(C11-B11)	=F11+273.15	=$O$25 + $O$26/(G11-$O$27)
12	0.000001	20	900	5	1060000	=B12+(ERF(D12/(SQRT(4*A12*E12))))*(C12-B12)	=F12+273.15	=$O$25 + $O$26/(G12-$O$27)
13	0.000001	20	900	5	1070000	=B13+(ERF(D13/(SQRT(4*A13*E13))))*(C13-B13)	=F13+273.15	=$O$25 + $O$26/(G13-$O$27)
14	0.000001	20	900	5	1080000	=B14+(ERF(D14/(SQRT(4*A14*E14))))*(C14-B14)	=F14+273.15	=$O$25 + $O$26/(G14-$O$27)
15	0.000001	20	900	5	1090000	=B15+(ERF(D15/(SQRT(4*A15*E15))))*(C15-B15)	=F15+273.15	=$O$25 + $O$26/(G15-$O$27)
16	0.000001	20	900	5	1100000	=B16+(ERF(D16/(SQRT(4*A16*E16))))*(C16-B16)	=F16+273.15	=$O$25 + $O$26/(G16-$O$27)
17	0.000001	20	900	5	1110000	=B17+(ERF(D17/(SQRT(4*A17*E17))))*(C17-B17)	=F17+273.15	=$O$25 + $O$26/(G17-$O$27)
18	0.000001	20	900	5	1120000	=B18+(ERF(D18/(SQRT(4*A18*E18))))*(C18-B18)	=F18+273.15	=$O$25 + $O$26/(G18-$O$27)
19	0.000001	20	900	5	1130000	=B19+(ERF(D19/(SQRT(4*A19*E19))))*(C19-B19)	=F19+273.15	=$O$25 + $O$26/(G19-$O$27)
20	0.000001	20	900	5	1140000	=B20+(ERF(D20/(SQRT(4*A20*E20))))*(C20-B20)	=F20+273.15	=$O$25 + $O$26/(G20-$O$27)
21	0.000001	20	900	5	1150000	=B21+(ERF(D21/(SQRT(4*A21*E21))))*(C21-B21)	=F21+273.15	=$O$25 + $O$26/(G21-$O$27)
22	0.000001	20	900	5	1160000	=B22+(ERF(D22/(SQRT(4*A22*E22))))*(C22-B22)	=F22+273.15	=$O$25 + $O$26/(G22-$O$27)
23	0.000001	20	900	5	1170000	=B23+(ERF(D23/(SQRT(4*A23*E23))))*(C23-B23)	=F23+273.15	=$O$25 + $O$26/(G23-$O$27)
24	0.000001	20	900	5	1180000	=B24+(ERF(D24/(SQRT(4*A24*E24))))*(C24-B24)	=F24+273.15	=$O$25 + $O$26/(G24-$O$27)
25	0.000001	20	900	5	1190000	=B25+(ERF(D25/(SQRT(4*A25*E25))))*(C25-B25)	=F25+273.15	=$O$25 + $O$26/(G25-$O$27)
26	0.000001	20	900	5	1200000	=B26+(ERF(D26/(SQRT(4*A26*E26))))*(C26-B26)	=F26+273.15	=$O$25 + $O$26/(G26-$O$27)
27	0.000001	20	900	5	1210000	=B27+(ERF(D27/(SQRT(4*A27*E27))))*(C27-B27)	=F27+273.15	=$O$25 + $O$26/(G27-$O$27)
28	0.000001	20	900	5	1220000	=B28+(ERF(D28/(SQRT(4*A28*E28))))*(C28-B28)	=F28+273.15	=$O$25 + $O$26/(G28-$O$27)
29	0.000001	20	900	5	1230000	=B29+(ERF(D29/(SQRT(4*A29*E29))))*(C29-B29)	=F29+273.15	=$O$25 + $O$26/(G29-$O$27)
30	0.000001	20	900	5	1240000	=B30+(ERF(D30/(SQRT(4*A30*E30))))*(C30-B30)	=F30+273.15	=$O$25 + $O$26/(G30-$O$27)

Table A4.4: Viscosity model of Giordano et al. (2008) incorporated into the cooling model to calculate viscosity at a given temperature.

M	N	O	P	Q	R	S	T	U	V	W	X	Y	Z
MODEL FOR VISCOSITY OF VOLATILE-BEARING MELTS						*MODEL COEFFICIENTS*							
Citation: Giordano D. Russell JK. & Dingwell DB (2008)						VFT EQ: log n (Pa s) = A + B/[T(K)-C]							
Viscosity of Magmatic Liquids: A Model. EPSL. Accepted 3/08.						*[Constants: Do Not Modify]*					*COMPUTED*		
						A	-4.55				*VALUES*		
Oxide	*Constant*	*INPUT*	*Normalize*	*Mol. %*		*B1*	159.60	*C1*	2.75	B1	*12651.51*	C1	*217.571*
Labels	*Molec. Wt.*	*(Wt. %)*	*(Wt. %)*	*Oxide Basis*		*B2*	-173.30	*C2*	15.70	B2	*-1490.13*	C2	*137.407*
SiO2	60.0850	73.29	73.330	79.117		*B3*	72.10	*C3*	8.30	B3	*171.02*	C3	*21.506*
TiO2	79.8800	0.189	0.189	0.153		*B4*	75.70	*C4*	10.20	B4	*17.49*	C4	*10.364*
Al2O3	101.9600	13.52	13.524	8.599		*B5*	-39.00	*C5*	-12.30	B5	*-39.63*	C5	*-100.270*
FeO(T)	71.8500	2.55	2.548	2.299		*B6*	-84.10	*C6*	-99.50	B6	*-479.01*	C6	*-30.618*
MnO	70.9400	0.067	0.067	0.061		*B7*	141.50	*C11*	0.30	B7	*94.53*	C11	*31.140*
MgO	40.3000	0.14	0.144	0.231		*B11*	-2.43			B11	*-499.11*		
CaO	56.0800	0.88	0.879	1.016		*B12*	-0.91			B12	*-680.74*		
Na2O	61.9800	5.10	5.101	5.335		*B13*	17.60			B13	*1233.69*		
K2O	94.2000	4.09	4.093	2.817									
P2O5	141.9400	0.026	0.026	0.012		*Colour Code to Cells*							
H2O	18.0010	0.10	0.100	0.360		*Constants For Viscosity Program*							
F2O-1	37.9968	0.00	0.000	0.000		*Values Set by User*							
Total		99.95	100.000	100.000		*Computed Properties*							
			GFW.	*64.8268*									

	Predicted Model Values	
T(oC)	1000	1200
A	*-4.55*	*-4.55*
B	*10979.6*	*10979.6*
C	*287.1*	*287.1*
Tg(K)	*951*	*951*
Fragility (m)	*23.7*	*23.7*
log η (Pas)	*6.58*	*4.71*

T(oC)	T(K)	*log η (Pa s)*
700	973.15	11.45
800	1073.15	9.42
900	1173.15	7.84
1000	1273.15	6.58
1100	1373.15	5.56
1200	1473.15	4.71

Table A4.5: Rhyolite stress accumulation model, using cooling model, where α is the thermal expansion coefficient, ν is Poisson's ratio, E is young's modulus and σ is the calculated stress

	A	B	C	D	E	F	G	H	I	J	K	L	M	N	O	P
1	K /m2s-1	T0 /C	Ti /C	z /m	time /s	Temp /C	Temp in K	Log10 (η) /Pa s	Δt	ΔT	η	α	1-ν	E	σ1	σ
2	1.0E-06	20	900	0.1	0	900.00	1173.15	7.84				7.0E-06	0.8	6.8E+10		0
3	1.0E-06	20	900	0.1	1	900.00	1173.15	7.84	1	0.0E+00	6.94E+07	7.0E-06	0.8	6.8E+10	0	0
4	1.0E-06	20	900	0.1	10	900.00	1173.15	7.84	9	0.0E+00	6.94E+07	7.0E-06	0.8	6.8E+10	0	0
5	1.0E-06	20	900	0.1	20	900.00	1173.15	7.84	10	0.0E+00	6.94E+07	7.0E-06	0.8	6.8E+10	0	0
6	1.0E-06	20	900	0.1	30	900.00	1173.15	7.84	10	0.0E+00	6.94E+07	7.0E-06	0.8	6.8E+10	0	0
7	1.0E-06	20	900	0.1	40	900.00	1173.15	7.84	10	0.0E+00	6.94E+07	7.0E-06	0.8	6.8E+10	0	0
8	1.0E-06	20	900	0.1	50	900.00	1173.15	7.84	10	0.0E+00	6.94E+07	7.0E-06	0.8	6.8E+10	0	0
9	1.0E-06	20	900	0.1	60	900.00	1173.15	7.84	10	0.0E+00	6.94E+07	7.0E-06	0.8	6.8E+10	0	0
10	1.0E-06	20	900	0.1	70	900.00	1173.15	7.84	10	0.0E+00	6.94E+07	7.0E-06	0.8	6.8E+10	0	0
11	1.0E-06	20	900	0.1	80	900.00	1173.15	7.84	10	0.0E+00	6.94E+07	7.0E-06	0.8	6.8E+10	0	0.00E+00
12	1.0E-06	20	900	0.1	90	900.00	1173.15	7.84	10	8.0E-11	6.94E+07	7.0E-06	0.8	6.8E+10	0	0.00E+00
13	1.0E-06	20	900	0.1	100	900.00	1173.15	7.84	10	1.3E-09	6.94E+07	7.0E-06	0.8	6.8E+10	0	0.00E+00
14	1.0E-06	20	900	0.1	110	900.00	1173.15	7.84	10	1.2E-08	6.94E+07	7.0E-06	0.8	6.8E+10	0	0.00E+00
15	1.0E-06	20	900	0.1	120	900.00	1173.15	7.84	10	8.2E-08	6.94E+07	7.0E-06	0.8	6.8E+10	0	0.00E+00
16	1.0E-06	20	900	0.1	130	900.00	1173.15	7.84	10	4.0E-07	6.94E+07	7.0E-06	0.8	6.8E+10	0	0.00E+00
17	1.0E-06	20	900	0.1	140	900.00	1173.15	7.84	10	1.5E-06	6.94E+07	7.0E-06	0.8	6.8E+10	0	0.00E+00
18	1.0E-06	20	900	0.1	150	900.00	1173.15	7.84	10	4.8E-06	6.94E+07	7.0E-06	0.8	6.8E+10	0	0.00E+00
19	1.0E-06	20	900	0.1	160	900.00	1173.15	7.84	10	1.3E-05	6.94E+07	7.0E-06	0.8	6.8E+10	0	0.00E+00
20	1.0E-06	20	900	0.1	170	900.00	1173.15	7.84	10	3.2E-05	6.94E+07	7.0E-06	0.8	6.8E+10	0	0.00E+00
21	1.0E-06	20	900	0.1	180	900.00	1173.15	7.84	10	6.8E-05	6.94E+07	7.0E-06	0.8	6.8E+10	0	0.00E+00
22	1.0E-06	20	900	0.1	190	900.00	1173.15	7.84	10	1.4E-04	6.94E+07	7.0E-06	0.8	6.8E+10	0	0.00E+00
23	1.0E-06	20	900	0.1	200	900.00	1173.149	7.84	10	2.5E-04	6.94E+07	7.0E-06	0.8	6.8E+10	0	0.00E+00
24	1.0E-06	20	900	0.1	210	900.00	1173.149	7.84	10	4.3E-04	6.94E+07	7.0E-06	0.8	6.8E+10	0	0.00E+00
25	1.0E-06	20	900	0.1	220	900.00	1173.148	7.84	10	7.1E-04	6.94E+07	7.0E-06	0.8	6.8E+10	0	0.00E+00
26	1.0E-06	20	900	0.1	230	900.00	1173.147	7.84	10	1.1E-03	6.94E+07	7.0E-06	0.8	6.8E+10	0	0.00E+00
27	1.0E-06	20	900	0.1	240	900.00	1173.146	7.84	10	1.7E-03	6.95E+07	7.0E-06	0.8	6.8E+10	0	0.00E+00
28	1.0E-06	20	900	0.1	250	899.99	1173.143	7.84	10	2.4E-03	6.95E+07	7.0E-06	0.8	6.8E+10	0	0.00E+00
29	1.0E-06	20	900	0.1	260	899.99	1173.14	7.84	10	3.4E-03	6.95E+07	7.0E-06	0.8	6.8E+10	0	0.00E+00
30	1.0E-06	20	900	0.1	270	899.99	1173.135	7.84	10	4.6E-03	6.95E+07	7.0E-06	0.8	6.8E+10	0	0.00E+00

Table A4.6: Basalt stress accumulation model, temperature step is set at 1°C and resulting time step, and thus cooling rate, is calculated from this.

	A	B	C	D	E	F	H	I	J	K	L	M	N	O	P	Q	R	S	T	U
1														Z=0.1				Z=0.5		
2	K /m^{2}s^{-1}	$T_{0/C}$	$T_{i/C}$	erf-1	Temp /C	Temp /K	Log10 η	ΔT	η	α	1-ν	E	Δt	time /s	σ1	σ	Δt	time /s	σ1	σ
3	6.5E-07	20	1150		1150	1423.15	2.12			7.0E-06	0.8	6.8E+10		0		0		0		0
4	6.5E-07	20	1150	2.3521	1149	1422.15	2.13	1	1.34E+02	7.0E-06	0.8	6.8E+10	695	695.229	0	0	17381	17380.73	0	0
5	6.5E-07	20	1150	2.2107	1148	1421.15	2.14	1	1.37E+02	7.0E-06	0.8	6.8E+10	92	787.0199	0	0	2295	19675.5	0	0
6	6.5E-07	20	1150	2.1253	1147	1420.15	2.15	1	1.40E+02	7.0E-06	0.8	6.8E+10	64	851.4816	0	0.0E+00	1612	21287.04	0	0.0E+00
7	6.5E-07	20	1150	2.0623	1146	1419.15	2.16	1	1.43E+02	7.0E-06	0.8	6.8E+10	53	904.3514	0	0.0E+00	1322	22608.79	0	0.0E+00
8	6.5E-07	20	1150	2.0128	1145	1418.15	2.17	1	1.46E+02	7.0E-06	0.8	6.8E+10	45	949.3542	0	0.0E+00	1125	23733.85	0	0.0E+00
9	6.5E-07	20	1150	1.9711	1144	1417.15	2.18	1	1.52E+02	7.0E-06	0.8	6.8E+10	41	989.9098	0	0.0E+00	1014	24747.74	0	0.0E+00
10	6.5E-07	20	1150	1.9357	1143	1416.15	2.20	1	1.59E+02	7.0E-06	0.8	6.8E+10	37	1026.443	0	0.0E+00	913	25661.07	0	0.0E+00
11	6.5E-07	20	1150	1.9043	1142	1415.15	2.22	1	1.67E+02	7.0E-06	0.8	6.8E+10	34	1060.633	0	0.0E+00	855	26515.84	0	0.0E+00
12	6.5E-07	20	1150	1.8765	1141	1414.15	2.24	1	1.75E+02	7.0E-06	0.8	6.8E+10	32	1092.277	0	0.0E+00	791	27306.92	0	0.0E+00
13	6.5E-07	20	1150	1.8511	1140	1413.15	2.26	1	1.84E+02	7.0E-06	0.8	6.8E+10	30	1122.498	0	0.0E+00	756	28062.44	0	0.0E+00
14	6.5E-07	20	1150	1.8281	1139	1412.15	2.29	1	1.93E+02	7.0E-06	0.8	6.8E+10	28	1150.91	0	0.0E+00	710	28772.76	0	0.0E+00
15	6.5E-07	20	1150	1.8066	1138	1411.15	2.31	1	2.03E+02	7.0E-06	0.8	6.8E+10	27	1178.388	0	0.0E+00	687	29459.71	0	0.0E+00
16	6.5E-07	20	1150	1.7869	1137	1410.15	2.33	1	2.13E+02	7.0E-06	0.8	6.8E+10	26	1204.488	0	0.0E+00	653	30112.21	0	0.0E+00
17	6.5E-07	20	1150	1.7684	1136	1409.15	2.35	1	2.25E+02	7.0E-06	0.8	6.8E+10	25	1229.945	0	0.0E+00	636	30748.62	0	0.0E+00
18	6.5E-07	20	1150	1.7511	1135	1408.15	2.37	1	2.37E+02	7.0E-06	0.8	6.8E+10	24	1254.299	0	0.0E+00	609	31357.48	0	0.0E+00
19	6.5E-07	20	1150	1.7347	1134	1407.15	2.40	1	2.49E+02	7.0E-06	0.8	6.8E+10	24	1278.198	0	0.0E+00	597	31954.96	0	0.0E+00
20	6.5E-07	20	1150	1.7193	1133	1406.15	2.42	1	2.63E+02	7.0E-06	0.8	6.8E+10	23	1301.184	0	0.0E+00	575	32529.6	0	0.0E+00
21	6.5E-07	20	1150	1.7045	1132	1405.15	2.44	1	2.77E+02	7.0E-06	0.8	6.8E+10	23	1323.844	0	0.0E+00	567	33096.1	0	0.0E+00
22	6.5E-07	20	1150	1.6906	1131	1404.15	2.47	1	2.92E+02	7.0E-06	0.8	6.8E+10	22	1345.726	0	0.0E+00	547	33643.15	0	0.0E+00
23	6.5E-07	20	1150	1.6771	1130	1403.15	2.49	1	3.08E+02	7.0E-06	0.8	6.8E+10	22	1367.375	0	0.0E+00	541	34184.38	0	0.0E+00
24	6.5E-07	20	1150	1.6644	1129	1402.15	2.51	1	3.25E+02	7.0E-06	0.8	6.8E+10	21	1388.348	0	0.0E+00	524	34708.7	0	0.0E+00
25	6.5E-07	20	1150	1.6521	1128	1401.15	2.54	1	3.44E+02	7.0E-06	0.8	6.8E+10	21	1409.157	0	0.0E+00	520	35228.92	0	0.0E+00

Appendix 5: Striae and column side width measurements from entablature-bearing basaltic lava flows

The following tables contain the full set of data collected from columns (both colonnade and columns in entablature) and pseudopillow fracture systems in entablature bearing flows, where S is striae width, W is column side width, σ is the standard deviation and # measurements is the number of measurements that produce any mean or standard deviation value. For measurement method see chapter 4, section 4.3.1.2 'Column-bounding fractures'.

Table A5.1: Striae and column side width measurements from entablature

Outcrop description	Location	Mean S /mm	σ S	# measurements	Mean W /mm	σ W	# measurements
Colonnade	Gljúfri	27.9	7.4	33	385.3	97.4	8
Colonnade, north, top of columns	Hjálparfoss	31.2	9.7	84	282.6	90.0	17
Colonnade, north, base of columns	Hjálparfoss	15.7	4.1	73	271.5	91.6	13
Colonnade, southern	Hjálparfoss	31.0	8.5	50	420.3	208.4	10
Colonnade, flow 4	Galtafell	58.5	12.6	63	372.4	95.4	13
Entablature	Gljúfri	13.0	4.1	54	118.1	28.3	15
Entablature	Hjálparfoss	26.2	6.7	47	221.8	70.1	12
Entablature near waterfall	Hjálparfoss	14.7	3.8	53	248.1	14.5	8
Entablature near waterfall 2	Hjálparfoss	16.2	4.0	73	269.3	83.7	12
Entablature, southern	Hjálparfoss	13.5	3.7	44	171.1	83.5	8
Cube-jointed entablature, flow 4	Galtafell	13.0	7.1	33	69.5	17.4	10
Cube-jointed entablature, flow 2	Galtafell	10.7	3.9	57	109.0	40.2	12
Subsidiary fracture striae	Hjálparfoss	10.7	2.8	76	-	-	-

Appendix 6: Slaga pseudopillow fracture system measurements in full

Pseudopillow fracture systems from the Slaga lava flow, where σ is the standard deviation and # measurements is the number of measurements that produce the mean or standard deviation.

Table A6.1: Pseudopillow fracture systems from the Slaga lava flow

Mean striae width /mm	σ	# measurements	Mean subsidiary fracture spacing /mm	σ	# measurements
4.3	2.9	14	10.7	3.5	9
3.1	1.2	12	10.6	3.2	9
5.5	2.9	27	11.0	4.7	41
3.5	0.9	5	7.6	1.9	11
8.9	7.8	27	17.8	10.5	14
6.1	2.1	43	11.0	3.7	29
7.1	3.7	11	18.8	3.7	5
12.4	2.5	8	12.0	3.0	11
13.0	4.1	8	26.9	5.0	4
7.3	2.7	18	14.9	3.4	10

For measurement method see chapter 2, section 2.3.3 'Measurements of long planar subsidiary fractures' and chapter 5, section 5.3.1.3 'Measurements from long planar subsidiary fractures'.

Appendix 7: XRF major and trace element data and TAS plot

All XRF analyses are from single, representative, unaltered/unhydrated lava samples. Major element analyses were performed on glass discs prepaired by mixing one part (by weight) finely powdered rock sample with five parts of lithium borate flux (Spectroflux 100B). This was then melted in a platinum crucible in the furnace at 1100°C, and the melt pressed in a mould to form a circular glass disc. Trace element analyses were performed on powder pellets which were produced by mixing finely powdered rock sample with a binding agent. This is then compressed into 35 mm diameter pellets.

Table A7.1 XRF major analyses from entablature lava flows

Sample:	Búrfell		Galtafell			Sheepfold	Þjórsárholt	Miðfell	Skarðsfjall
wt %	Hjálparfoss	Gjáin	Flow 4	Flow 3	Flow 2				
SiO_2	49.25	49.89	49.17	49.63	49.36	50.76	51.52	49.03	50.74
TiO_2	1.800	1.536	3.467	3.454	2.896	3.265	3.204	2.846	3.161
Al_2O_3	14.53	14.90	13.00	13.14	13.36	13.23	13.06	13.32	13.12
Fe_2O_3	12.45	12.22	16.15	16.20	15.46	15.46	15.12	15.30	15.03
MnO	0.194	0.191	0.233	0.230	0.227	0.225	0.227	0.221	0.226
MgO	7.37	7.73	5.26	5.39	6.06	5.09	4.79	6.06	4.86
CaO	12.34	12.80	9.67	9.82	10.63	9.36	9.02	10.51	9.03
Na_2O	2.20	2.03	2.53	2.59	2.43	2.69	2.79	2.41	2.72
K_2O	0.23	0.14	0.59	0.59	0.38	0.67	0.75	0.39	0.71
P_2O_5	0.265	0.144	0.410	0.424	0.293	0.402	0.402	0.281	0.386
LOI	-0.55	-0.75	-0.61	-0.38	-0.34	-0.32	-0.40	-0.56	-0.14
Total	100.08	100.83	99.87	101.09	100.76	100.83	100.47	99.82	99.83

Table A7.2 XRF major analyses from rhyolite columnar jointing

Sample:	Tangahraun	Slaga	R1	G1	G2	B	Blåhnúkur mean	
wt %								±2σ
SiO_2	57.62	57.04	73.56	73.29	73.42	70.76	70.09	1.17
TiO_2	1.507	1.598	0.289	0.189	0.188	0.277	0.29	0.03
Al_2O_3	16.08	14.02	12.83	13.52	13.50	14.13	14.11	0.19
Fe_2O_3	9.25	14.08	3.27	2.55	2.51	3.31	3.35	0.21
MnO	0.243	0.331	0.123	0.067	0.063	0.085	0.08	0.00
MgO	2.10	1.49	0.10	0.14	0.16	0.22	0.32	0.21
CaO	5.01	5.53	0.70	0.88	0.87	0.94	0.97	0.31
Na_2O	5.03	5.00	5.48	5.10	4.94	5.77	5.57	0.19
K_2O	2.63	1.65	3.89	4.09	4.04	4.28	4.33	0.14
P_2O_5	0.606	0.588	0.022	0.026	0.026	0.037	0.03	0.00
LOI	-0.11	-0.34	0.28	0.46	0.87	0.90	0.72	0.77
Total	99.95	100.98	100.55	100.31	100.59	100.71	99.87	0.90

Table A7.3 XRF trace analyses from entablature lava flows

Sample:	Detection	Búrfell		Galtafell			Sheepfold	Þjórsárholt	Miðfell	Skarðsfjall
ppm	Limit	Hjálparfoss	Gjáin	Flow 4	Flow 3	Flow 2				
Rb	2	4	2	11	10	6	13	14	7	14
Sr	2	198	161	253	259	217	251	246	216	251
Y	2.0	29	26	47	45	39	50	53	39	53
Zr	2	105	82	241	242	177	270	293	182	292
Nb	1.5	14	9	29	30	21	32	35	21	35
Ba	12	59	44	132	139	98	151	168	97	158
Pb	5	4	5	5	4	6	6	6	3	4
Th	4	2	3	5	4	3	3	4	2	4
U	3	3	1	1	0	1	0	3	0	3
Sc	5	42	42	36	35	40	36	32	40	34
V	5	304	308	431	427	430	388	368	422	378
Cr	4	150	161	28	29	82	36	32	80	29
Co	2	40	43	39	39	42	35	35	40	33
Ni	3	73	78	40	40	59	39	32	55	35
Cu	3	129	109	124	127	125	111	106	161	108
Zn	3	88	78	134	132	118	136	132	118	139
Ga	3	19	18	23	23	21	23	24	22	24

Table A7.4 XRF trace analyses from rhyolite columnar jointing

Sample: ppm	Detection Limit	Tangahraun	Slaga	R1	G1	G2	B
Rb	2	61	34	99	101	102	106
Sr	2	471	310	48	47	48	58
Y	2.0	57	84	118	90	97	87
Zr	2	509	462	851	441	437	807
Nb	1.5	98	48	163	70	69	120
Ba	12	1025	422	483	694	686	471
Pb	5	1	5	11	9	11	9
Th	4	9	3	17	15	13	18
U	3	4	2	6	4	4	6
Sc	5	14	23	2	2	2	3
V	5	46	1	4	2	1	4
Cr	4	34	6	5	8	5	4
Co	2	6	6	1	1	0	1
Ni	3	2	5	6	4	3	4
Cu	3	10	18	4	10	9	8
Zn	3	120	164	186	98	100	127
Ga	3	22	27	33	25	25	30

Where R1 is a lobe from Rauðufossafjöll, Torfajökull; B is a sample from Bláhnúkur, Torfajökull; G1 and G2 are lobes from Goðafjall, Öræfajökull.

Fig. A7.1 TAS (total alkali vs. silica) plot for all samples in the study, demonstrating compositional domains. The data for the TAS plot are taken directly from the XRF data.

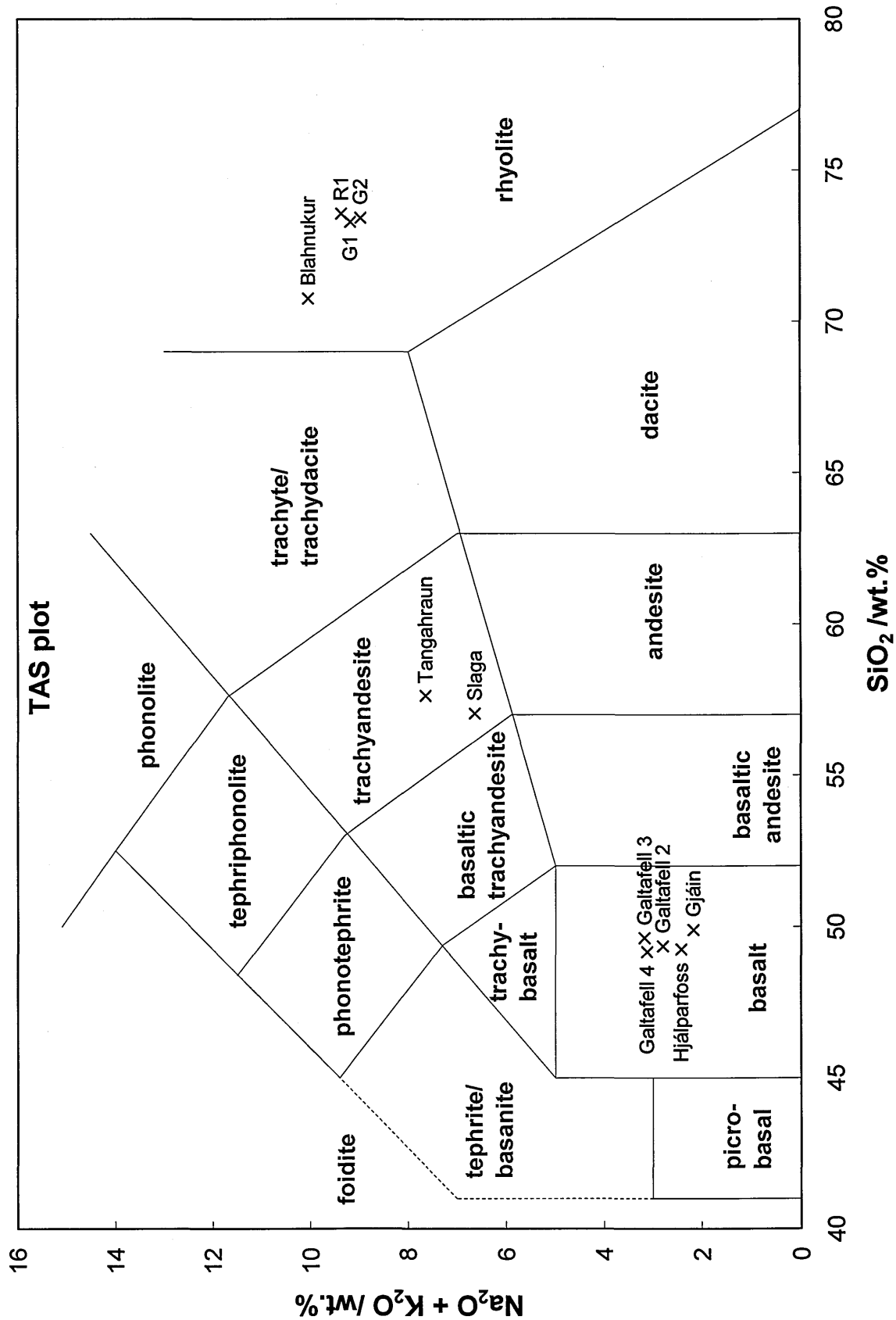

Where R1 is a lobe from Rauðufossafjöll, Torfajökull; Bláhnúkur is a sample from Bláhnúkur, Torfajökull; G1 and G2 are lobes from Goðafjall, Öræfajökull.